NSTX U

Torques On TF Conductors & Resulting Torsion & Shear Stress in NSTX CSU

NSTXU CALC 132-03-00

Rev 0

September 19 2011

Prepared By:

Robert D Woolley

Digitally signed by Robert D Woolley
DN: cn=Robert D Woolley, o, ou, email=rwoolley@pppl.gov, c=US
Date: 2011.09.19 17:26:50 -04'00'

R. Woolley

Reviewed By:

Peter Titus

Digitally signed by Peter Titus
DN: cn=Peter Titus, o, ou, email=ptitus@pppl.gov, c=US
Date: 2011.09.20 08:28:16 -04'00'

Peter H. Titus, PPPL Engineering Analysis Branch

Reviewed By:

Peter Titus

Digitally signed by Peter Titus
DN: cn=Peter Titus, o, ou, email=ptitus@pppl.gov, c=US
Date: 2011.09.20 08:28:29 -04'00'

Peter H. Titus Cognizant Engineer

PPPL Calculation Form

Calculation # NSTXU CALC 132-03-00 Revision # 00 WP #, 0029,0037 (ENG-032)

Purpose of Calculation: (Define why the calculation is being performed.)

The purpose of the calculation is to provide:

1. A means of calculating the torsional moments acting on the TF system for use to the Design Point Spreadsheet. These moments are used to size many of the OOP support structures, and /or to check Lorentz force calculations.

2. Calculations of the inner leg torsional shear stress and an appropriate algorithm for the DCPS to compute the torsional shear stresses to qualify the TF and/or to qualify similar results in ref 5.

References (List any source of design information including computer program titles and revision levels.

1. **R. Woolley memo 13-260709, "Out-Of-Plane (OOP) PF/TF Torques On TF Conductors in NSTX CSU", 26 July 2009,**
2. **P. Titus memo, "Maximum TF Torsional Shear", 29 July 2009**
3. **P. Titus paper, "Provisions for Out-of-Plane Support of the TF Coils in Recent Tokamaks",28September1999**
4. **R. Woolley memo 13-110211, "Torques On TF Conductors & Resulting Torsion & Shear Stress in NSTX CSU, 04May2010 Design Point", 11 February 2011**
5. **P. Titus, NSTXU*-CALC-132-07-00 Rev0, "TF Inner Leg Torsional Shear, Including Input to the DCPS", 9Sept2011**

Assumptions (Identify all assumptions made as part of this calculation.)

Stiffnesses for segments of the global structure have come from other FEA calculations. These are assumed to be correct, and in so far as they produce torsional shear stresses similar to [5] the stiffnesses used, are judged adequate

Calculation (Calculation is either documented here or attached)

Two Memos are included in the body of the calculation. A Feb 11 2011 memo which includes the torsional moment summation used in the design point, and a September 18th 2011 memo. The Feb 11 memo also includes a calculation of the torsional shear stress in the TF inner leg that was corrected in the September 18th memo.

Conclusion (Specify whether or not the purpose of the calculation was accomplished.)

The torsional moment equation has been implemented in the design point spreadsheet,. Torsional shear stress has been calculated to be 25.23 MPa. This is higher than the ref 5 result of 22 MPa but the difference is small given the complexity of the calculations and the different approaches used, and the results and DCPS algorithms are judged consistent. Choice of the final DCPS algorithm will be deferred to the time the DCPS is implemented.

Cognizant Engineer's printed name, signature, and date

Peter H. Titus Peter Titus

Digitally signed by Peter Titus
DN: cn=Peter Titus, o, ou, email=ptitus@pppl.gov, c=US
Date: 2011.09.20 08:28:48 -04'00'

I have reviewed this calculation and, to my professional satisfaction, it is properly performed and correct.

Checker's printed name, signature, and date

Peter H. Titus Peter Titus

Digitally signed by Peter Titus
DN: cn=Peter Titus, o, ou, email=ptitus@pppl.gov, c=US
Date: 2011.09.20 08:29:09 -04'00'

To: Distribution Date: 11 February 2011

From: R. Woolley Subject Torques On TF Conductors & Resulting Torsion & ShearStress in NSTX CSU, 04May2010 Design Point

References:

1. **R. Woolley memo 13-260709, "Out-Of-Plane (OOP) PF/TF Torques On TF Conductors in NSTX CSU", 26 July 2009,**
2. **P. Titus memo, "Maximum TF Torsional Shear", 29 July 2009**
3. **P. Titus paper, "Provisions for Out-of-Plane Support of the TF Coils in Recent Tokamaks",28September1999**

Summary

This updates Ref.1 bringing its calculation of out-o-plane (OOP) torques on TF coil conductors up to date for the design point adopted on 04May2010. It also includes a linear elastic model for the TF conductors and their supporting structures to estimate TF conductor torsion for any specified set of currents in the PF coils, OH coil, and plasma. For the 96 previously defined plasma equilibria and for the +24 kA maximum OH precharge case, the **peak torsional shear stress in the TF centerstack calculated by these methods is 25.18 MPa.**

As in Ref.1, this memo advances a simple but accurate algorithm for evaluating out-of-plane torques due to magnetic interactions of poloidal magnetic fields with TF conductor current. This is the subcect of pages 1-14 and Appendix 1 (pages 43-50). The torsional response model is the subject of pages 15- -42 and Appendix 2 (pages 51-69). Instead of the conventional complicated approach involving numerical integration of vector cross products of position vectors, current density vectors and poloidal magnetic field vectors at many evaluation points chosen along a segment of the TF conductor, this torque algorithm multiplies the [(130kA)(36turn)=4,680,000 A] TF current magnitude by the difference of the per radian poloidal magnetic fluxes evaluated at the two ends of the segment. (Note that the product of amperes and webers has the torque units, newton-meters.) The results are mathematically equivalent to numerically integrating the vector cross product of position and force over the TF conductor, but the torque algorithm advanced herein requires far less computation and is subject to far less numerical error. A full exposition of the torque algorithm is given in Appendix 1.

This torque algorithm is applied to the NSTX CS upgrade, using the latest layout for the TF conductor outline and using the PF/OH coil set of the 04May2010 design point. To increase numerical accuracy the TF conductor is partitioned into subregions separated by internal current streamlines estimated by equally subdividing the conductor cross section area. Torque loading densities for current ranges in each of the 12 PF and 1 OH coil circuits and for the plasma current are plotted. MATLAB version R2010b was used for all numerical calculations and plots.

Total Torque is Zero

The sum total of Z-axis Lorenz magnetic torques on the TF conductor system is identically zero. starting and ending poloidal fluxes by definition have zero difference. However, it also logically follows from the facts that (1) the sum total of Lorenz torques on all NSTX conductors is always zero (in order for conservation of total angular momentum to hold true), and (2) Lorenz torques on coaxial PF and OH coil conductors are identically zero due to their axisymmetric shape and their alignment with the toroidal field. However, although the total TF system torque is zero, the torques on *portions* of the TF system can be large enough to require attention to providing sufficient support or in avoiding excessive stresses.

Torque Algorithm Results

Concerns have been expressed about supporting net torques on the TF outer legs by the opposing net torques on the TF central bundle and radial conductor assemblies. A simple algebraic formula is obtained from the torque algorithm for net torque on the TF outer legs, as Eq.(1). (Different from Ref.1, the TF outer leg boundary is here set at the umbrella clamps.)

$$\left[\frac{\text{Net TF System OuterLeg Torque}}{1\,\text{N - m}}\right] = 3519.9\left[\frac{I_{PF1AU} - I_{PF1AL}}{1\,\text{kA}}\right] + 3692.0\left[\frac{I_{PF1BU} - I_{PF1BL}}{1\,\text{kA}}\right] + 4293.8\left[\frac{I_{PF1CU} - I_{PF1CL}}{1\,\text{kA}}\right] + 13191\left[\frac{I_{PF2U} - I_{PF2L}}{1\,\text{kA}}\right] + 16497\left[\frac{I_{PF3U} - I_{PF3L}}{1\,\text{kA}}\right] \quad (1)$$

Note that vertically symmetric currents in OH, PF4 and PF5 circuits do not contribute to net TF OuterLeg torque, nor does plasma current in the vertically symmetric plasma model used herein. Larger typical values are predicted for net torque summed over the entire top half of the TF system, including the upper half of the TF central bundle, the upper radial assemblies, and the upper half of the TF outer legs. These torques are of course balanced by opposing torques developed in the bottom half of the TF system. A formula for net torque on the top half of the TF system is as follows:

$$\left[\frac{\text{Net Upper Half TF System Torque}}{1\,\text{N - m}}\right] = 13563.1\left[\frac{I_{OH}}{1\,\text{kA}}\right] + 2260.9\left[\frac{I_{PF1AU} + I_{PF1AL}}{1\,\text{kA}}\right] + 1580.6\left[\frac{I_{PF1BU} + I_{PF1BL}}{1\,\text{kA}}\right] + 1851.5\left[\frac{I_{PF1CU} + I_{PF1CL}}{1\,\text{kA}}\right] + 5197.5\left[\frac{I_{PF2U} + I_{PF2L}}{1\,\text{kA}}\right] + 21915.7\left[\frac{I_{PF3U} + I_{PF3L}}{1\,\text{kA}}\right] + 56813.9\left[\frac{I_{PF4}}{1\,\text{kA}}\right] + 118636.5\left[\frac{I_{PF5U}}{1\,\text{kA}}\right] + 713308.9\left[\frac{I_{plasma}}{1\,\text{MA}}\right] \quad (2)$$

Similar torque formulae can be obtained for out-of-plane torques on any TF conductor circuit segment, using poloidal magnetic flux values calculated at that segment's ends. Note that the shape of the TF conductor segment between its ends is not needed to determine its net torque.

Poloidal magnetic flux can be evaluated by use of the Ref.(2) Excel spreadsheet. This tool automatically calculates poloidal flux on a grid of 5 cm (r,z) squares extending throughout the entire NSTX CSU poloidal half-plane out past its TF conductors, for any user-specified set of currents in the OH coil, PF coils, and plasma.

OOP Torque Analysis of NSTX CSU

As in Ref.1, the NSTX CSU TF conductor shape definition was provided by Peter Titus on 26 June 2009 in a file containing XYZ 3D coordinates of 4229 nodal points delimiting hexahedral elements in a 30 degree sector global TF model. These were subsequently culled and sorted by various automated MATLAB methods to obtain a poloidal half-plane outline consisting of 322 points, including an inner outline trace of 159 points and an outer outline trace of 163 points. These points were only modified from the provided file by setting their third coordinate values to zero without changing their other two coordinates. The resulting TF conductor outline appears in the following Fig.(1) MATLAB plot.

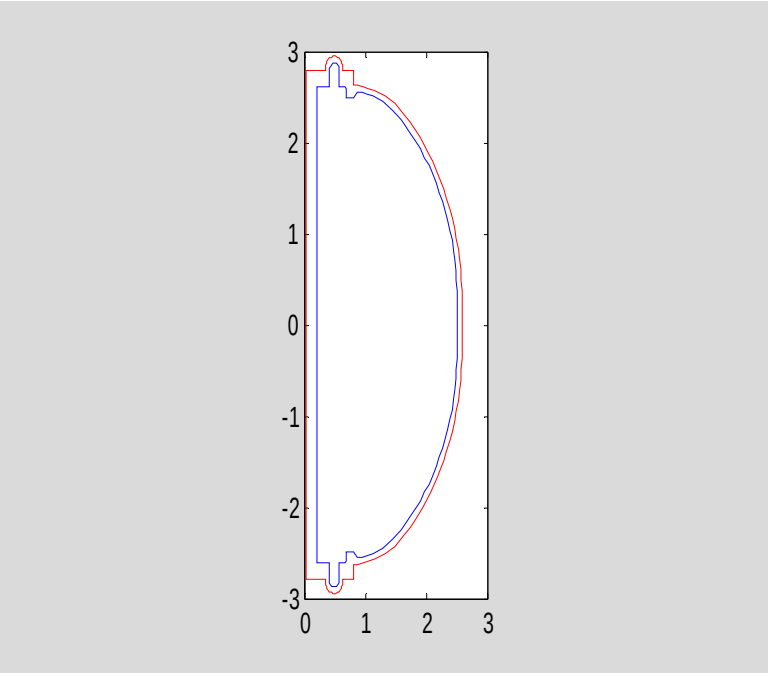

Figure 1: Poloidal Projection Outline of TF Conductor, 322 points

Parametric variables were then calculated and saved for each point in each of the two outline traces, starting from zero at their radially innerpoints on the (z=0) horizontal midplane and adding the distances to each successive point while proceeding in the counterclockwise direction. After returning to the starting points, the saved parametric values were then normalized by

dividing each cumulative distance value by its contour's total perimeter length. The resulting parametric variables, which range from 0 to 1, roughly represent poloidal angle.

Finally, 2000 uniformly spaced values of this poloidal angle variable ranging from 0 to 1 were generated and 2000 corresponding r and z coordinate values were obtained for each of the TF coil's inner and outer outline curves by using MATLAB's standard interpolation m-file subroutines. The two resulting 2000-point outlines are plotted below in Fig. (2). Note that although they appear almost identical to the previous TF outline plot, each outline here consists of 2000 equally spaced points which are now linked to each other through their common normalized poloidal "angle" location parametric variable values. In each contour of this model, node point number 1 is also number 2000, located at Z=0 in the TF centerstack. Constant radius points on the centerstack's outer edge include 1 through 363 at the bottom and from 1638 at the top through 2000. TF leads extending to the flexes encompass nodes out to 371 and to 1630.

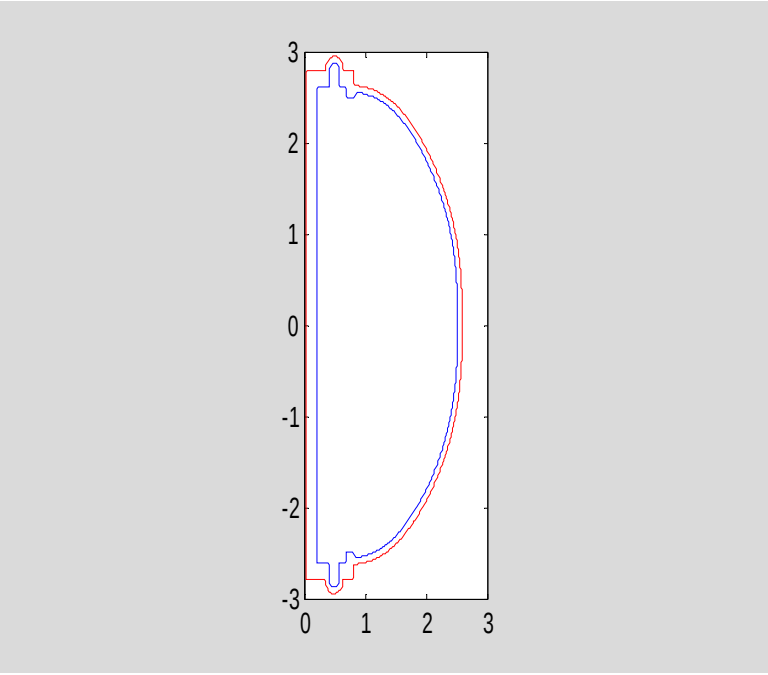

Figure 2: Poloidal Projection Outline of TF Conductor, 4000 points

Note that the TF current stream function which varies with the (r,z) location in the poloidal half-plane is defined as the total TF system current that passes through the 3D circle sharing those cylindrical coordinates. It varies from zero at (r,z) locations not linking the TF coils to the total TF current (i.e., number of turns times current per turn) at locations within the TF coil system bore. At intermediate locations within the TF conductor it varies between those values. Level set contours of the TF current stream function are also streamlines of the TF current flow.

As plotted, the (red) outer outline is the zero value contour of the TF current stream function and the (blue) inner outline is the contour of the TF current stream function at its full, 100% of TF system current, value. It was decided for calculations herein to try to improve accuracy by estimating how the TF current is distributed within the TF conductor. This was done by estimating the (r,z) coordinate locations at each of 2000 poloidal variable points for TF current stream function contours enclosing 25%, 50%, and 75%, respectively, of the total TF current. Ideally these contour estimates would be obtained by solving conductive media equations using ohms law, but this was not done. Instead, the estimated contours were obtained by interpolation between the outline coordinates for common poloidal angle variables. For the vertical (z) coordinates, linear interpolation was used directly. However, a different method was used to interpolate the r coordinate since conductor thickness in the toroidal direction varies in proportion to r for locations in and near the TF central bundle but takes on constant thickness for outer locations. Linear interpolation of a nonlinear function was used, where that function switched from a quadratic for inner locations to a straight line for outer locations. For this purpose the switchover radius between variable and constant toroidal thickness was estimated as r=0.3339 meters, based on inspection of plots showing the 4229 points of the global model.

The Fig.(3) plot follows showing the resulting estimated three internal contours and the two bounding contours of the TF current stream function.

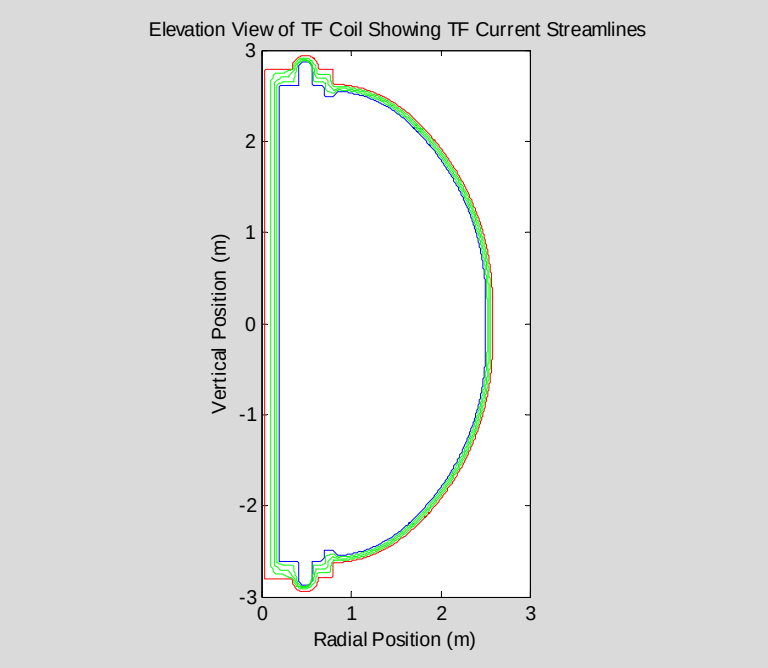

Figure 3: Poloidal Projection of TF Current Stream Function Contours, 10000 points

It may be useful to have plots showing r and z for the bounding outlines and internal contours as functions of the poloidal angle parametric variable. These follow:

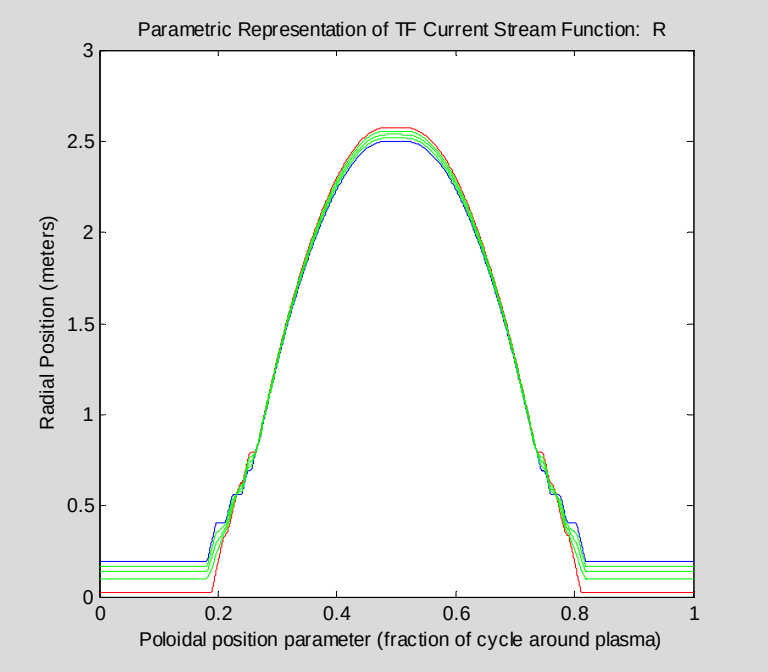

Figure 4: Radial Coordinates of TF Current Stream Function Contours vs Poloidal Variable

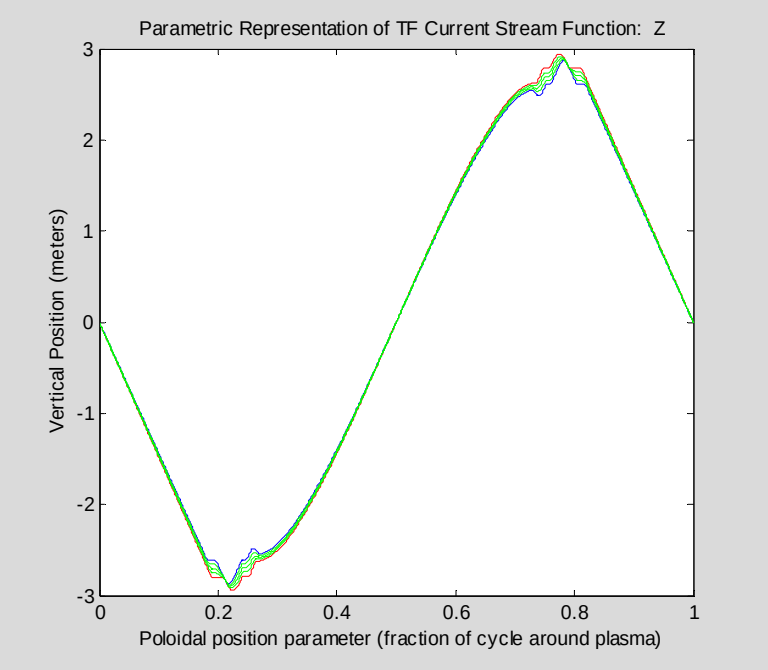

Figure 5: Vertical Coordinates of TF Current Stream Function Contours vs Poloidal Variable

The primary change requiring this update is modification of the designs for the OH coil and for th six coils, PF1AU, PF1BU, PF1CU, PF1CL, PF1BL, and PF1AL which led to the present design point which was adopted 04May2010. These changes included small changes in the dimensions and locations of the seven altered coils but quite large changes in the numbers of turns

incorporated within each coil. Details of the poloidal field system for the 04May2010 design point have been reproduced here as Table 1 and are depicted in Fig.6. These include 23 coil windings that are configured into 13 series-connected circuits. They also include a crude. approximate magnetics model representing the plasma as a rectangular cross section uniform current density single-turn coil winding.

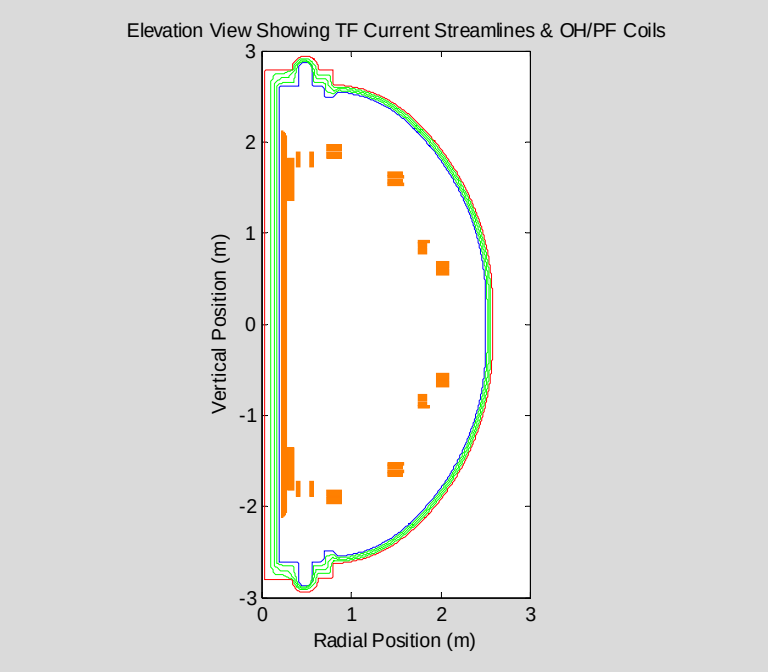

Figure 6: Poloidal Projection of PF&OH coils, with TF Current Stream Function Contours

Table 1: 04May2010 Design Point Poloidal Field System for PF Coils, OH Coil, Plasma (As Used For Magnetics Calculations)

Coil Power	Series-connected Winding Geometry					Rectangular Matrix of Turns		
Circuit Name	Rectangular Winding Name	R (center) cm	ΔR cm	Z (center) cm	ΔZ cm	# in z direction	# in r direction	Total # turns
PF1AU	PF1AU	31.93	5.9268	159.06	46.3533	16	4	64
PF1BU	PF1BU	40.038	3.36	180.42	18.1167	16	2	32
PF1CU	PF1CU	55.052	3.7258	181.36	16.6379	10	2	20
	PF2AU	79.9998	16.2712	193.3473	6.797	2	7	14
PF2U	PF2BU	79.9998	16.2712	185.26	6.797	2	7	14
	PF3AU	149.446	18.6436	163.3474	6.797	2	7.5	15
PF3U	PF3BU	149.446	18.6436	155.26	6.797	2	7.5	15
	PF4BU	179.4612	9.1542	80.7212	6.797	4	2	8
	PF4CU	180.6473	11.5265	88.8086	6.797	2	4.5	9
	PF4BL	179.4612	9.1542	-80.7212	6.797	4	2	8
PF4	PF4CL	180.6473	11.5265	-88.8086	6.797	2	4.5	9
	PF5AU	201.2798	13.5331	65.2069	6.858	2	6	12
	PF5BU	201.2798	13.5331	57.8002	6.858	2	6	12
	PF5AL	201.2798	13.5331	-65.2069	6.858	2	6	12
PF5	PF5BL	201.2798	13.5331	-57.8002	6.858	2	6	12
	PF3BL	149.446	18.6436	-155.26	6.797	2	7.5	15
PF3L	PF3AL	149.446	18.6436	-163.347	6.797	2	7.5	15
	PF2LA	79.9998	16.2712	-193.347	6.797	2	7	14
PF2L	PF2LB	79.9998	16.2712	-185.26	6.797	2	7	14
PF1CL	PF1CL	55.052	3.7258	-181.36	16.6379	10	2	20
PF1BL	PF1BL	40.038	3.36	-180.42	18.1167	16	2	32
PF1AL	PF1AL	31.93	5.9268	-159.06	46.3533	16	4	64
OH	OH	24.2083	6.934	0	424.16	221	4	884
PLASMA	PL	107.000	110.000	0.000	200.000	1	1	1

Next, poloidal flux was calculated for each of the 2000 locations on each of the five contours for each of the 13 coil circuits and for a crude electromagnetic model of a "plasma" having uniform current density and a rectangular cross section extending over 0.52<r<1.63 and -1<z<1, all in meters. Plots of the computed poloidal magnetic fluxes appear below in Figs.(7)-(11).

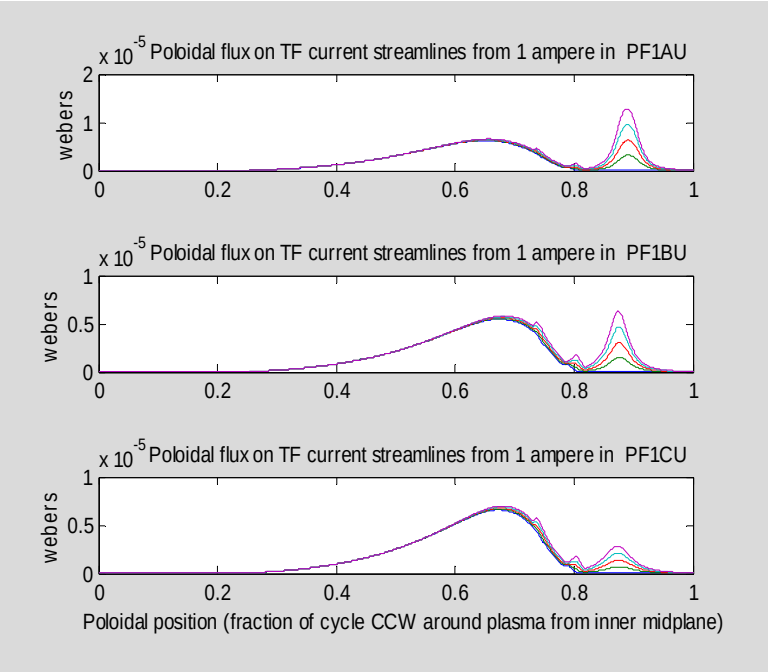

Figure 7: Poloidal Flux Per Ampere Excitation in Circuits 1-3

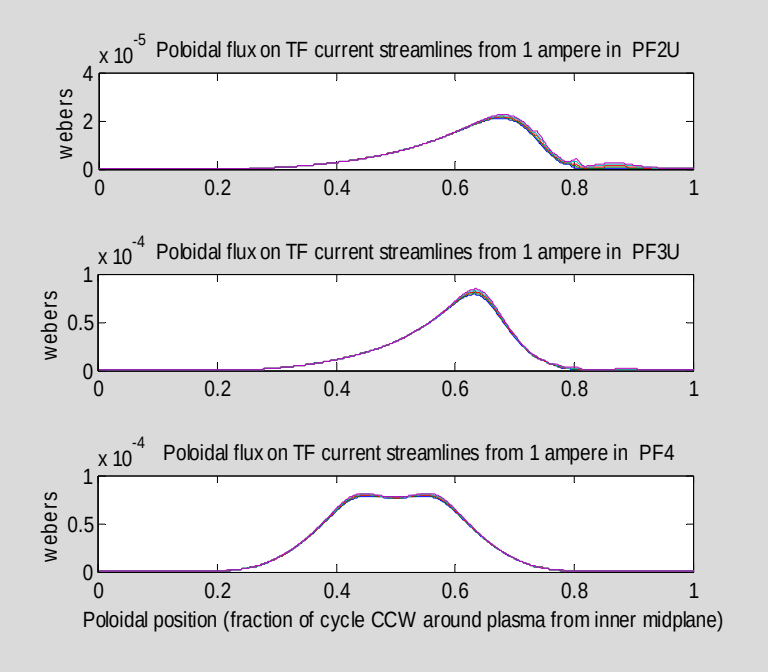

Figure 8: Poloidal Flux Per Ampere Excitation in Circuits 4-6

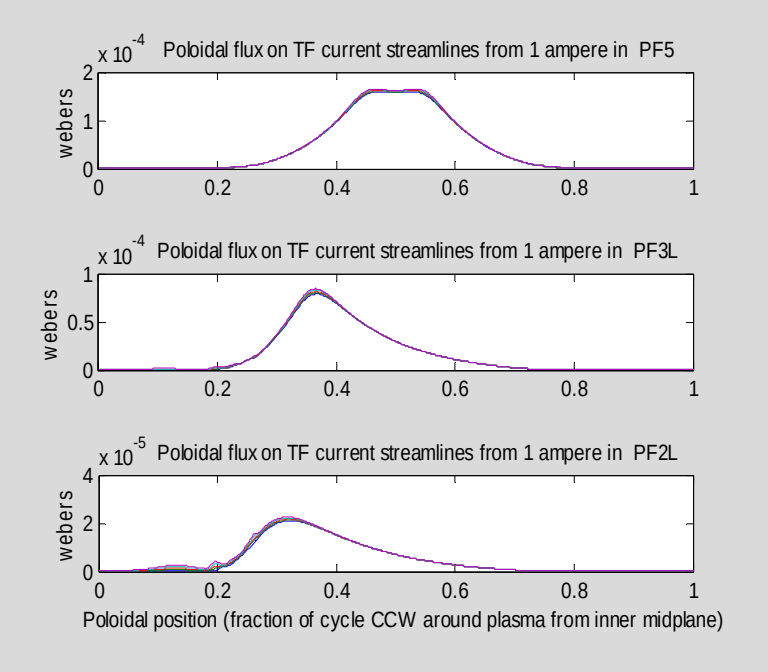

Figure 9: Poloidal Flux Per Ampere Excitation in Circuits 7-9

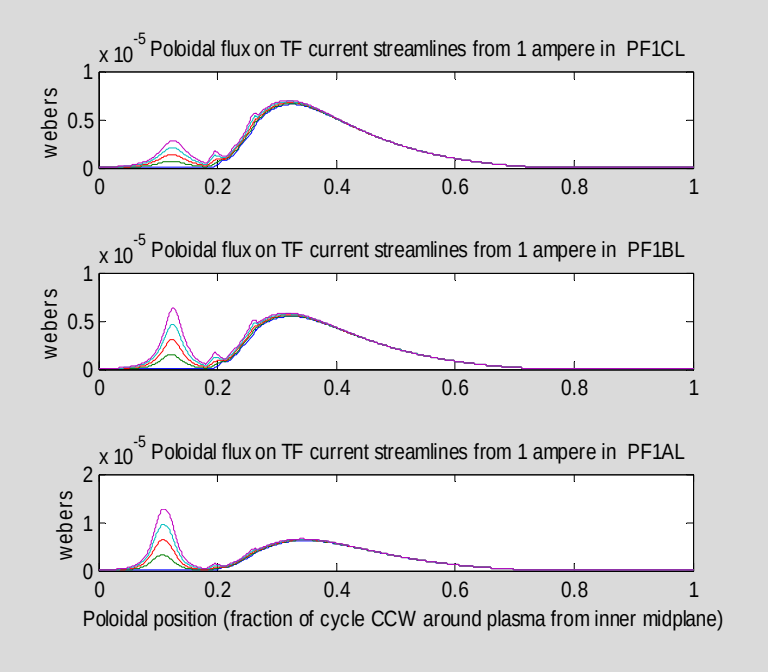

Figure 10: Poloidal Flux Per Ampere Excitation in Circuits 10-12

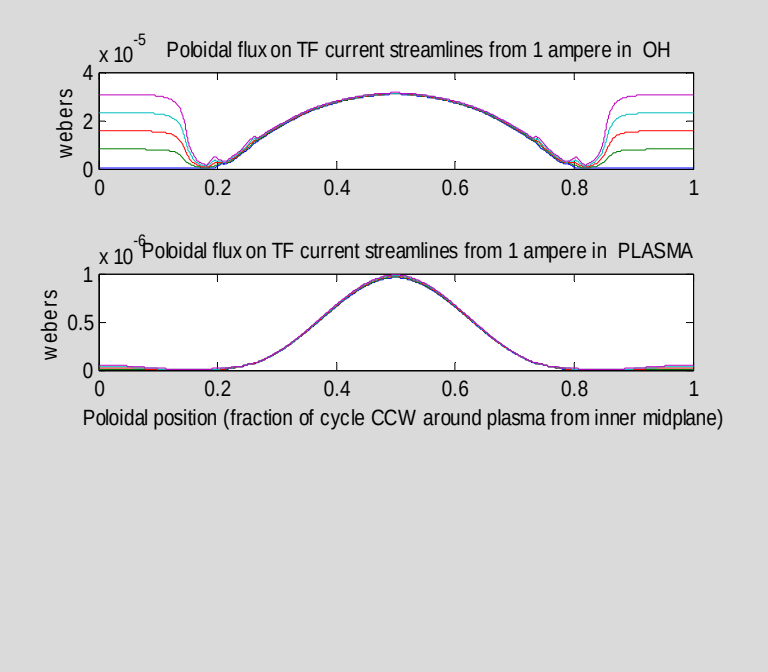

Figure 11: Poloidal Flux Per Ampere Excitation in Circuits 13-14

For each coil circuit, the mean flux was next calculated for each poloidal location as a weighted average of the flux values on the five current stream function contours, using weighting factors [0.125 0.25 0.25 0.25 0.125]. Local torque densities per ampere of circuit current are then evaluated as the product of total TF current times the finite difference derivative with respect to the poloidal angle variable of the mean flux divided by 2π. The resulting profiles were multiplied respectively by the Table 2 maximum and minimum circuit currents to establish the ranges of torque densities versus poloidal locations. Results appear in Figs.12-16.

Table 2: Coil And Plasma Current Ranges Assumed for Torque Load Range Calculations

COIL CIRCUIT NAME	MINIMUM CURRENT (Amperes)	MAXIMUM CURRENT (Amperes)
'PF1AU'	-7000	18000
'PF1BU'	0	13000
'PF1CU'	0	16000
'PF2U'	-11000	15000
'PF3U'	-16000	12000
'PF4'	0	16000
'PF5'	0	34000
'PF3L'	-16000	12000
'PF2L'	-11000	15000
'PF1CL'	0	16000
'PF1BL'	0	13000
'PF1AL'	-7000	18000
'OH'	-24000	24000
'PLASMA'	0	2000000

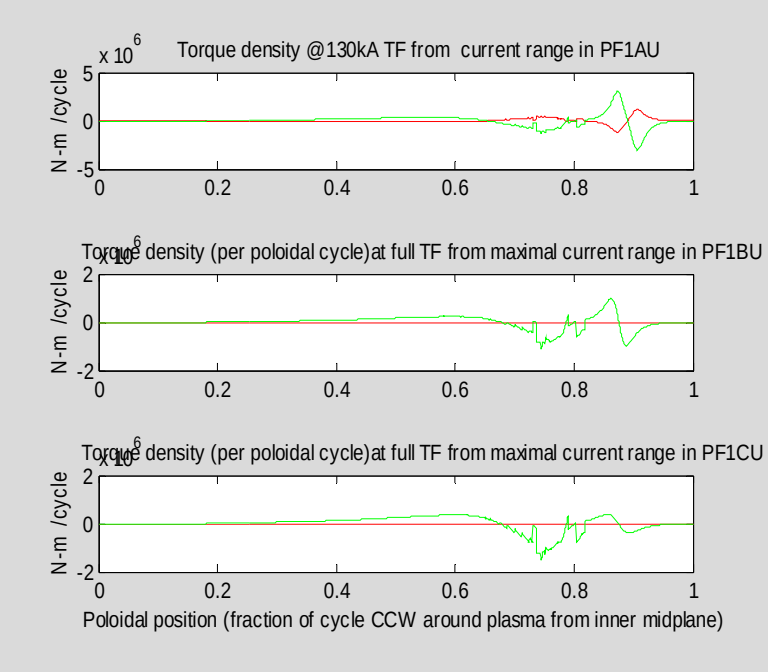

Figure 12: Torque Density For Maximal Range of Currents in Circuits 1-3

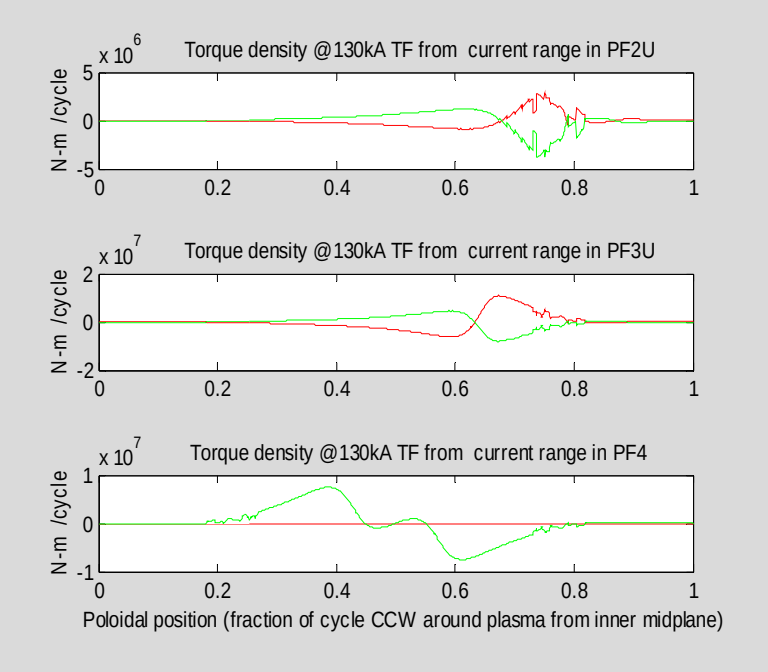

Figure 13: Torque Density For Maximal Range of Currents in Circuits 4-6

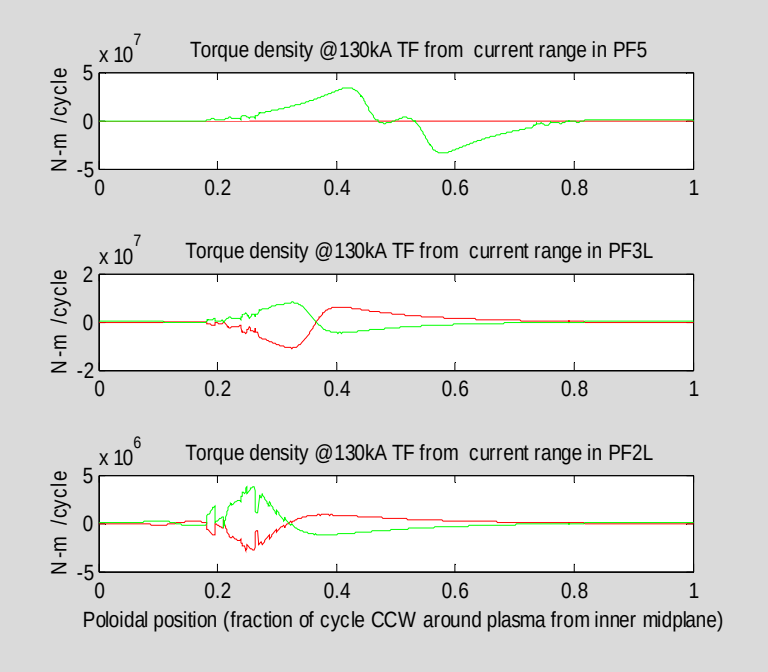

Figure 14: Torque Density For Maximal Range of Currents in Circuits 7-9

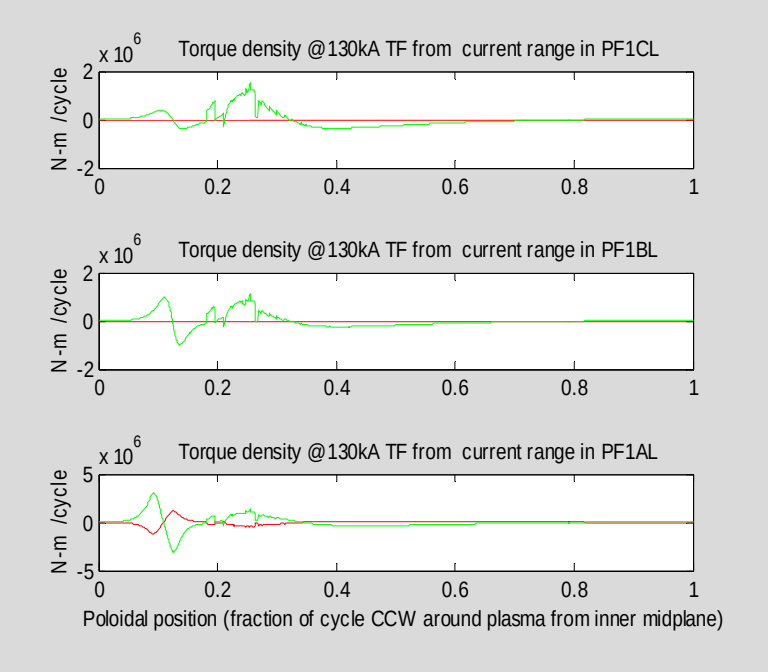

Figure 15: Torque Density For Maximal Range of Currents in Circuits 10-12

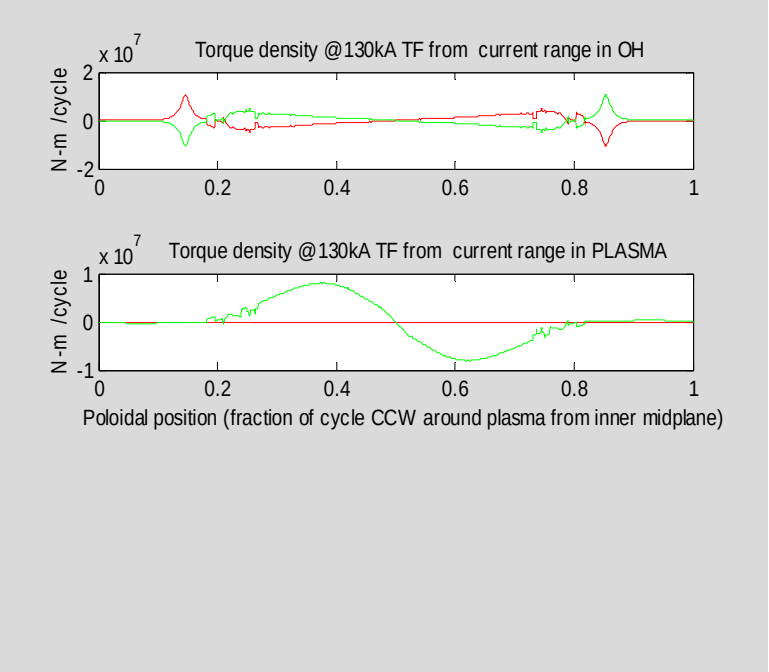

Figure 16: Torque Density For Maximal Range of Currents in Circuits 13-14

TORSIONAL RESPONSE ALGORITHMS: Overview

Although magnetic Lorenz torque loading on the TF coil system is completely determined by its electrical currents and magnetic fields, the torsion response of the system also reflects the mechanical propagation of torques and rotational deflections between different conductor assemblies and structural supports. The ***internal torque*** state at any imaginary section cut through the TF conductor system is defined as the external torque that would need to be applied to one side of that cut to maintain its mechanical equilibrium. This torque is oppositely directed for the two sides of the cut, so by convention the cut side in the direction of node numbering advancement around the TF loop is used herein. Maximum shear stress in a section through elastic material is directly proportional to the internal torque state, so this quantity is of special interest. The complete torsion model predicts the distribution of internal torque along with associated small rotational deformations. That necessarily includes the structural support torques and the resulting torsional shear stresses. The model includes, in addition to the distributed current-dependent Lorenz torque loads, the various torsion spring stiffnesses and interconnections that are relevant to rotational deformations.

Since force and torque equilibrium necessarily exist throughout the entire TF system, it follows that the difference in internal torque states between any two sections through the TF conductors is equal to the total external torque acting on the TF conductor region between them. Between the upper and lower leads of the TF centerstack there are no connections able to mechanically transmit torque, so within this region the profile of internal torque state vs location is equal to an additive torque constant plus the electromagnetic torque loading distribution described earlier in this memo. The additive torque constant depends on torsion spring responses of the entire TF conductor and support system, while the electromagnetic torque loading distribution is a known function of currents and position only, independent of any torsion spring responses.

The model approach taken employs the toroidal membrane methods advanced in section VII of Peter Titus' 1999 paper, but extends it in certain ways. For the centerstack portion of the TF system, torsion formulae for thick-walled tubular shafts are used instead of thin-walled approximations. More significantly, discrete mechanical springs augmenting the toroidal membrane model are used to represent effects on the TF conductor system of additional external mechanical support structures and interconnections. These springs include upper and lower umbrella lids together with their ties to the upper and lower umbrella structures, the upper and support rod connections between TF conductor outer legs and the vacuum vessel, the vacuum vessel itself, and the mechanical connections between the vacuum vessel through its gravity support legs to the floor and up through the pedestal pad supporting the TF centerstack. These additional modeled springs are interconnected with each other outside the modeled toroidal membrane and are attached to the toroidal membrane at specific poloidal nodes. Important node numbers in the toroidal membrane model are listed in Table 3 and their locations are depicted in Fig.17.

Table 3: Important Nodes in Toroidal Membrane Model of TF System Conductors

Node Number	R (m)	Z (m)	Importance
1	0.1942	0	Starting node in centerstack's middle
363	0.1942	-2.6000	Bottom of centerstack's straight section
371	0.2450	-2.6067	Bolts Attaching Stepped G10 Ring to Lower SplineLid
383	0.3312	-2.6067	End of Toroidally Continuous TF Lead Conductors
513	0.6923	-2.4916	TF Outer Leg's Lower End
566	1.0489	-2.5165	TF Outer Leg Clamped to Lower Umbrella Structure
838	2.3411	-1.1489	TF Outer Leg Clamp to Rods Connecting to Vacuum Vessel
1163	2.3411	1.1489	TF Outer Leg Clamp to Rods Connecting to Vacuum Vessel
1435	1.0489	2.5165	TF Outer Leg Clamped to Upper Umbrella Structure
1488	0.6923	2.4916	TF Outer Leg's Upper End
1618	0.3312	2.6067	End of Toroidally Continuous TF Lead Conductors
1630	0.2450	2.6067	Bolts Attaching Stepped G10 Ring to Upper SplineLid
1638	0.1942	2.6000	Top of centerstack's straight section
2000	0.1942	0	Ending node in centerstack's middle

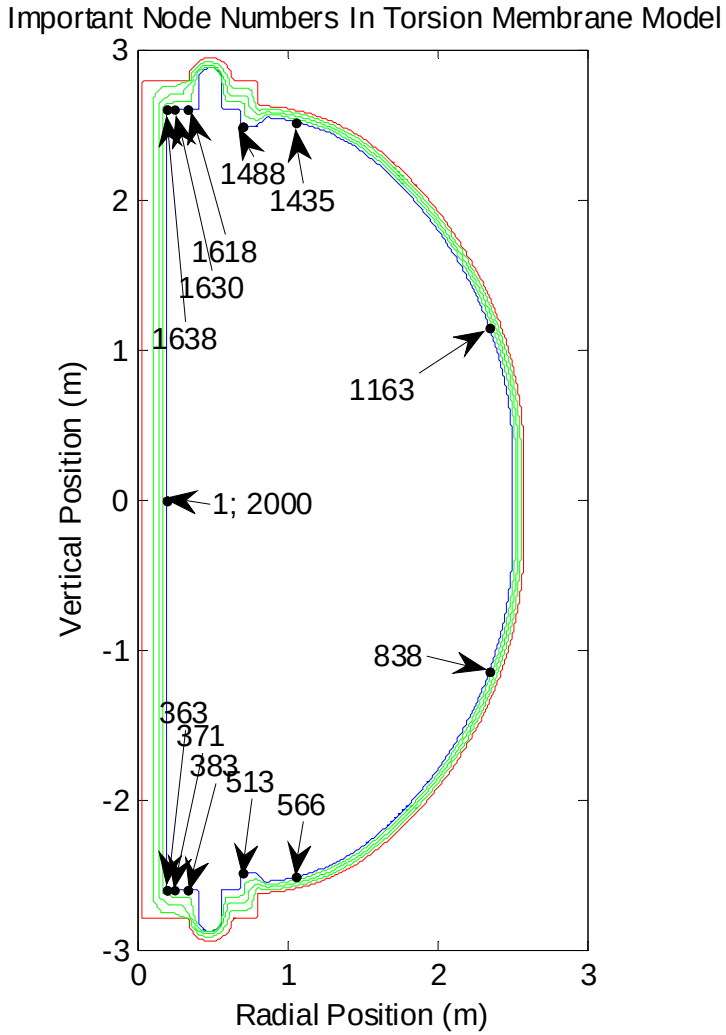

Figure 17: Important Node Numbers in the TF Conductor's Toroidal Membrane Model

The constant-radius portion of the centerstack TF is represented by node numbers 1 through 363 which extend vertically from the centerstack's middle to its bottom of its constant-radius part, and by node numbers 1630 through 2000 which extend vertically from the top of the centerstack's constant-radius part to its middle, where it started at node 1. The centerstack's lower TF lead extensions are node numbers 364 through 383 and its upper TF lead extensions are node numbers 1618 through 1637. The remaining nodes, 384 through 1617, represent the TF outer leg, the TF radial conductors, and the TF flex loops which connect to the centerstack's lead extensions. Electrical connections between the lower and upper ends of each TF outer leg and the lower and upper TF radials are located respectively at node numbers 513 and 1488, each at r=0.6923 meters.

External interconnection paths modeled via discrete torsional springs include the following:

(1) From the upper TF outer legs at node 1435 clamped by a split aluminum block to the vacuum vessel's upper umbrella, to the upper umbrella's bolted lid, radially inwards though the lid to an upper inner bolt plate, then to an annular "crown" disk insulator locked by tight-fitting radial pins to the centerstack's upper leads at node 1630.
(2) The vertical mirror image of (1) on the bottom, i.e., from the lower TF outer legs clamped to the vacuum vessel's lower umbrella at node 566, to its bolted lid, radially inwards to the lower inner bolt plate and insulating "crown" annulus, then to the centerstack's lower leads at node 371.
(3) From the TF outer legs just above horizontal mid-plane ports at node 1163, through rod connections to clevises mounted on the vacuum vessel. The vacuum vessel's upper dome continues this path to the upper umbrella legs then to TF conductor node 1435.
(4) The vertical mirror image of (3) below the midplane, i.e., from the outer legs just below mid-plane ports at node 838, through connecting rods to aa clevis connected to the vacuum vessel, then through the vesse's lower dome, umbrella legs and Aluminum block clamp to node 566.
(5) From node 838 through lower clevis rods, through the vacuum vessel's cylindrical middle section to upper radius rods connections to node 1163.
(6) From the lower vacuum vessel through its mounting legs to the floor, then up through the centerstack's lower pedestal pad support, meeting the centerstack at node 363.

Of primary interest in the investigations for which this torsion model may be applied is how shear stress is distributed within the CenterStack (i.e., the central bundle of turns) portion of the TF system, i.e., in the TF centerstack, since the interturn insulation there must withstand peak values of this stress. Although this is primarily affected by the electromagnetic Lorenz torques

directly acting on the TF centerstack, it is also partly dependent on the structures outside the centerstack since mechanical connections with the TF centerstack at its top and bottom allow mechanical transfer of torques there.

TORSIONAL SPRING STIFFNESS FORMULAE

For toroidally continuous portions of a TF conductor system resembling a thin membrane, it is appropriate to model the local rotational deflection due to torsion as follows:

$$\frac{d\phi}{ds} = \frac{T}{2\pi r^3 tG} \tag{3}$$

where

s represents the independent variable representing poloidal location in the toroidal membrane as a curvilinear distance measured in the membrane's poloidal (r,z) halfplane projection from an arbitrarily chosen reference location on the membrane,

$\phi(s)$ represents the azimuthal (i.e., toroidal) rotation angle at poloidal location s due to torsion,

$\frac{d\phi}{ds}$ is the density of that torsional rotation deflection at location s, that is, the rate of deflection angle increase per unit change in poloidal location,

$T(s)$ is the local internal torque state in the TF membrane conductor at poloidal location s,

G, is the shear modulus of the membrane material,

$r(s)$, is the radius from the z axis of the membrane at poloidal location s, and

t, that is, $t(s)$, is the membrane's thickness at poloidal location s.

Relating s to r allows Eq.(1) to be integrated, e.g., if a section of the toroidal membrane is planar so that ds in Eq.(1) equals dr, then integration over the resulting disk-annulus between inner and outer radii yields the following:

$$\phi = \frac{T}{4\pi tG}\left(\frac{1}{r_i^2} - \frac{1}{r_o^2}\right) \tag{3a}$$

Another commonly occurring situation has the toroidal membrane in a non-planar configuration. For those cases a small axisymmetric portion of the membrane can be approximated as having a straight line segment for its poloidal projection, extending from (r_1,z_1) to (r_2,z_2). For example, this would apply to a thin approximately conical section taken though a vacuum vessel dome. Integrating over the resulting frustrum of a cone results in the following:

$$\phi = \left(\frac{\sqrt{(r_2 - r_1)^2 + (z_2 - z_1)^2}}{r_2 - r_1}\right)\frac{T}{4\pi tG}\left(\frac{1}{r_1^2} - \frac{1}{r_2^2}\right) \tag{3b}$$

In such portions of the TF conductor system where the thin toroidal membrane model is an appropriate approximation, the shear stress is constant over the thickness of each perpendicular section and varies according to the following formula:

$$\tau = Gr\frac{d\phi}{ds} \tag{4}$$

where $\tau(s)$ the shear stress in the perpendicular section at location s.

In the NSTX CS upgrade's TF system the centerstack bundle of TF turns is sufficiently thick that it should not be modeled as a thin membrane. It is more appropriate to instead model it as an elastic thick-walled tubular shaft in which shear stress in a section perpendicular to the axis varies linearly with radius within that section. For the centerstack portion of the TF conductor system where the inner and outer radii of the TF are constant, the following formulae are used:

$$\frac{d\phi}{ds} = \frac{T}{JG} \tag{5}$$

where J is the rotational moment of inertia of the centerstack TF cross section,

$$J = \frac{\pi}{2}\left(r_{OUTER}^4 - r_{INNER}^4\right) \tag{6}$$

In this thick tubular shaft model the maximum shear stress in each section occurs at its outer radius and is given by the following:

$$\tau_{MAX} = Gr_{OUTER}\frac{d\phi}{ds} \equiv \frac{Tr_{OUTER}}{J} \tag{7}$$

These formulae for thick-walled tubular shafts are also used for lead extension regions of the TF centerstack which extend from r=0.1942 meters out to r=0.3329 meters where toroidal continuity of the TF conductor's mechanical configuration ends. In this 0.1942<r<0.3329 lead extension region the torsion formulae are less accurate since stress concentrations where radii abruptly change are not modeled.

For the present toroidal membrane model of the TF conductor, the blue contour of Figs. 1 through 3 is used for all r>0.3329 outer locations where the thin membrane representation is used. For r<0.3329 locations in the centerstack and its lead extensions where the thick-walled tubular shaft model is more appropriate, the blue contour is used to determine the r_{OUTER} value and the corresponding poloidal point on the red contour is used for r_{INNER}. Together these are used to calculate the local rotational moment of inertia, J, and also the peak shear stress.

Torsional stiffness formulae based on simple first-principles mechanical models are accurate wherever the TF system is nominally continuous in the toroidal direction, which for the NSTX CSU includes all parts of the TF system at locations inboard from the flex loops where the radius is less than 0.3329 meters. However, the same torsion formulae are also used herein to approximately model TF conductor deformation in outer regions where r>0.3329. The TF conductors and their supporting structures are not toroidally continuous in outer regions but instead are broken up by air gaps. The air gaps permit structures to deform in nonaxisymmetric ways not modeled by torsional stiffness formulae. Thus, the present approximation neglecting toroidal air gaps must therefore artificially reduce the stiffness of its assumed toroidally

continuous model in order to match its predictions to the actual nonaxisymmetric system. Estimates and other information supplied by Mark Smith and by Tom Willard have been used to adjust these model parameter values.

ESTIMATION OF PARAMETER VALUES

The following section documents both my own ball-park estimates of some stiffness parameters and also torsional stiffness estimates developed by Mark Smith using a global 3D model, which I have preferentially adopted.

Centerstack:

The TF centerstack's new inner radius is 0.0512 m, and its new outer radius is 0.194238 m, not including its lead extensions. The shear modulus of its copper is taken as G=48 GPa, i.e., 4.8e10 Pa. Applying Eq.(3), its twist angle per unit length per unit torque is as follows:

$$\frac{1}{T}\frac{d\phi}{ds} = \frac{1}{JG} = \frac{1}{\frac{\pi}{2}\left(r_{OUTER}^4 - r_{INNER}^4\right)G} = \frac{2}{\pi\left((0.194238)^4 - (0.0512)^4\right)(4.8E10)} =$$

$$= 9.36275866886577e-009 \text{ radian N}^{-1}m^{-2}$$

The total centerstack straight section length from node 1 through 363 and 1638 through 2000 is 5.200 m, so its torsional stiffness parameter is

K_{CS}=1/[(9.3627587E-9 radian/N-m^2)(5.200 m)] = 2.054E7 N-m/radian =
= 3.176E6 inch-lbf/degree

Its reciprocal stiffness parameter is then
R_{CS}= 1/(2.054E7 N-m/radian) =4.85853E-8 radians/N-m.

Its reciprocal stiffness parameter per element is as follows:
$R_{CS/elt}$= (4.85853E-8 radians/N-m)/(724 elts) = 6.711e-11radians/N-m/elt

TF Centerstack Lead Extensions

The same formula is used for the lead extension portions of the TF centerstack, nodes 363 through 383 and 1618 through 1638. Its inner radius is also taken as 0.0512 m, but its outer radius varies. Summing the resulting individual reciprocal stiffness terms (using MATLAB) results in

R_{Leads}= 5.835E-10 radians/N-m

for upper lead extensions and the same again result separately for the lower lead extensions.

The average value per element of this constant is as follows:
$R_{Leads/elt}$= (5.835E-10 radians/N-m)/(19 elts) = 3.071E-11 radians/N-m/elt

The equivalent spring stiffness constant for the lead extensions is the reciprocal, i.e.,

K_{Leads}=1/(5.835E-010 radians/N-m= 1.71E9 N-m/radian

The upper lead extension is included with the straight part of the centerstack, so
r1=3.87007e-010+4.85853E-8= 4.89723e-8 radians per newton-meter

Insulating Annular "Crown" pinned to leads, bolting plate

I do not have a proper estimate for the stiffness of these assemblies, but will assume that the reciprocal stiffness of each (top and bottom) is about

R_{crown}=5E-9 radian/N-m

Outer Umbrella and Lid:

I had earlier estimated a reciprocal stiffness for the portion of the umbrella between TF clamps and lid as follows:

$$R_{OuterUmbrella} = \left(\frac{1}{T}\frac{d\phi}{ds}\right)(\Delta s) = \left(\frac{\Delta s}{2\pi r^3 t}\right) = \left(\frac{(0.35542)}{2\pi(1.0477521)^3(0.0254)(7.72E10)}\right) = 2.508\text{E-}11$$

radians/N-m.

At that time the lid design was envisioned as a stainless steel disk-annulus, assumed to be 1" thick. Its outer and inner radii are assumed to be respectively 1.047752 m and 15.375"/2= 0.1953 m, which resulted in a lid reciprocal stiffness of

$$R = \frac{\phi}{T} = \frac{1}{4\pi t G}\left(\frac{1}{r_i^2} - \frac{1}{r_o^2}\right) = \frac{1}{4\pi(0.0254)(7.72E10)}\left(\frac{1}{(0.1953)^2} - \frac{1}{(1.0477521)^2}\right) =$$

=1.02702e-009 radians per Newton-meter

Using those values as ballpark estimates, then the net reciprocal stiffness from TF coil clamp to crown interface would have been
2.508e011+1.02702e-009 = 1.052E-9 radian/N-m

A better estimate of the stiffness via this path was provided by Mark Smith by fitting a global 3D model, as copied into the following text box. The reciprocal stiffness derived from his data is

$R_{umbrella+lid}$=3.338E-9 radians/N-m

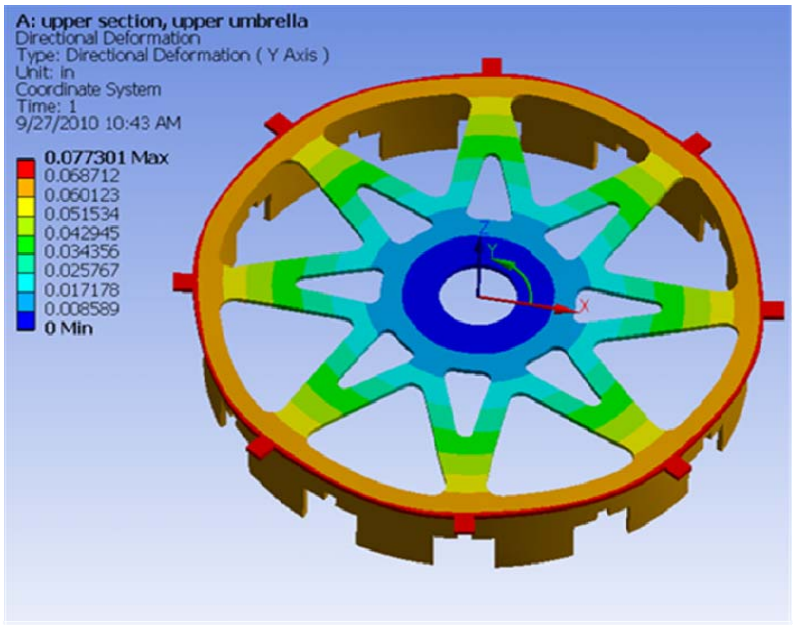

12*10000 lbf = 120000 lbf

R = 41.3 inch

T = 4.956E6 lbf-in

Θ = s/r =~ .077301 inch/41.3 inch = 0.001872 radians

K1 = T/Θ = 4.956E6 lbf-in/0.001872 radians
K1 = 2.64787E9 lbf-in/radians

K1 = 4.6214E7 lbf-in/°

Mark Smith's Global Model Data 1

Inner Umbrella

Each umbrella is a nominally cylindrical stainless steel (G=77.2 GPa) structure of radius r=1.0477521 m, thickness t=1"=0.0254 m, and height from base to the middle of the cutouts for TF outer legs is 32.12"=0.8158 m. Eq.(3) could be used to estimate its stiffness parameter if it had no cutouts. However, it has not only the cutouts for TF outer legs but also ten arch-shaped cutouts near its base. If its thickness were reduced by 67% from 1" to t=0.33"=0.00847 m as a ballpark "guestimate" to match actual nonaxisymmetric deflections under torsion loading .the stiffness parameter would become the following:

$$R_{\text{InnerUmbrella}} = \left(\frac{1}{T}\frac{d\phi}{ds}\right)(\Delta s) = \left(\frac{\Delta s}{2\pi r^3 t}\right) = \left(\frac{(0.8158)}{2\pi(1.0477521)^3(0.00847)(7.72E10)}\right) =$$

=1.727E-010 radians per newton-meter

A better estimate of the stiffness of this path was provided by Mark Smith by fitting a global 3D model, as copied into the following text box. It is equivalent to

$R_{\text{InnerUmbrela}}$=4.44E-9 radian/N-m

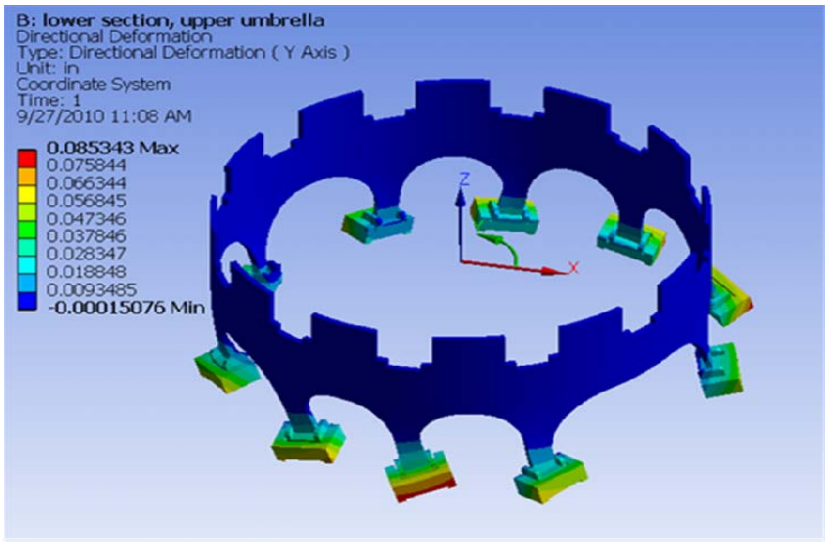

M = 4.13E6 lbf-in

R = 41.3 inch

Θ = s/r --> .085343 inch/41.3 inch = 0.002066 radians

K2a = T/Θ = 4.13E6 lbf-in/0.002066 radians
K2a= 1.99E9 lbf-in/radians

K2a = 3.48827E7 lbf-in/°

Mark Smith's Global Model Data2

Vacuum Vessel Division

Connecctions to the TF outer legs above and below the horizontal midplane were identified as TF conductor node numbers 838 and 1163, located at (r,z)=(2.3411, ±1.1489) m. These connections go to the vacuum vessel, meeting it at locations closer to the midplane. For the present analysis they are assumed to meet the vacuum vessel at the interface between the vacuum vessel's cylindrical midsection and its upper or lower domes, i.e., at (r,z)=(1.74, 1.00) m. Therefore, for the calculation of spring stiffnesses, one value is for the cylindrical central portion of the vacuum vessel and another is for a vacuum vessel dome connected in series with the portion of the umbrella between the vacuum vessel and thee TF outer leg's aluminum block clamp.

Central cylindrical section of the vacuum vessel:

The vacuum vessel is made of stainless steel (shear modulus G=77.2 GPa) of thickness t=0.625"= t=0.01875 m. The radius of the vacuum vessel's central section is about 1.705 m and its height is 2.00 m. Therefore, Eq.(3) could be used for a rough reciprocal stiffness estimate, $R_{VV\text{-}middle}$=4.4367E-11 radians/ N-m. For the effect of port cutouts it was decided to reduce the assumed cylindrical membrane thickness by 50%, to t=0.009375. This would increase the reciprocal stiffness parameter to $R_{VV\text{-}middle}$=8.87E-11 radians/ N-m.

A better estimate of the stiffness of this path was provided by Mark Smith by fitting a global 3D model, as copied into the following text box. It is equivalent to

$R_{VV\text{-}middle}$=5.634-10 radian/N-m

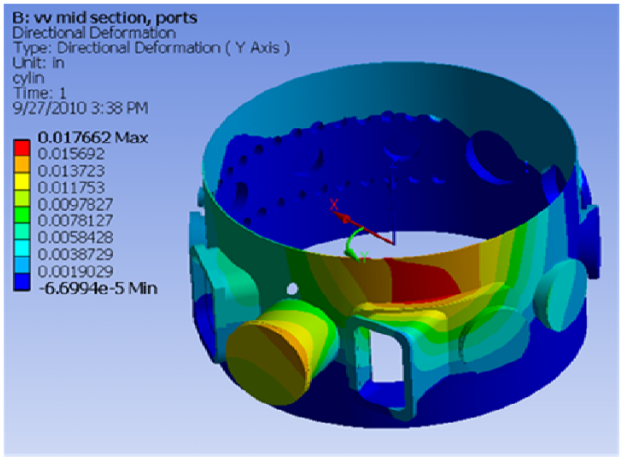

M = 4.13E6 lbf-in

R = 67.1 inch

Θ = s/r =\ 0.017662 inch/67.1 inch = 0.000263 radians

K3 = T/Θ = 4.13E6 lbf-in/0.000263 radians
K3= 1.569e10 lbf-in/radians

K3 = 2.738e8 lbf-in/°

Mark Smith's Global Model Data 3

Vacuum vessel dome

Vacuum vessel drawings identified (r.z) coordinates of the upper dome from the dome's mouth to its interface with the vacuum vessel's cylindrical section, as listed in the following table.

Table 4: Vacuum Vessel Dome Coordinates

Point #	r (m)	z (m)
1	0.6121	1.7500
2	0.7442	1.7170
3	1.1455	1.5545
4	1.5392	1.3106
5	1.6612	1.1735
6	1.7068	1.0033

The total rotation angle per unit torque for the five unbroken conical frustrum regions bounded by the points is then estimated as follows:

$$R_{dome} = \frac{\phi}{T} = \frac{1}{4\pi t G}\sum_{i=1}^{i=5}\left(\frac{\sqrt{(r_{i+1}-r_i)^2+(z_{i+1}-z_i)^2}}{r_{i+1}-r_i}\right)\left(\frac{1}{r_i^2}-\frac{1}{r_{i+1}^2}\right) = \frac{1}{4\pi(0.01875)(7.72E10)}(2.57940) =$$

= 1.41805e-010 radians per newton-meter. If one arbitrarily reduces the thickness by 50% to account for port cutouts, this leads to the following guestimate for the reciprocal stiffness of each of the domes:

R_{dome}=2.8361E-10 radian/ N-m

A better estimate of the stiffness of this path was provided by Mark Smith by fitting a global 3D model, as copied into the following text box. It is equivalent to

R_{dome}=1.72E-10 radian/ N-m

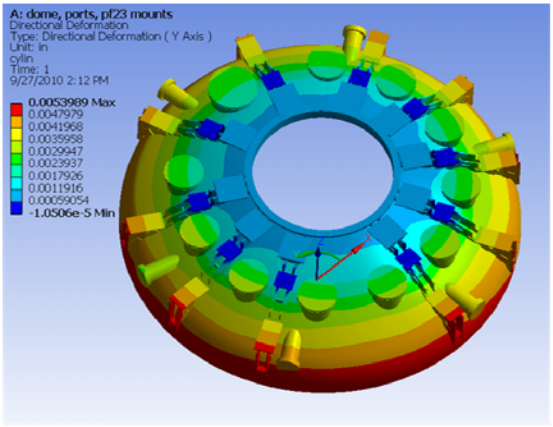

M = 4.13E6 lbf-in

R = 67.1 inch

Θ = s/r ~ 0.005399 inch/67.1 inch = 0.00008 radians

K2b = T/Θ = 4.13E6 lbf-in/0.00008 radians

K2b= 5.133e10 lbf-in/radians

K2b = 8.96e8 lbf-in/°

Mark Smith's Global Model Data 4

Vacuum Vessel Connections to TF Outer Legs

A rough stiffness estimate was made based on assumed 1.5"=0.0381 m diameter solid steel cylindrical rod attached to the vacuum vessel through pin connections at clevis attachments midway between TF outer legs. Coordinates of these connection points are (R,Z)=(1.7068, ±1.00) m, while the coordinates of the TF out legs where they attach to the tangential rods are (R,Z)=(2.3411, ±1.1489) m. Taking into account the 12-fold symmetry and the geometric angles, the resulting reciprocal stiffness parameter estimate is as follows:

$R_{ClevisRods}$=1.22e-010 radian/N-m

Vacuum Vessel Legs and Pedestal Support for TF Centerstack

Without nonaxisymmetric analyses it is not possible to estimate the rotational stiffness of the torque path through vacuum vessel support legs, floor, and TF centerstack pedestal support. However, Mark Smith has provided such estimates by fitting a nonaxisymmetric global 3D model, as copied into the following two text boxes. The equivalent reciprocal stiffness parameter for the VV support legs is

R_{Legs}=3.72E-8 radian/N-m

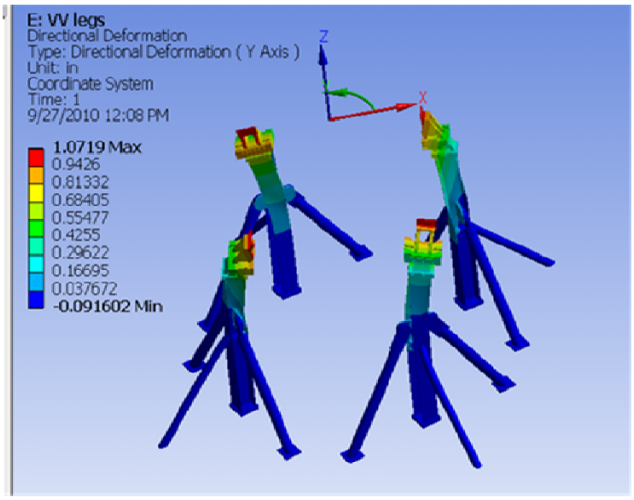

M = 4.13E6 lbf-in

R = 67.1 inch

Θ = s/r ⇒ 1.0719 inch/61.7 inch = 0.017373 radians

K_{legs} = T/Θ = 4.13E6 lbf-in/0.017373 radians

K_{legs} = 2.37728e8 lbf-in/radians

K_{legs} = 4.14914e6 lbf-in/°

Mark Smith's Global Model Data 5

The equivalent reciprocal stiffness parameter for the pedestal pad supporting the centerstack is:

R_{Ped}=2.17E-8 radian/N-m

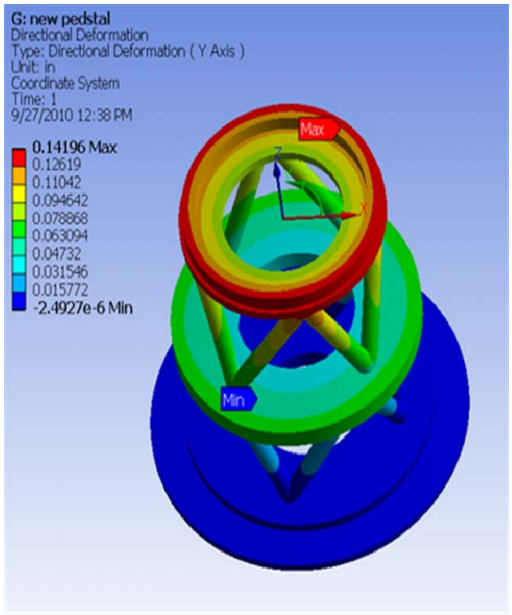

M = 4.13E6 lbf-in

R = 14 inch

Θ = s/r => 0.14196 inch/14 inch = 0.01014 radians

K_{pnew} = T/Θ = 4.13E6 lbf-in/0.01014 radians

K_{pnew} = 4.073e8 lbf-in/radians

K_{pnew} = 7.109e6 lbf-in/°

Mark Smith's Global Model Data 6

TF Conductor Portions Lacking Structural Continuity in Toroidal Direction

The remaining portions of the system are TF conductors which are interspersed with toroidal air gaps lacking any structural rigidity. This situation exists everywhere that the TF conductors have major radius locations exceeding the threshold value, i.e., for R>0.3329 m. Although at certain locations the TF conductors are clamped to other structures, such clamping is not the issue here since those other structures and their TF conductor attachment points are expressly modeled as external springs. Thus, any torsional stiffness parameters to be assigned to toroidally discontiuous portions of TF conductors must be chosen to match the TF conductors' nonaxisymmetric beam-like toroidal deflection behaviors to the axisymmetric model.

Recall that for a straight beam, the deflection distance, *y*, is governed by the following fourth order system of differential equations:

$$\frac{dV}{ds} = q(s)$$

$$\frac{dM}{ds} = V(s)$$

$$\frac{d\theta}{ds} = \frac{M(s)}{EI}$$

$$\frac{dy_f}{ds} = \theta(s)$$

$$\frac{dy_s}{ds} = \frac{V(s)}{AG}$$

$$y = y_s + y_f$$

where

s is the distance along the straight beam,
q is the perpendicular running load force per unit distance,
V is the internal section shear force,
M is the internal section bending moment,
q is the deflection angle
y_f is the deflection distance due to flexure
y_s is the deflection distance due to shear
E is the elastic modulus
G is the shear modulus
I is the cross section's moment of inertia with respect to the loading direction
A is the cross section's area

Note that the torsion system of equations matches the shear part of the beam deflection system but has no way of modeling beam flexure. Thus, there is no first-principles approach to matching the models. As an intuitive example of this mismatch, a continuous toroidal membrane representing the TF outer legs would develop nonzero internal torque if its top were rotated by,

say, 0.001 radians with respect to its bottom, but the collection of 12 TF outer legs could sustain such a relative rotation without elastically deforming them (to first order), i.e., with twelve different small rigid body tilting motions of the separate outer legs.

Thus, the best that can be done is to make a very approximate, order-of-magnitude torsional stiffness estimate for the outer TF conductor, as a "kludge". To this end, Tom Willard supplied ANSYS calculated results for the out-of-plane deflection of an isolated TF Outer Leg under defined loading conditions. The model imposed cantilever restraints on the conductor at the upper and lower locations where the actual outer leg is clamped to the umbrellas by aluminum blocks (i.e., the torsion model's nodes 566 and 1435) It applied 1000 lbf=4454.5 N out-of-plane load forces to the outer legs at the locations where each acual outer leg will be connected to vacuum vessel clevises via rods (i.e., the torsion model's nodes 838 and 1163). Maximum calculated OOP deflection was 0.073 inches with a single OOP force applied and 0.140 inches=3.56 mm with both OOP forces applied in the same direction. The torsion model's stiffness value is then set by the second of these results, based on the deflection of the top half only. A torque of

$$T=(12 \text{ outer legs})(F=4454.5 \text{ N})(R=2.3411 \text{ m}) = 125{,}142 \text{ N-m}$$

is predicted by ANSYS to cause the TF conductor portion between the upper umbrella's clamp (node 1435) and the clevis rod clamp (node 1163) to rotate through and angle of

$$\Delta\phi = (0.00356 \text{ m})/(2.3411 \text{ m}) = 0.0015189 \text{ radians}$$

The corresponding reciprocal stiffness value is then

$$R_{1163:1435} = \Delta\phi / T = (0.0015189 \text{ radians})/(125{,}142 \text{ N-m}) =$$
$$=1.2138\text{e-}008 \text{ radian/N-m}$$

In order to assign a consistent stiffness to other portions of the TF outer legs, a single-element value is first obtained by dividing the above result by the 1435-1163+1= 273 elements to obtain

$$R_{TFOL/elt}=R_{1163:1435} /(1435\text{-}1163+1 \text{ elts}) = 4.45\text{E-}11 \text{ radian/N-m/elt}$$

This per element value is then used to generate reciprocal stiffness values for the other portions of the TF outer legs. For the portion between lower and upper rod attachments to clevises,

$$R_{838:1163}=(1163\text{-}838+1)R_{TFOL\text{-}node} = 1.45\text{E-}8 \text{ radian/N-m}$$

For the Outer leg TF portion inboard of each umbrella clamp, including the flex straps for which no better "kludge" estimate of torsional stiffness has been derived, the reciprocal stiffness values are as follows:

$$R_{1435:1618}= R_{383:566}== (184)R_{TFOL\text{-}node} = 5.26\text{E-}8 \text{ radian/N-m}$$

THE EQUIVALENT ELECTRICAL MODEL

This analysis uses an analogy between the torsional mechanical system and a hypothetical electrical network. The angular twist of an axisymmetic portion of the TF system is analogous to the voltage developed across a length of resistive conductor in the hypothetical analogous electrical network, and the internal torque developed in that axisymmetric section is analogous to the current flowing through the analogous resistor. Torsional spring stiffnesses, expressed in units of torque per unit angular deflection, are analogous to conductances (i.e., reciprocal resistances) in the hypothetical electrical network.

Since electromagnetic torque loading on the TF centerstack is not spatially umiform, the TF centerstack can best be modeled as a series-connected sequence of many small torsion springs. The nodes between the resistors represent a sequence of physical locations within the centerstack. The nonuniform distributed torque loading is then modeled by assigning the Lorenz torque increment for each region between two adjacent nodes to one of those two nodes. (Little error is introduced by this asymmetrical assignment if nodes are closely spaced.) As developed in the Appendix, this torque is equal to the product of total TF threading current, $N_{TF} I_{TF}$, times the difference in poloidal flux per radian between the modeled element's two ends, i.e.,

$$T_j = N_{TF} I_{TF} \frac{\Psi_{j+1} - \Psi_j}{2\pi}$$

An electrical analogy shown in Fig.18a is a series connected string of resistors interleaved with current sources that inject increments of electrical current from a common reference node.

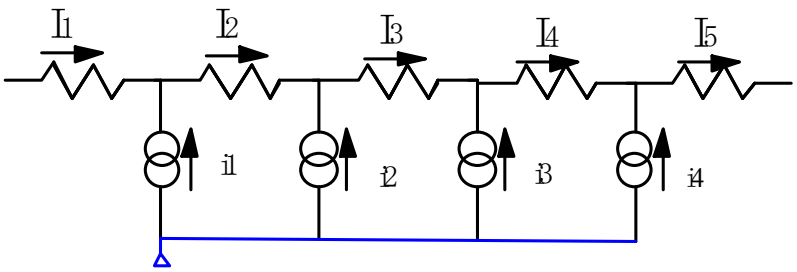

Figure 18a: Electrical Analogy of Series-Connected Torsion Springs And External Torques

Currents I_j flowing through the Fig.18a resistors represent the internal torque state at different vertical locations in the TF centerstack. Resistor currents can thus differ from each other according to:

$$I_{j+1} = I_j + i_j$$

where i_j is an injected current. Since the injected currents, i_j, represent the incremental torques, T_j, the electrical analogy model's resistor currents are related to actual poloidal fluxes as follows:

$$I_j = N_{TF} I_{TF} \frac{\Psi_j}{2\pi} + C$$

where *C* is any fixed constant value.

This Fig18a model can be continued beyond the TF centerstack through the outer parts of the TF conductor system where mechanical supports interconnecting portions of the system must also be modeled. The fact that the total net Lorenz torque on the entire TF system is necessarily zero translates in the full TF system model's analogous electrical network into the net current from the common reference node being zero. This allows the Fig.18b alternative equivalent circuit model to be used instead for the analogy.

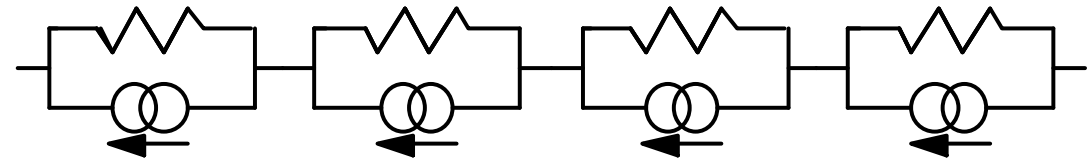

Figure 18b: Alternative Analogy of Series-Connected Torsion Springs And External Torques

In Fig.18b, the current in each external current source is assigned as:

$$i_j = N_{TF} I_{TF} \frac{\Psi_j}{2\pi}$$

where *j* is the node number of the location at one of the current source's ends. With this assignment, the current in each of the model's resistors is related to actual poloidal flux as

$$I_j = N_{TF} I_{TF} \frac{\Psi_j}{2\pi} + C\,,$$

where *C* si the common constant value of current flowing between series blocks of Fig.18b. This also clearly matches the resistor current in the Fig.18a model.

Fig.19 depicts the electrical analogy of the full toroidal membrane model of the TF conductor, which includes 1999 copies of the basic blocks of Fig.18b, all connected in series to form a single loop. Fig.19 shows only 25 of the 1999 copies, but the rest are implied.

The current in each Fig.19 primary resistor representing the TF centerstack equals the current in its parallel current source plus the loop current in the ccw direction. Analogously, the internal torque state at any location is the applied differential Lorenz torque plus the torque mechanically transferred in. Other parts of Fig.19 are also interconnected through external resistors lacking any parallel current sources (i.e., lacking any applied EM torques). Figure 19 depicts these external paths with bold symbols, using resistance numberings keyed to the previously numbered external paths for mechanical torques.

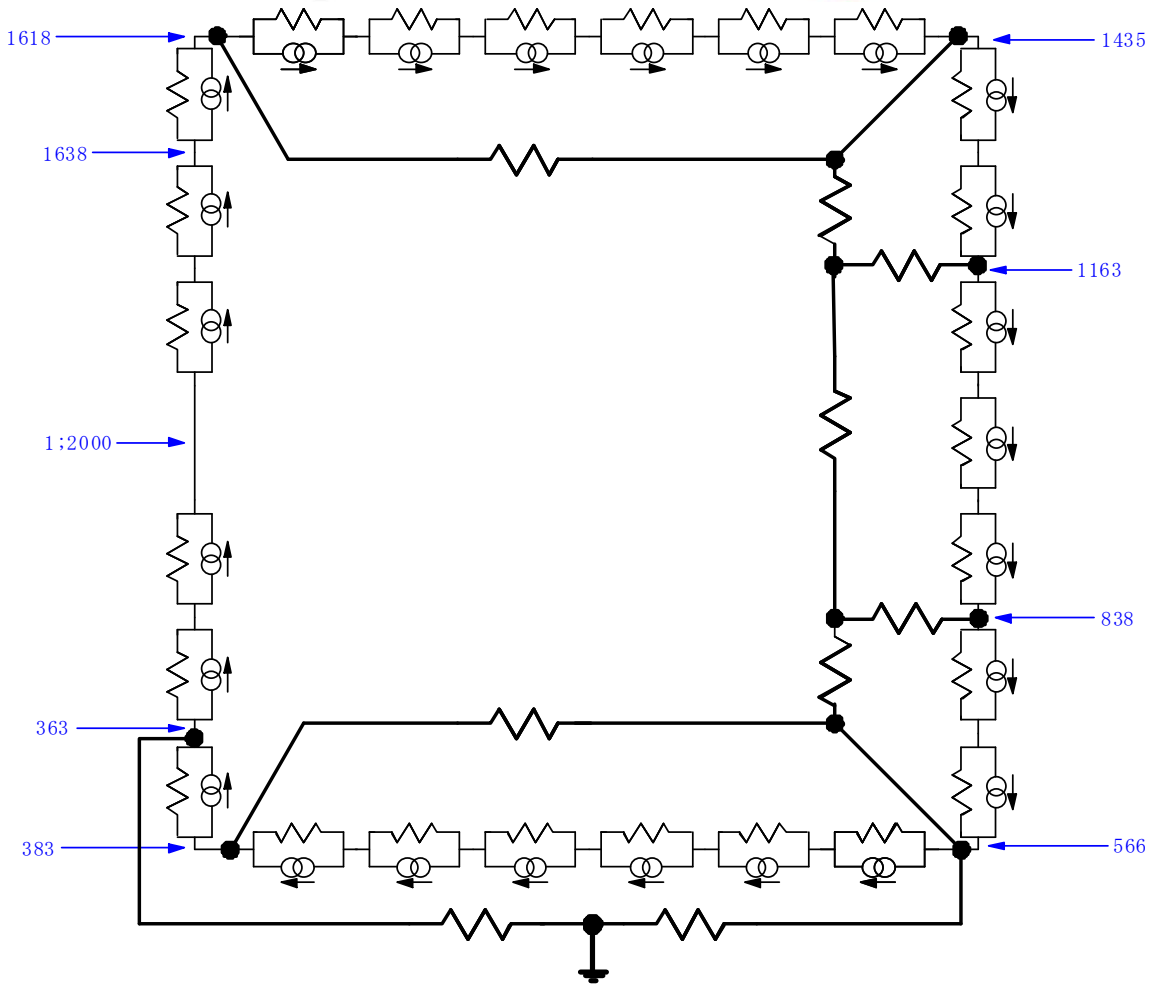

Figure 19: Electrical Analogy TF Torsional Model for NSTX CSU

The external resistors of Fig.19 are identified as follows. R(1) and R(2) represent series mechanical connection paths from respectively upper and lower aluminum block TF conductor clamps through the upper or lower umbrella to the umbrella lid and its radial connection to the insulating crown bolted to the centerstack's TF leads. R(3A) represents the upper system of rods connecting between TF outer leg clamps and clevis attachments to the vacuum vessel. R3B represents the series combination of the upper dome portion of the vacuum vessel above the upper clevis attachments, the upper umbrella mounting, and the upper umbrella up to where aluminum block TF conductor clamps are attached. R(4A) and R(4B) represent the lower mirror image of R(3A) and R(3B). R(5), together with R(3A) and R(4A), implement the previously listed interconnection path (5). R(6A) in series with R(6B) together model path (6) which transmits torque through the vacuum vessel's legs to the floor and then up through the pedestal pad to the centerstack's bottom. In this model, the torque through path (6) is transmitted into the inner part of the centerstack's bottom without going through the lower lead extensions.

The following table summarizes electrical analogy model resistances from the previous section.

Table 5: Electrical Analogy Model Resistance Values

Parameter	Comments	Analogous Resistance Value (radian/N-m)
R(1)	$R_{crown}+R_{umbrella+lid}$	8.38E-9
R(2)	$R_{crown}+R_{umbrella+lid}$	8.38E-9
R(3B)	$R_{InnerUmbrela}+R_{dome}$	4.962E-9
R(4B)	$R_{InnerUmbrela}+R_{dome}$	4.962E-9
R(3A)	$R_{ClevisRods}$	1.22E-10
R(4A)	$R_{ClevisRods}$	1.22E-10
R(5)	$R_{VV\text{-}middle}$	5.634-10
R(6A)	R_{Ped}	2.17E-8
R(6B)	R_{Legs}	3.72E-8
$R_{1638:2000\&1:363}$	R_{CS}	4.86E-8
$R_{363:383}$	R_{Leads}	5.835E-10
$R_{1618:1638}$	R_{Leads}	5.835E-10
$R_{383:566}$		5.26E-8
$R_{1435:1618}$		5.26E-8
$R_{566:838}$		1.214E-8
$R_{1163:1435}$		1.214E-8
$R_{838:1163}$		1.45E-8

SOLUTION OF NSTX CSU ELECTRICAL ANALOGY TF TORSIONAL MODEL

In order to calculate the shear stress profile in the TF centerstack it is necessary to first determine the internal torque state as a function of location, $T(s_j)$. In terms of the Fig.19 electrical analogy model this is equivalent to calculating resistor currents in each of the Fig.18b-style blocks representing the centerstack, i.e., between nodes 1 and 371 and between nodes 1630 and 2000 (a.k.a. 1). However, each such resistor current is simply the sum of the constant value of current passing between all of the centerstack's Fig.18b-type blocks and the known poloidal-flux-dependent current in its parallel current source. Thus, only two constant current values need to be determined to evaluate centerstack shear stress profiles. One current value is needed for nodes 1630 through 2000 and 1 through363, while the other is needed for nodes 363 through 371 which represent the lower lead extensions. Furthermore, inspection of Fig.19 shows that the entire TF system model could be similarly treated by solving for a total of seven (7) such "constant" values of mesh currents.

Determining terminal currents is simplified by equivalent-circuit reductions. A Thevenin equivalent of the basic block in the Fig.18b circuit employing an ideal series voltage source is shown in Fig.20. The voltage of this source is the product of the Fig.18b block's source current and resistance, i.e.,

$$V_j = R_j N_{TF} I_{TF} \frac{\Psi_j}{2\pi}$$

and its resistance is equal to R_j, the same as in the Fig.18b block. It has the same external terminal node voltage/current characteristics as Fig 18b, ***but its internal resistor current does not match the current through Fig.18's resistor***.

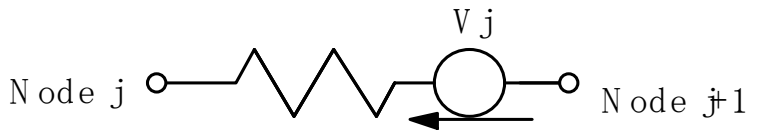

Figure 20: Thevenin Equivalent of the Fig.21 Circuit, Using A Voltage Source

Converting from Fig.18b-type blocks to the Fig.20 form allows many series-connected blocks to be merged into a single block by adding their resistances and adding their source voltages. Applying this substitution to Fig. 19 and combining blocks results in the Fig.21 circuit, which for mesh currents is equivalent to the Fig.19 circuit but easier to calculate. After solving for them, they are substituted into the Fig.19 circuit in order to calculate each resistor current there which is analogous and proportional to the internal torque state of the corresponding part of the mechanical system.

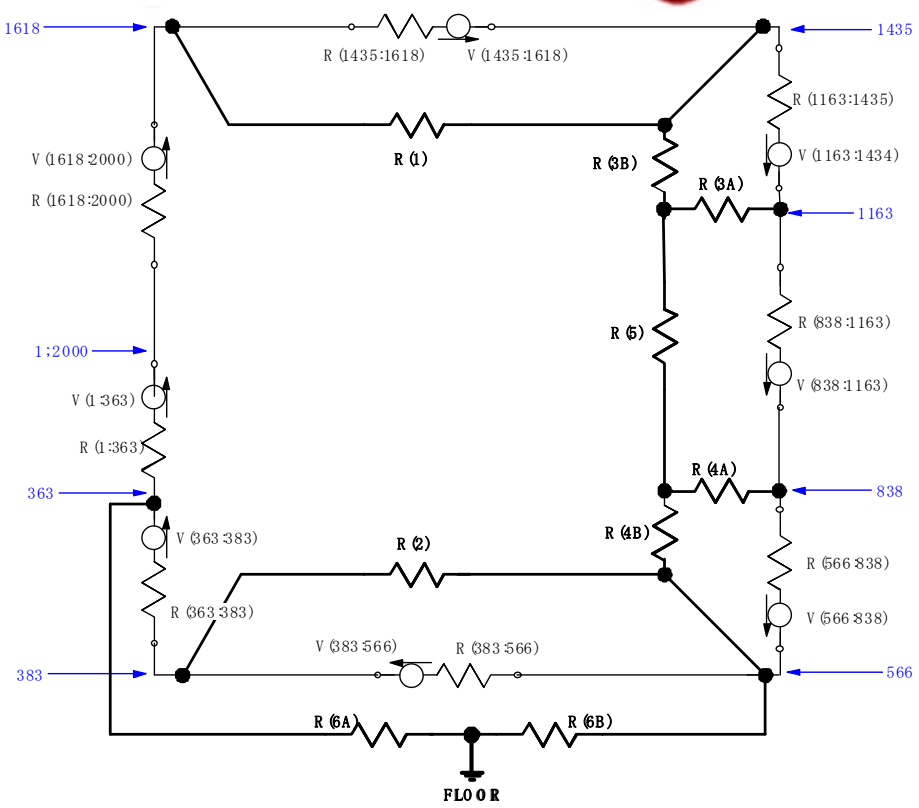

Figure 21: Equivalent Electrical Analogy TF Torsional Model for NSTX CSU

To help solve the Fig.21 circuit it is appropriate to first combine series elements and assign more compact names to designate the resistances, voltage source parameters, and distinct mesh currents in the circuit. This is done in the following diagram which uses 7 mesh loops. Note that the mesh loop carrying the current, i1, is the large loop that contains all seven voltage sources.

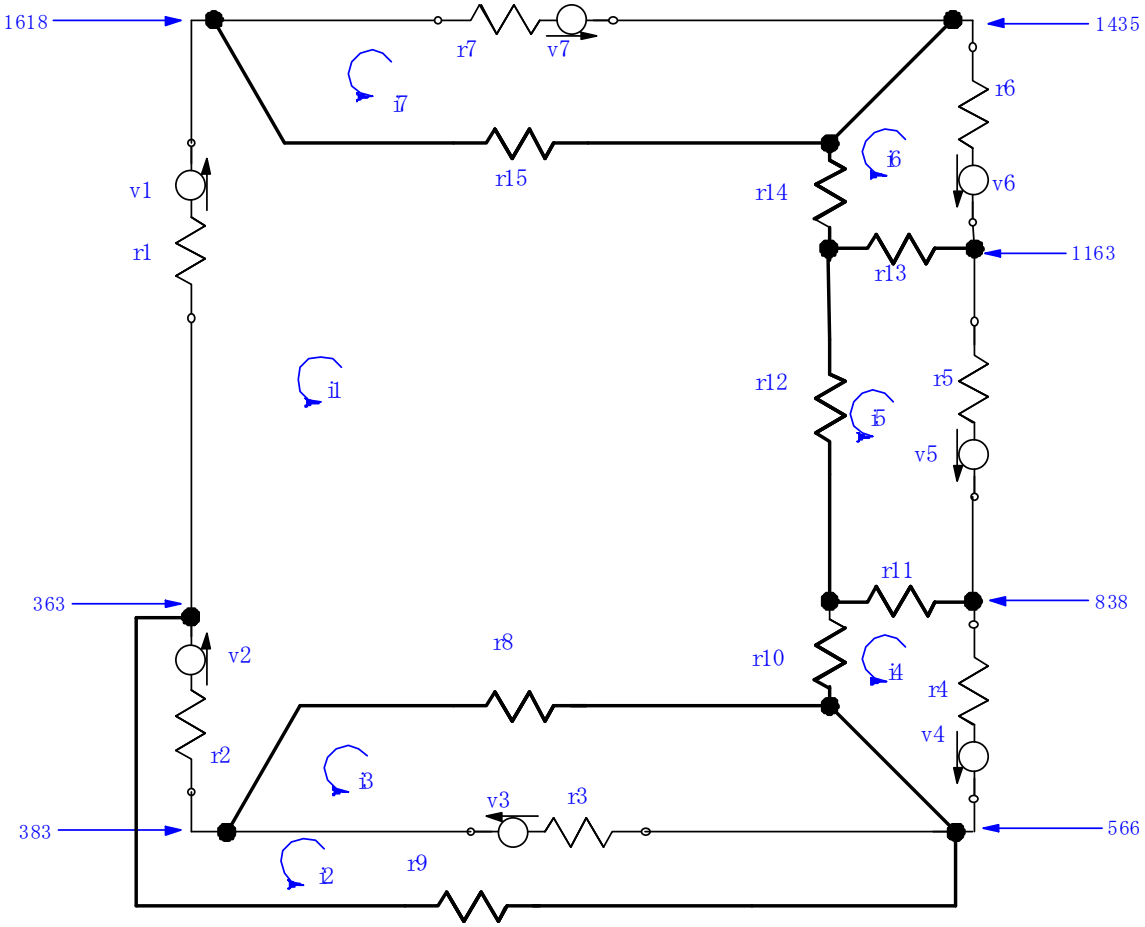

Figure 22: Simplified equivalent circuit of electrical analogy torsion model

The correspondences with symbols of earlier diagrams and parameter values are as follows:

r1=R(1:363)+R(1638:2000) +R(1618:1638)
= 4.86E-8 + 5.835E-10 = 4.92E-8 radian/N-m

r2=R(363:383)= 5.835E-10 radian/N-m

r3=R(383:566) = 5.26E-8 radian/N-m

r4=R(566:838)= 1.214E-8 radian/N-m

r5=R(838:1163) = 1.45E-8 radian/N-m

r6=R(1163:1435) = 1.214E-8 radian/N-m

r7=R(1435:1618)= 5.26E-8 radian/N-m

r8=R(2) = 8.38E-9 radian/N-m

r9=R(6A)+R(6B) = 2.17E-8 +3.72E-8 = 5.89E-8 radian/N-m

r10 = R(4B) = 4.61E-9 radian/N-m

r11=R(4A)= 1.22E-10 radian/N-m

r12 = R(5) = 5.634-10 radian/N-m

r13 = R(3A) = 1.22E-10 radian/N-m

r14 = R(3B) = 4.61E-9 radian/N-m

r15 = R(1) = 8.38E-9 radian/N-m

The analogous voltage sources result from the series connection of a sequence of elements each containing its own voltage source. When a series sequence of such elements have common torsional "resistance" values which multiply their equivalent current sources, these common resistances can be factored out of the voltage sums yielding a sum over the equivalent sequence of analog current sources. However, since each analog current source is proportional to a difference of successive poloidal flux values, a simplifying cancelation occurs which eliminates poloidal flux at the intermediate nodes results.

In the reciprocal stiffnesses calculated for the TF conductors, constant elemental resistance values result for the constant-radius portions of the TF center-stack. A second constant value per element has been selected for the TF outer leg conductor, extending inwards to the flex straps. The lead extensions were not modeled as having such a constant value but will nevertheless be approximated with their constant average value in order to simplify calculations. The three constant resistance values per element are as follows.

$R_{CS/elt}$= 6.7e-11radians/N-m/elt = R_{CSe}

$R_{Leads/elt}$=3.071E-11 radians/N-m/elt =R_{Le}

$R_{TFOL/elt}$=4.45E-11 radian/N-m/elt =R_{TFOLe}

Then the analogy model's ideal voltage sources can be expressed as follows

v1=V(1:363)+V1618:1638)+V(1638:2000)=

$=((\Psi_{1638}-\Psi_{363})*R_{CS/elt}+(\Psi_{1618}-\Psi_{1638})*R_{Leads/elt})*N_{TF}I_{TF}/2\pi$

v2= V(363:383) $=(\Psi_{363}-\Psi_{383})*R_{Leads/elt}*N_{TF}I_{TF}/2\pi$

v3=V(383:566) = $(\Psi_{383}-\Psi_{566})*R_{TFOL/elt}*N_{TF}I_{TF}/2\pi$

v4= V(566:838)= $(\Psi_{566}-\Psi_{838})*R_{TFOL/elt}*N_{TF}I_{TF}/2\pi$

v5=V(838:1163) = $(\Psi_{838}-\Psi_{1163})*R_{TFOL/elt}*N_{TF}I_{TF}/2\pi$

v6=V(1163:1435) = $(\Psi_{1163}-\Psi_{1435})*R_{TFOL/elt}*N_{TF}I_{TF}/2\pi$

v7=V(1435:1618) = $(\Psi_{1435}-\Psi_{1618})*R_{TFOL/elt}*N_{TF}I_{TF}/2\pi$

Using these variables the seven mesh equations to be solved for mesh currents are as follows:

$$r1*i1+r2*(i1-i2)+r3*(i1-i2+i3)+r4*(i1+i4)+r5*(i1+i5)+r6*(i1+i6)+r7*(i1+i7)$$
$$=-(v1+v2+v3+v4+v5+v6+v7)$$

$$r9*i2+r3*(i2-i1-i3)+r2*(i2-i1)=v2+v3$$

$$r3*(i3+i1-i2)+r8*i3=-v3$$

$$r4*(i1+i4)+r11*(i4-i5)+r10*i4=-v4$$

$$r5*(i1+i5)+r13*(i5-i6)+r12*i5+r11*(i5-i4)=-v5$$

$$r6*(i1+i6)+r14*i6+r13*(i6-i5)=-v6$$

$$r7*(i1+i7)+r15*i7=-v7$$

These equations can be expressed more compactly in vector-matrix form , as follows:

$$\begin{bmatrix} (r1+r2+r3+r4+r5+r6+r7) & -(r2+r3) & r3 & r4 & r5 & r6 & r7 \\ -(r2+r3) & (r2+r3+r9) & -r3 & 0 & 0 & 0 & 0 \\ r3 & -r3 & (r3+r8) & 0 & 0 & 0 & 0 \\ r4 & 0 & 0 & (r11+r4+r10) & -r11 & 0 & 0 \\ r5 & 0 & 0 & -r11 & (r5+r11+r12+r13) & -r13 & 0 \\ r6 & 0 & 0 & 0 & -r13 & (r6+r13+r14) & 0 \\ r7 & 0 & 0 & 0 & 0 & 0 & (r7+r15) \end{bmatrix} \begin{bmatrix} i1 \\ i2 \\ i3 \\ i4 \\ i5 \\ i6 \\ i7 \end{bmatrix}$$

$$= \begin{bmatrix} -1 & -1 & -1 & -1 & -1 & -1 & -1 \\ 0 & 1 & 1 & 0 & 0 & 0 & 0 \\ 0 & 0 & -1 & 0 & 0 & 0 & 0 \\ 0 & 0 & 0 & -1 & 0 & 0 & 0 \\ 0 & 0 & 0 & 0 & -1 & 0 & 0 \\ 0 & 0 & 0 & 0 & 0 & -1 & 0 \\ 0 & 0 & 0 & 0 & 0 & 0 & -1 \end{bmatrix} \begin{bmatrix} v1 \\ v2 \\ v3 \\ v4 \\ v5 \\ v6 \\ v7 \end{bmatrix}$$

where

$$\begin{bmatrix} v1 \\ v2 \\ v3 \\ v4 \\ v5 \\ v6 \\ v7 \end{bmatrix} = \begin{bmatrix} -R_{CSe} & 0 & 0 & 0 & 0 & 0 & R_{Le} & (R_{CSe}-R_{Le}) \\ R_{Le} & -R_{Le} & 0 & 0 & 0 & 0 & 0 & 0 \\ 0 & R_{TFOLe} & -R_{TFOLe} & 0 & 0 & 0 & 0 & 0 \\ 0 & 0 & R_{TFOLe} & -R_{TFOLe} & 0 & 0 & 0 & 0 \\ 0 & 0 & 0 & R_{TFOLe} & -R_{TFOLe} & 0 & 0 & 0 \\ 0 & 0 & 0 & 0 & R_{TFOLe} & -R_{TFOLe} & 0 & 0 \\ 0 & 0 & 0 & 0 & 0 & R_{TFOLe} & -R_{TFOLe} & 0 \end{bmatrix} \begin{bmatrix} \Psi_{363} \\ \Psi_{383} \\ \Psi_{566} \\ \Psi_{838} \\ \Psi_{1163} \\ \Psi_{1435} \\ \Psi_{1618} \\ \Psi_{1638} \end{bmatrix} \left(\frac{N_{TF} I_{TF}}{2\pi} \right)$$

ANALYSIIS RESULTS

For the stiffness parameter values chosen herein and for each of 97 coil current combination cases including the 96 plasma equilibria (specified previously by J. Menard) and a single OH-only +24 kA precharge case, the model's solution was obtained via MATLAB. Once the fixed currents i1 and i2 for a parameter case were numerically found the were used to determine the corresponding internal torque and shear stress profile in the TF centerstack. The resulting shear stress profiles are plotted in Appendix 2.

The maximum peak absolute shear stress over all 97 cases examined was 25.18 MPa, but many cases had almost this large a value of peak absolute shear stress. Inspection of the profiles shows that the OH coil's effect on peak shear stress is far stronger than the combined effects of the other PF coils or the plasma. All cases with peak shear stresses near 25 MPa had the absolute value of OH current at 24 kA, and all cases with smaller absolute values of OH current had correspondingly smaller values of peak shear stress.

APPENDIX 1

Out-Of-Plane (OOP) Torque Algorithm Exposition

Derivation of Torsion Load Formulae for Out-Of-Plane (OOP) forces on Toroidal Field Coils

In general, the total moment (i.e., torque) vector of electromagnetic forces about an origin is the volume integral of the following differential:

$$d\vec{M} = \vec{r} \times \left(\vec{J} \times \vec{B}\right) dV \tag{A1}$$

where $\vec{r}$ is the position vector of a differential volume, dV, $\vec{J}$ is the current density vector and $\vec{B}$ is the magnetic field vector. For a toroidal field coil system it is appropriate to use a cylindrical coordinate system. (r,θ,z), in which the vertically oriented z axis is the central axis of symmetry which includes the origin. To analyze OOP forces in a near-axisymmetric system it is sufficient to consider only current densities and magnetic fields lying within the local poloidal plane and depending only on the position vector within that same plane. Thus, these vectors can be rewritten as follows:

$$\begin{aligned} \vec{r} &\equiv r\hat{r} + z\hat{z} \\ \vec{J} &\equiv J_r\hat{r} + J_z\hat{z} \\ \vec{B} &\equiv B_r\hat{r} + B_z\hat{z} \end{aligned} \tag{A2}$$

where $\hat{r}, \hat{\theta}, \hat{z}$ are unit vectors aligned with the local coordinate system directions.

The volume differential in cylindrical coordinates becomes:

$$dV \equiv r\, dr d\theta\, dz \tag{A3}$$

Substituting and combining terms to simplify the result, the differential moment vector is rewritten as follows in Eq. (A4)

$$d\vec{M} = \left(J_z B_r - J_r B_z\right)\left(r\hat{z} + z\hat{r}\right) r dr d\theta dz \tag{A4}$$

When integrating Eq.(A4) over the full range of toroidal angle, $0 \le \theta < 2\pi$, the radial unit vector term, $\hat{r}$, cancels itself out for rotationally symmetric poloidal magnetic fields and TF coil current densities. The remaining nonzero part of the integral is stated in Eq.(A5).

$$\vec{M} = \hat{z}\iiint \left(J_z B_r - J_r B_z\right) r^2 dr d\theta dz = \hat{z}\, 2\pi \iint \left(J_z B_r - J_r B_z\right) r^2 dr dz \tag{A5}$$

In this last form, the double integral is taken over the (r,z) poloidal half-plane. However, current density components are zero everywhere outside the TF coils so the integration region only needs to include the (r,z) projection of TF coil conductors.

An important simplification results from changing over to stream function variables. For axisymmetric systems the poloidal flux stream function, $\Psi(r,z)$, is the total magnetic flux enclosed by the circle centered on and normal to the z axis which passes through (r,z). Poloidal magnetic flux is related to the poloidal magnetic field as stated by Eq.(A6).

$$B_r(r,z) = -\frac{1}{2\pi r}\frac{d\Psi(r,z)}{dz}$$
$$B_z(r,z) = \frac{1}{2\pi r}\frac{d\Psi(r,z)}{dr} \qquad \text{(A6)}$$

so

$$\vec{B} = \frac{1}{2\pi r}\hat{\theta}\times\nabla\Psi \qquad \text{(A7)}$$

We similarly define the toroidal field coil current stream function, *I(r,z)*, as the total TF coil current enclosed by the circle about the z axis passing through (r,z). This current stream function is related to the TF current density as stated by Eq.(A8).

$$J_r(r,z) = -\frac{1}{2\pi r}\frac{dI(r,z)}{dz}$$
$$J_z(r,z) = \frac{1}{2\pi r}\frac{dI(r,z)}{dr} \qquad \text{(A8)}$$

so

$$\vec{J} = \frac{1}{2\pi r}\hat{\theta}\times\nabla I \qquad \text{(A9)}$$

Substituting these stream functions of Eqs.(A7) and (A9) into the previous integral yields Eq.(A10a).

$$\vec{M} = \iiint \vec{r}\times\left(\vec{J}\times\vec{B}\right)dV =$$
$$= \iiint \left(r\hat{r}+z\hat{z}\right)\times\left(\left(\frac{1}{2\pi r}\hat{\theta}\times\nabla I\right)\times\left(\frac{1}{2\pi r}\hat{\theta}\times\nabla\Psi\right)\right)rdrdzd\theta = \qquad \text{(A10a)}$$
$$= \frac{1}{4\pi^2}\iiint\left(\hat{z}-\frac{z}{r}\hat{r}\right)\left(\hat{\theta}\bullet\left(\nabla I\times\nabla\Psi\right)\right)drdzd\theta$$

As stated previously, the radially oriented term cancels out while integrating over toroidal angle, leaving Eq.(A10b) as the result.

$$\vec{M} = \frac{\hat{z}}{2\pi}\iint drdz\left(\frac{\partial I}{\partial r}\frac{\partial\Psi}{\partial z}-\frac{\partial I}{\partial z}\frac{\partial\Psi}{\partial r}\right) = \frac{\hat{z}}{2\pi}\iint\left(\hat{\theta}\bullet\left(\nabla I\times\nabla\Psi\right)\right)drdz \qquad \text{(A10b)}$$

This is a particularly simple and compact formula involving the integral of the cross product of gradients of two scalar functions. The poloidal magnetic flux function can be directly obtained to any desired accuracy by use of Greens functions involving the standard elliptic integral functions, K() and E(), and the current stream function can be approximated using the projected outline of TF conductors. Furthermore, the integral itself can be approximated from these data using very simple algorithms.

Limit for the case of a slender TF conductor

Vector identities applied to Eq.(A10b) imply that

$$\vec{M} = -\frac{\hat{z}}{2\pi}\iint drdz\left(\left(\nabla I \times \hat{\theta}\right)\bullet \nabla\Psi\right) \tag{A11}$$

Here, the integration is over the area of the poloidal projection of the TF conductor segment whose net torque is to be calculated. If the conductor's projection is slender with a small width, w, we can change the element of poloidal area from dA=drdz to dA=dldw where l represents distance along the conductor's length. Assuming constant current density in the conductor the gradient vector of the current stream function, ∇I , has a magnitude equal to the total TF urrent divided by the width, $\left|\nabla I\right| = \frac{I_{TF}}{w}$, and the gradient vector 's direction is perpendicular to the local TF current streamline, pointing towards the coil's bore. It follows that $\left(\nabla I \times \hat{\theta}\right)$ has the same magnitude but is pointed in the same direction as the flowing TF current, a direction denoted here by the unit vector, $\hat{n}$. With these substitutions, the net torque over a slender TF conductor segment extending from point A to point B can be rewritten as in Eq.(A12).

$$\begin{aligned}\vec{M} &= -\frac{\hat{z}}{2\pi}\iint drdz\left(\left(\nabla I \times \hat{\theta}\right)\bullet \nabla\Psi\right)\\ &= -\frac{\hat{z}}{2\pi}\frac{I_{TF}}{w}\int_0^w dw\int_A^B dl\ \hat{n}\bullet\nabla\Psi \\ &= -\frac{\hat{z}}{2\pi}I_{TF}\int_A^B dl\ \hat{n}\bullet\nabla\Psi\end{aligned} \tag{A12}$$

However, this last integral expression in Eq.(A12) may be immediately recognized as the line integral of the gradient of a scalar function, so it has the following Eq.(A13)exact solution:

$$\vec{M} = \hat{z}\ I_{TF}\ \frac{\Psi_A - \Psi_B}{2\pi} \tag{A13}$$

Thus, the general formula of Eq.(A12), when interpreted for slender conductors, asserts that the net torque over a poloidal length of TF conductor is simply the product of the difference between the poloidal flux values at the conductor's ends, divided by 2π, then multiplied by the TF current.

Derivation of Approximation For Wider TF Conductors

Consider a triangular region in the poloidal half-plane, ΔABC, on which the exact scalar functions *I(r,z)* and *Ψ(r,z)* are to be linearly approximated by $\tilde{I}(r,z)$ and $\tilde{\Psi}(r,z)$ using function values that are exact at the triangle's three corners. The linear models are as follows:

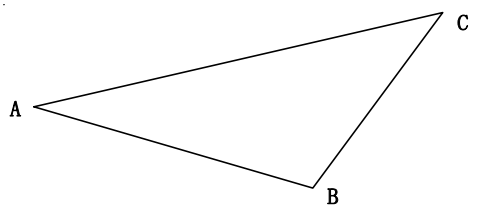

$$I(r,z) \approx \tilde{I}(r,z) = \left(\tilde{I}_0\right) + \left(\frac{\partial \tilde{I}}{\partial r}\right) r + \left(\frac{\partial \tilde{I}}{\partial z}\right) z$$
$$\Psi(r,z) \approx \tilde{\Psi}(r,z) = \left(\tilde{\Psi}_0\right) + \left(\frac{\partial \tilde{\Psi}}{\partial r}\right) r + \left(\frac{\partial \tilde{\Psi}}{\partial z}\right) z \quad \text{(A14)}$$

where $\left(\tilde{I}_0\right), \left(\frac{\partial \tilde{I}}{\partial r}\right), \left(\frac{\partial \tilde{I}}{\partial z}\right), \left(\tilde{\Psi}_0\right), \left(\frac{\partial \tilde{\Psi}}{\partial r}\right), \left(\frac{\partial \tilde{\Psi}}{\partial z}\right)$ are linear model coefficient parameters that have constant values throughout the triangle. The requirement to match the approximation to actual function values at triangle corners yields the following matrix equations, where $(r_A, z_A), (r_B, z_B), (r_C, z_C)$ are the coordinates of the triangle's corners:

$$\begin{bmatrix} 1 & r_A & z_A \\ 1 & r_B & z_B \\ 1 & r_C & z_C \end{bmatrix} \begin{bmatrix} \left(\tilde{I}_0\right) \\ \left(\frac{\partial \tilde{I}}{\partial r}\right) \\ \left(\frac{\partial \tilde{I}}{\partial z}\right) \end{bmatrix} = \begin{bmatrix} I_A \\ I_B \\ I_C \end{bmatrix} \quad \text{(A15)}$$

$$\begin{bmatrix} 1 & r_A & z_A \\ 1 & r_B & z_B \\ 1 & r_C & z_C \end{bmatrix} \begin{bmatrix} \left(\tilde{\Psi}_0\right) \\ \left(\frac{\partial \tilde{\Psi}}{\partial r}\right) \\ \left(\frac{\partial \tilde{\Psi}}{\partial z}\right) \end{bmatrix} = \begin{bmatrix} \Psi_A \\ \Psi_B \\ \Psi_C \end{bmatrix} \quad \text{(A16)}$$

These can be readily solved in closed form to find the appropriate coefficient parameter values. For the partial derivative coefficient parameters the solutions are as follows:

$$\left(\frac{\partial \tilde{I}}{\partial r}\right) = \frac{I_A(z_B - z_C) + I_B(z_C - z_A) + I_C(z_A - z_B)}{r_A(z_B - z_C) + r_B(z_C - z_A) + r_C(z_A - z_B)}$$
$$\left(\frac{\partial \tilde{I}}{\partial z}\right) = \frac{I_A(r_B - r_C) + I_B(r_C - r_A) + I_C(r_A - r_B)}{z_A(r_B - r_C) + z_B(r_C - r_A) + z_C(r_A - r_B)}$$
$$\left(\frac{\partial \tilde{\Psi}}{\partial r}\right) = \frac{\Psi_A(z_B - z_C) + \Psi_B(z_C - z_A) + \Psi_C(z_A - z_B)}{r_A(z_B - z_C) + r_B(z_C - z_A) + r_C(z_A - z_B)}$$
$$\left(\frac{\partial \tilde{\Psi}}{\partial z}\right) = \frac{\Psi_A(r_B - r_C) + \Psi_B(r_C - r_A) + \Psi_C(r_A - r_B)}{z_A(r_B - r_C) + z_B(r_C - r_A) + z_C(r_A - r_B)} \quad \text{(A17)}$$

Using this approximation the previous integrand becomes:

$$\hat{\theta}\bullet\left(\nabla I\times\nabla\Psi\right)\equiv\left(\frac{\partial I}{\partial r}\frac{\partial\Psi}{\partial z}-\frac{\partial I}{\partial z}\frac{\partial\Psi}{\partial r}\right)\approx\left(\frac{\partial\tilde{I}}{\partial r}\frac{\partial\tilde{\Psi}}{\partial z}-\frac{\partial\tilde{I}}{\partial z}\frac{\partial\tilde{\Psi}}{\partial r}\right)= \\ =\frac{I_A\left(\Psi_B-\Psi_C\right)+I_B\left(\Psi_C-\Psi_A\right)+I_C\left(\Psi_A-\Psi_B\right)}{r_A\left(z_B-z_C\right)+r_B\left(z_C-z_A\right)+r_C\left(z_A-z_B\right)} \tag{A18}$$

Note that as a result of assuming a linear model over the triangle, this approximation gives a constant value of the integrand over the triangle. Thus, the *integral* over the triangle is simply this integrand's constant value times the triangle's area, which, assuming the ABC point sequence is counterclockwise, is:

$$\left[\text{Area of Triangle }\Delta\text{ABC}\right]=\frac{1}{2}\begin{vmatrix}1 & r_A & z_A\\ 1 & r_B & z_B\\ 1 & r_C & z_C\end{vmatrix}=\frac{r_A\left(z_B-z_C\right)+r_B\left(z_C-z_A\right)+r_C\left(z_A-z_B\right)}{2} \tag{A19}$$

This cancels all (r,z) coordinates, so the integral over the triangle becomes as stated in Eq.(A20).

$$\vec{M}_{\Delta ABC}\approx\hat{z}\left(\frac{I_A\left(\Psi_B-\Psi_C\right)+I_B\left(\Psi_C-\Psi_A\right)+I_C\left(\Psi_A-\Psi_B\right)}{4\pi}\right) \tag{A20}$$

This formula can be applied to an adjacent bordering triangle, ΔACD, by changing indices as in Eq.(A21).

$$\vec{M}_{\Delta ACD}\approx\hat{z}\left(\frac{I_A\left(\Psi_C-\Psi_D\right)+I_C\left(\Psi_D-\Psi_A\right)+I_D\left(\Psi_A-\Psi_C\right)}{4\pi}\right) \tag{A21}$$

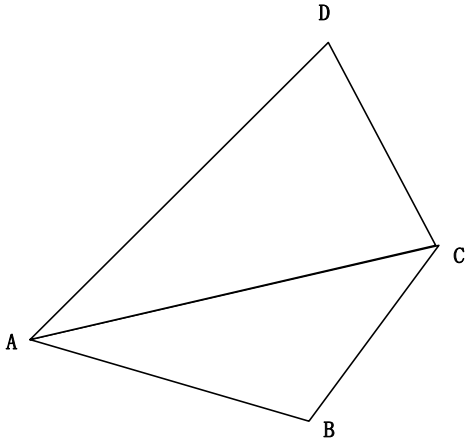

The two triangles together form a quadrilateral, ABCD, so the integral over the entire quadrilateral is the sum of the two triangle integrals:

$$\vec{M}_{ABCD}=\vec{M}_{\Delta ABC}+\vec{M}_{\Delta ACD}\approx \\ \approx\hat{z}\left(\begin{array}{l}\dfrac{I_A\left(\Psi_B-\Psi_C\right)+I_B\left(\Psi_C-\Psi_A\right)+I_C\left(\Psi_A-\Psi_B\right)}{4\pi}\\ +\dfrac{I_A\left(\Psi_C-\Psi_D\right)+I_C\left(\Psi_D-\Psi_A\right)+I_D\left(\Psi_A-\Psi_C\right)}{4\pi}\end{array}\right)= \\ =\hat{z}\left(\frac{\left(I_A-I_C\right)\left(\Psi_B-\Psi_D\right)-\left(I_B-I_D\right)\left(\Psi_A-\Psi_C\right)}{4\pi}\right) \tag{A22}$$

The quadrilateral, ABCD, could alternatively be decomposed in a different way into two triangles, i.e., into triangle ΔABD and triangle ΔBCD. Although the linear coefficient parameter sets that would apply for these triangles would be different from the above, the final resulting formula for the moment integral over the quadrilateral ABCD turns out to be identically the same!

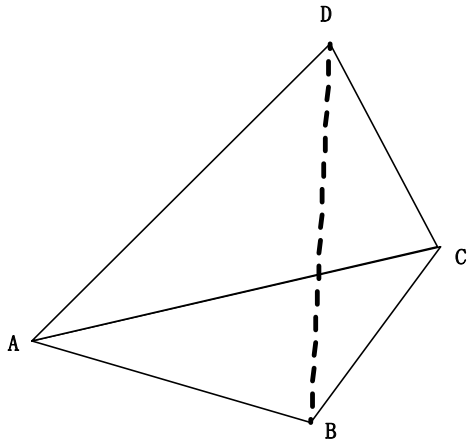

Note that in the important special case wherein the quadrilateral's corner points are located on two TF current stream function contour lines, it follows that $I_A=I_D$ and $I_B=I_C$. In that case the approximate formula for net torque in the quadrilateral region of the poloidal half-plane becomes simplified to Eq.(A23).

$$\vec{M}^{\text{AD\&BC on TFCurrent Streamlines}}_{\text{ABCD}} = \hat{z}\left(I_A - I_B\right)\left(\frac{\Psi_A + \Psi_B - \Psi_C - \Psi_D}{4\pi}\right). \qquad \text{(A23)}$$

This is the simple average of the differences between per radian poloidal magnetic fluxes at the two ends of each of the two bounding current stream function contours, multiplied by the TF current enclosed between those two current stream function contours.

Thus, the torsional OOP loading of the TF coil system can be evaluated by taking simple sums and differences of poloidal flux evaluated at points located on TF current streamlines.

A Higher Accuracy Numerical Approximation

In the present case of this memo's calculations of net torque in the NSTX CSU TF conductor due to poloidal field interactions with TF current, five TF current streamlines have been chosen and their separation in terms of contour levels is the total TF current divided by four. The adjacent diagram illustrates the five contours and flux evaluation points on those contours for two adjacent poloidal angle locations. Applying the torque formula to each of the for quadrilaterals having the ten indicated locations as their corners, the sum of the net torque is as stated in Eq.(A24).

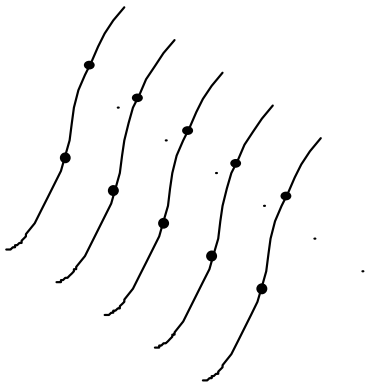

$$\begin{aligned}\vec{M} &= \hat{z}\left(\frac{I_{TF}}{4}\right)\left(\frac{\Psi_1^1 + \Psi_2^1 - \Psi_2^2 - \Psi_1^2}{4\pi}\right) + \hat{z}\left(\frac{I_{TF}}{4}\right)\left(\frac{\Psi_2^1 + \Psi_3^1 - \Psi_3^2 - \Psi_2^2}{4\pi}\right) \\ &+ \hat{z}\left(\frac{I_{TF}}{4}\right)\left(\frac{\Psi_3^1 + \Psi_4^1 - \Psi_4^2 - \Psi_3^2}{4\pi}\right) + \hat{z}\left(\frac{I_{TF}}{4}\right)\left(\frac{\Psi_4^1 + \Psi_5^1 - \Psi_5^2 - \Psi_4^2}{4\pi}\right) \qquad \text{(A24)}\end{aligned}$$

$$= \hat{z}\,\frac{I_{TF}}{2\pi}\begin{pmatrix} 0.125\left(\Psi_1^1 - \Psi_1^2\right) + 0.25\left(\Psi_2^1 - \Psi_2^2\right) + 0.25\left(\Psi_3^1 - \Psi_3^2\right) \\ + 0.25\left(\Psi_4^1 - \Psi_4^2\right) + 0.125\left(\Psi_5^1 - \Psi_5^2\right) \end{pmatrix}$$

Thus, in the sum over one poloidal interval we must premultiply the column vector of five local flux values by the row vector, [1 2 2 2 1], then divide by 16π before subtracting from the corresponding result for the other poloidal location.

Note that if all five flux values at one poloidal location were identical to each other the result would be that single value divided by 2π.

Note also that there is no benefit from repeating this summation procedure over many poloidal intervals in a TF conductor segment and summing their results, since the quantities evaluated at all intermediate poloidal locations would identically cancel each other out in taking the poloidal intervals sum. It is mathematically equivalent to directly subtract the quantities calculated on the five contours at the TF conductor segment's ends.

APPENDIX 2

Torsion Analysis Results

Shear stress stress profiles were calculated for the 96 plasma equilibrium cases previously defined by J. Menard and for a single +24 kA OH precharge case. The different shear profiles are all graphed on the following pages. Peak shear stress values are collected in the following table for these cases. The maximum absolute shear was -25.184 MPa, observed for equilibrium case #1 and almost reached again in equilibrium case #16.

The table and plots show shear stress is mostly due to OH. PF coils and plasma contribute little.

Table A2: TF Centerstack MAx Absolute Shear Stress ; Precharge and Plasma Cases

Case# -24 kA OH	Peak Shear MPa	Case# 0 kA OH	Peak Shear MPa	Case# 13 kA OH	Peak Shear MPa	Case 24 kA OH	Peak Shear MPa
						Precharge	24.45
1	-25.184	2	2.0659	3	15.421		
4	-23.862	5	2.0733	6	15.428		
7	-23.422	8	2.3851	9	15.528		
10	-23.272	11	2.7436	12	16.023		
13	-23.248	14	2.8179	15	16.112		
16	-25.184	17	2.0659	18	15.421		
19	-23.104	20	3.5128	21	16.814		
22	-23.152	23	3.2479	24	16.517		
25	-23.216	26	2.9997	27	16.255		
28	-23.316	29	2.8479	30	15.994		
31	-23.442	32	3.0592	33	16.015		
34	-23.133	35	6.4557	36	19.960		
37	-23.096	38	6.1462	39	19.669		
40	-23.124	41	5.7567	42	19.271		
43	-23.196	44	5.0989	45	18.688		
46	-23.278	47	4.4391	38	18.096		
49	-22.982	50	6.6023	51	20.108		
52	-22.989	53	6.2348	54	19.786		
55	-23.046	56	5.7607	57	19.304		
58	-23.132	59	5.1357	60	18.715		
61	-23.242	62	4.3503	63	17.968		
64	-23.289	65	3.176	66	16.591		
67	-23.295	68	3.1136	69	16.529		
70	-23.284	71	3.0578	72	16.497		
73	-23.245	74	3.1616	75	16.616		
76	-23.206	77	3.3256	78	16.783		
79	-23.149	80	3.5554	81	17.019		
82	-23.045	83	4.8323	84	18.114		
85	-23.117	86	3.9819	87	17.246		
88	-23.187	89	3.3987	90	16.663		
91	-23.264	92	2.9525	93	16.203		
94	-23.349	95	2.5611	96	15.802		

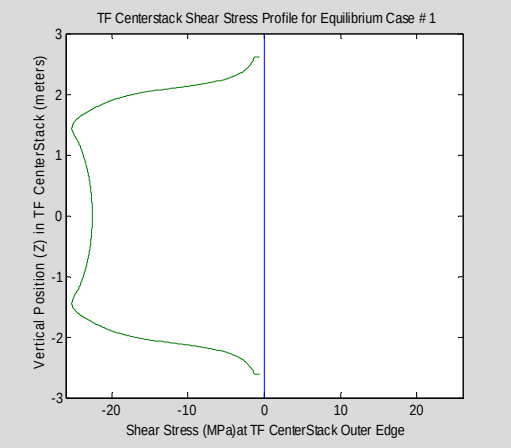
TF Centerstack Shear Stress Profile for Equilibrium Case # 1
Vertical Position (Z) in TF CenterStack (meters)
Shear Stress (MPa)at TF CenterStack Outer Edge

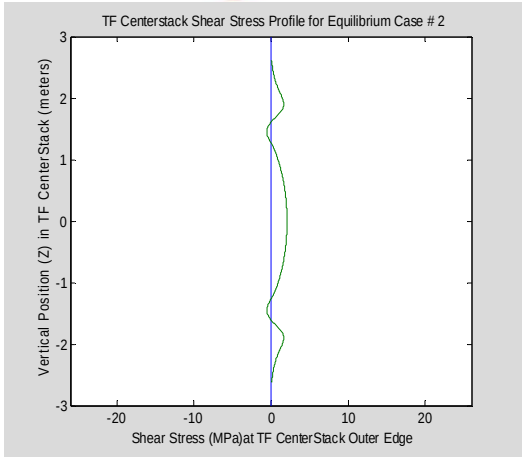
TF Centerstack Shear Stress Profile for Equilibrium Case # 2
Vertical Position (Z) in TF CenterStack (meters)
Shear Stress (MPa)at TF CenterStack Outer Edge

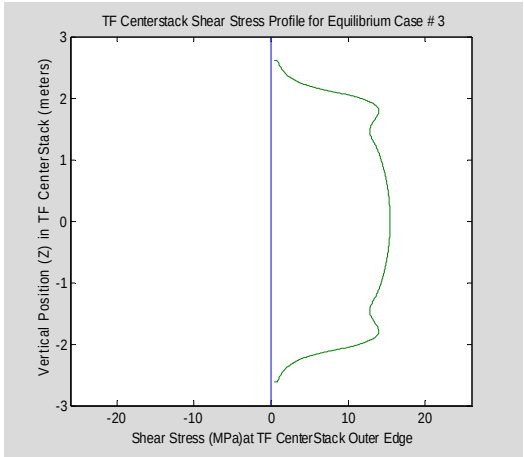
TF Centerstack Shear Stress Profile for Equilibrium Case # 3
Vertical Position (Z) in TF CenterStack (meters)
Shear Stress (MPa)at TF CenterStack Outer Edge

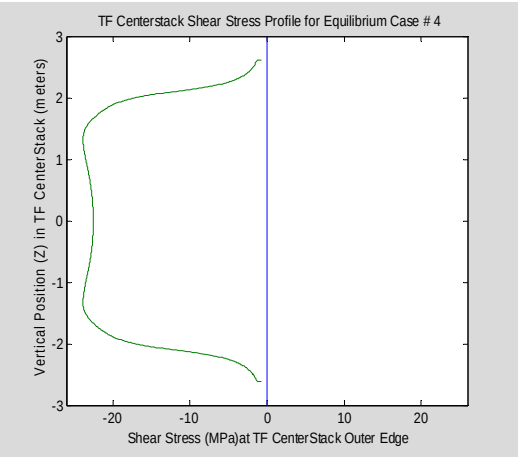
TF Centerstack Shear Stress Profile for Equilibrium Case # 4
Vertical Position (Z) in TF CenterStack (meters)
Shear Stress (MPa)at TF CenterStack Outer Edge

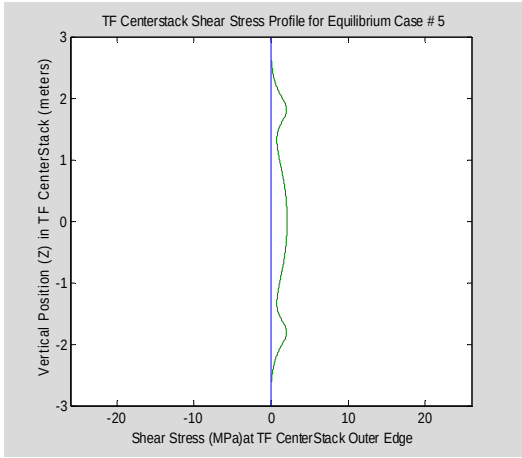
TF Centerstack Shear Stress Profile for Equilibrium Case # 5
Vertical Position (Z) in TF CenterStack (meters)
Shear Stress (MPa)at TF CenterStack Outer Edge

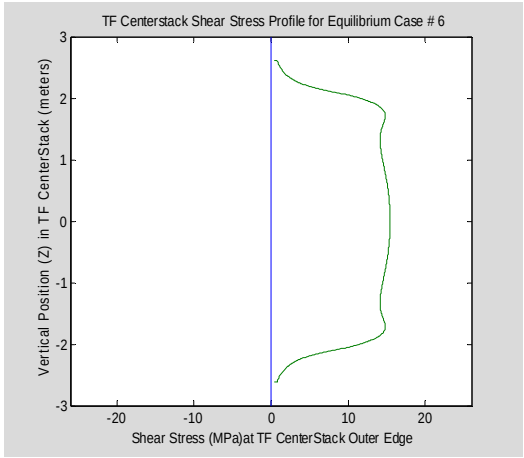
TF Centerstack Shear Stress Profile for Equilibrium Case # 6
Vertical Position (Z) in TF CenterStack (meters)
Shear Stress (MPa)at TF CenterStack Outer Edge

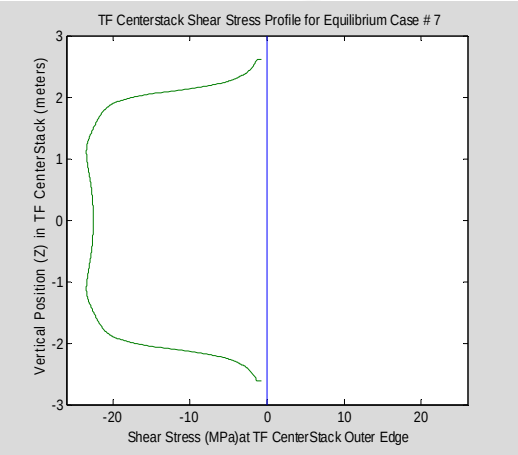
TF Centerstack Shear Stress Profile for Equilibrium Case # 7
Vertical Position (Z) in TF CenterStack (meters)
Shear Stress (MPa)at TF CenterStack Outer Edge

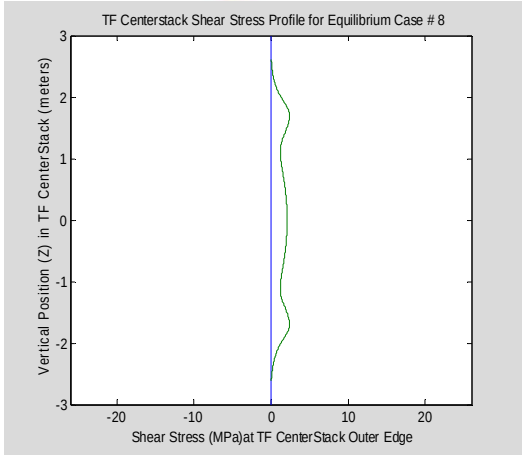
TF Centerstack Shear Stress Profile for Equilibrium Case # 8
Vertical Position (Z) in TF CenterStack (meters)
Shear Stress (MPa)at TF CenterStack Outer Edge

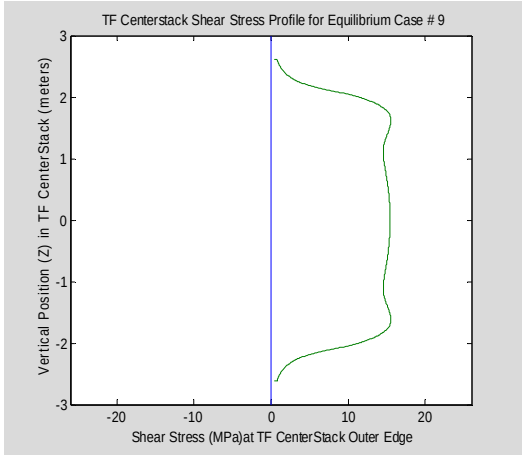
TF Centerstack Shear Stress Profile for Equilibrium Case # 9
Vertical Position (Z) in TF CenterStack (meters)
Shear Stress (MPa)at TF CenterStack Outer Edge

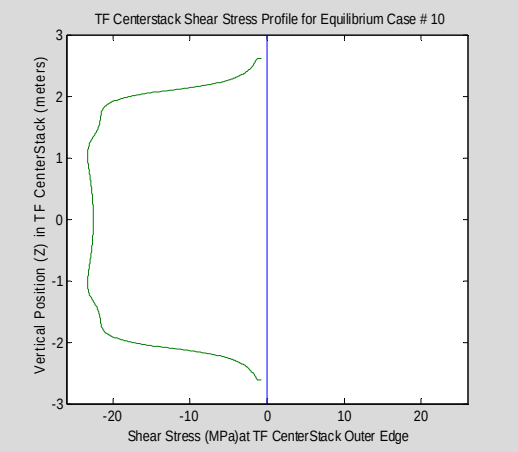
TF Centerstack Shear Stress Profile for Equilibrium Case # 10
Vertical Position (Z) in TF CenterStack (meters)
Shear Stress (MPa)at TF CenterStack Outer Edge

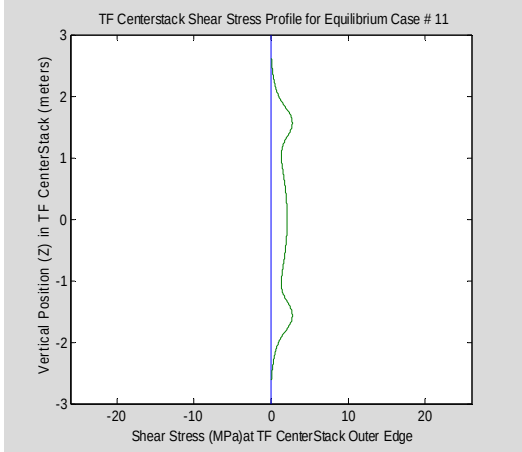
TF Centerstack Shear Stress Profile for Equilibrium Case # 11
Vertical Position (Z) in TF CenterStack (meters)
Shear Stress (MPa)at TF CenterStack Outer Edge

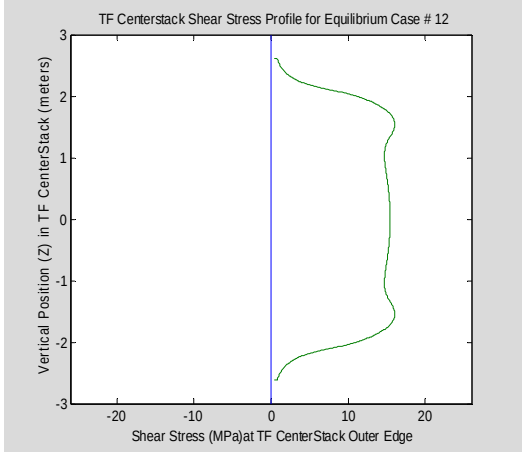
TF Centerstack Shear Stress Profile for Equilibrium Case # 12
Vertical Position (Z) in TF CenterStack (meters)
Shear Stress (MPa)at TF CenterStack Outer Edge

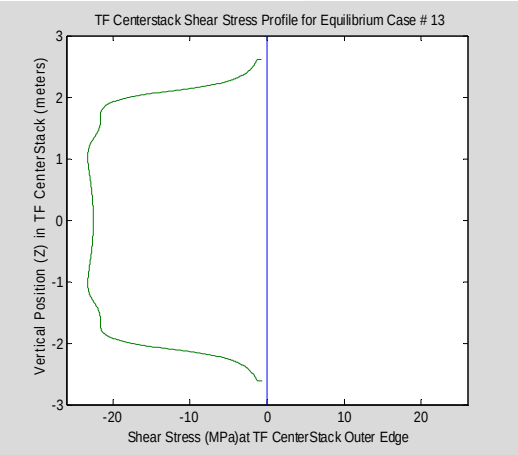
TF Centerstack Shear Stress Profile for Equilibrium Case # 13
Vertical Position (Z) in TF CenterStack (meters)
Shear Stress (MPa)at TF CenterStack Outer Edge

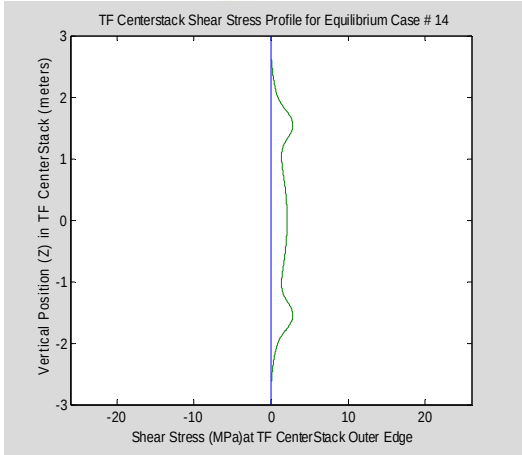
TF Centerstack Shear Stress Profile for Equilibrium Case # 14
Vertical Position (Z) in TF CenterStack (meters)
Shear Stress (MPa)at TF CenterStack Outer Edge

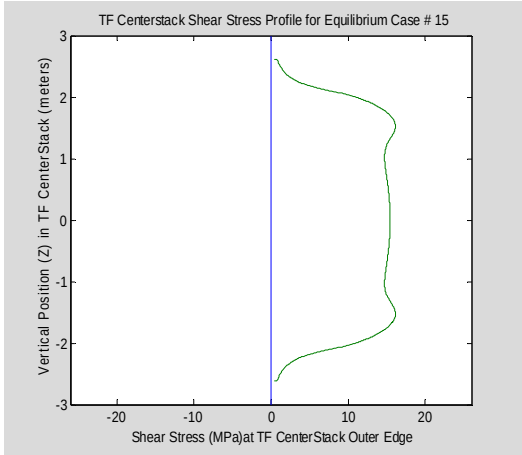
TF Centerstack Shear Stress Profile for Equilibrium Case # 15
Vertical Position (Z) in TF CenterStack (meters)
Shear Stress (MPa)at TF CenterStack Outer Edge

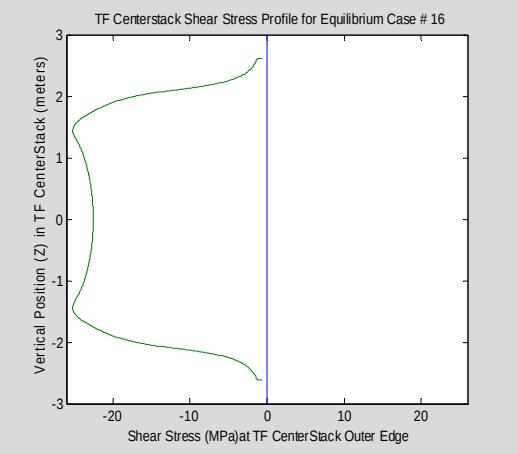
TF Centerstack Shear Stress Profile for Equilibrium Case # 16
Vertical Position (Z) in TF CenterStack (meters)
Shear Stress (MPa)at TF CenterStack Outer Edge

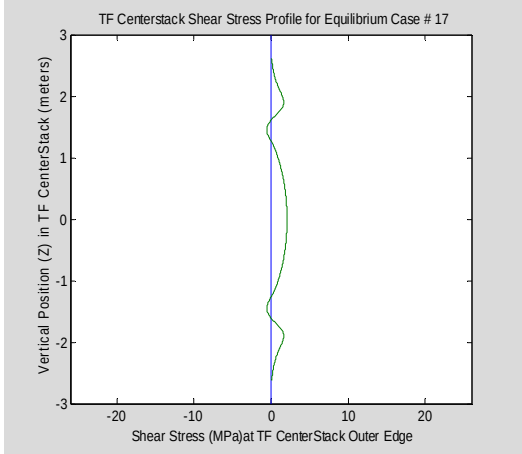
TF Centerstack Shear Stress Profile for Equilibrium Case # 17
Vertical Position (Z) in TF CenterStack (meters)
Shear Stress (MPa)at TF CenterStack Outer Edge

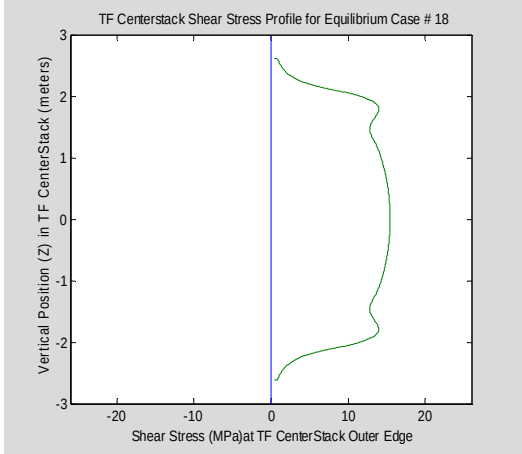
TF Centerstack Shear Stress Profile for Equilibrium Case # 18
Vertical Position (Z) in TF CenterStack (meters)
Shear Stress (MPa)at TF CenterStack Outer Edge

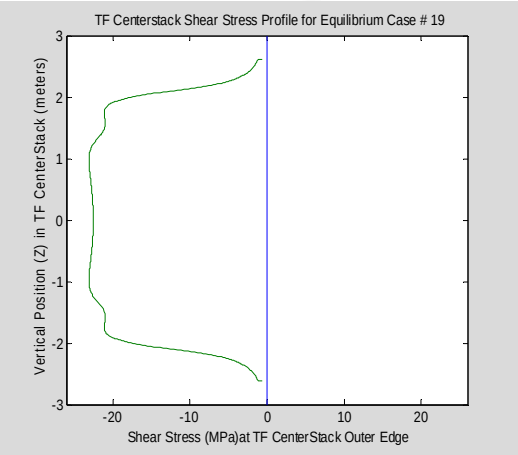
TF Centerstack Shear Stress Profile for Equilibrium Case # 19
Vertical Position (Z) in TF CenterStack (meters)
Shear Stress (MPa)at TF CenterStack Outer Edge

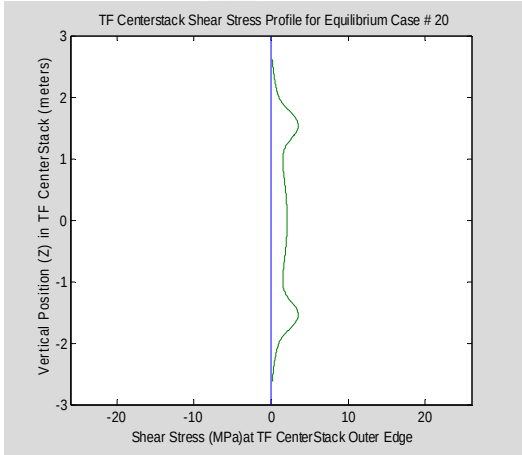
TF Centerstack Shear Stress Profile for Equilibrium Case # 20
Vertical Position (Z) in TF CenterStack (meters)
Shear Stress (MPa)at TF CenterStack Outer Edge

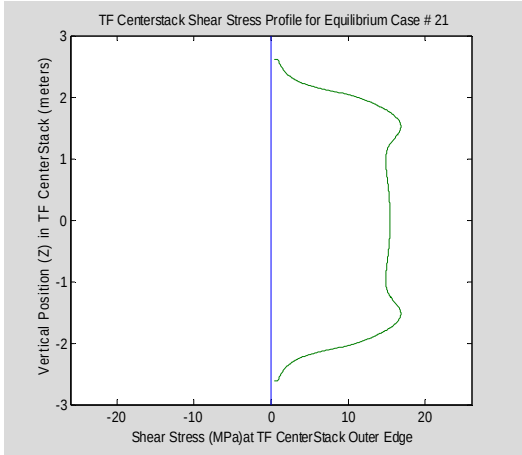
TF Centerstack Shear Stress Profile for Equilibrium Case # 21
Vertical Position (Z) in TF CenterStack (meters)
Shear Stress (MPa)at TF CenterStack Outer Edge

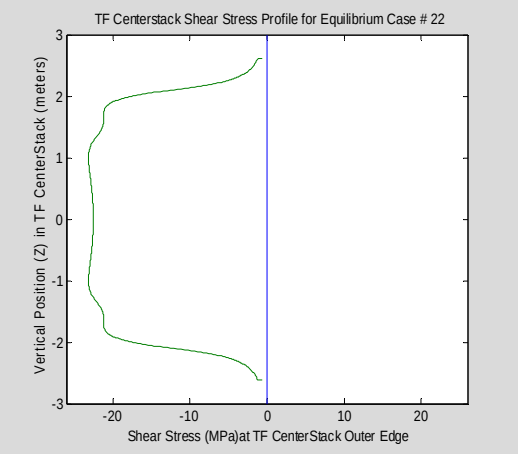
TF Centerstack Shear Stress Profile for Equilibrium Case # 22
Vertical Position (Z) in TF CenterStack (meters)
Shear Stress (MPa)at TF CenterStack Outer Edge

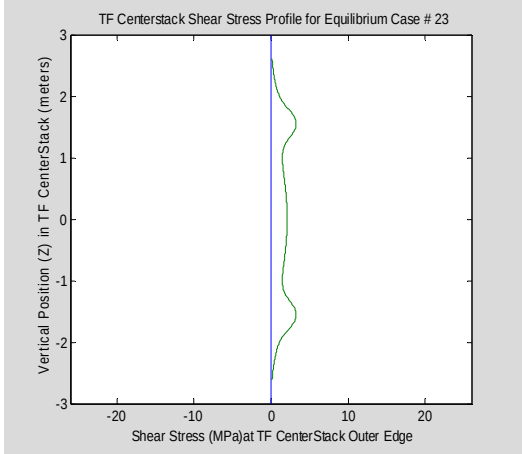
TF Centerstack Shear Stress Profile for Equilibrium Case # 23
Vertical Position (Z) in TF CenterStack (meters)
Shear Stress (MPa)at TF CenterStack Outer Edge

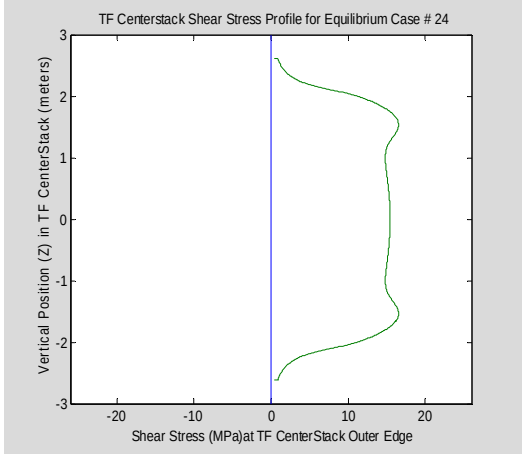
TF Centerstack Shear Stress Profile for Equilibrium Case # 24
Vertical Position (Z) in TF CenterStack (meters)
Shear Stress (MPa)at TF CenterStack Outer Edge

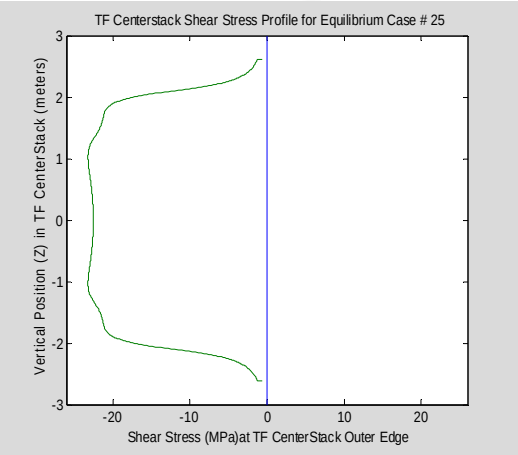
TF Centerstack Shear Stress Profile for Equilibrium Case # 25
Vertical Position (Z) in TF CenterStack (meters)
Shear Stress (MPa)at TF CenterStack Outer Edge

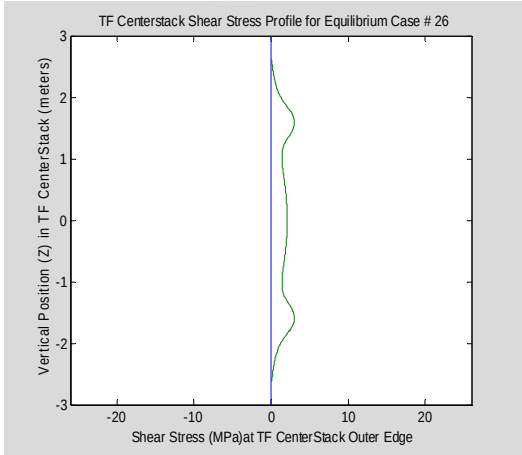
TF Centerstack Shear Stress Profile for Equilibrium Case # 26
Vertical Position (Z) in TF CenterStack (meters)
Shear Stress (MPa)at TF CenterStack Outer Edge

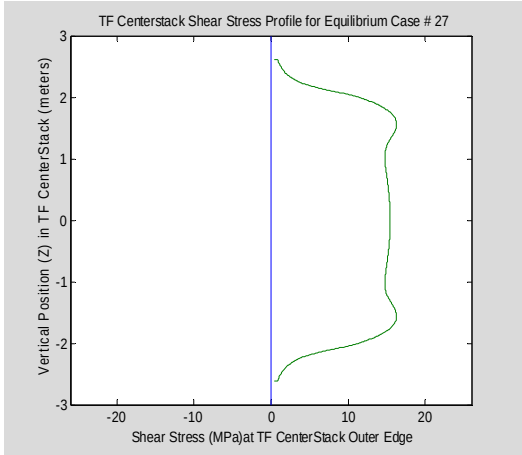
TF Centerstack Shear Stress Profile for Equilibrium Case # 27
Vertical Position (Z) in TF CenterStack (meters)
Shear Stress (MPa)at TF CenterStack Outer Edge

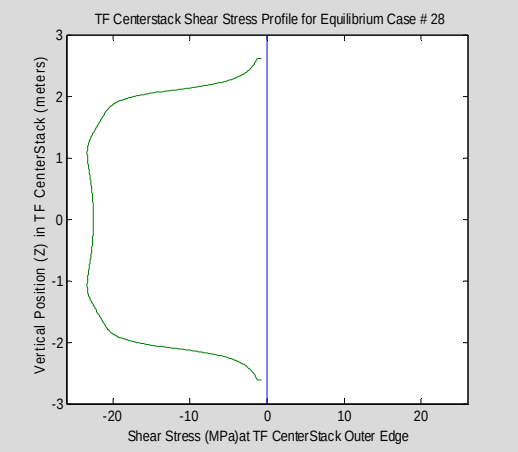
TF Centerstack Shear Stress Profile for Equilibrium Case # 28
Vertical Position (Z) in TF CenterStack (meters)
Shear Stress (MPa)at TF CenterStack Outer Edge

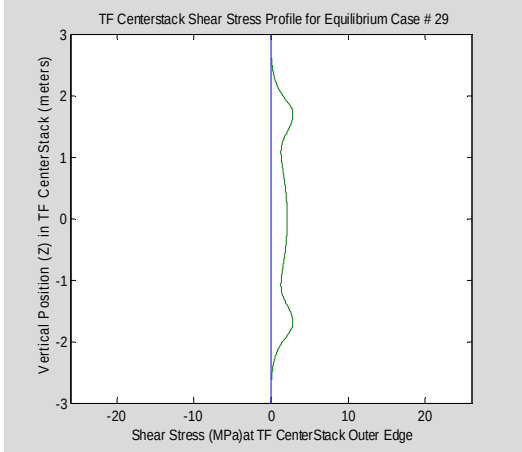
TF Centerstack Shear Stress Profile for Equilibrium Case # 29
Vertical Position (Z) in TF CenterStack (meters)
Shear Stress (MPa)at TF CenterStack Outer Edge

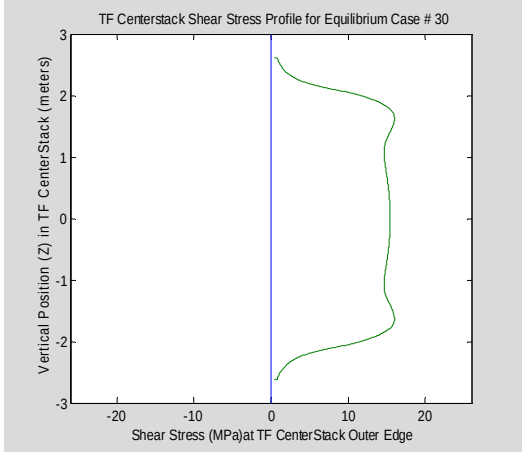
TF Centerstack Shear Stress Profile for Equilibrium Case # 30
Vertical Position (Z) in TF CenterStack (meters)
Shear Stress (MPa)at TF CenterStack Outer Edge

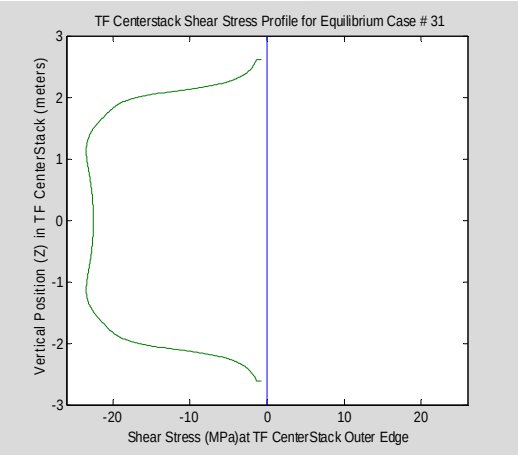
TF Centerstack Shear Stress Profile for Equilibrium Case # 31
Vertical Position (Z) in TF CenterStack (meters)
Shear Stress (MPa)at TF CenterStack Outer Edge

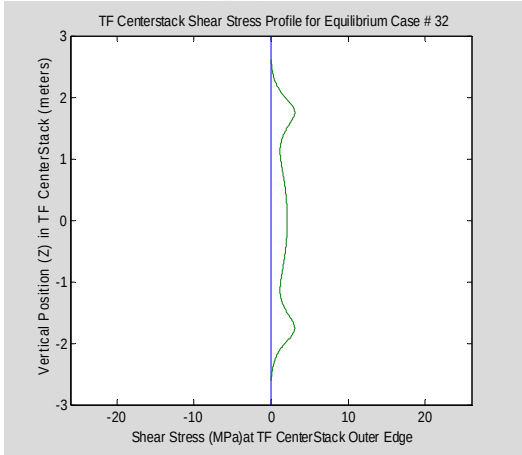
TF Centerstack Shear Stress Profile for Equilibrium Case # 32
Vertical Position (Z) in TF CenterStack (meters)
Shear Stress (MPa)at TF CenterStack Outer Edge

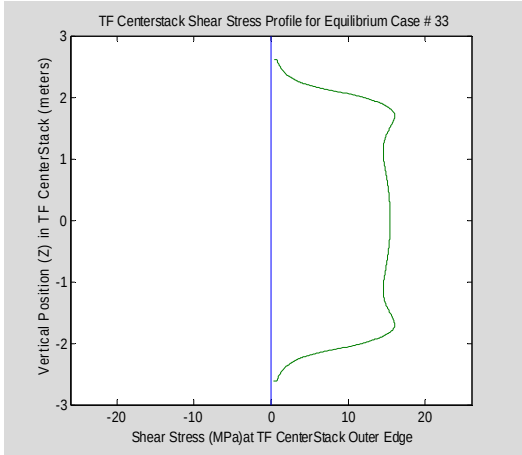
TF Centerstack Shear Stress Profile for Equilibrium Case # 33
Vertical Position (Z) in TF CenterStack (meters)
Shear Stress (MPa)at TF CenterStack Outer Edge

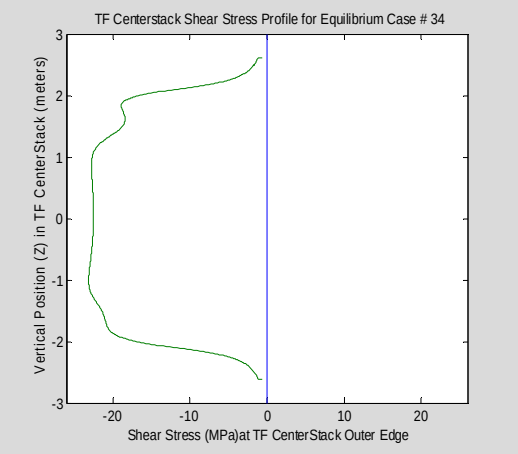
TF Centerstack Shear Stress Profile for Equilibrium Case # 34
Vertical Position (Z) in TF CenterStack (meters)
Shear Stress (MPa)at TF CenterStack Outer Edge

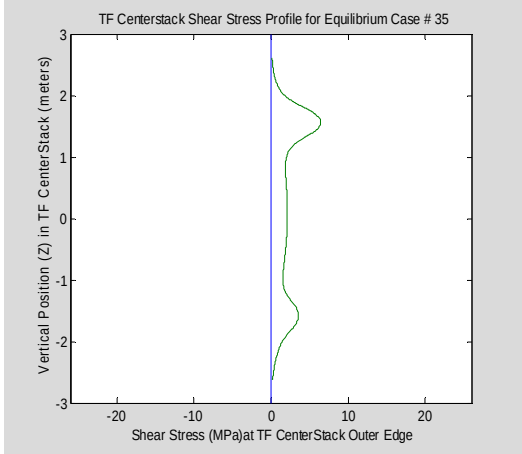
TF Centerstack Shear Stress Profile for Equilibrium Case # 35
Vertical Position (Z) in TF CenterStack (meters)
Shear Stress (MPa)at TF CenterStack Outer Edge

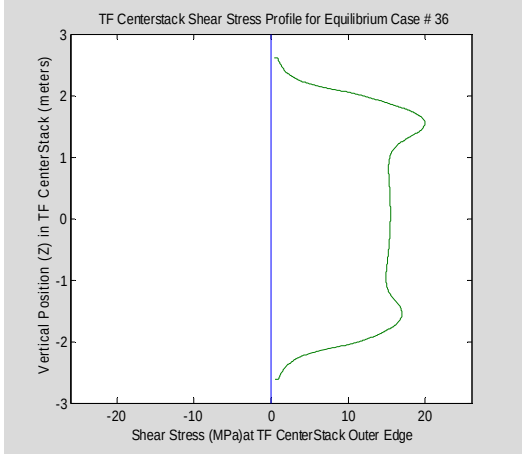
TF Centerstack Shear Stress Profile for Equilibrium Case # 36
Vertical Position (Z) in TF CenterStack (meters)
Shear Stress (MPa)at TF CenterStack Outer Edge

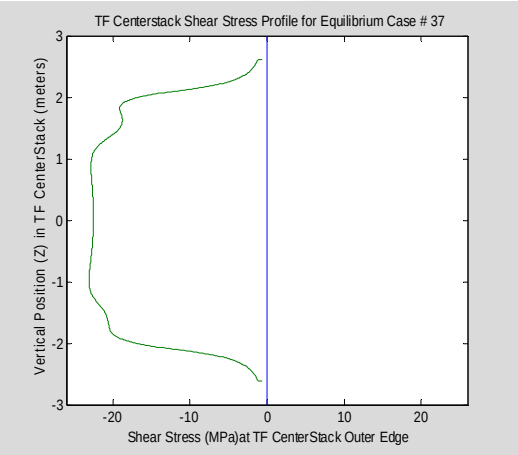
TF Centerstack Shear Stress Profile for Equilibrium Case # 37
Vertical Position (Z) in TF CenterStack (meters)
Shear Stress (MPa)at TF CenterStack Outer Edge

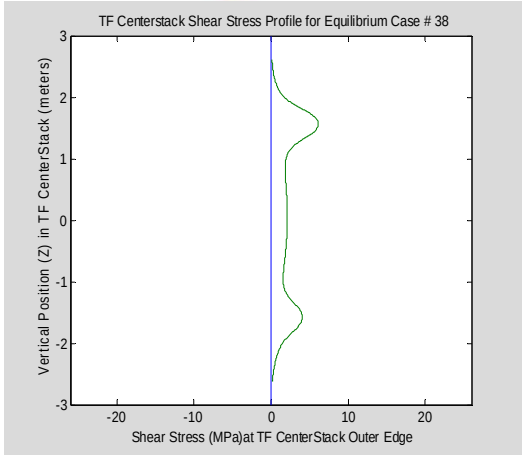
TF Centerstack Shear Stress Profile for Equilibrium Case # 38
Vertical Position (Z) in TF CenterStack (meters)
Shear Stress (MPa)at TF CenterStack Outer Edge

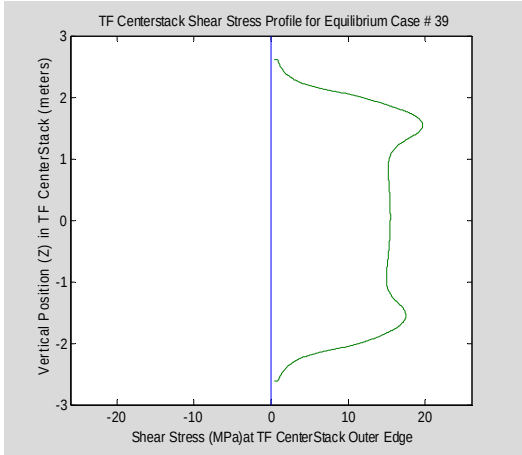
TF Centerstack Shear Stress Profile for Equilibrium Case # 39
Vertical Position (Z) in TF CenterStack (meters)
Shear Stress (MPa)at TF CenterStack Outer Edge

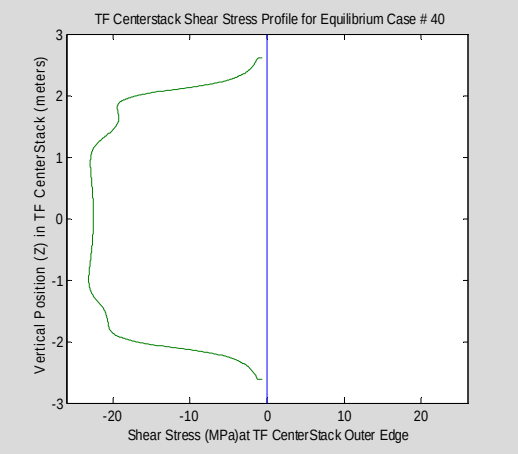
TF Centerstack Shear Stress Profile for Equilibrium Case # 40
Vertical Position (Z) in TF CenterStack (meters)
Shear Stress (MPa)at TF CenterStack Outer Edge

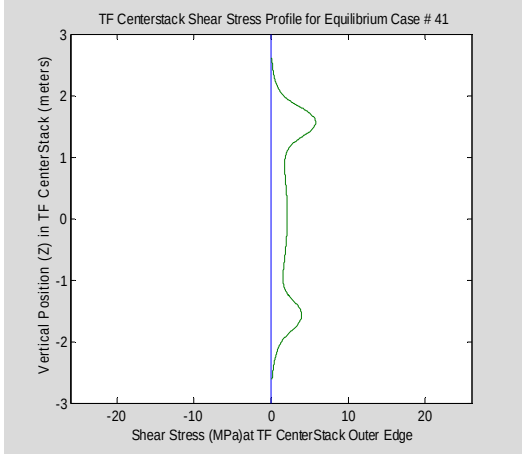
TF Centerstack Shear Stress Profile for Equilibrium Case # 41
Vertical Position (Z) in TF CenterStack (meters)
Shear Stress (MPa)at TF CenterStack Outer Edge

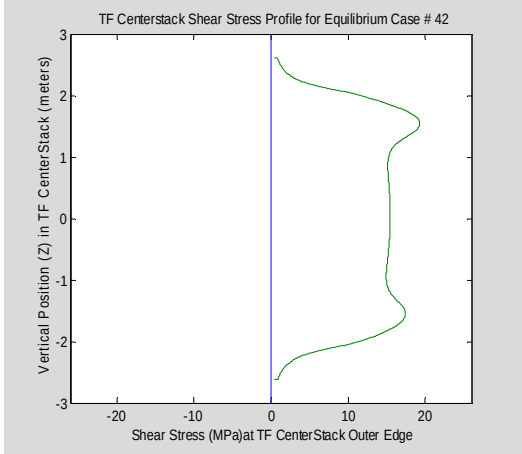
TF Centerstack Shear Stress Profile for Equilibrium Case # 42
Vertical Position (Z) in TF CenterStack (meters)
Shear Stress (MPa)at TF CenterStack Outer Edge

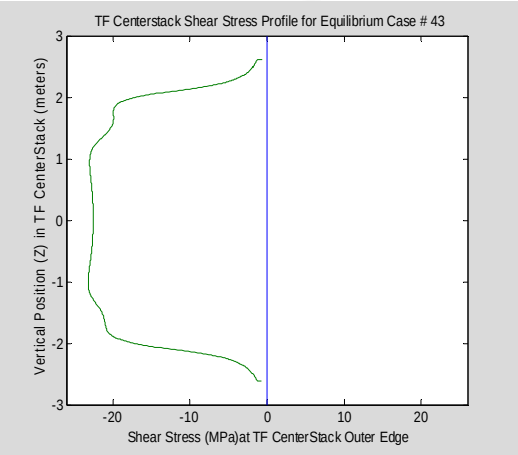
TF Centerstack Shear Stress Profile for Equilibrium Case # 43
Vertical Position (Z) in TF CenterStack (meters)
Shear Stress (MPa)at TF CenterStack Outer Edge

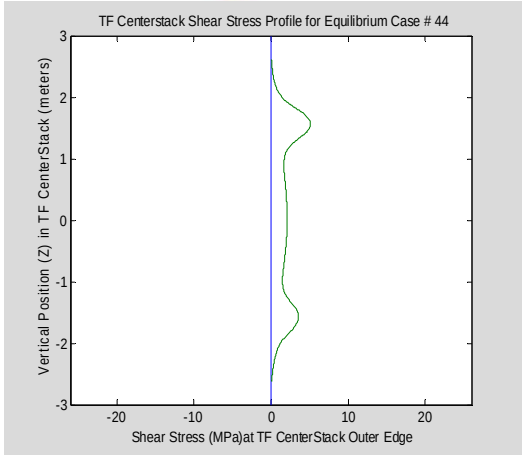
TF Centerstack Shear Stress Profile for Equilibrium Case # 44
Vertical Position (Z) in TF CenterStack (meters)
Shear Stress (MPa)at TF CenterStack Outer Edge

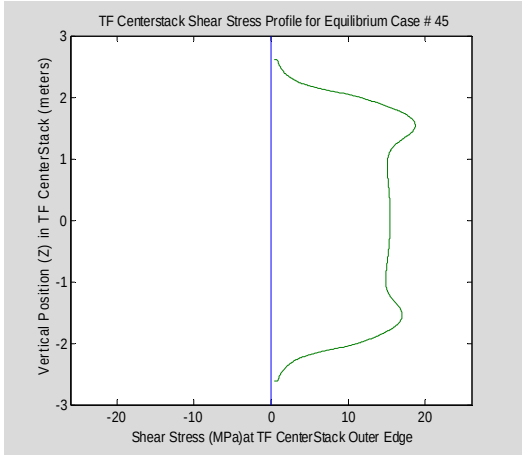
TF Centerstack Shear Stress Profile for Equilibrium Case # 45
Vertical Position (Z) in TF CenterStack (meters)
Shear Stress (MPa)at TF CenterStack Outer Edge

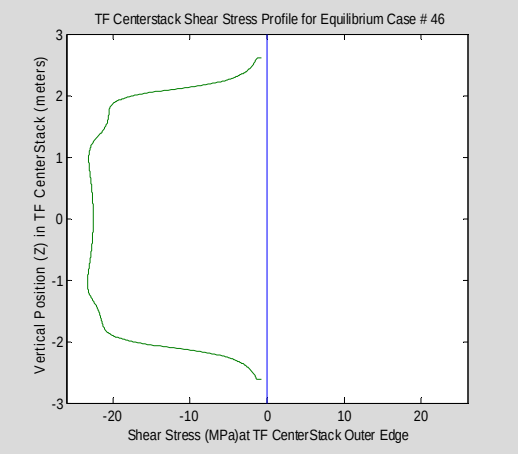
TF Centerstack Shear Stress Profile for Equilibrium Case # 46
Vertical Position (Z) in TF CenterStack (meters)
Shear Stress (MPa)at TF CenterStack Outer Edge

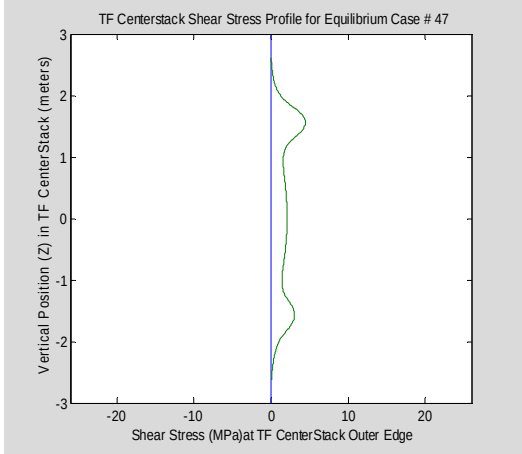
TF Centerstack Shear Stress Profile for Equilibrium Case # 47
Vertical Position (Z) in TF CenterStack (meters)
Shear Stress (MPa)at TF CenterStack Outer Edge

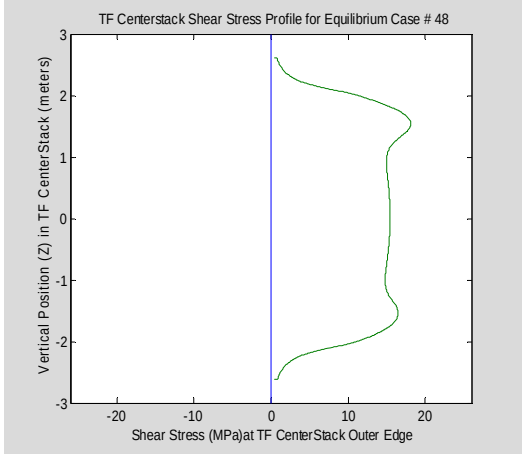
TF Centerstack Shear Stress Profile for Equilibrium Case # 48
Vertical Position (Z) in TF CenterStack (meters)
Shear Stress (MPa)at TF CenterStack Outer Edge

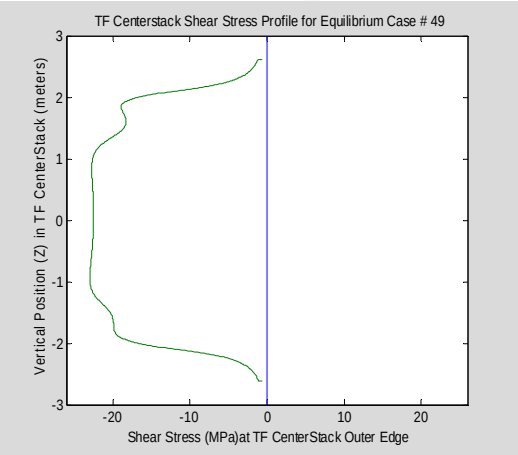
TF Centerstack Shear Stress Profile for Equilibrium Case # 49
Vertical Position (Z) in TF CenterStack (meters)
Shear Stress (MPa)at TF CenterStack Outer Edge

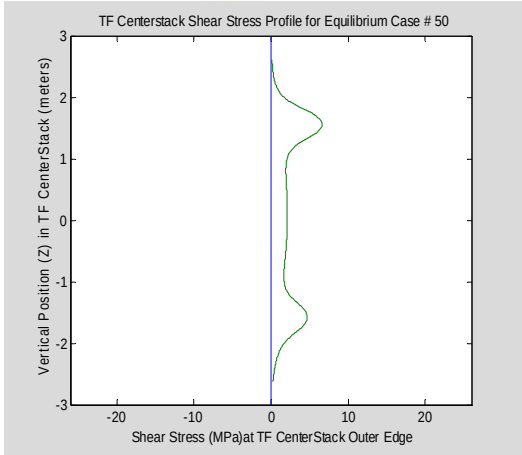
TF Centerstack Shear Stress Profile for Equilibrium Case # 50
Vertical Position (Z) in TF CenterStack (meters)
Shear Stress (MPa)at TF CenterStack Outer Edge

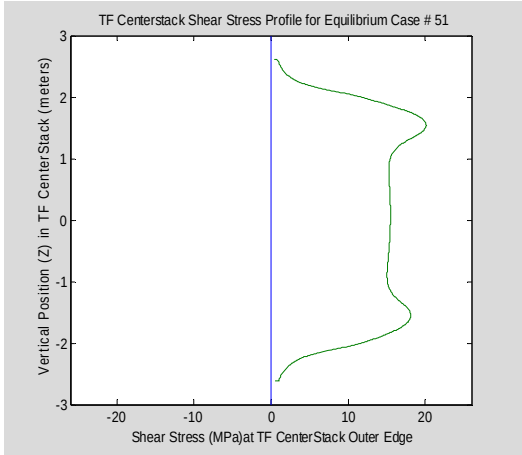
TF Centerstack Shear Stress Profile for Equilibrium Case # 51
Vertical Position (Z) in TF CenterStack (meters)
Shear Stress (MPa)at TF CenterStack Outer Edge

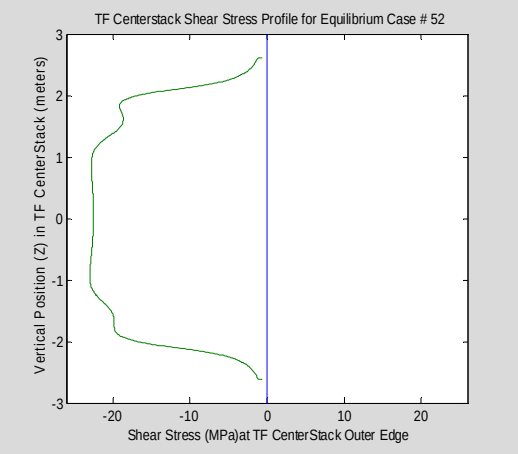
TF Centerstack Shear Stress Profile for Equilibrium Case # 52
Vertical Position (Z) in TF CenterStack (meters)
Shear Stress (MPa)at TF CenterStack Outer Edge

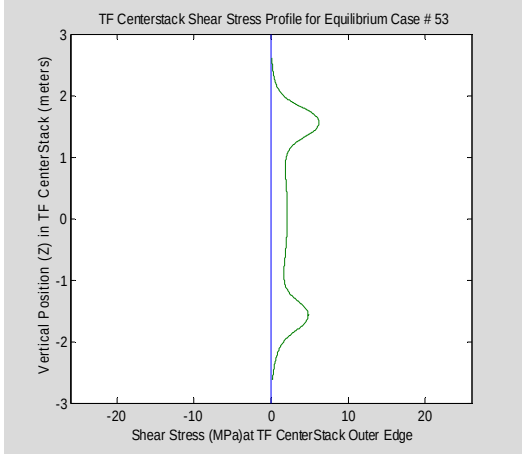
TF Centerstack Shear Stress Profile for Equilibrium Case # 53
Vertical Position (Z) in TF CenterStack (meters)
Shear Stress (MPa)at TF CenterStack Outer Edge

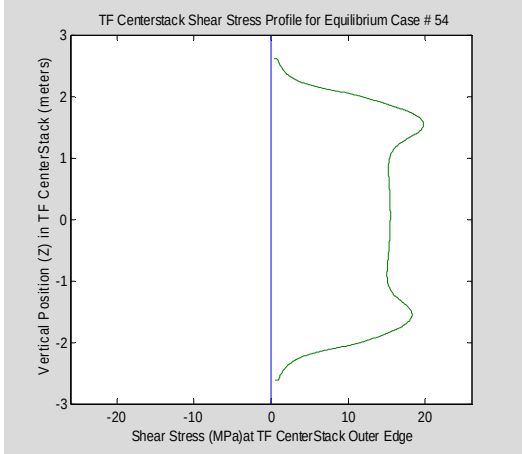
TF Centerstack Shear Stress Profile for Equilibrium Case # 54
Vertical Position (Z) in TF CenterStack (meters)
Shear Stress (MPa)at TF CenterStack Outer Edge

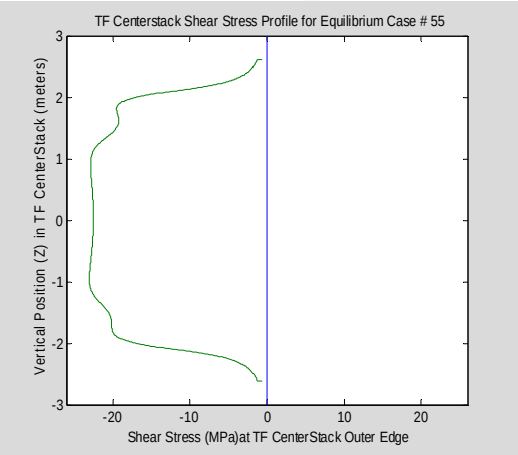
TF Centerstack Shear Stress Profile for Equilibrium Case # 55
Vertical Position (Z) in TF CenterStack (meters)
Shear Stress (MPa)at TF CenterStack Outer Edge

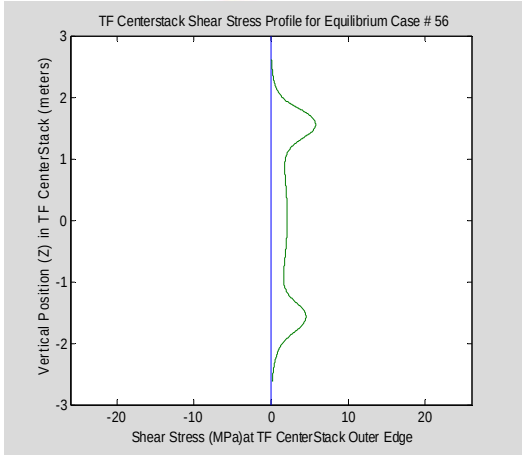
TF Centerstack Shear Stress Profile for Equilibrium Case # 56
Vertical Position (Z) in TF CenterStack (meters)
Shear Stress (MPa)at TF CenterStack Outer Edge

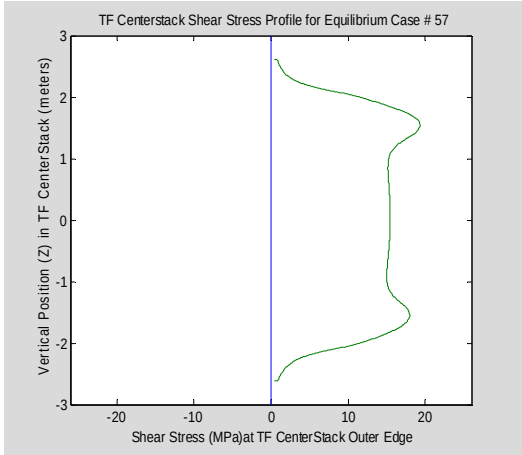
TF Centerstack Shear Stress Profile for Equilibrium Case # 57
Vertical Position (Z) in TF CenterStack (meters)
Shear Stress (MPa)at TF CenterStack Outer Edge

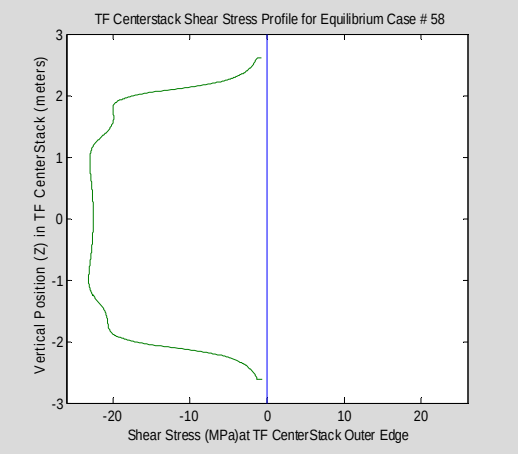
TF Centerstack Shear Stress Profile for Equilibrium Case # 58
Vertical Position (Z) in TF CenterStack (meters)
Shear Stress (MPa)at TF CenterStack Outer Edge

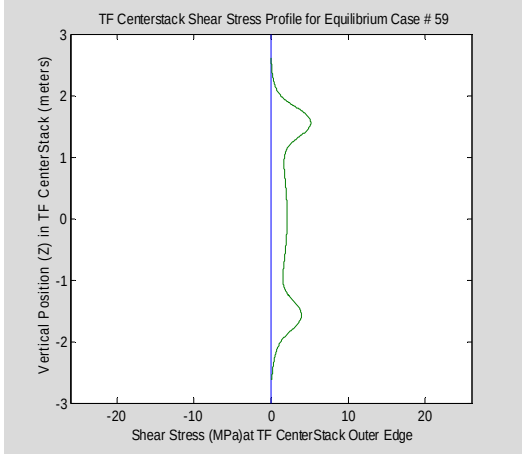
TF Centerstack Shear Stress Profile for Equilibrium Case # 59
Vertical Position (Z) in TF CenterStack (meters)
Shear Stress (MPa)at TF CenterStack Outer Edge

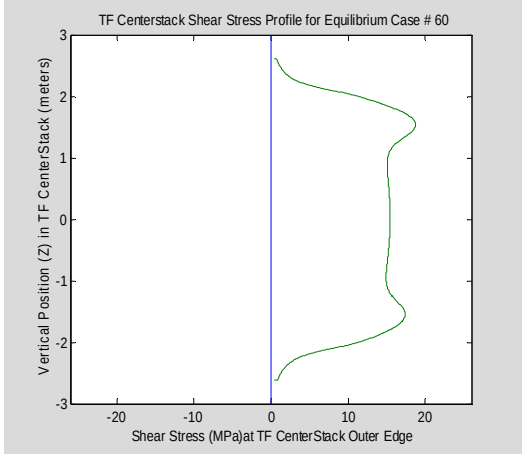
TF Centerstack Shear Stress Profile for Equilibrium Case # 60
Vertical Position (Z) in TF CenterStack (meters)
Shear Stress (MPa)at TF CenterStack Outer Edge

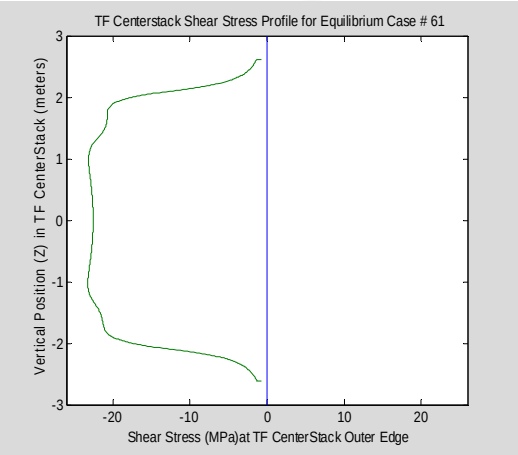
TF Centerstack Shear Stress Profile for Equilibrium Case # 61
Vertical Position (Z) in TF CenterStack (meters)
Shear Stress (MPa)at TF CenterStack Outer Edge

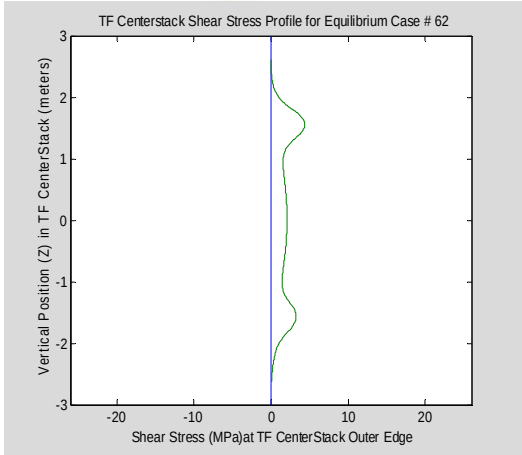
TF Centerstack Shear Stress Profile for Equilibrium Case # 62
Vertical Position (Z) in TF CenterStack (meters)
Shear Stress (MPa)at TF CenterStack Outer Edge

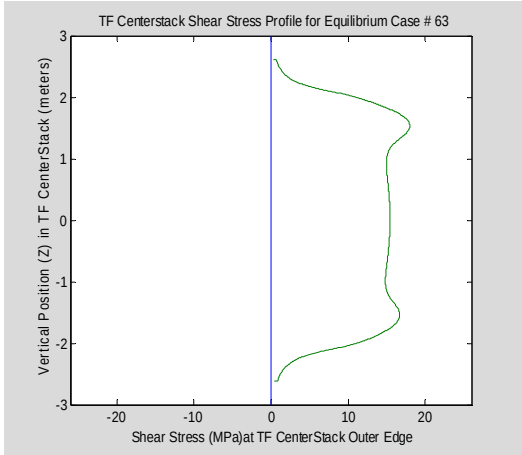
TF Centerstack Shear Stress Profile for Equilibrium Case # 63
Vertical Position (Z) in TF CenterStack (meters)
Shear Stress (MPa)at TF CenterStack Outer Edge

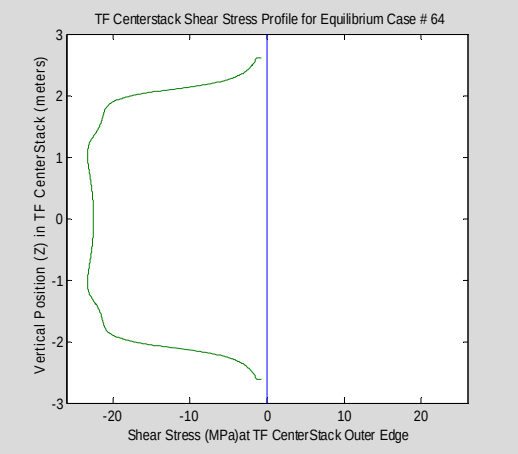
TF Centerstack Shear Stress Profile for Equilibrium Case # 64
Vertical Position (Z) in TF CenterStack (meters)
Shear Stress (MPa)at TF CenterStack Outer Edge

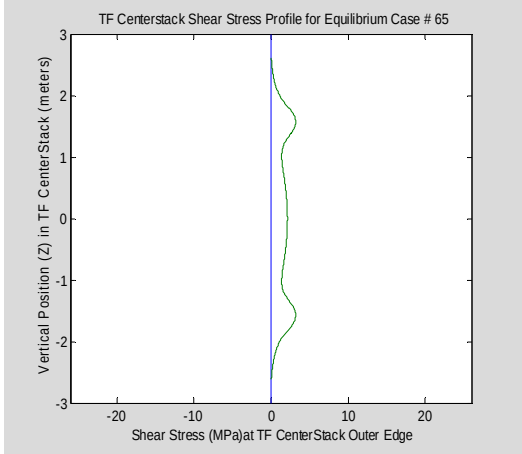
TF Centerstack Shear Stress Profile for Equilibrium Case # 65
Vertical Position (Z) in TF CenterStack (meters)
Shear Stress (MPa)at TF CenterStack Outer Edge

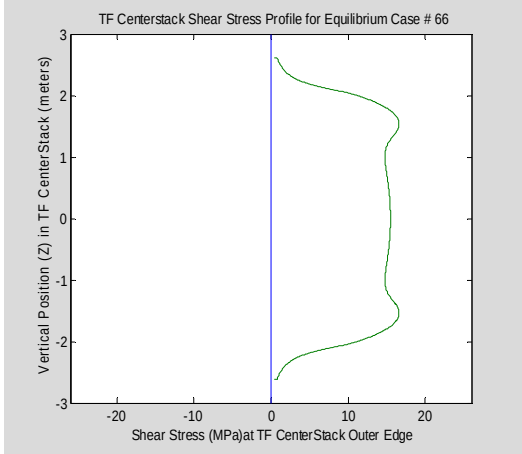
TF Centerstack Shear Stress Profile for Equilibrium Case # 66
Vertical Position (Z) in TF CenterStack (meters)
Shear Stress (MPa)at TF CenterStack Outer Edge

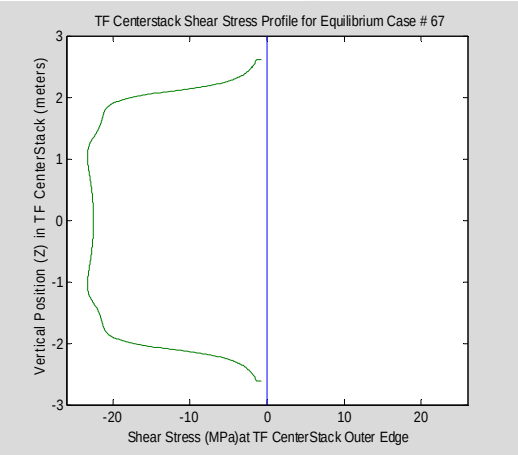
TF Centerstack Shear Stress Profile for Equilibrium Case # 67
Vertical Position (Z) in TF CenterStack (meters)
Shear Stress (MPa)at TF CenterStack Outer Edge

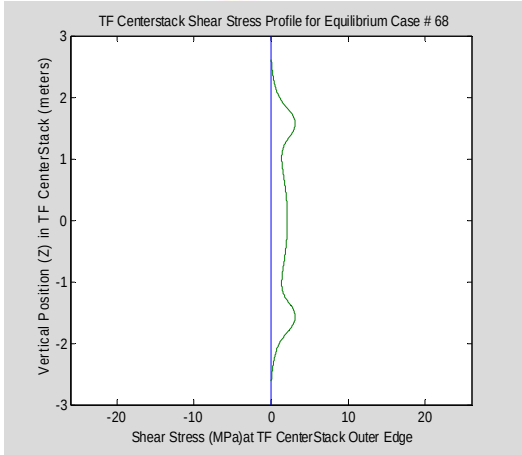
TF Centerstack Shear Stress Profile for Equilibrium Case # 68
Vertical Position (Z) in TF CenterStack (meters)
Shear Stress (MPa)at TF CenterStack Outer Edge

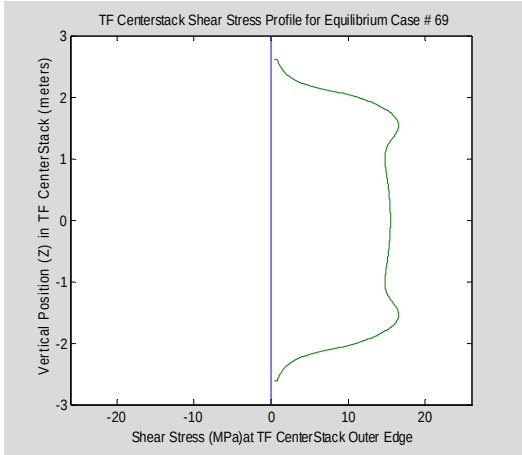
TF Centerstack Shear Stress Profile for Equilibrium Case # 69
Vertical Position (Z) in TF CenterStack (meters)
Shear Stress (MPa)at TF CenterStack Outer Edge

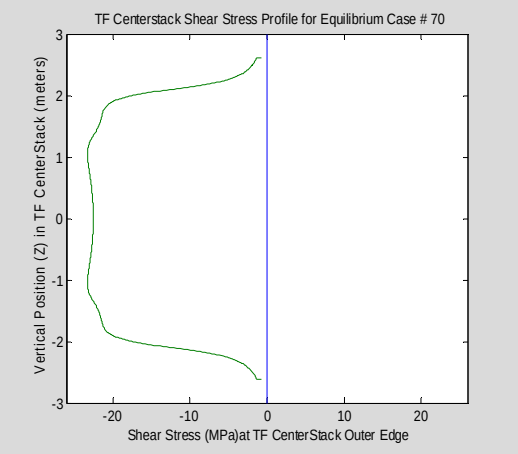
TF Centerstack Shear Stress Profile for Equilibrium Case # 70
Vertical Position (Z) in TF CenterStack (meters)
Shear Stress (MPa)at TF CenterStack Outer Edge

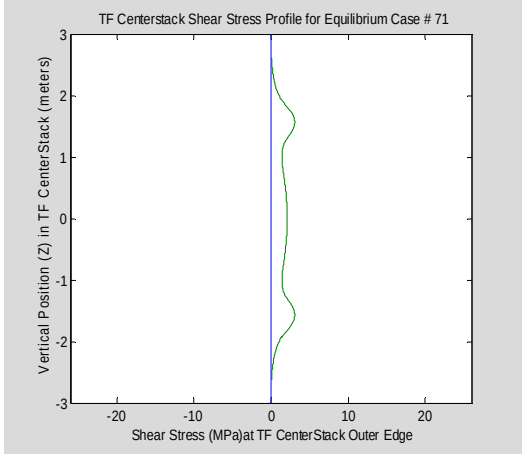
TF Centerstack Shear Stress Profile for Equilibrium Case # 71
Vertical Position (Z) in TF CenterStack (meters)
Shear Stress (MPa)at TF CenterStack Outer Edge

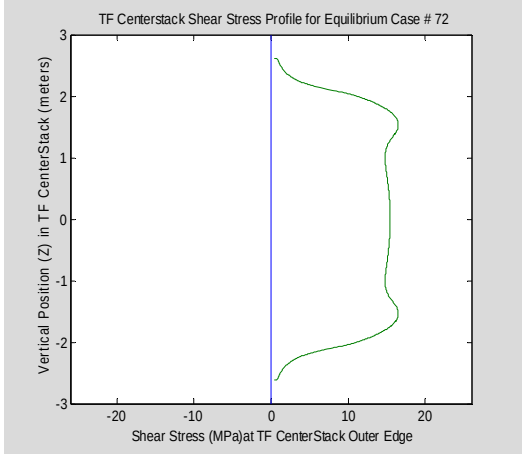
TF Centerstack Shear Stress Profile for Equilibrium Case # 72
Vertical Position (Z) in TF CenterStack (meters)
Shear Stress (MPa)at TF CenterStack Outer Edge

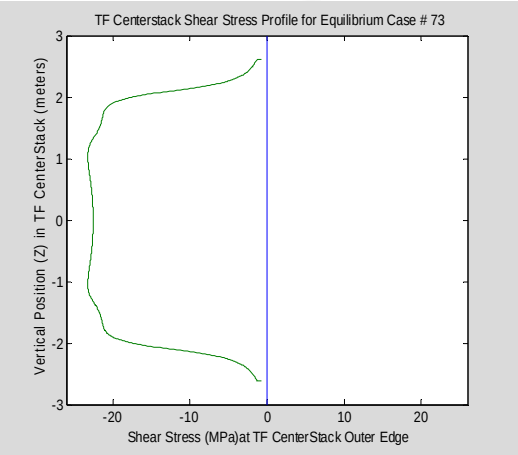
TF Centerstack Shear Stress Profile for Equilibrium Case # 73
Vertical Position (Z) in TF CenterStack (meters)
Shear Stress (MPa)at TF CenterStack Outer Edge

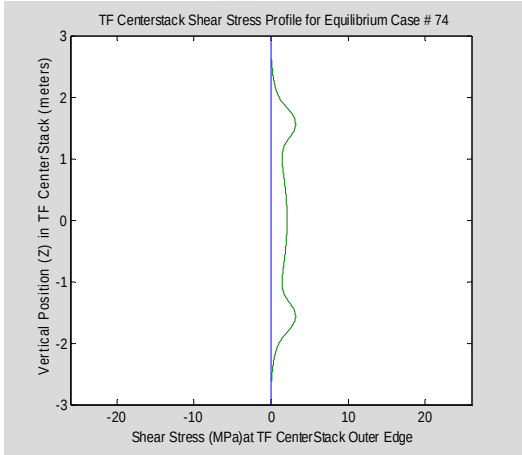
TF Centerstack Shear Stress Profile for Equilibrium Case # 74
Vertical Position (Z) in TF CenterStack (meters)
Shear Stress (MPa)at TF CenterStack Outer Edge

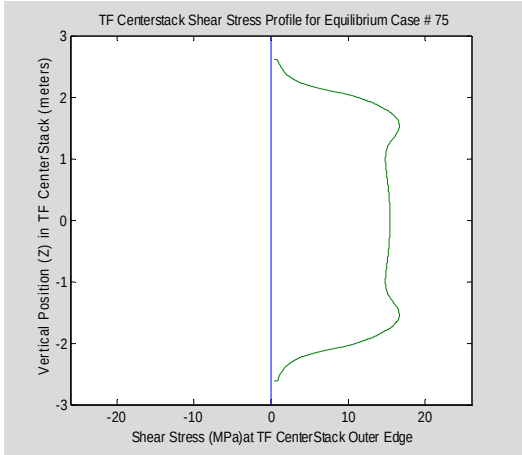
TF Centerstack Shear Stress Profile for Equilibrium Case # 75
Vertical Position (Z) in TF CenterStack (meters)
Shear Stress (MPa)at TF CenterStack Outer Edge

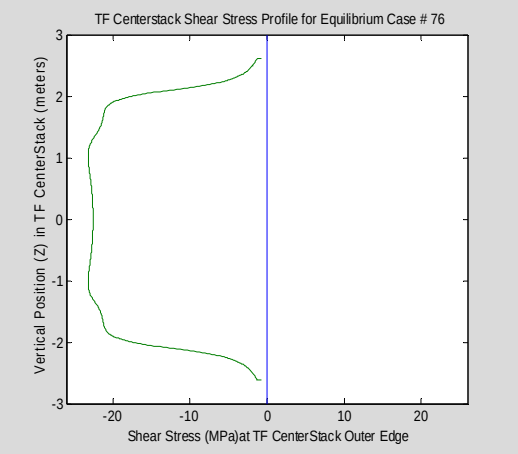
TF Centerstack Shear Stress Profile for Equilibrium Case # 76
Vertical Position (Z) in TF CenterStack (meters)
Shear Stress (MPa)at TF CenterStack Outer Edge

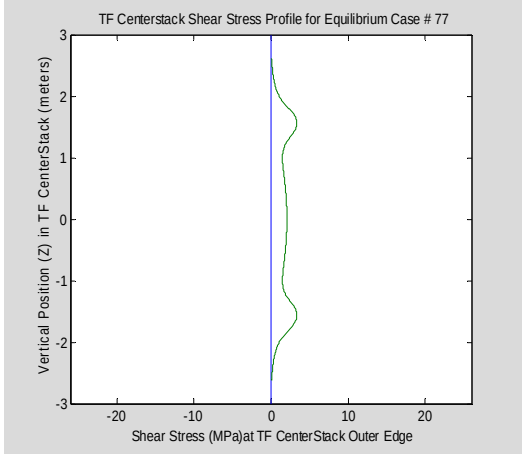
TF Centerstack Shear Stress Profile for Equilibrium Case # 77
Vertical Position (Z) in TF CenterStack (meters)
Shear Stress (MPa)at TF CenterStack Outer Edge

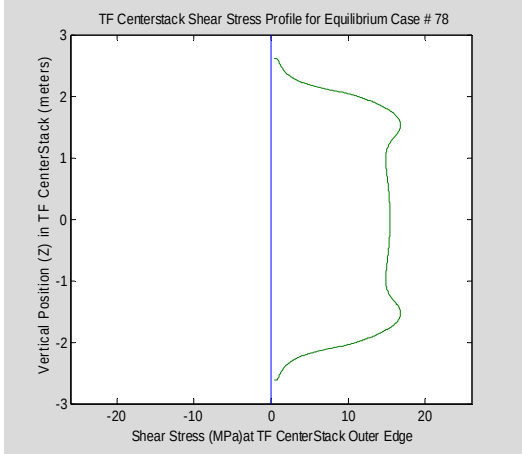
TF Centerstack Shear Stress Profile for Equilibrium Case # 78
Vertical Position (Z) in TF CenterStack (meters)
Shear Stress (MPa)at TF CenterStack Outer Edge

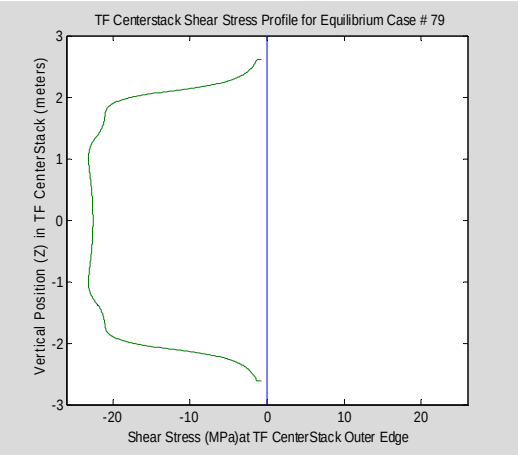
TF Centerstack Shear Stress Profile for Equilibrium Case # 79
Vertical Position (Z) in TF CenterStack (meters)
Shear Stress (MPa)at TF CenterStack Outer Edge

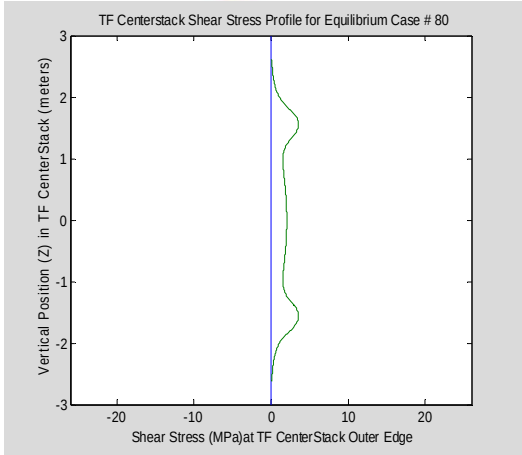
TF Centerstack Shear Stress Profile for Equilibrium Case # 80
Vertical Position (Z) in TF CenterStack (meters)
Shear Stress (MPa)at TF CenterStack Outer Edge

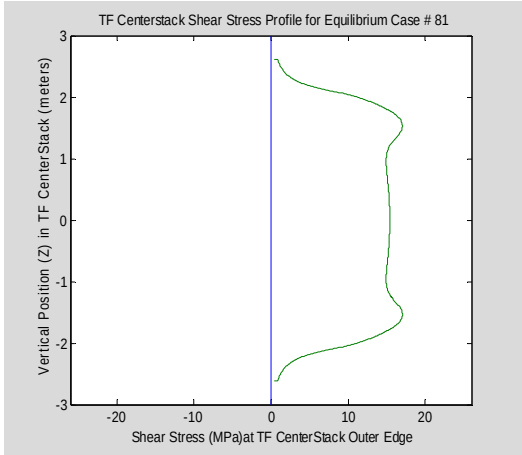
TF Centerstack Shear Stress Profile for Equilibrium Case # 81
Vertical Position (Z) in TF CenterStack (meters)
Shear Stress (MPa)at TF CenterStack Outer Edge

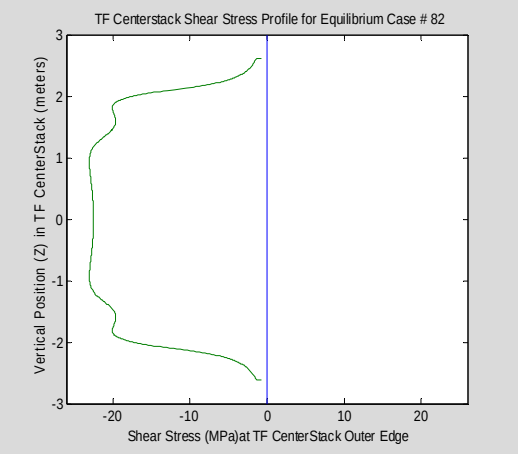
TF Centerstack Shear Stress Profile for Equilibrium Case # 82
Vertical Position (Z) in TF CenterStack (meters)
Shear Stress (MPa)at TF CenterStack Outer Edge

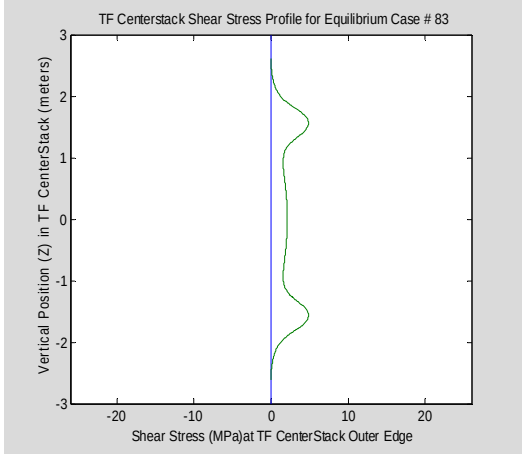
TF Centerstack Shear Stress Profile for Equilibrium Case # 83
Vertical Position (Z) in TF CenterStack (meters)
Shear Stress (MPa)at TF CenterStack Outer Edge

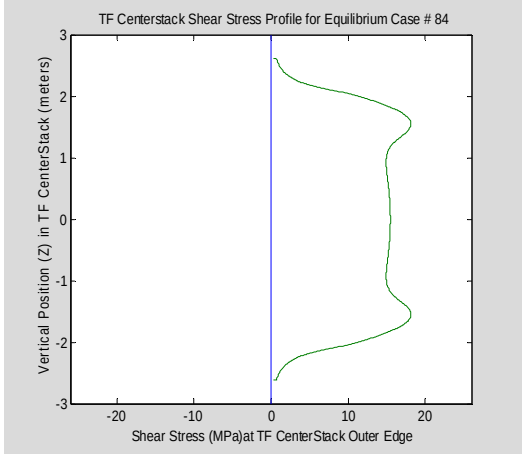
TF Centerstack Shear Stress Profile for Equilibrium Case # 84
Vertical Position (Z) in TF CenterStack (meters)
Shear Stress (MPa)at TF CenterStack Outer Edge

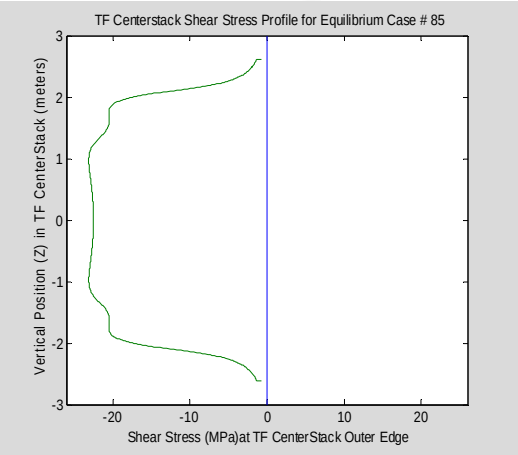
TF Centerstack Shear Stress Profile for Equilibrium Case # 85
Vertical Position (Z) in TF CenterStack (meters)
Shear Stress (MPa)at TF CenterStack Outer Edge

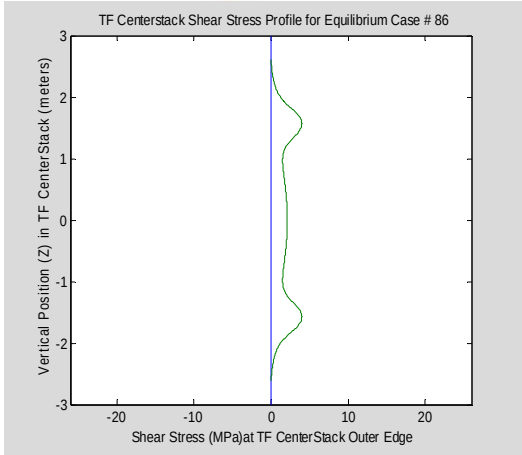
TF Centerstack Shear Stress Profile for Equilibrium Case # 86
Vertical Position (Z) in TF CenterStack (meters)
Shear Stress (MPa)at TF CenterStack Outer Edge

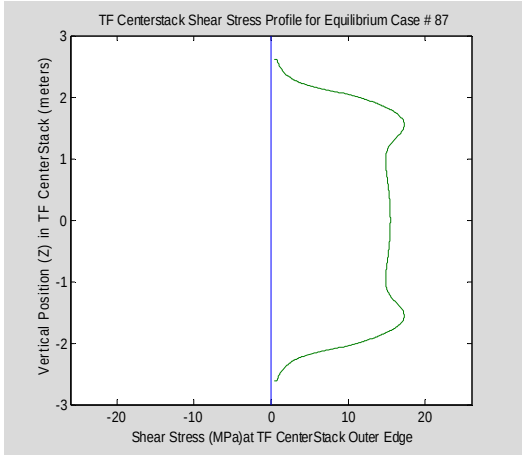
TF Centerstack Shear Stress Profile for Equilibrium Case # 87
Vertical Position (Z) in TF CenterStack (meters)
Shear Stress (MPa)at TF CenterStack Outer Edge

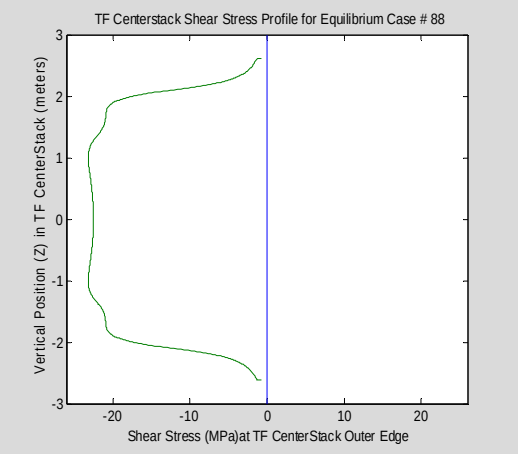
TF Centerstack Shear Stress Profile for Equilibrium Case # 88
Vertical Position (Z) in TF CenterStack (meters)
Shear Stress (MPa)at TF CenterStack Outer Edge

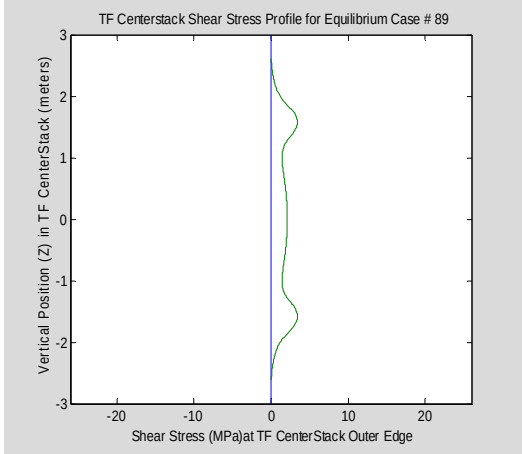
TF Centerstack Shear Stress Profile for Equilibrium Case # 89
Vertical Position (Z) in TF CenterStack (meters)
Shear Stress (MPa)at TF CenterStack Outer Edge

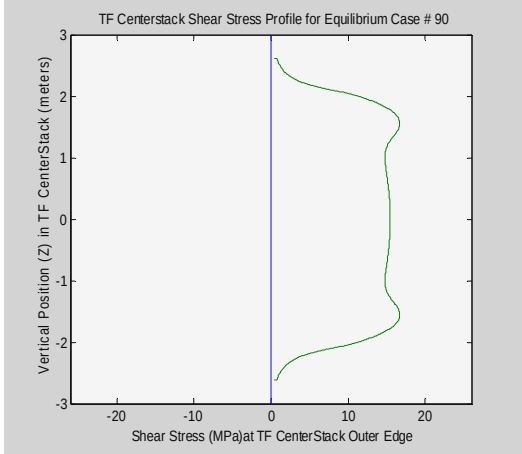
TF Centerstack Shear Stress Profile for Equilibrium Case # 90
Vertical Position (Z) in TF CenterStack (meters)
Shear Stress (MPa)at TF CenterStack Outer Edge

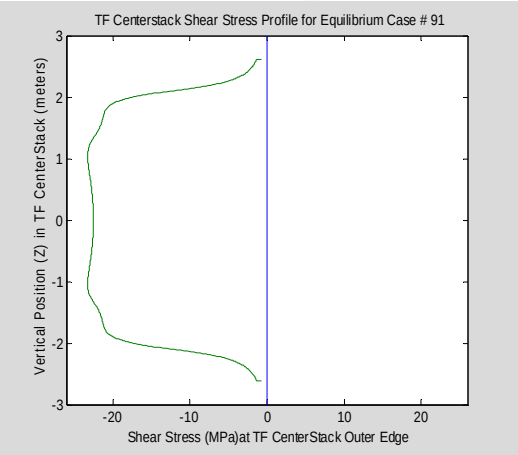
TF Centerstack Shear Stress Profile for Equilibrium Case # 91
Vertical Position (Z) in TF CenterStack (meters)
Shear Stress (MPa)at TF CenterStack Outer Edge

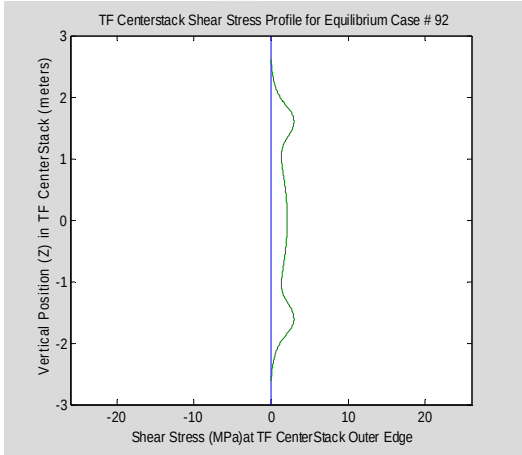
TF Centerstack Shear Stress Profile for Equilibrium Case # 92
Vertical Position (Z) in TF CenterStack (meters)
Shear Stress (MPa)at TF CenterStack Outer Edge

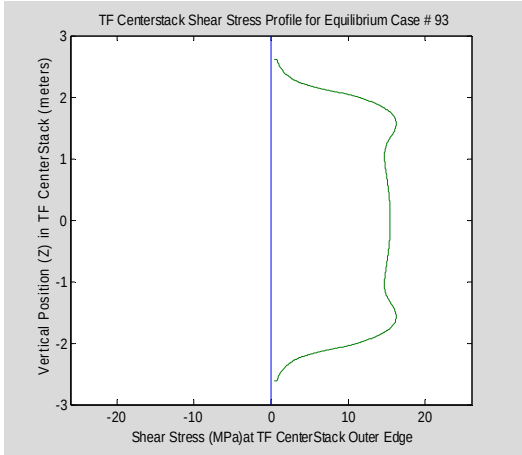
TF Centerstack Shear Stress Profile for Equilibrium Case # 93
Vertical Position (Z) in TF CenterStack (meters)
Shear Stress (MPa)at TF CenterStack Outer Edge

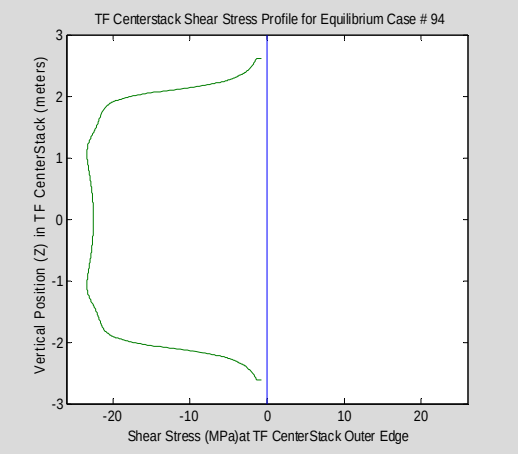
TF Centerstack Shear Stress Profile for Equilibrium Case # 94
Vertical Position (Z) in TF CenterStack (meters)
Shear Stress (MPa)at TF CenterStack Outer Edge

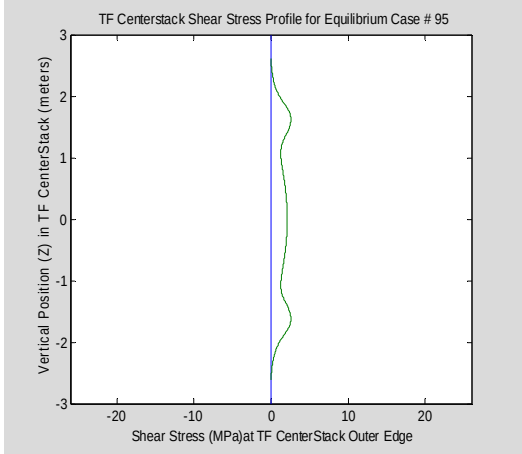
TF Centerstack Shear Stress Profile for Equilibrium Case # 95
Vertical Position (Z) in TF CenterStack (meters)
Shear Stress (MPa)at TF CenterStack Outer Edge

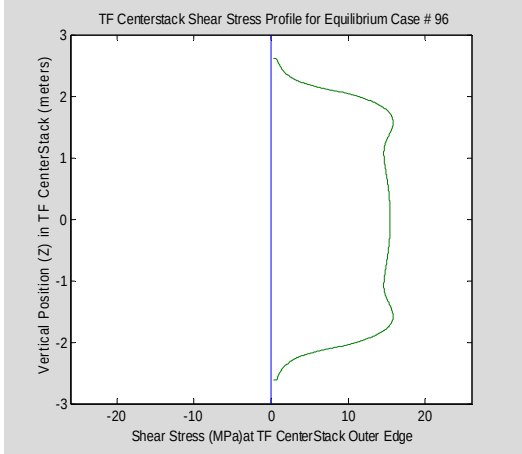
TF Centerstack Shear Stress Profile for Equilibrium Case # 96
Vertical Position (Z) in TF CenterStack (meters)
Shear Stress (MPa)at TF CenterStack Outer Edge

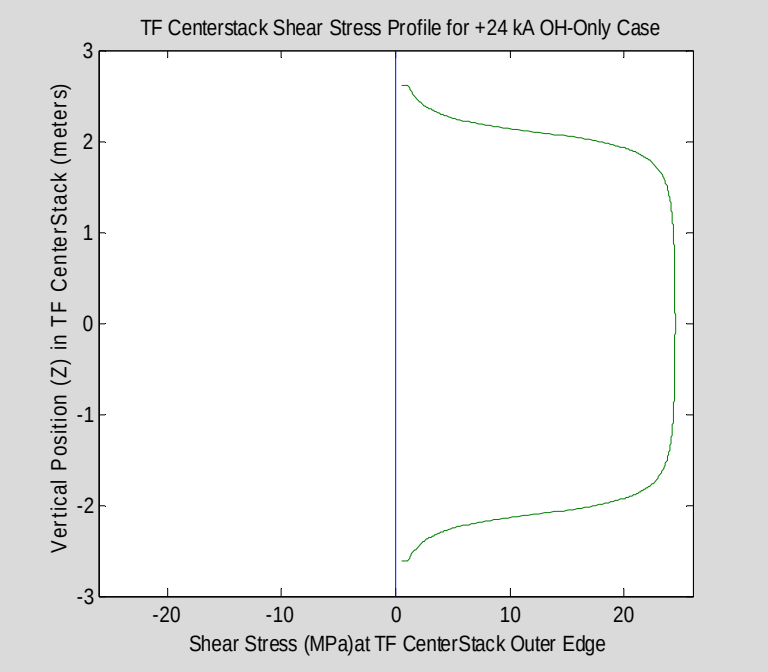
TF Centerstack Shear Stress Profile for +24 kA OH-Only Case
Vertical Position (Z) in TF CenterStack (meters)
3
2
1
0
-1
-2
-3
-20
-10
0
10
20
Shear Stress (MPa)at TF CenterStack Outer Edge

13-180911

To: Distribution Date: 18 September 2011

From: R. Woolley Subject TF Inner Leg Shear Stress in NSTX CSU

References:

1. **R. Woolley memo 13-260709, "Out-Of-Plane (OOP) PF/TF Torques On TF Conductors in NSTX CSU", 26 July 2009,**
2. **P. Titus memo, "Maximum TF Torsional Shear", 29 July 2009**
3. **P. Titus paper, "Provisions for Out-of-Plane Support of the TF Coils in Recent Tokamaks",28September1999**
4. **R. Woolley memo 13-110211, "Torques On TF Conductors & Resulting Torsion & Shear Stress in NSTX CSU, 04May2010 Design Point", 11 February 2011**
5. **P. Titus, NSTXU*-CALC-132-07-00 Rev0, "TF Inner Leg Torsional Shear, Including Input to the DCPS", 9Sept2011**

Summary

This memo replaces Ref.4. It results from my review of P. Titus' Ref.5 and comparisons of its predicted shear stress results with those of my own Ref.4 analyses. Findings are as follows:

(1) Ref.5 is confirmed as following correct calculation methods and should therefore be just as accurate as the Global Model on which it is based. (The Global Model review is by others.)

(2) My Ref.4 calculations contained an error which had the effect of underestimating structural supporting torques, thus resulting in distorted torsional shear distributions within the TF inner leg. The present memo corrects this error (see Eqs.27) and documents the resulting shear stress distributions for NSTX-U's 96 prescribed plasma equilibria and for its OH precharge condition.

(3) Maximum local shear stress (a) occurs when PF coil currents are combined with maximally negative OH current, and (b) are spatially localized in small regions near the ends of the inner leg before reaching the lead extensions. This qualitatively matches the behavior predicted in Ref.5.

(4) Peak local shear stress of **25.234 MPa** is predicted for equilibria #1 and #16, using nominal stiffness parameters estimated for the NSTX design as of December 2010. (Note that this peak value only applies at a point location; any finite region has a lower average.) The 97 shear stress distributions for the inner leg are documented in Appendix 2 (i.e., page 50).

(5) An effort was undertaken to investigate whether deliberate changes in stiffnesses could reduce peak torsional shear stress. It was found that ***reduction in stiffness*** of either umbrella lid reduces peak inner leg shear. For example, a 95% reduction of upper lid stiffness reduces peak local shear stress in the inner leg by 22.5% to **19.553 MPa**. The 97 shear stress distributions for the inner leg with this reduced upper lid stiffness are documented in Appendix 3 (i.e., page 70).

As in Ref.4, this memo advances and uses a simple algorithm based on magnetic flux differences for evaluating out-of-plane torques due to magnetic interactions of poloidal magnetic fields with TF conductor current. This is the subject of Appendix 1 (i.e., page 42). The torsional elastic response model is the subject of pages 2-40. Analysis results are discussed on page 41.

As in Refs.1 & 4, the NSTX CSU TF conductor shape definition was provided by Peter Titus on 26 June 2009 in a file containing XYZ 3D coordinates of 4229 nodal points delimiting hexahedral elements in a 30 degree sector global TF model. These were subsequently culled and sorted by various automated MATLAB methods to obtain a poloidal half-plane outline consisting of 322 points, including an inner outline trace of 159 points and an outer outline trace of 163 points. These points were only modified from the provided file by setting their third coordinate values to zero without changing their other two coordinates. The resulting TF conductor outline appears in the following Fig.(1) MATLAB plot.

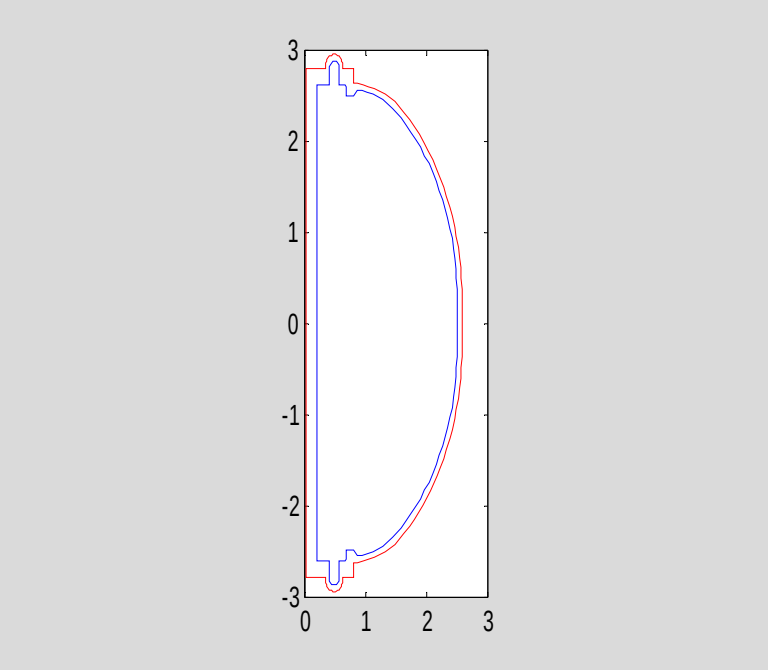

Figure 1: Poloidal Projection Outline of TF Conductor, 322 points

Parametric variables were then calculated and saved for each point in each of the two outline traces, starting from zero at their radially inner points on the (z=0) horizontal midplane and adding the distances to each successive point while proceeding in the counterclockwise direction. After returning to the starting points, the saved parametric values were then normalized by dividing each cumulative distance value by its contour's total perimeter length. The resulting parametric variables, which range from 0 to 1, roughly represent poloidal angle.

Finally, 2000 uniformly spaced values of this poloidal angle variable ranging from 0 to 1 were generated and 2000 corresponding r and z coordinate values were obtained for each of the TF coil's inner and outer outline curves by using MATLAB's standard interpolation m-file subroutines. The two resulting 2000-point outlines are plotted below in Fig. (2). Note that although they appear almost identical to the previous TF outline plot, each outline here consists

of 2000 equally spaced points which are now linked to each other through their common normalized poloidal "angle" location parametric variable values. In each contour of this model, node point number 1 is also number 2000, located at Z=0 in the TF centerstack. Constant radius points on the centerstack's outer edge include 1 through 363 at the bottom and from 1638 at the top through 2000. TF leads extending to the flexes encompass nodes out to 371 and to 1630.

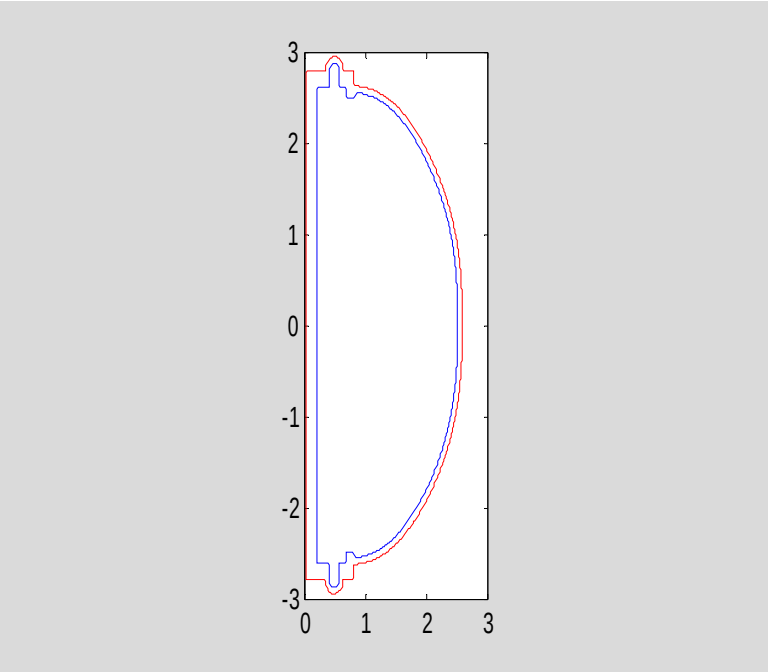

Figure 2: Poloidal Projection Outline of TF Conductor, 4000 points

Note that the TF current stream function which varies with the (r,z) location in the poloidal half-plane is defined as the total TF system current that passes through the 3D circle sharing those cylindrical coordinates. It varies from zero at (r,z) locations not linking the TF coils to the total TF current (i.e., number of turns times current per turn) at locations within the TF coil system bore. At intermediate locations within the TF conductor it varies between those values. Level set contours of the TF current stream function are also streamlines of the TF current flow.

As plotted, the (red) outer outline is the zero value contour of the TF current stream function and the (blue) inner outline is the contour of the TF current stream function at its full, 100% of TF system current, value. It was decided for calculations herein to try to improve accuracy by estimating how the TF current is distributed within the TF conductor. This was done by estimating the (r,z) coordinate locations at each of 2000 poloidal variable points for TF current stream function contours enclosing 25%, 50%, and 75%, respectively, of the total TF current. Ideally these contour estimates would be obtained by solving conductive media equations using

ohms law, but this was not done. Instead, the estimated contours were obtained by interpolation between the outline coordinates for common poloidal angle variables. For the vertical (z) coordinates, linear interpolation was used directly. However, a different method was used to interpolate the r coordinate since conductor thickness in the toroidal direction varies in proportion to r for locations in and near the TF central bundle but takes on constant thickness for outer locations. Linear interpolation of a nonlinear function was used, where that function switched from a quadratic for inner locations to a straight line for outer locations. For this purpose the switchover radius between variable and constant toroidal thickness was estimated as r=0.3339 meters, based on inspection of plots showing the 4229 points of the global model.

The Fig.(3) plot follows showing the resulting estimated three internal contours and the two bounding contours of the TF current stream function.

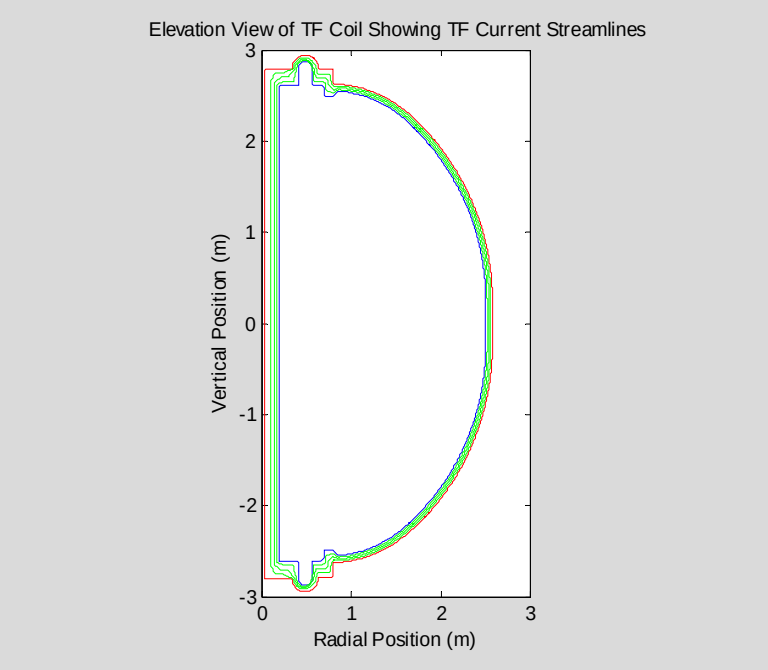

Figure 3: Poloidal Projection of TF Current Stream Function Contours, 10000 points

It may be useful to have plots showing r and z for the bounding outlines and internal contours as functions of the poloidal angle parametric variable. These follow:

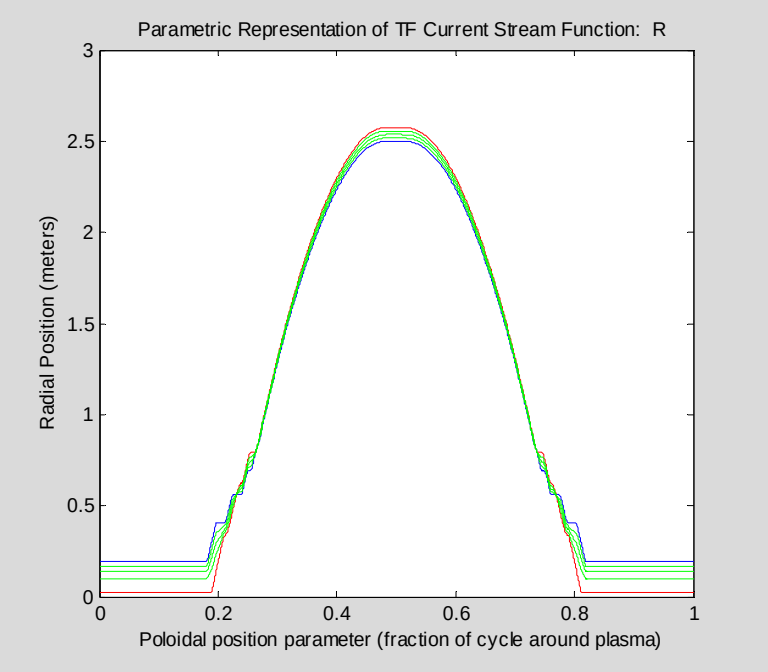

Figure 4: Radial Coordinates of TF Current Stream Function Contours vs Poloidal Variable

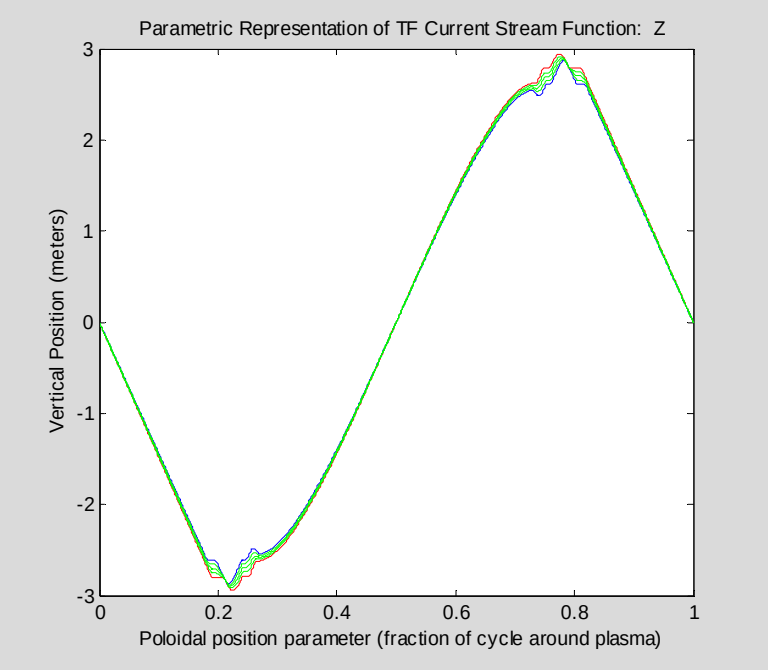

Figure 5: Vertical Coordinates of TF Current Stream Function Contours vs Poloidal Variable

The magnetics designs assumed herein for the OH coil and for the six coils, PF1AU, PF1BU, PF1CU, PF1CL, PF1BL, and PF1AL were adopted 04May2010. Later changes have been minor, and have not been explicitly addressed. Details of the poloidal field system for the 04May2010 design point have been reproduced here as Table 1 and are depicted in Fig.6. These include 23

coil windings that are configured into 13 series-connected circuits. They also include a crude. approximate magnetics model representing the plasma as a rectangular cross section uniform current density single-turn coil winding.

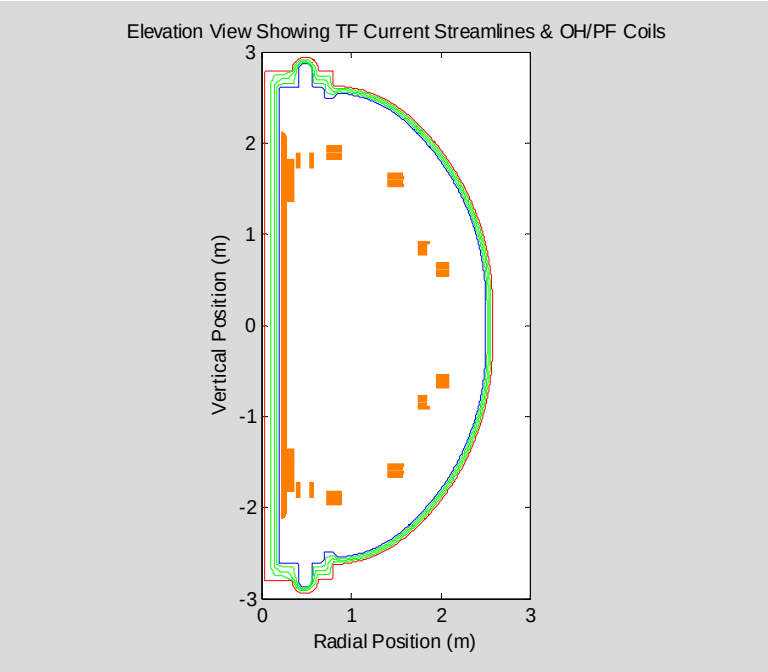

Figure 6: Poloidal Projection of PF&OH coils, with TF Current Stream Function Contours

Table 1: 04May2010 Design Point Poloidal Field System for PF Coils, OH Coil, Plasma (As Used For Magnetics Calculations)

Coil Power	Series-connected Winding Geometry					Rectangular Matrix of Turns		
Circuit Name	Rectangular Winding Name	R (center) cm	ΔR cm	Z (center) cm	ΔZ cm	# in z direction	# in r direction	Total # turns
PF1AU	PF1AU	31.93	5.9268	159.06	46.3533	16	4	64
PF1BU	PF1BU	40.038	3.36	180.42	18.1167	16	2	32
PF1CU	PF1CU	55.052	3.7258	181.36	16.6379	10	2	20
	PF2AU	79.9998	16.2712	193.3473	6.797	2	7	14
PF2U	PF2BU	79.9998	16.2712	185.26	6.797	2	7	14
	PF3AU	149.446	18.6436	163.3474	6.797	2	7.5	15
PF3U	PF3BU	149.446	18.6436	155.26	6.797	2	7.5	15
	PF4BU	179.4612	9.1542	80.7212	6.797	4	2	8
	PF4CU	180.6473	11.5265	88.8086	6.797	2	4.5	9
	PF4BL	179.4612	9.1542	-80.7212	6.797	4	2	8
PF4	PF4CL	180.6473	11.5265	-88.8086	6.797	2	4.5	9
	PF5AU	201.2798	13.5331	65.2069	6.858	2	6	12
	PF5BU	201.2798	13.5331	57.8002	6.858	2	6	12
	PF5AL	201.2798	13.5331	-65.2069	6.858	2	6	12
PF5	PF5BL	201.2798	13.5331	-57.8002	6.858	2	6	12
	PF3BL	149.446	18.6436	-155.26	6.797	2	7.5	15
PF3L	PF3AL	149.446	18.6436	-163.347	6.797	2	7.5	15
	PF2LA	79.9998	16.2712	-193.347	6.797	2	7	14
PF2L	PF2LB	79.9998	16.2712	-185.26	6.797	2	7	14
PF1CL	PF1CL	55.052	3.7258	-181.36	16.6379	10	2	20
PF1BL	PF1BL	40.038	3.36	-180.42	18.1167	16	2	32
PF1AL	PF1AL	31.93	5.9268	-159.06	46.3533	16	4	64
OH	OH	24.2083	6.934	0	424.16	221	4	884
PLASMA	PL	107.000	110.000	0.000	200.000	1	1	1

Next, poloidal flux was calculated for each of the 2000 locations on each of the five contours for each of the 13 coil circuits and for a crude electromagnetic model of a "plasma" having uniform current density and a rectangular cross section extending over $0.52<r<1.63$ and $-1<z<1$, all in meters. Plots of the computed poloidal magnetic fluxes appear below in Figs.(7)-(11).

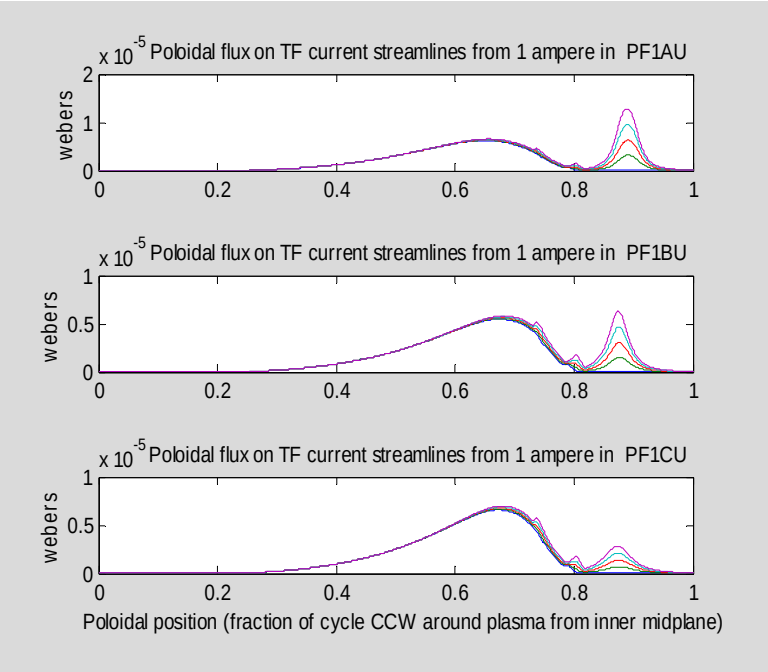

Figure 7: Poloidal Flux Per Ampere Excitation in Circuits 1-3

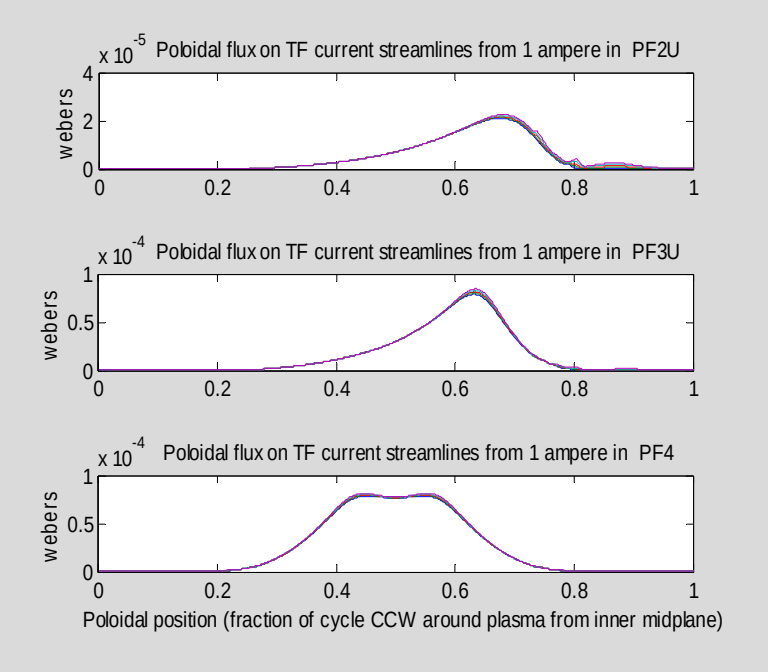

Figure 8: Poloidal Flux Per Ampere Excitation in Circuits 4-6

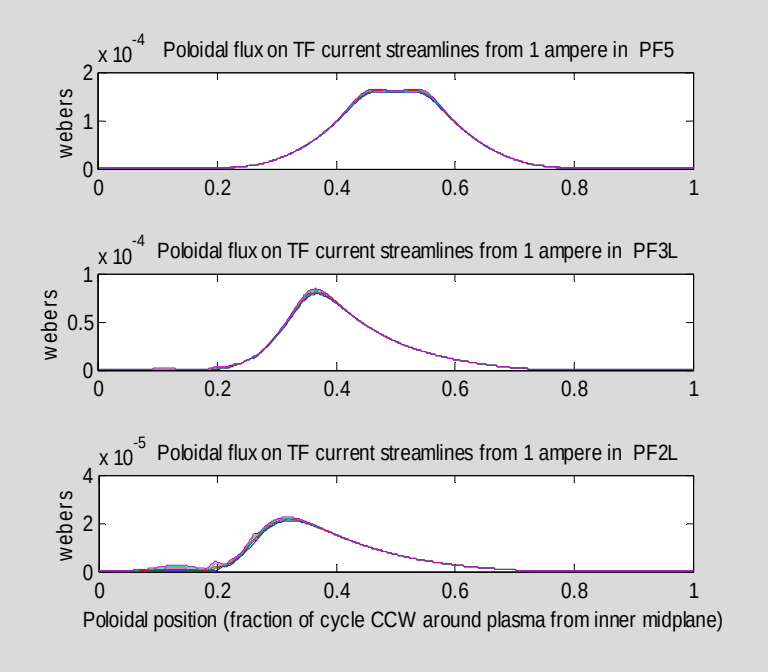

Figure 9: Poloidal Flux Per Ampere Excitation in Circuits 7-9

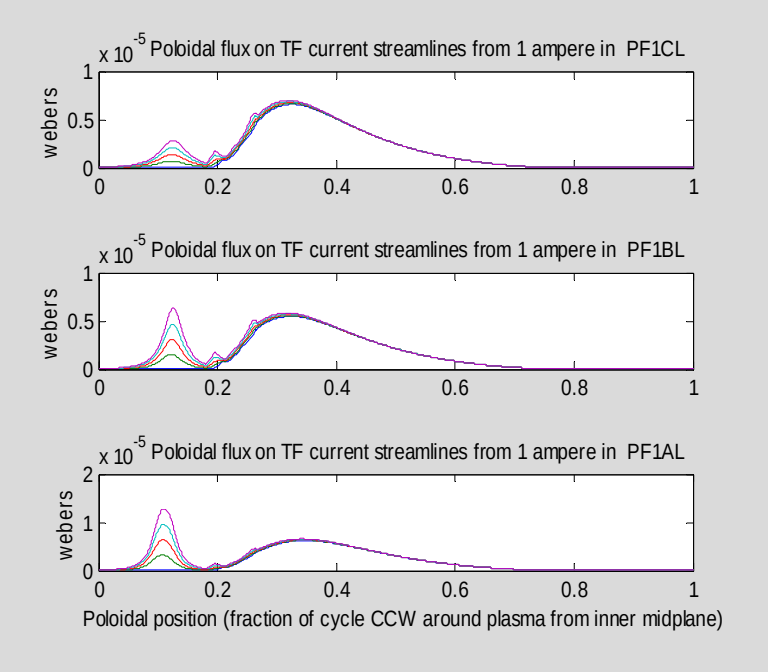

Figure 10: Poloidal Flux Per Ampere Excitation in Circuits 10-12

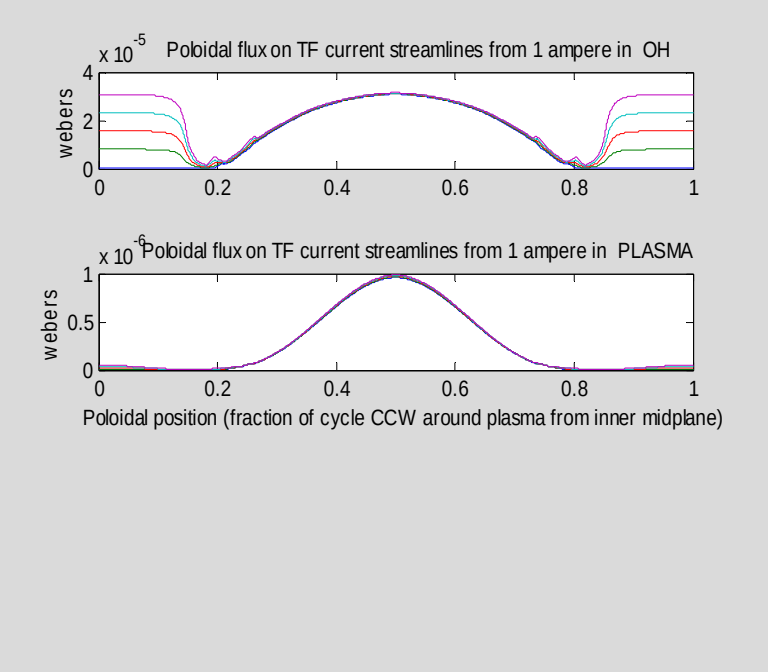

Figure 11: Poloidal Flux Per Ampere Excitation in Circuits 13-14

For each coil circuit, the mean flux was next calculated for each poloidal location as a weighted average of the flux values on the five current stream function contours, using weighting factors [0.125 0.25 0.25 0.25 0.125]. Local torque densities per ampere of circuit current are then evaluated as the product of total TF current times the finite difference derivative with respect to the poloidal angle variable of the mean flux divided by 2π. The resulting profiles were multiplied respectively by the Table 2 maximum and minimum circuit currents to establish the ranges of torque densities versus poloidal locations. Results appear in Figs.12-16.

Table 2: Coil And Plasma Current Ranges Assumed for Torque Load Range Calculations

COIL CIRCUIT NAME	MINIMUM CURRENT (Amperes)	MAXIMUM CURRENT (Amperes)
'PF1AU'	-7000	18000
'PF1BU'	0	13000
'PF1CU'	0	16000
'PF2U'	-11000	15000
'PF3U'	-16000	12000
'PF4'	0	16000
'PF5'	0	34000
'PF3L'	-16000	12000
'PF2L'	-11000	15000
'PF1CL'	0	16000
'PF1BL'	0	13000
'PF1AL'	-7000	18000
'OH'	-24000	24000
'PLASMA'	0	2000000

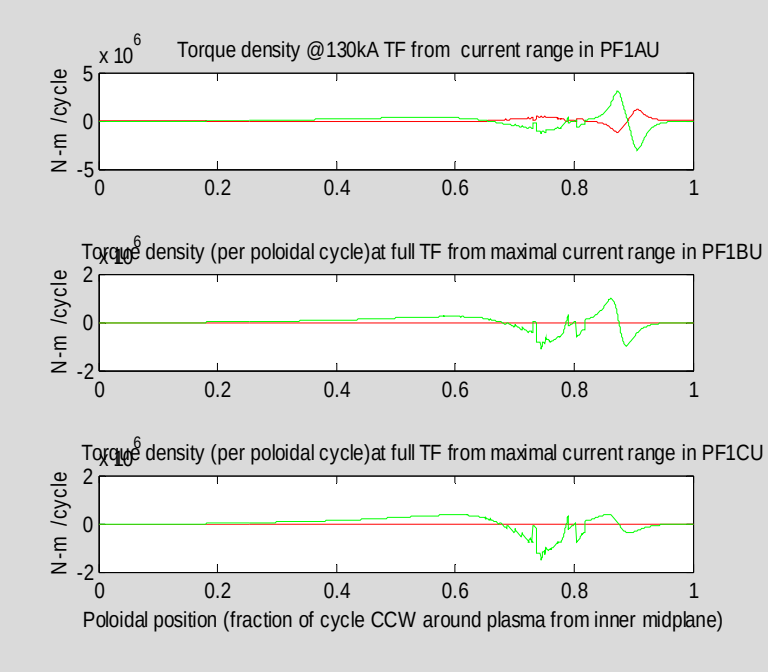

Figure 12: Torque Density For Maximal Range of Currents in Circuits 1-3

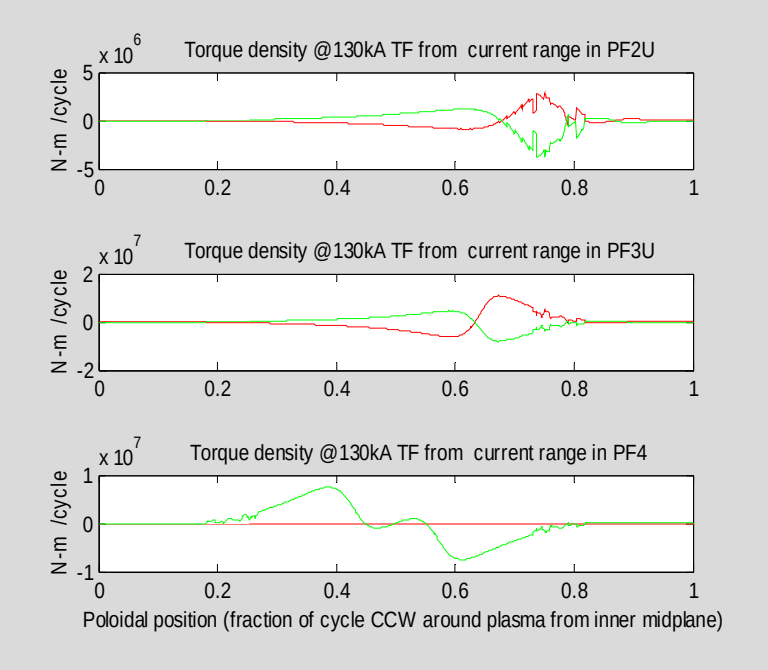

Figure 13: Torque Density For Maximal Range of Currents in Circuits 4-6

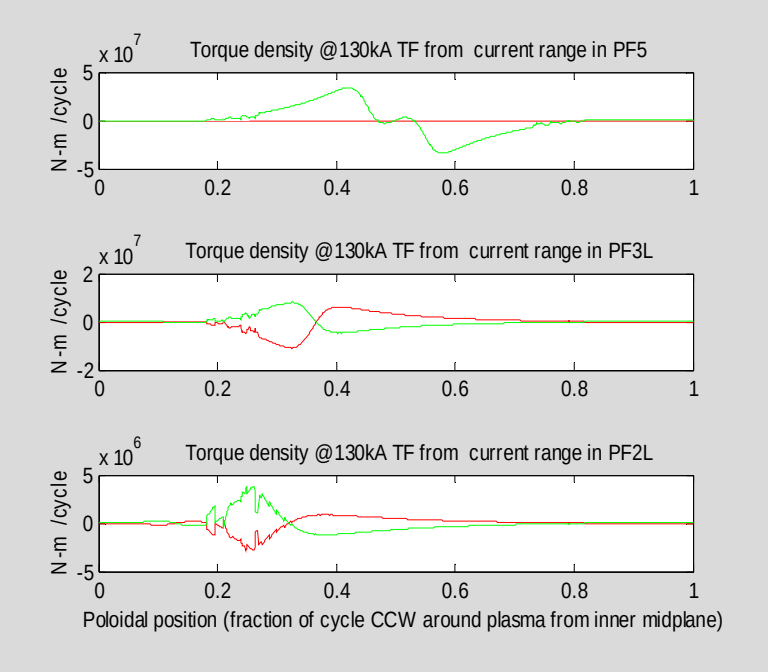

Figure 14: Torque Density For Maximal Range of Currents in Circuits 7-9

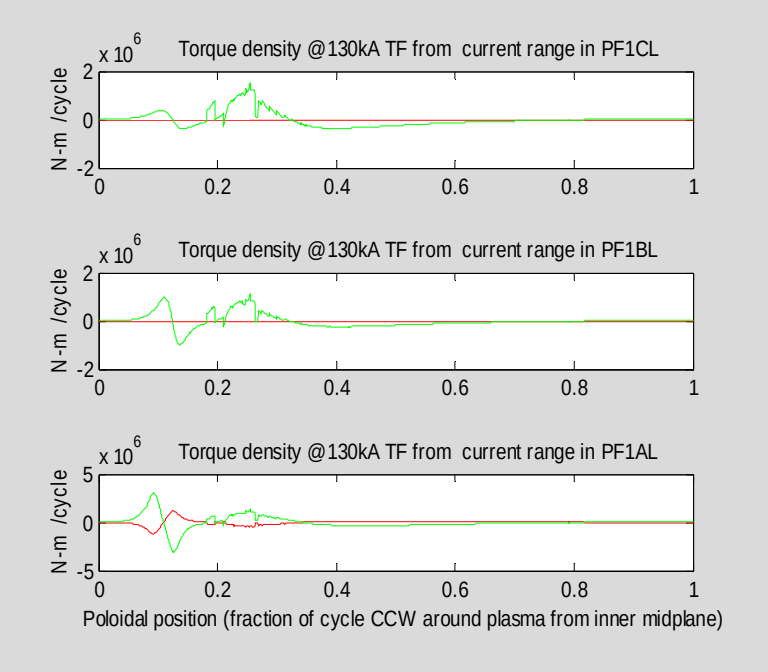

Figure 15: Torque Density For Maximal Range of Currents in Circuits 10-12

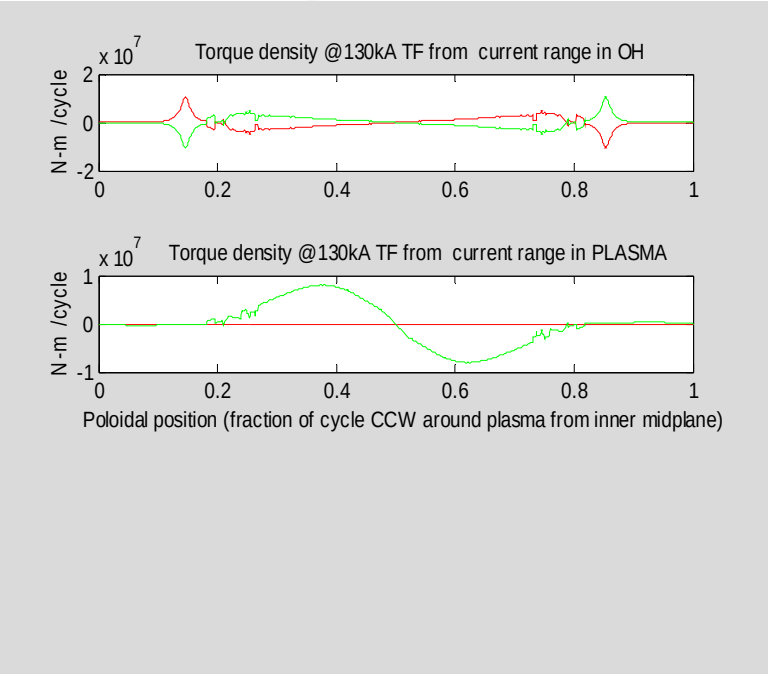

Figure 16: Torque Density For Maximal Range of Currents in Circuits 13-14

TORSIONAL RESPONSE ALGORITHMS: Overview

Although magnetic Lorenz torque loading on the TF coil system is completely determined by its electrical currents and magnetic fields, the torsion response of the system also reflects the mechanical propagation of torques and rotational deflections between different conductor assemblies and structural supports. The ***internal torque*** state at any imaginary section cut through the TF conductor system is defined as the external torque that would need to be applied to one side of that cut to maintain its mechanical equilibrium. This torque is oppositely directed for the two sides of the cut, so by convention the cut side in the direction of node numbering advancement around the TF loop is used herein. Maximum shear stress in a section through elastic material is directly proportional to the internal torque state, so this quantity is of special interest. The complete torsion model predicts the distribution of internal torque along with associated small rotational deformations. That necessarily includes the structural support torques and the resulting torsional shear stresses. The model includes, in addition to the distributed current-dependent Lorenz torque loads, the various torsion spring stiffnesses and interconnections that are relevant to rotational deformations.

Since force and torque equilibrium necessarily exist throughout the entire TF system, it follows that the difference in internal torque states between any two sections through the TF conductors is equal to the total external torque acting on the TF conductor region between them. Between the upper and lower leads of the TF centerstack there are no connections able to mechanically transmit torque, so within this region the profile of internal torque state vs location is equal to an additive torque constant plus the electromagnetic torque loading distribution described earlier in this memo. The additive torque constant depends on torsion spring responses of the entire TF conductor and support system, while the electromagnetic torque loading distribution is a known function of currents and position only, independent of any torsion spring responses.

The model approach taken employs the toroidal membrane methods advanced in section VII of Peter Titus' 1999 paper, but extends it in certain ways. For the centerstack portion of the TF system, torsion formulae for thick-walled tubular shafts are used instead of thin-walled approximations. More significantly, discrete mechanical springs augmenting the toroidal membrane model are used to represent effects on the TF conductor system of additional external mechanical support structures and interconnections. These springs include upper and lower umbrella lids together with their ties to the upper and lower umbrella structures, the upper and support rod connections between TF conductor outer legs and the vacuum vessel, the vacuum vessel itself, and the mechanical connections between the vacuum vessel through its gravity support legs to the floor and up through the pedestal pad supporting the TF centerstack. These additional modeled springs are interconnected with each other outside the modeled toroidal membrane and are attached to the toroidal membrane at specific poloidal nodes. Important node numbers in the toroidal membrane model are listed in Table 3 and their locations are depicted in Fig.17.

Table 3: Important Nodes in Toroidal Membrane Model of TF System Conductors

Node Number	R (m)	Z (m)	Importance
1	0.1942	0	Starting node in centerstack's middle
363	0.1942	-2.6000	Bottom of centerstack's straight section
371	0.2450	-2.6067	Bolts Attaching Stepped G10 Ring to Lower SplineLid
383	0.3312	-2.6067	End of Toroidally Continuous TF Lead Conductors
513	0.6923	-2.4916	TF Outer Leg's Lower End
566	1.0489	-2.5165	TF Outer Leg Clamped to Lower Umbrella Structure
838	2.3411	-1.1489	TF Outer Leg Clamp to Rods Connecting to Vacuum Vessel
1163	2.3411	1.1489	TF Outer Leg Clamp to Rods Connecting to Vacuum Vessel
1435	1.0489	2.5165	TF Outer Leg Clamped to Upper Umbrella Structure
1488	0.6923	2.4916	TF Outer Leg's Upper End
1618	0.3312	2.6067	End of Toroidally Continuous TF Lead Conductors
1630	0.2450	2.6067	Bolts Attaching Stepped G10 Ring to Upper SplineLid
1638	0.1942	2.6000	Top of centerstack's straight section
2000	0.1942	0	Ending node in centerstack's middle

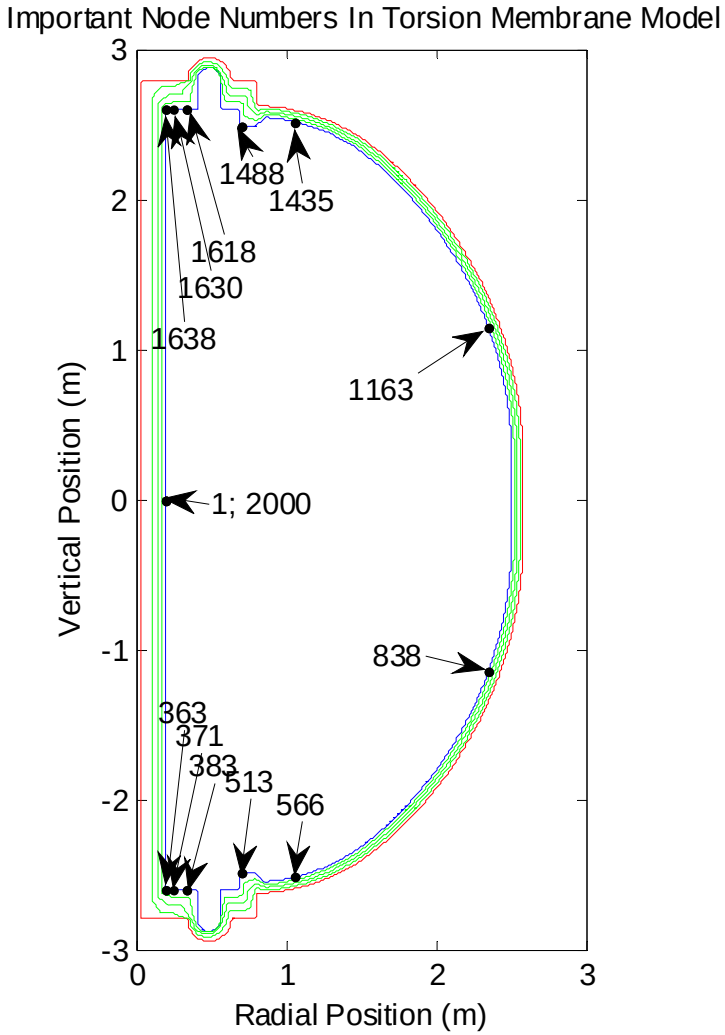

Figure 17: Important Node Numbers in the TF Conductor's Toroidal Membrane Model

The constant-radius portion of the centerstack TF is represented by node numbers 1 through 363 which extend vertically from the centerstack's middle to its bottom of its constant-radius part, and by node numbers 1630 through 2000 which extend vertically from the top of the centerstack's constant-radius part to its middle, where it started at node 1. The centerstack's lower TF lead extensions are node numbers 364 through 383 and its upper TF lead extensions are node numbers 1618 through 1637. The remaining nodes, 384 through 1617, represent the TF outer leg, the TF radial conductors, and the TF flex loops which connect to the centerstack's lead extensions. Electrical connections between the lower and upper ends of each TF outer leg and the lower and upper TF radials are located respectively at node numbers 513 and 1488, each at r=0.6923 meters.

External interconnection paths modeled via discrete torsional springs include the following:

(1) From the upper TF outer legs at node 1435 clamped by a split aluminum block to the vacuum vessel's upper umbrella, to the upper umbrella's bolted lid, radially inwards though the lid to an upper inner bolt plate, then to an annular "crown" disk insulator locked by tight-fitting radial pins to the centerstack's upper leads at node 1630.
(2) The vertical mirror image of (1) on the bottom, i.e., from the lower TF outer legs clamped to the vacuum vessel's lower umbrella at node 566, to its bolted lid, radially inwards to the lower inner bolt plate and insulating "crown" annulus, then to the centerstack's lower leads at node 371.
(3) From the TF outer legs just above horizontal mid-plane ports at node 1163, through rod connections to clevises mounted on the vacuum vessel. The vacuum vessel's upper dome continues this path to the upper umbrella legs then to TF conductor node 1435.
(4) The vertical mirror image of (3) below the midplane, i.e., from the outer legs just below mid-plane ports at node 838, through connecting rods to aa clevis connected to the vacuum vessel, then through the vesse's lower dome, umbrella legs and Aluminum block clamp to node 566.
(5) From node 838 through lower clevis rods, through the vacuum vessel's cylindrical middle section to upper radius rods connections to node 1163.
(6) From the lower vacuum vessel through its mounting legs to the floor, then up through the centerstack's lower pedestal pad support, meeting the centerstack at node 363.

Of primary interest in the investigations for which this torsion model may be applied is how shear stress is distributed within the CenterStack (i.e., the central bundle of turns) portion of the TF system, i.e., in the TF centerstack, since the interturn insulation there must withstand peak values of this stress. Although this is primarily affected by the electromagnetic Lorenz torques

directly acting on the TF centerstack, it is also partly dependent on the structures outside the centerstack since mechanical connections with the TF centerstack at its top and bottom allow mechanical transfer of torques there.

TORSIONAL SPRING STIFFNESS FORMULAE

For toroidally continuous portions of a TF conductor system resembling a thin membrane, it is appropriate to model the local rotational deflection due to torsion as follows:

$$\frac{d\phi}{ds} = \frac{T}{2\pi r^3 tG} \tag{3}$$

where

s represents the independent variable representing poloidal location in the toroidal membrane as a curvilinear distance measured in the membrane's poloidal (r,z) halfplane projection from an arbitrarily chosen reference location on the membrane,

$\phi(s)$ represents the azimuthal (i.e., toroidal) rotation angle at poloidal location s due to torsion,

$\frac{d\phi}{ds}$ is the density of that torsional rotation deflection at location s, that is, the rate of deflection angle increase per unit change in poloidal location,

$T(s)$ is the local internal torque state in the TF membrane conductor at poloidal location s,

G, is the shear modulus of the membrane material,

$r(s)$, is the radius from the z axis of the membrane at poloidal location s, and

t, that is, $t(s)$, is the membrane's thickness at poloidal location s.

Relating s to r allows Eq.(1) to be integrated, e.g., if a section of the toroidal membrane is planar so that ds in Eq.(1) equals dr, then integration over the resulting disk-annulus between inner and outer radii yields the following:

$$\phi = \frac{T}{4\pi tG}\left(\frac{1}{r_i^2} - \frac{1}{r_o^2}\right) \tag{3a}$$

Another commonly occurring situation has the toroidal membrane in a non-planar configuration. For those cases a small axisymmetric portion of the membrane can be approximated as having a straight line segment for its poloidal projection, extending from (r_1,z_1) to (r_2,z_2). For example, this would apply to a thin approximately conical section taken though a vacuum vessel dome. Integrating over the resulting frustrum of a cone results in the following:

$$\phi = \left(\frac{\sqrt{(r_2 - r_1)^2 + (z_2 - z_1)^2}}{r_2 - r_1}\right)\frac{T}{4\pi tG}\left(\frac{1}{r_1^2} - \frac{1}{r_2^2}\right) \tag{3b}$$

In such portions of the TF conductor system where the thin toroidal membrane model is an appropriate approximation, the shear stress is constant over the thickness of each perpendicular section and varies according to the following formula:

$$\tau = Gr\frac{d\phi}{ds} \tag{4}$$

where $\tau(s)$ the shear stress in the perpendicular section at location s.

In the NSTX CS upgrade's TF system the centerstack bundle of TF turns is sufficiently thick that it should not be modeled as a thin membrane. It is more appropriate to instead model it as an elastic thick-walled tubular shaft in which shear stress in a section perpendicular to the axis varies linearly with radius within that section. For the centerstack portion of the TF conductor system where the inner and outer radii of the TF are constant, the following formulae are used:

$$\frac{d\phi}{ds} = \frac{T}{JG} \tag{5}$$

where J is the rotational moment of inertia of the centerstack TF cross section,

$$J = \frac{\pi}{2}\left(r_{OUTER}^4 - r_{INNER}^4\right) \tag{6}$$

In this thick tubular shaft model the maximum shear stress in each section occurs at its outer radius and is given by the following:

$$\tau_{MAX} = Gr_{OUTER}\frac{d\phi}{ds} \equiv \frac{Tr_{OUTER}}{J} \tag{7}$$

These formulae for thick-walled tubular shafts are also used for lead extension regions of the TF centerstack which extend from r=0.1942 meters out to r=0.3329 meters where toroidal continuity of the TF conductor's mechanical configuration ends. In this 0.1942<r<0.3329 lead extension region the torsion formulae are less accurate since stress concentrations where radii abruptly change are not modeled.

For the present toroidal membrane model of the TF conductor, the blue contour of Figs. 1 through 3 is used for all r>0.3329 outer locations where the thin membrane representation is used. For r<0.3329 locations in the centerstack and its lead extensions where the thick-walled tubular shaft model is more appropriate, the blue contour is used to determine the r_{OUTER} value and the corresponding poloidal point on the red contour is used for r_{INNER}. Together these are used to calculate the local rotational moment of inertia, J, and also the peak shear stress.

Torsional stiffness formulae based on simple first-principles mechanical models are accurate wherever the TF system is nominally continuous in the toroidal direction, which for the NSTX CSU includes all parts of the TF system at locations inboard from the flex loops where the radius is less than 0.3329 meters. However, the same torsion formulae are also used herein to approximately model TF conductor deformation in outer regions where r>0.3329. The TF conductors and their supporting structures are not toroidally continuous in outer regions but instead are broken up by air gaps. The air gaps permit structures to deform in nonaxisymmetric ways not modeled by torsional stiffness formulae. Thus, the present approximation neglecting toroidal air gaps must therefore artificially reduce the stiffness of its assumed toroidally

continuous model in order to match its predictions to the actual nonaxisymmetric system. Estimates and other information supplied by Mark Smith and by Tom Willard have been used to adjust these model parameter values.

ESTIMATION OF PARAMETER VALUES

The following section documents both my own ball-park estimates of some stiffness parameters and also torsional stiffness estimates developed by Mark Smith using a global 3D model, which I have preferentially adopted.

Centerstack:

The TF centerstack's new inner radius is 0.0512 m, and its new outer radius is 0.194238 m, not including its lead extensions. The shear modulus of its copper is taken as G=48 GPa, i.e., 4.8e10 Pa. Applying Eq.(3), its twist angle per unit length per unit torque is as follows:

$$\frac{1}{T}\frac{d\phi}{ds} = \frac{1}{JG} = \frac{1}{\frac{\pi}{2}\left(r_{OUTER}^4 - r_{INNER}^4\right)G} = \frac{2}{\pi\left((0.194238)^4 - (0.0512)^4\right)(4.8E10)} =$$

$$= 9.36275866886577\text{e-}009 \text{ radian N}^{-1}m^{-2} \qquad (8)$$

The total centerstack straight section length from node 1 through 363 and 1638 through 2000 is 5.200 m, so its torsional stiffness parameter is

K_{CS}=1/[(9.3627587E-9 radian/N-m^2)(5.200 m)] = 2.054E7 N-m/radian =
= 3.176E6 inch-lbf/degree (9a)

Its reciprocal stiffness parameter is then
R_{CS}= 1/(2.054E7 N-m/radian) =4.85853E-8 radians/N-m. (9b)

Its reciprocal stiffness parameter per element is as follows:
$R_{CS/elt}$= (4.85853E-8 radians/N-m)/(724 elts) = 6.711e-11radians/N-m/elt (9c)

TF Centerstack Lead Extensions

The same formula is used for the lead extension portions of the TF centerstack, nodes 363 through 383 and 1618 through 1638. Its inner radius is also taken as 0.0512 m, but its outer radius varies. Summing the resulting individual reciprocal stiffness terms (using MATLAB) results in

R_{Leads}= 5.835E-10 radians/N-m (10a)

for upper lead extensions and the same again result separately for the lower lead extensions.

The average value per element of this constant is as follows:
$R_{Leads/elt}$= (5.835E-10 radians/N-m)/(19 elts) = 3.071E-11 radians/N-m/elt (10b)

The equivalent spring stiffness constant for the lead extensions is the reciprocal, i.e.,

K_{Leads}=1/(5.835E-010 radians/N-m= 1.71E9 N-m/radian (10c)

The upper lead extension is included with the straight part of the centerstack, so
r1=5.8835e-010+4.85853E-8= 4.95e-8 radians per newton-meter (10d)

Insulating Annular "Crown" pinned to leads, bolting plate

Recent design information as of September 2011 is that the upper and lower Crpwn assemblies are axisymmetric structures machined from G10, with each taking the shape of two axially adjacent coaxial rings. Estimated ring dimensions are as follows:

Table 4: Upper Crown Assembly Dimensions (inches)

	Ring 1	Ring 2
Inner Diameter	**16.0"**	**17.6"**
Outer Diameter	**21.5"**	**19.4"**
Height	**4.0"**	**2.0"**

Table 5: Lower Crown Assembly Dimensions (inches)

	Ring 1	Ring 2
Inner Diameter	**16.0"**	**20.1"**
Outer Diameter	**27.0"**	**23.0"**
Height	**4.0"**	**2.0"**

Assuming the shear modulus of G10 material is 7,69E9 Pa, this results in upper and lower reciprocal stiffnesses (i.e., compliences) of **respectively 5.60E-9 and 2.05E-9 radians/N-m**. (Note that Ref.4 had assumed 5E-9 for both of these.)

Outer Umbrella and Lid:

I had earlier estimated a reciprocal stiffness for the portion of the umbrella between TF clamps and lid as follows:

$$R_{OuterUmbrella} = \left(\frac{1}{T}\frac{d\phi}{ds}\right)(\Delta s) = \left(\frac{\Delta s}{2\pi r^3 t}\right) = \left(\frac{(0.35542)}{2\pi(1.0477521)^3(0.0254)(7.72E10)}\right) =$$

=2.508E-11 radians/N-m. ((11a)

At that time the lid design was envisioned as a stainless steel disk-annulus, assumed to be 1" thick. Its outer and inner radii are assumed to be respectively 1.047752 m and 15.375"/2= 0.1953 m, which resulted in a lid reciprocal stiffness of

$$R = \frac{\phi}{T} = \frac{1}{4\pi tG}\left(\frac{1}{r_i^2} - \frac{1}{r_o^2}\right) = \frac{1}{4\pi(0.0254)(7.72E10)}\left(\frac{1}{(0.1953)^2} - \frac{1}{(1.0477521)^2}\right) =$$

=1.02702e-009 radians per Newton-meter (11b)

Using those values as ballpark estimates, then the net reciprocal stiffness from TF coil clamp to crown interface would have been

2.508e011+1.02702e-009 = 1.052E-9 radian/N-m (11c)

A better estimate of the stiffness via this path was provided by Mark Smith by fitting a global 3D model, as copied into the following text box. The reciprocal stiffness derived from his data is

$R_{umbrella+lid}$=3.338E-9 radians/N-m (11d)

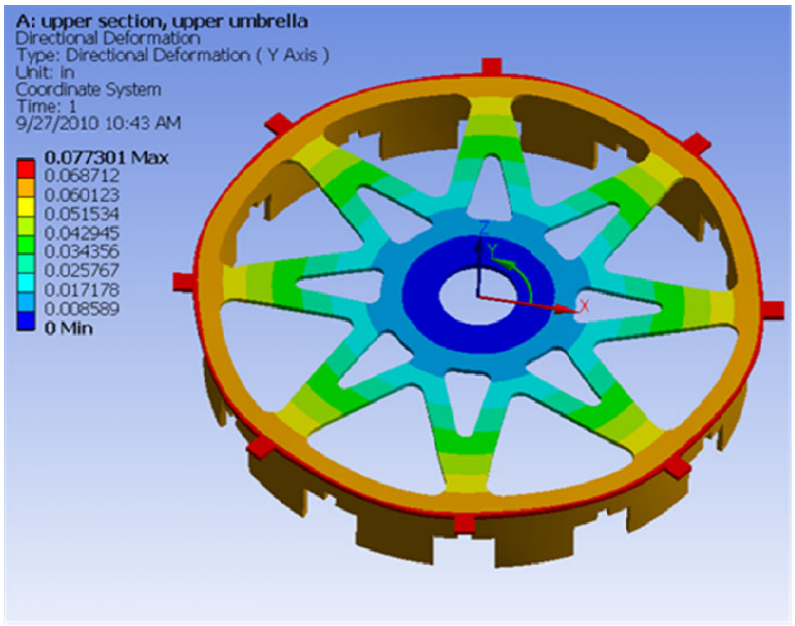

12*10000 lbf = 120000 lbf

R = 41.3 inch

T = 4.956E6 lbf-in

Θ = s/r =~ .077301 inch/41.3 inch = 0.001872 radians

K1 = T/Θ = 4.956E6 lbf-in/0.001872 radians
K1 = 2.64787E9 lbf-in/radians

K1 = 4.6214E7 lbf-in/°

Mark Smith's Global Model Data 1

Inner Umbrella

Each umbrella is a nominally cylindrical stainless steel (G=77.2 GPa) structure of radius r=1.0477521 m, thickness t=1"=0.0254 m, and height from base to the middle of the cutouts for TF outer legs is 32.12"=0.8158 m. Eq.(3) could be used to estimate its stiffness parameter if it had no cutouts. However, it has not only the cutouts for TF outer legs but also ten arch-shaped cutouts near its base. If its thickness were reduced by 67% from 1" to t=0.33"=0.00847 m as a ballpark "guestimate" to match actual nonaxisymmetric deflections under torsion loading .the stiffness parameter would become the following:

$$R_{\text{InnerUmbrella}} = \left(\frac{1}{T}\frac{d\phi}{ds}\right)(\Delta s) = \left(\frac{\Delta s}{2\pi r^3 t}\right) = \left(\frac{(0.8158)}{2\pi(1.0477521)^3(0.00847)(7.72E10)}\right) =$$

$$=1.727\text{E-}010 \text{ radians per newton-meter} \qquad (12a)$$

A better estimate of the stiffness of this path was provided by Mark Smith by fitting a global 3D model, as copied into the following text box. It is equivalent to

$$R_{\text{InnerUmbrela}}=4.44\text{E-}9 \text{ radian/N-m} \qquad (12b)$$

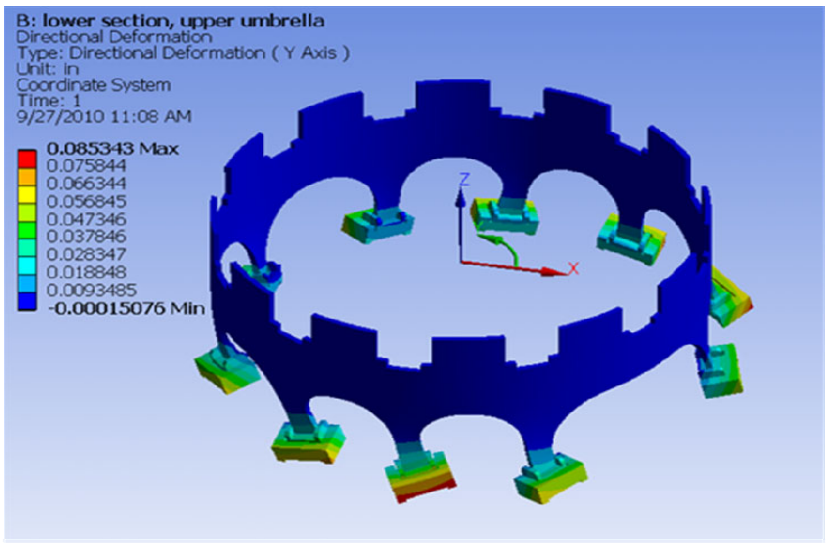

M = 4.13E6 lbf-in

R = 41.3 inch

Θ = s/r =\ .085343 inch/41.3 inch = 0.002066 radians

K2a = T/Θ = 4.13E6 lbf-in/0.002066 radians
K2a= 1.99E9 lbf-in/radians

K2a = 3.48827E7 lbf-in/°

Mark Smith's Global Model Data2

Vacuum Vessel Division

Connecctions to the TF outer legs above and below the horizontal midplane were identified as TF conductor node numbers 838 and 1163, located at (r,z)=(2.3411, ±1.1489) m. These connections go to the vacuum vessel, meeting it at locations closer to the midplane. For the present analysis they are assumed to meet the vacuum vessel at the interface between the vacuum vessel's cylindrical midsection and its upper or lower domes, i.e., at (r,z)=(1.74, 1.00) m. Therefore, for the calculation of spring stiffnesses, one value is for the cylindrical central portion of the vacuum vessel and another is for a vacuum vessel dome connected in series with the portion of the umbrella between the vacuum vessel and the TF outer leg's aluminum block .

Central cylindrical section of the vacuum vessel:

The vacuum vessel is made of stainless steel (shear modulus G=77.2 GPa) of thickness t=0.625"= t=0.01875 m. The radius of the vacuum vessel's central section is about 1.705 m and its height is 2.00 m. Therefore, Eq.(3) could be used for a rough reciprocal stiffness estimate, $R_{VV\text{-}middle}$=4.4367E-11 radians/ N-m. For the effect of port cutouts it was decided to reduce the assumed cylindrical membrane thickness by 50%, to t=0.009375. This would increase the reciprocal stiffness parameter to $R_{VV\text{-}middle}$=8.87E-11 radians/ N-m.

A better estimate of the stiffness of this path was provided by Mark Smith by fitting a global 3D model, as copied into the following text box. It is equivalent to

$$R_{VV\text{-}middle}=5.634\text{-}10 \text{ radian/N-m} \qquad (13)$$

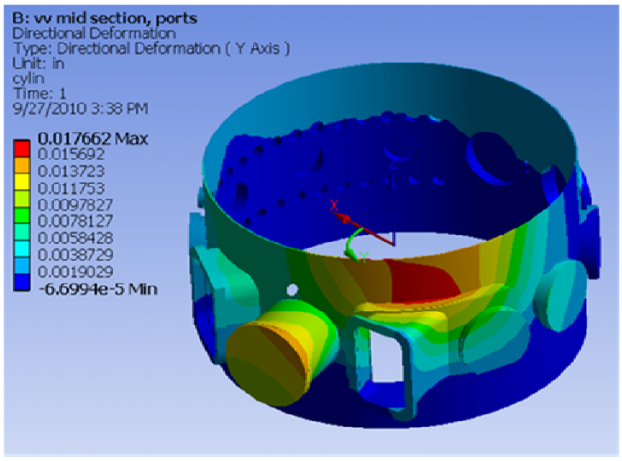

M – 4.13E6 lbf-in

R = 67.1 inch

Θ = s/r => 0.017662 inch/67.1 inch = 0.000263 radians

K3 = T/Θ = 4.13E6 lbf-in/0.000263 radians

K3= 1.569e10 lbf-in/radians

K3 = 2.738e8 lbf-in/°

Mark Smith's Global Model Data 3

Vacuum vessel dome

Vacuum vessel drawings identified (r.z) coordinates of the upper dome from the dome's mouth to its interface with the vacuum vessel's cylindrical section, as listed in the following table.

Table6: Vacuum Vessel Dome Coordinates

Point #	r (m)	z (m)
1	0.6121	1.7500
2	0.7442	1.7170
3	1.1455	1.5545
4	1.5392	1.3106
5	1.6612	1.1735
6	1.7068	1.0033

The total rotation angle per unit torque for the five unbroken conical frustrum regions bounded by the points is then estimated as follows:

$$R_{dome} = \frac{\phi}{T} = \frac{1}{4\pi t G}\sum_{i=1}^{i=5}\left(\frac{\sqrt{(r_{i+1}-r_i)^2+(z_{i+1}-z_i)^2}}{r_{i+1}-r_i}\right)\left(\frac{1}{r_i^2}-\frac{1}{r_{i+1}^2}\right) = \frac{1}{4\pi(0.01875)(7.72E10)}(2.57940) =$$

= 1.41805e-010 radians per newton-meter. If one arbitrarily reduces the thickness by 50% to account for port cutouts, this leads to the following guestimate for the reciprocal stiffness of each of the domes:

R_{dome}=2.8361E-10 radian/ N-m (14a)

A better estimate of the stiffness of this path was provided by Mark Smith by fitting a global 3D model, as copied into the following text box. It is equivalent to

R_{dome}=1.72E-10 radian/ N-m (14b)

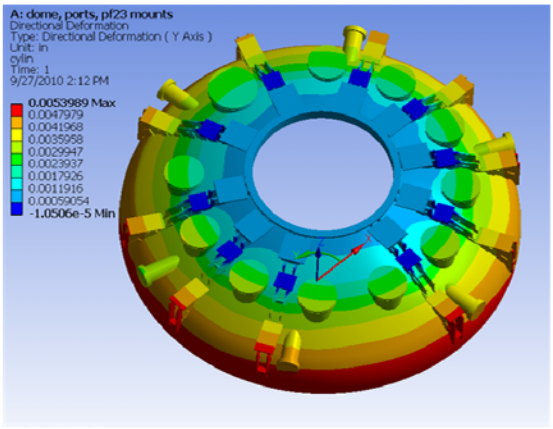

M = 4.13E6 lbf-in

R = 67.1 inch

Θ = s/r = 0.005399 inch/67.1 inch = 0.00008 radians

K2b = T/Θ = 4.13E6 lbf-in/0.00008 radians

K2b= 5.133e10 lbf-in/radians

K2b = 8.96e8 lbf-in/°

Mark Smith's Global Model Data 4

Vacuum Vessel Connections to TF Outer Legs

A rough stiffness estimate was made based on assumed 1.5"=0.0381 m diameter solid steel cylindrical rod attached to the vacuum vessel through pin connections at clevis attachments midway between TF outer legs. Coordinates of these connection points are (R,Z)=(1.7068, ±1.00) m, while the coordinates of the TF out legs where they attach to the tangential rods are (R,Z)=(2.3411, ±1.1489) m. Taking into account the 12-fold symmetry and the geometric angles, the resulting reciprocal stiffness parameter estimate is as follows:

$$R_{ClevisRods}=1.22e\text{-}010 \text{ radian/N-m} \quad (15)$$

Vacuum Vessel Legs and Pedestal Support for TF Centerstack

Without nonaxisymmetric analyses it is not possible to estimate the rotational stiffness of the torque path through vacuum vessel support legs, floor, and TF centerstack pedestal support. However, Mark Smith has provided such estimates by fitting a nonaxisymmetric global 3D model, as copied into the following two text boxes. The equivalent reciprocal stiffness parameter for the VV support legs is

$$R_{Legs}=3.72E\text{-}8 \text{ radian/N-m} \quad (16)$$

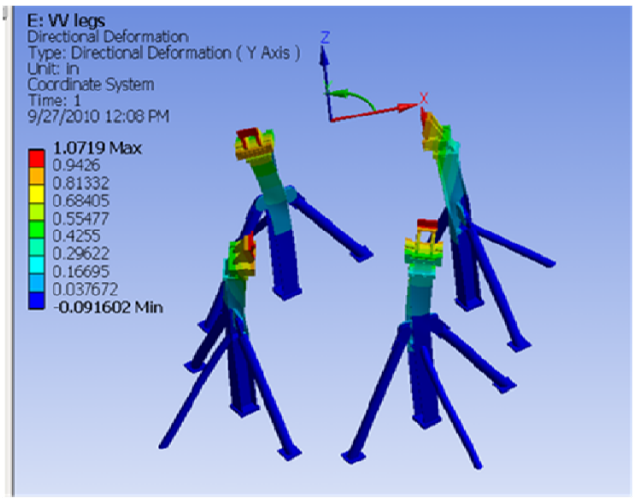

M = 4.13E6 lbf-in

R = 67.1 inch

Θ = s/r => 1.0719 inch/61.7 inch = 0.017373 radians

K_{Legs} = T/Θ = 4.13E6 lbf-in/0.017373 radians

K_{Legs} = 2.37728e8 lbf-in/radians

K_{Legs} = 4.14914e6 lbf-in/°

Mark Smith's Global Model Data 5

The equivalent reciprocal stiffness parameter for the pedestal pad supporting the centerstack is:

R_{Ped}=2.17E-8 radian/N-m (17)

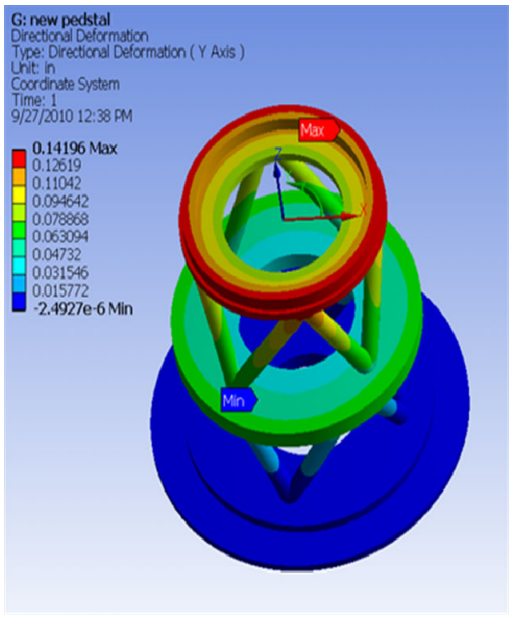

M = 4.13E6 lbf-in

R = 14 inch

$\Theta = s/r$ => 0.14196 inch/14 inch = 0.01014 radians

$K_{p\,new} = T/\Theta$ = 4.13E6 lbf-in/0.01014 radians

$K_{p\,new}$ = 4.073e8 lbf-in/radians

$K_{p\,new}$ = 7.109e6 lbf-in/°

Mark Smith's Global Model Data 6

TF Conductor Portions Lacking Structural Continuity in Toroidal Direction

The remaining portions of the system are TF conductors which are interspersed with toroidal air gaps lacking any structural rigidity. This situation exists everywhere that the TF conductors have major radius locations exceeding the threshold value, i.e., for R>0.3329 m. Although at certain locations the TF conductors are clamped to other structures, such clamping is not the issue here since those other structures and their TF conductor attachment points are expressly modeled as external springs. Thus, any torsional stiffness parameters to be assigned to toroidally discontiuous portions of TF conductors must be chosen to match the TF conductors' nonaxisymmetric beam-like toroidal deflection behaviors to the axisymmetric model.

Recall that for a straight beam, the deflection distance, *y*, is governed by the following fourth order system of differential equations:

$$\frac{dV}{ds} = q(s)$$
$$\frac{dM}{ds} = V(s)$$
$$\frac{d\theta}{ds} = \frac{M(s)}{EI}$$
$$\frac{dy_f}{ds} = \theta(s)$$
$$\frac{dy_s}{ds} = \frac{V(s)}{AG}$$
$$y = y_s + y_f$$

(18a)

where
s is the distance along the straight beam,
q is the perpendicular running load force per unit distance,
V is the internal section shear force,
M is the internal section bending moment,
q is the deflection angle
y_f is the deflection distance due to flexure
y_s is the deflection distance due to shear
E is the elastic modulus
G is the shear modulus
I is the cross section's moment of inertia with respect to the loading direction
A is the cross section's area

Note that the torsion system of equations matches the shear part of the beam deflection system but has no way of modeling beam flexure. Thus, there is no first-principles approach to matching the models. As an intuitive example of this mismatch, a continuous toroidal membrane

representing the TF outer legs would develop nonzero internal torque if its top were rotated by, say, 0.001 radians with respect to its bottom, but the collection of 12 TF outer legs could sustain such a relative rotation without elastically deforming them (to first order), i.e., with twelve different small rigid body tilting motions of the separate outer legs.

Thus, the best that can be done is to make a very approximate, order-of-magnitude torsional stiffness estimate for the outer TF conductor, as a "kludge". To this end, Tom Willard supplied ANSYS calculated results for the out-of-plane deflection of an isolated TF Outer Leg under defined loading conditions. The model imposed cantilever restraints on the conductor at the upper and lower locations where the actual outer leg is clamped to the umbrellas by aluminum blocks (i.e., the torsion model's nodes 566 and 1435) It applied 1000 lbf=4454.5 N out-of-plane load forces to the outer legs at the locations where each acual outer leg will be connected to vacuum vessel clevises via rods (i.e., the torsion model's nodes 838 and 1163). Maximum calculated OOP deflection was 0.073 inches with a single OOP force applied and 0.140 inches=3.56 mm with both OOP forces applied in the same direction. The torsion model's stiffness value is then set by the second of these results, based on the deflection of the top half only. A torque of

$$T=(12 \text{ outer legs})(F=4454.5 \text{ N})(R=2.3411 \text{ m}) = 125{,}142 \text{ N-m}$$

is predicted by ANSYS to cause the TF conductor portion between the upper umbrella's clamp (node 1435) and the clevis rod clamp (node 1163) to rotate through and angle of

$$\Delta\phi = (0.00356 \text{ m})/(2.3411 \text{ m}) = 0.0015189 \text{ radians}$$

The corresponding reciprocal stiffness value is then

$$R_{1163:1435} = \Delta\phi / T = (0.0015189 \text{ radians})/(125{,}142 \text{ N-m}) =$$
$$= 1.2138\text{e-}008 \text{ radian/N-m} \qquad (18b)$$

In order to assign a consistent stiffness to other portions of the TF outer legs, a single-element value is first obtained by dividing the above result by the 1435-1163+1= 273 elements to obtain

$$R_{TFOL/elt} = R_{1163:1435} /(1435\text{-}1163\text{+}1 \text{ elts}) = 4.45\text{E-}11 \text{ radian/N-m/elt} \qquad (18c)$$

This per element value is then used to generate reciprocal stiffness values for the other portions of the TF outer legs. For the portion between lower and upper rod attachments to clevises,

$$R_{838:1163} = (1163\text{-}838\text{+}1)R_{TFOL\text{-}node} = 1.45\text{E-}8 \text{ radian/N-m} \qquad (18d)$$

For the Outer leg TF portion inboard of each umbrella clamp, including the flex straps for which no better "kludge" estimate of torsional stiffness has been derived, the reciprocal stiffness values are as follows:

$$R_{1435:1618} = R_{383:566} == (184)R_{TFOL\text{-}node} = 5.26\text{E-}8 \text{ radian/N-m} \qquad (18e)$$

THE EQUIVALENT ELECTRICAL MODEL

This analysis uses an analogy between the torsional mechanical system and a hypothetical electrical network. The angular twist of an axisymmetic portion of the TF system is analogous to the voltage developed across a length of resistive conductor in the hypothetical analogous electrical network, and the internal torque developed in that axisymmetric section is analogous to the current flowing through the analogous resistor. Torsional spring stiffnesses, expressed in units of torque per unit angular deflection, are analogous to conductances (i.e., reciprocal resistances) in the hypothetical electrical network.

Since electromagnetic torque loading on the TF centerstack is not spatially umiform, the TF centerstack can best be modeled as a series-connected sequence of many small torsion springs. The nodes between the resistors represent a sequence of physical locations within the centerstack. The nonuniform distributed torque loading is then modeled by assigning the Lorenz torque increment for each region between two adjacent nodes to one of those two nodes. (Little error is introduced by this asymmetrical assignment if nodes are closely spaced.) As developed in the Appendix, this torque is equal to the product of total TF threading current, $N_{TF} I_{TF}$, times the difference in poloidal flux per radian between the modeled element's two ends, i.e.,

$$T_j = N_{TF} I_{TF} \frac{\Psi_{j+1} - \Psi_j}{2\pi} \qquad (!9)$$

An electrical analogy shown in Fig.18a is a series connected string of resistors interleaved with current sources that inject increments of electrical current from a common reference node.

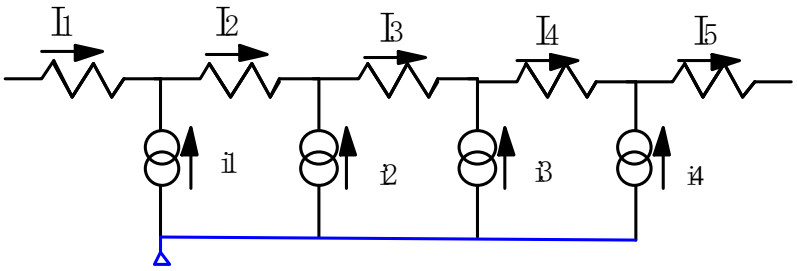

Figure 18a: Electrical Analogy of Series-Connected Torsion Springs And External Torques

Currents I_j flowing through the Fig.18a resistors represent the internal torque state at different vertical locations in the TF centerstack. Resistor currents can thus differ from each other according to:

$$I_{j+1} = I_j + i_j \qquad (20)$$

where i_j is an injected current. Since the injected currents, i_j, represent the incremental torques, T_j, the electrical analogy model's resistor currents are related to actual poloidal fluxes as follows:

$$I_j = N_{TF} I_{TF} \frac{\Psi_j}{2\pi} + C \qquad (21)$$

where C is any fixed constant value.

This Fig18a model can be continued beyond the TF centerstack through the outer parts of the TF conductor system where mechanical supports interconnecting portions of the system must also be modeled. The fact that the total net Lorenz torque on the entire TF system is necessarily zero translates in the full TF system model's analogous electrical network into the net current from the common reference node being zero. This allows the Fig.18b alternative equivalent circuit model to be used instead for the analogy.

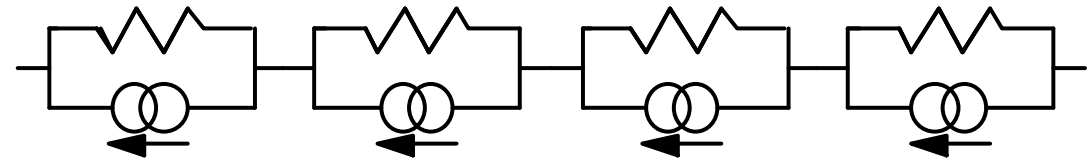

Figure 18b: Alternative Analogy of Series-Connected Torsion Springs And External Torques

In Fig.18b, the current in each external current source is assigned as:

$$i_j = N_{TF} I_{TF} \frac{\Psi_j}{2\pi} \tag{22}$$

where j is the node number of the location at one of the current source's ends. With this assignment, the current in each of the model's resistors is related to actual poloidal flux as

$$I_j = N_{TF} I_{TF} \frac{\Psi_j}{2\pi} + C\,, \tag{23}$$

where C is the common constant value of current flowing between series blocks of Fig.18b. This also clearly matches the resistor current in the Fig.18a model.

Fig.19 depicts the electrical analogy of the full toroidal membrane model of the TF conductor, which includes 1999 copies of the basic blocks of Fig.18b, all connected in series to form a single loop. Fig.19 shows only 25 of the 1999 copies, but the rest are implied.

The current in each Fig.19 primary resistor representing the TF centerstack equals the current in its parallel current source plus the loop current in the ccw direction. Analogously, the internal torque state at any location is the applied differential Lorenz torque plus the torque mechanically transferred in. Other parts of Fig.19 are also interconnected through external resistors lacking any parallel current sources (i.e., lacking any applied EM torques). Figure 19 depicts these external paths with bold symbols, using resistance numberings keyed to the previously numbered external paths for mechanical torques.

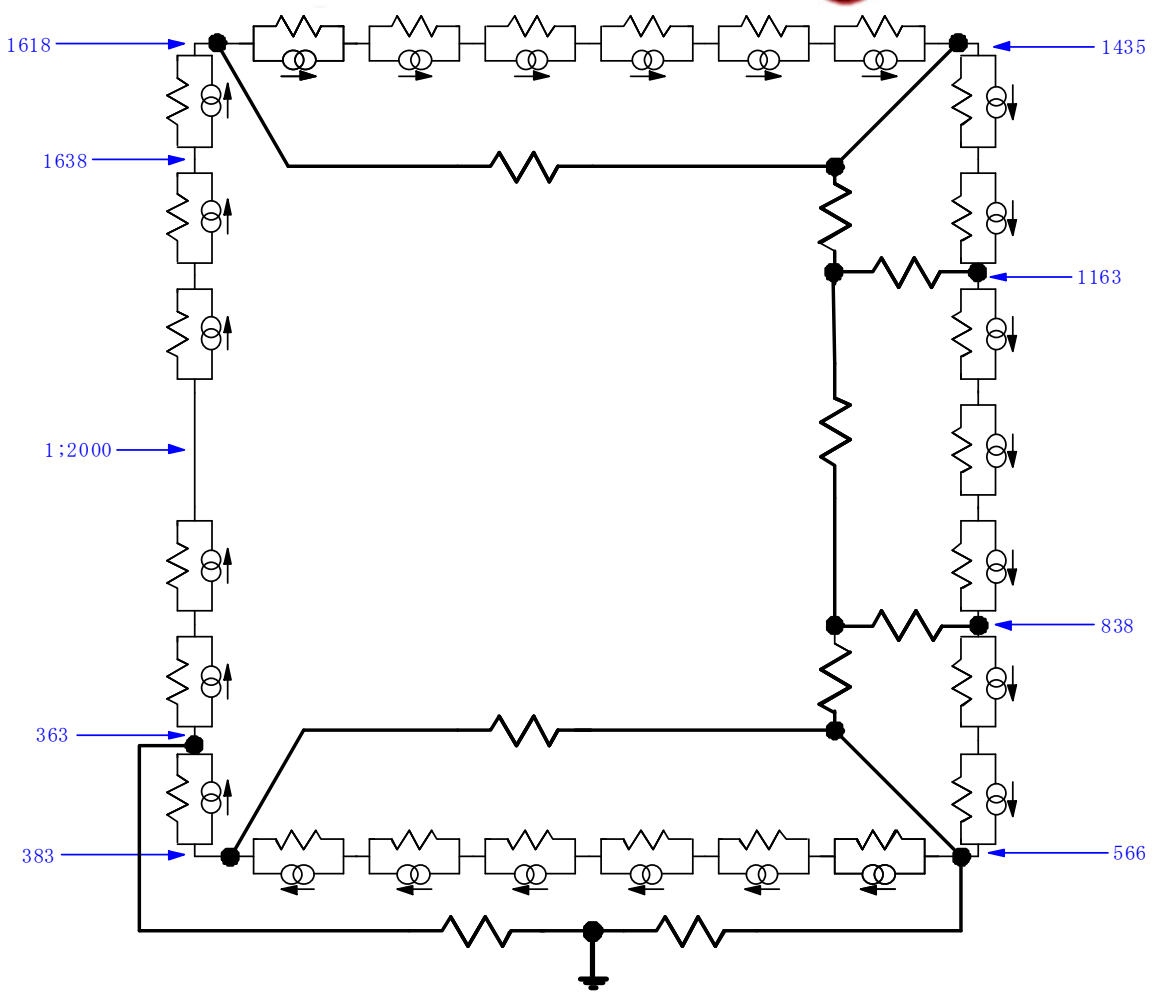

Figure 19: Electrical Analogy TF Torsional Model for NSTX CSU

The external resistors of Fig.19 are identified as follows. R(1) and R(2) represent series mechanical connection paths from respectively upper and lower aluminum block TF conductor clamps through the upper or lower umbrella to the umbrella lid and its radial connection to the insulating crown bolted to the centerstack's TF leads. R(3A) represents the upper system of rods connecting between TF outer leg clamps and clevis attachments to the vacuum vessel. R3B represents the series combination of the upper dome portion of the vacuum vessel above the upper clevis attachments, the upper umbrella mounting, and the upper umbrella up to where aluminum block TF conductor clamps are attached. R(4A) and R(4B) represent the lower mirror image of R(3A) and R(3B). R(5), together with R(3A) and R(4A), implement the previously listed interconnection path (5). R(6A) in series with R(6B) together model path (6) which transmits torque through the vacuum vessel's legs to the floor and then up through the pedestal pad to the centerstack's bottom. In this model, the torque through path (6) is transmitted into the inner part of the centerstack's bottom without going through the lower lead extensions.

The following table summarizes electrical analogy model resistances from the previous section.

Table 7: Electrical Analogy Model Resistance Values

Parameter	Comments	Analogous Resistance Value (radian/N-m)
R(1)	$R_{crown}+R_{umbrella+lid}$	8.938E-9
R(2)	$R_{crown}+R_{umbrella+lid}$	5.388E-9
R(3B)	$R_{InnerUmbrela}+R_{dome}$	4.962E-9
R(4B)	$R_{InnerUmbrela}+R_{dome}$	4.962E-9
R(3A)	$R_{ClevisRods}$	1.22E-10
R(4A)	$R_{ClevisRods}$	1.22E-10
R(5)	$R_{VV\text{-}middle}$	5.634-10
R(6A)	R_{Ped}	2.17E-8
R(6B)	R_{Legs}	3.72E-8
$R_{1638:2000\&1:363}$	R_{CS}	4.86E-8
$R_{363:383}$	R_{Leads}	5.835E-10
$R_{1618:1638}$	R_{Leads}	5.835E-10
$R_{383:566}$		5.26E-8
$R_{1435:1618}$		5.26E-8
$R_{566:838}$		1.214E-8
$R_{1163:1435}$		1.214E-8
$R_{838:1163}$		1.45E-8

SOLUTION OF NSTX CSU ELECTRICAL ANALOGY TF TORSIONAL MODEL

In order to calculate the shear stress profile in the TF centerstack it is necessary to first determine the internal torque state as a function of location, $T(s_j)$. In terms of the Fig.19 electrical analogy model this is equivalent to calculating resistor currents in each of the Fig.18b-style blocks representing the centerstack, i.e., between nodes 1 and 371 and between nodes 1630 and 2000 (a.k.a. 1). However, each such resistor current is simply the sum of the constant value of current passing between all of the centerstack's Fig.18b-type blocks and the known poloidal-flux-dependent current in its parallel current source. Thus, only two constant current values need to be determined to evaluate centerstack shear stress profiles. One current value is needed for nodes 1630 through 2000 and 1 through363, while the other is needed for nodes 363 through 371 which represent the lower lead extensions. Furthermore, inspection of Fig.19 shows that the entire TF system model could be similarly treated by solving for a total of seven (7) such "constant" values of mesh currents.

Determining terminal currents is simplified by equivalent-circuit reductions. A Thevenin equivalent of the basic block in the Fig.18b circuit employing an ideal series voltage source is shown in Fig.20. The voltage of this source is the product of the Fig.18b block's source current and resistance, i.e.,

$$V_j = R_j N_{TF} I_{TF} \frac{\Psi_j}{2\pi} \tag{24}$$

and its resistance is equal to R_j, the same as in the Fig.18b block. It has the same external terminal node voltage/current characteristics as Fig 18b, ***but its internal resistor current does not match the current through Fig.18's resistor***.

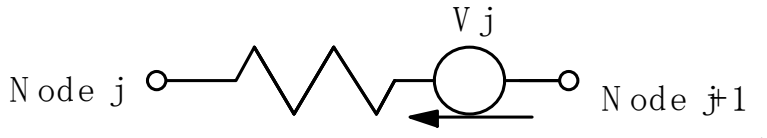

Figure 20: Thevenin Equivalent of the Fig.21 Circuit, Using A Voltage Source

Converting from Fig.18b-type blocks to the Fig.20 form allows many series-connected blocks to be merged into a single block by adding their resistances and adding their source voltages. Applying this substitution to Fig. 19 and combining blocks results in the Fig.21 circuit, which for mesh currents is equivalent to the Fig.19 circuit but easier to calculate. After solving for them, they are substituted into the Fig.19 circuit in order to calculate each resistor current there which is analogous and proportional to the internal torque state of the corresponding part of the mechanical system.

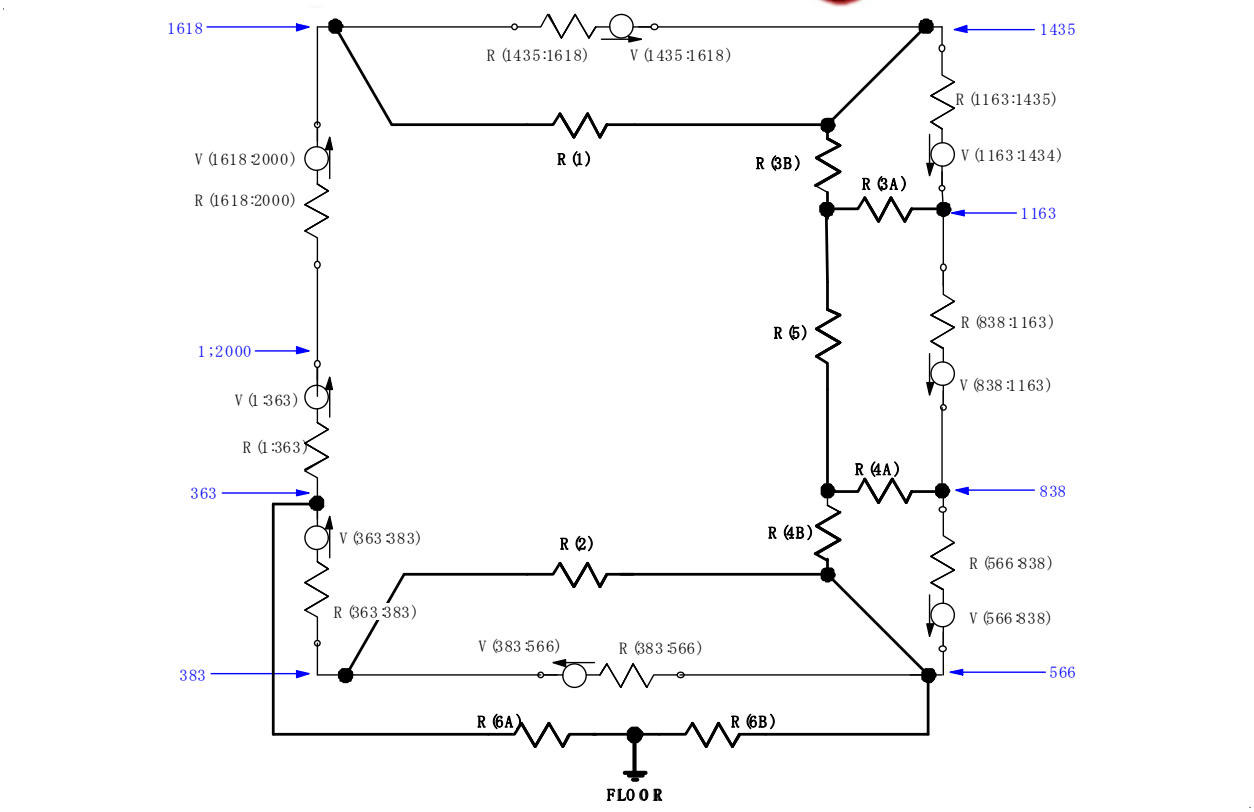

Figure 21: Equivalent Electrical Analogy TF Torsional Model for NSTX CSU

To help solve the Fig.21 circuit it is appropriate to first combine series elements and assign more compact names to designate the resistances, voltage source parameters, and distinct mesh currents in the circuit. This is done in the following diagram which uses 7 mesh loops. Note that the mesh loop carrying the current, i1, is the large loop that contains all seven voltage sources.

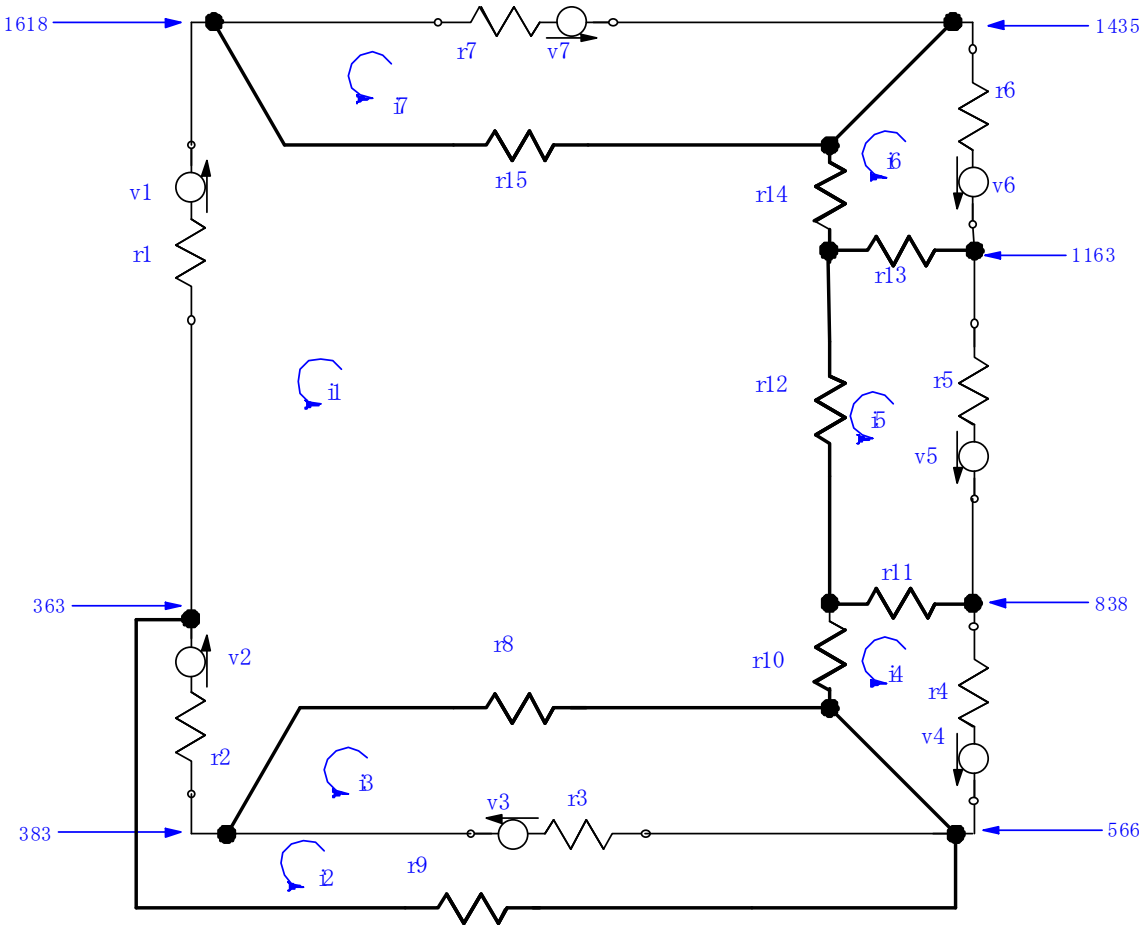

Figure 22: Simplified equivalent circuit of electrical analogy torsion model

The correspondences with symbols of earlier diagrams and parameter values are as follows:

r1=R(1:363)+R(1638:2000) +R(1618:1638)
= 4.86E-8 + 5.8835E-10 = 4.95E-8 radian/N-m

r2=R(363:383)= 5.8835E-10 radian/N-m

r3=R(383:566) = 5.26E-8 radian/N-m

r4=R(566:838)= 1.214E-8 radian/N-m

r5=R(838:1163) = 1.45E-8 radian/N-m

r6=R(1163:1435) = 1.214E-8 radian/N-m

r7=R(1435:1618)= 5.26E-8 radian/N-m

r8=R(2) = 5.388E-9 radian/N-m

r9=R(6A)+R(6B) = 2.17E-8 +3.72E-8 = 5.89E-8 radian/N-m

r10 = R(4B) = 4.61E-9 radian/N-m

r11=R(4A)= 1.22E-10 radian/N-m

r12 = R(5) = 5.634-10 radian/N-m

r13 = R(3A) = 1.22E-10 radian/N-m

r14 = R(3B) = 4.61E-9 radian/N-m

r15 = R(1) = 8.938E-9 radian/N-m

(25a-25o)

The analogous voltage sources result from the series connection of a sequence of elements each containing its own voltage source. When a series sequence of such elements have common torsional "resistance" values which multiply their equivalent current sources, these common resistances can be factored out of the voltage sums yielding a sum over the equivalent sequence of analog current sources. However, since each analog current source is proportional to a difference of successive poloidal flux values, a simplifying cancelation occurs which eliminates poloidal flux at the intermediate nodes results.

In the reciprocal stiffnesses calculated for the TF conductors, constant elemental resistance values result for the constant-radius portions of the TF center-stack. A second constant value per element has been selected for the TF outer leg conductor, extending inwards to the flex straps. The lead extensions were not modeled as having such a constant value but will nevertheless be approximated with their constant average value in order to simplify calculations. The three constant resistance values per element are as follows.

$R_{CS/elt}$= 6.7e-11radians/N-m/elt = R_{CSe}

$R_{Leads/elt}$=3.071E-11 radians/N-m/elt =R_{Le}

$R_{TFOL/elt}$=4.45E-11 radian/N-m/elt =R_{TFOLe} (26)

Then the analogy model's ideal voltage sources can be expressed as follows

$$v1 = \left(R_{\mathrm{CS/elt}} \left(\sum_{i=1638}^{1999} \Psi_i + \sum_{i=1}^{363} \Psi_i \right) + R_{\mathrm{Leads/elt}} \sum_{i=1618}^{1637} \Psi_i \right) \frac{N_{TF} I_{TF}}{2\pi} \qquad (27a)$$

$$v2 = \left(R_{\text{Leads/elt}} \sum_{i=364}^{383} \Psi_i \right) \frac{N_{TF} I_{TF}}{2\pi} \tag{27b}$$

$$v3 = \left(R_{\text{TFOL/elt}} \sum_{i=384}^{565} \Psi_i \right) \frac{N_{TF} I_{TF}}{2\pi} \tag{27c}$$

$$v4 = \left(R_{\text{TFOL/elt}} \sum_{i=566}^{837} \Psi_i \right) \frac{N_{TF} I_{TF}}{2\pi} \tag{27d}$$

$$v5 = \left(R_{\text{TFOL/elt}} \sum_{i=838}^{1163} \Psi_i \right) \frac{N_{TF} I_{TF}}{2\pi} \tag{27e_}$$

$$v6 = \left(R_{\text{TFOL/elt}} \sum_{i=1164}^{1434} \Psi_i \right) \frac{N_{TF} I_{TF}}{2\pi} \tag{27f}$$

$$v7 = \left(R_{\text{TFOL/elt}} \sum_{i=1435}^{1617} \Psi_i \right) \frac{N_{TF} I_{TF}}{2\pi} \tag{27g}$$

Using these variables the seven mesh equations to be solved for mesh currents are as follows:

$$r1*i1+r2*(i1-i2)+r3*(i1-i2+i3)+r4*(i1+i4)+r5*(i1+i5)+r6*(i1+i6)+r7*(i1+i7)$$
$$=-(v1+v2+v3+v4+v5+v6+v7)$$

$$r9*i2+r3*(i2-i1-i3)+r2*(i2-i1)=v2+v3$$

$$r3*(i3+i1-i2)+r8*i3=-v3$$

$$r4*(i1+i4)+r11*(i4-i5)+r10*i4=-v4$$

$$r5*(i1+i5)+r13*(i5-i6)+r12*i5+r11*(i5-i4)=-v5$$

$$r6*(i1+i6)+r14*i6+r13*(i6-i5)=-v6$$

$$r7*(i1+i7)+r15*i7=-v7$$

(28)

(These equations can be expressed more compactly in vector-matrix form , as follows:

$$\begin{bmatrix} (r1+r2+r3+r4+r5+r6+r7) & -(r2+r3) & r3 & r4 & r5 & r6 & r7 \\ -(r2+r3) & (r2+r3+r9) & -r3 & 0 & 0 & 0 & 0 \\ r3 & -r3 & (r3+r8) & 0 & 0 & 0 & 0 \\ r4 & 0 & 0 & (r11+r4+r10) & -r11 & 0 & 0 \\ r5 & 0 & 0 & -r11 & (r5+r11+r12+r13) & -r13 & 0 \\ r6 & 0 & 0 & 0 & -r13 & (r6+r13+r14) & 0 \\ r7 & 0 & 0 & 0 & 0 & 0 & (r7+r15) \end{bmatrix} \begin{bmatrix} i1 \\ i2 \\ i3 \\ i4 \\ i5 \\ i6 \\ i7 \end{bmatrix}$$

$$= \begin{bmatrix} -1 & -1 & -1 & -1 & -1 & -1 & -1 \\ 0 & 1 & 1 & 0 & 0 & 0 & 0 \\ 0 & 0 & -1 & 0 & 0 & 0 & 0 \\ 0 & 0 & 0 & -1 & 0 & 0 & 0 \\ 0 & 0 & 0 & 0 & -1 & 0 & 0 \\ 0 & 0 & 0 & 0 & 0 & -1 & 0 \\ 0 & 0 & 0 & 0 & 0 & 0 & -1 \end{bmatrix} \begin{bmatrix} v1 \\ v2 \\ v3 \\ v4 \\ v5 \\ v6 \\ v7 \end{bmatrix} \tag{29}$$

where

$$\begin{bmatrix} v1 \\ v2 \\ v3 \\ v4 \\ v5 \\ v6 \\ v7 \end{bmatrix} = \begin{bmatrix} 0 & 0 & 0 & 0 & 0 & 0 & R_{Le} & R_{CSe} \\ R_{Le} & 0 & 0 & 0 & 0 & 0 & 0 & 0 \\ 0 & R_{TFOLe} & 0 & 0 & 0 & 0 & 0 & 0 \\ 0 & 0 & R_{TFOLe} & 0 & 0 & 0 & 0 & 0 \\ 0 & 0 & 0 & R_{TFOLe} & 0 & 0 & 0 & 0 \\ 0 & 0 & 0 & 0 & R_{TFOLe} & 0 & 0 & 0 \\ 0 & 0 & 0 & 0 & 0 & R_{TFOLe} & 0 & 0 \end{bmatrix} \begin{bmatrix} \Psi_{364:383} \\ \Psi_{384:565} \\ \Psi_{566:837} \\ \Psi_{838:1163} \\ \Psi_{1164:1434} \\ \Psi_{1435:1617} \\ \Psi_{1618:1637} \\ \Psi_{1638:1999} + \Psi_{1:363} \end{bmatrix} \left(\frac{N_{TF} I_{TF}}{2\pi} \right) \tag{30}$$

DISCUSSION OF ANALYSIS RESULTS

For the stiffness parameter values chosen herein and for each of 97 coil current combination cases including the 96 plasma equilibria (specified previously by J. Menard) and a single OH-only +24 kA precharge case, the model's solution was obtained via MATLAB. Once the fixed currents i1 and i2 for a parameter case were numerically found the were used to determine the corresponding internal torque and shear stress profile in the TF centerstack. The resulting shear stress profiles are plotted in Appendix 2. The maximum peak absolute shear stress over all 97 cases examined was 25.234 MPa, but many cases had almost this large a value of peak absolute shear stress. Inspection of the profiles shows that the OH coil's effect on peak shear stress is stronger than the combined effects of the other PF coils and the plasma, but that the 25 MPa peak shear only occurs when the OH current magnitude is maximized with the polarity (negative) that reinforces the polarity of shear stress resulting from the equilibrium PF coil and plasma currents alone. In such cases the shear stress at the middle of the inner leg is near zero, indicating that almost all of the torsion load is carried through the vacuum vessel with essentially none is carried through the inner leg.

Stiffness parameters were then perturbed to find their effects on peak shear stress. It was found that reducing the stiffness connecting the TF inner leg to the vacuum vessel reduces the peak shear stress in the inner leg. The stiffness reduction achieves this by reducing the load carried through the vacuum vessel, thus increasing the load share carried through the inner leg. This shifts the inner leg's shear stress profile by a constant amount at all vertical locations, thus decreasing peak torsion in the critical regions near the inner leg's top and bottom while increasing the oppositely directed torsion at the inner leg's middle. Appendix 3 presents results for a case in which the upper lid's stiffness is reduced by 95%, without any other changes. Comparison of stress distribution plots in Appendix 3 with those of Appendix 2 reveals how this stress profile shift causes peak torsion shear stress to be reduced by 22.5%.

APPENDIX 1

Out-Of-Plane (OOP) Torque Algorithm Exposition

Derivation of Torsion Load Formulae for Out-Of-Plane (OOP) forces on Toroidal Field Coils

In general, the total moment (i.e., torque) vector of electromagnetic forces about an origin is the volume integral of the following differential:

$$d\vec{M} = \vec{r} \times \left(\vec{J} \times \vec{B}\right) dV \tag{A1}$$

where $\vec{r}$ is the position vector of a differential volume, dV, $\vec{J}$ is the current density vector and $\vec{B}$ is the magnetic field vector. For a toroidal field coil system it is appropriate to use a cylindrical coordinate system. (r,θ,z), in which the vertically oriented z axis is the central axis of symmetry which includes the origin. To analyze OOP forces in a near-axisymmetric system it is sufficient to consider only current densities and magnetic fields lying within the local poloidal plane and depending only on the position vector within that same plane. Thus, these vectors can be rewritten as follows:

$$\begin{aligned} \vec{r} &\equiv r\hat{r} + z\hat{z} \\ \vec{J} &\equiv J_r\hat{r} + J_z\hat{z} \\ \vec{B} &\equiv B_r\hat{r} + B_z\hat{z} \end{aligned} \tag{A2}$$

where $\hat{r}, \hat{\theta}, \hat{z}$ are unit vectors aligned with the local coordinate system directions.

The volume differential in cylindrical coordinates becomes:

$$dV \equiv r\, dr d\theta\, dz \tag{A3}$$

Substituting and combining terms to simplify the result, the differential moment vector is rewritten as follows in Eq. (A4)

$$d\vec{M} = \left(J_z B_r - J_r B_z\right)\left(r\hat{z} + z\hat{r}\right) r dr d\theta dz \tag{A4}$$

When integrating Eq.(A4) over the full range of toroidal angle, $0 \le \theta < 2\pi$, the radial unit vector term, $\hat{r}$, cancels itself out for rotationally symmetric poloidal magnetic fields and TF coil current densities. The remaining nonzero part of the integral is stated in Eq.(A5).

$$\vec{M} = \hat{z}\iiint \left(J_z B_r - J_r B_z\right) r^2 dr d\theta dz = \hat{z}\, 2\pi \iint \left(J_z B_r - J_r B_z\right) r^2 dr dz \tag{A5}$$

In this last form, the double integral is taken over the (r,z) poloidal half-plane. However, current density components are zero everywhere outside the TF coils so the integration region only needs to include the (r,z) projection of TF coil conductors.

An important simplification results from changing over to stream function variables. For axisymmetric systems the poloidal flux stream function, $\Psi(r,z)$, is the total magnetic flux enclosed by the circle centered on and normal to the z axis which passes through (r,z). Poloidal magnetic flux is related to the poloidal magnetic field as stated by Eq.(A6).

$$B_r(r,z) = -\frac{1}{2\pi r}\frac{d\Psi(r,z)}{dz}$$
$$B_z(r,z) = \frac{1}{2\pi r}\frac{d\Psi(r,z)}{dr} \qquad \text{(A6)}$$

so

$$\vec{B} = \frac{1}{2\pi r}\hat{\theta}\times\nabla\Psi \qquad \text{(A7)}$$

We similarly define the toroidal field coil current stream function, *I(r,z)*, as the total TF coil current enclosed by the circle about the z axis passing through (r,z). This current stream function is related to the TF current density as stated by Eq.(A8).

$$J_r(r,z) = -\frac{1}{2\pi r}\frac{dI(r,z)}{dz}$$
$$J_z(r,z) = \frac{1}{2\pi r}\frac{dI(r,z)}{dr} \qquad \text{(A8)}$$

so

$$\vec{J} = \frac{1}{2\pi r}\hat{\theta}\times\nabla I \qquad \text{(A9)}$$

Substituting these stream functions of Eqs.(A7) and (A9) into the previous integral yields Eq.(A10a).

$$\vec{M} = \iiint \vec{r}\times\left(\vec{J}\times\vec{B}\right)dV =$$
$$= \iiint \left(r\hat{r}+z\hat{z}\right)\times\left(\left(\frac{1}{2\pi r}\hat{\theta}\times\nabla I\right)\times\left(\frac{1}{2\pi r}\hat{\theta}\times\nabla\Psi\right)\right)rdrdzd\theta = \qquad \text{(A10a)}$$
$$= \frac{1}{4\pi^2}\iiint\left(\hat{z}-\frac{z}{r}\hat{r}\right)\left(\hat{\theta}\bullet\left(\nabla I\times\nabla\Psi\right)\right)drdzd\theta$$

As stated previously, the radially oriented term cancels out while integrating over toroidal angle, leaving Eq.(A10b) as the result.

$$\vec{M} = \frac{\hat{z}}{2\pi}\iint drdz\left(\frac{\partial I}{\partial r}\frac{\partial\Psi}{\partial z}-\frac{\partial I}{\partial z}\frac{\partial\Psi}{\partial r}\right) = \frac{\hat{z}}{2\pi}\iint\left(\hat{\theta}\bullet\left(\nabla I\times\nabla\Psi\right)\right)drdz \qquad \text{(A10b)}$$

This is a particularly simple and compact formula involving the integral of the cross product of gradients of two scalar functions. The poloidal magnetic flux function can be directly obtained to any desired accuracy by use of Greens functions involving the standard elliptic integral functions, K() and E(), and the current stream function can be approximated using the projected outline of TF conductors. Furthermore, the integral itself can be approximated from these data using very simple algorithms.

Limit for the case of a slender TF conductor

Vector identities applied to Eq.(A10b) imply that

$$\vec{M} = -\frac{\hat{z}}{2\pi}\iint drdz\left(\left(\nabla I \times \hat{\theta}\right)\bullet \nabla\Psi\right) \tag{A11}$$

Here, the integration is over the area of the poloidal projection of the TF conductor segment whose net torque is to be calculated. If the conductor's projection is slender with a small width, w, we can change the element of poloidal area from dA=drdz to dA=dldw where l represents distance along the conductor's length. Assuming constant current density in the conductor the gradient vector of the current stream function, ∇I , has a magnitude equal to the total TF urrent divided by the width, $\left|\nabla I\right| = \frac{I_{TF}}{w}$, and the gradient vector 's direction is perpendicular to the local TF current streamline, pointing towards the coil's bore. It follows that $\left(\nabla I \times \hat{\theta}\right)$ has the same magnitude but is pointed in the same direction as the flowing TF current, a direction denoted here by the unit vector, $\hat{n}$. With these substitutions, the net torque over a slender TF conductor segment extending from point A to point B can be rewritten as in Eq.(A12).

$$\begin{aligned}\vec{M} &= -\frac{\hat{z}}{2\pi}\iint drdz\left(\left(\nabla I \times \hat{\theta}\right)\bullet \nabla\Psi\right)\\ &= -\frac{\hat{z}}{2\pi}\frac{I_{TF}}{w}\int_0^w dw\int_A^B dl\ \hat{n}\bullet\nabla\Psi \\ &= -\frac{\hat{z}}{2\pi}I_{TF}\int_A^B dl\ \hat{n}\bullet\nabla\Psi\end{aligned} \tag{A12}$$

However, this last integral expression in Eq.(A12) may be immediately recognized as the line integral of the gradient of a scalar function, so it has the following Eq.(A13)exact solution:

$$\vec{M} = \hat{z}\ I_{TF}\ \frac{\Psi_A - \Psi_B}{2\pi} \tag{A13}$$

Thus, the general formula of Eq.(A12), when interpreted for slender conductors, asserts that the net torque over a poloidal length of TF conductor is simply the product of the difference between the poloidal flux values at the conductor's ends, divided by 2π, then multiplied by the TF current.

Derivation of Approximation For Wider TF Conductors

Consider a triangular region in the poloidal half-plane, ΔABC, on which the exact scalar functions *I(r,z)* and *Ψ(r,z)* are to be linearly approximated by $\tilde{I}(r,z)$ and $\tilde{\Psi}(r,z)$ using function values that are exact at the triangle's three corners. The linear models are as follows:

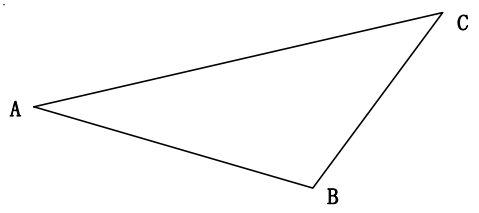

$$I(r,z) \approx \tilde{I}(r,z) = \left(\tilde{I}_0\right) + \left(\frac{\partial \tilde{I}}{\partial r}\right) r + \left(\frac{\partial \tilde{I}}{\partial z}\right) z$$
$$\Psi(r,z) \approx \tilde{\Psi}(r,z) = \left(\tilde{\Psi}_0\right) + \left(\frac{\partial \tilde{\Psi}}{\partial r}\right) r + \left(\frac{\partial \tilde{\Psi}}{\partial z}\right) z \qquad \text{(A14)}$$

where $\left(\tilde{I}_0\right), \left(\frac{\partial \tilde{I}}{\partial r}\right), \left(\frac{\partial \tilde{I}}{\partial z}\right), \left(\tilde{\Psi}_0\right), \left(\frac{\partial \tilde{\Psi}}{\partial r}\right), \left(\frac{\partial \tilde{\Psi}}{\partial z}\right)$ are linear model coefficient parameters that have constant values throughout the triangle. The requirement to match the approximation to actual function values at triangle corners yields the following matrix equations, where $(r_A, z_A), (r_B, z_B), (r_C, z_C)$ are the coordinates of the triangle's corners:

$$\begin{bmatrix} 1 & r_A & z_A \\ 1 & r_B & z_B \\ 1 & r_C & z_C \end{bmatrix} \begin{bmatrix} \left(\tilde{I}_0\right) \\ \left(\frac{\partial \tilde{I}}{\partial r}\right) \\ \left(\frac{\partial \tilde{I}}{\partial z}\right) \end{bmatrix} = \begin{bmatrix} I_A \\ I_B \\ I_C \end{bmatrix} \qquad \text{(A15)}$$

$$\begin{bmatrix} 1 & r_A & z_A \\ 1 & r_B & z_B \\ 1 & r_C & z_C \end{bmatrix} \begin{bmatrix} \left(\tilde{\Psi}_0\right) \\ \left(\frac{\partial \tilde{\Psi}}{\partial r}\right) \\ \left(\frac{\partial \tilde{\Psi}}{\partial z}\right) \end{bmatrix} = \begin{bmatrix} \Psi_A \\ \Psi_B \\ \Psi_C \end{bmatrix} \qquad \text{(A16)}$$

These can be readily solved in closed form to find the appropriate coefficient parameter values. For the partial derivative coefficient parameters the solutions are as follows:

$$\left(\frac{\partial \tilde{I}}{\partial r}\right) = \frac{I_A(z_B - z_C) + I_B(z_C - z_A) + I_C(z_A - z_B)}{r_A(z_B - z_C) + r_B(z_C - z_A) + r_C(z_A - z_B)}$$
$$\left(\frac{\partial \tilde{I}}{\partial z}\right) = \frac{I_A(r_B - r_C) + I_B(r_C - r_A) + I_C(r_A - r_B)}{z_A(r_B - r_C) + z_B(r_C - r_A) + z_C(r_A - r_B)}$$
$$\left(\frac{\partial \tilde{\Psi}}{\partial r}\right) = \frac{\Psi_A(z_B - z_C) + \Psi_B(z_C - z_A) + \Psi_C(z_A - z_B)}{r_A(z_B - z_C) + r_B(z_C - z_A) + r_C(z_A - z_B)} \qquad \text{(A17)}$$
$$\left(\frac{\partial \tilde{\Psi}}{\partial z}\right) = \frac{\Psi_A(r_B - r_C) + \Psi_B(r_C - r_A) + \Psi_C(r_A - r_B)}{z_A(r_B - r_C) + z_B(r_C - r_A) + z_C(r_A - r_B)}$$

Using this approximation the previous integrand becomes:

$$\hat{\theta}\bullet\left(\nabla I\times\nabla\Psi\right)\equiv\left(\frac{\partial I}{\partial r}\frac{\partial\Psi}{\partial z}-\frac{\partial I}{\partial z}\frac{\partial\Psi}{\partial r}\right)\approx\left(\frac{\partial\tilde{I}}{\partial r}\frac{\partial\tilde{\Psi}}{\partial z}-\frac{\partial\tilde{I}}{\partial z}\frac{\partial\tilde{\Psi}}{\partial r}\right)= \\ =\frac{I_A\left(\Psi_B-\Psi_C\right)+I_B\left(\Psi_C-\Psi_A\right)+I_C\left(\Psi_A-\Psi_B\right)}{r_A\left(z_B-z_C\right)+r_B\left(z_C-z_A\right)+r_C\left(z_A-z_B\right)} \tag{A18}$$

Note that as a result of assuming a linear model over the triangle, this approximation gives a constant value of the integrand over the triangle. Thus, the *integral* over the triangle is simply this integrand's constant value times the triangle's area, which, assuming the ABC point sequence is counterclockwise, is:

$$\left[\text{Area of Triangle }\Delta\text{ABC}\right]=\frac{1}{2}\begin{vmatrix}1 & r_A & z_A\\ 1 & r_B & z_B\\ 1 & r_C & z_C\end{vmatrix}=\frac{r_A\left(z_B-z_C\right)+r_B\left(z_C-z_A\right)+r_C\left(z_A-z_B\right)}{2} \tag{A19}$$

This cancels all (r,z) coordinates, so the integral over the triangle becomes as stated in Eq.(A20).

$$\vec{M}_{\Delta ABC}\approx\hat{z}\left(\frac{I_A\left(\Psi_B-\Psi_C\right)+I_B\left(\Psi_C-\Psi_A\right)+I_C\left(\Psi_A-\Psi_B\right)}{4\pi}\right) \tag{A20}$$

This formula can be applied to an adjacent bordering triangle, ΔACD, by changing indices as in Eq.(A21).

$$\vec{M}_{\Delta ACD}\approx\hat{z}\left(\frac{I_A\left(\Psi_C-\Psi_D\right)+I_C\left(\Psi_D-\Psi_A\right)+I_D\left(\Psi_A-\Psi_C\right)}{4\pi}\right) \tag{A21}$$

The two triangles together form a quadrilateral, ABCD, so the integral over the entire quadrilateral is the sum of the two triangle integrals:

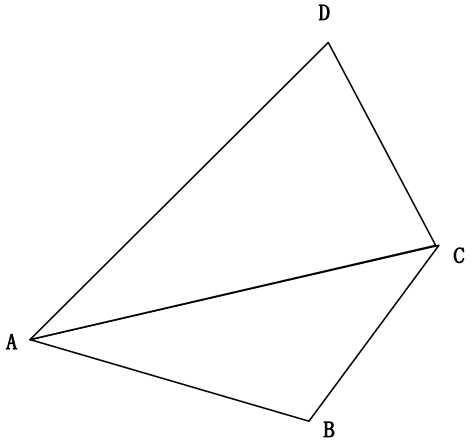

$$\vec{M}_{ABCD}=\vec{M}_{\Delta ABC}+\vec{M}_{\Delta ACD}\approx \\ \approx\hat{z}\left(\begin{array}{l}\dfrac{I_A\left(\Psi_B-\Psi_C\right)+I_B\left(\Psi_C-\Psi_A\right)+I_C\left(\Psi_A-\Psi_B\right)}{4\pi}\\ +\dfrac{I_A\left(\Psi_C-\Psi_D\right)+I_C\left(\Psi_D-\Psi_A\right)+I_D\left(\Psi_A-\Psi_C\right)}{4\pi}\end{array}\right)= \\ =\hat{z}\left(\frac{\left(I_A-I_C\right)\left(\Psi_B-\Psi_D\right)-\left(I_B-I_D\right)\left(\Psi_A-\Psi_C\right)}{4\pi}\right) \tag{A22}$$

The quadrilateral, ABCD, could alternatively be decomposed in a different way into two triangles, i.e., into triangle ΔABD and triangle ΔBCD. Although the linear coefficient parameter sets that would apply for these triangles would be different from the above, the final resulting formula for the moment integral over the quadrilateral ABCD turns out to be identically the same!

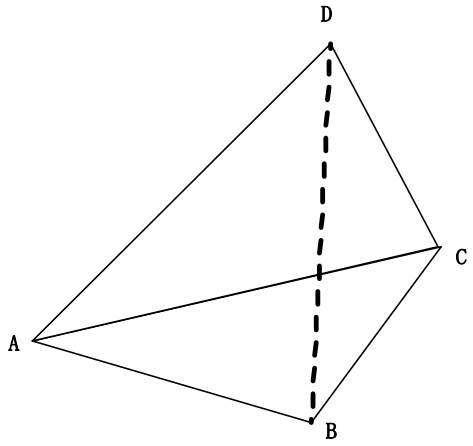

Note that in the important special case wherein the quadrilateral's corner points are located on two TF current stream function contour lines, it follows that $I_A=I_D$ and $I_B=I_C$. In that case the approximate formula for net torque in the quadrilateral region of the poloidal half-plane becomes simplified to Eq.(A23).

$$\vec{M}^{\text{AD\&BC on TFCurrent Streamlines}}_{\text{ABCD}} = \hat{z}\left(I_A - I_B\right)\left(\frac{\Psi_A + \Psi_B - \Psi_C - \Psi_D}{4\pi}\right). \qquad \text{(A23)}$$

This is the simple average of the differences between per radian poloidal magnetic fluxes at the two ends of each of the two bounding current stream function contours, multiplied by the TF current enclosed between those two current stream function contours.

Thus, the torsional OOP loading of the TF coil system can be evaluated by taking simple sums and differences of poloidal flux evaluated at points located on TF current streamlines.

A Higher Accuracy Numerical Approximation

In the present case of this memo's calculations of net torque in the NSTX CSU TF conductor due to poloidal field interactions with TF current, five TF current streamlines have been chosen and their separation in terms of contour levels is the total TF current divided by four. The adjacent diagram illustrates the five contours and flux evaluation points on those contours for two adjacent poloidal angle locations. Applying the torque formula to each of the for quadrilaterals having the ten indicated locations as their corners, the sum of the net torque is as stated in Eq.(A24).

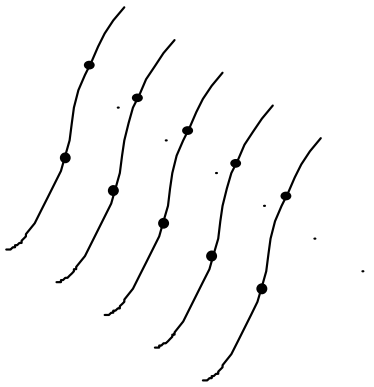

$$\begin{aligned}\vec{M} &= \hat{z}\left(\frac{I_{TF}}{4}\right)\left(\frac{\Psi_1^1 + \Psi_2^1 - \Psi_2^2 - \Psi_1^2}{4\pi}\right) + \hat{z}\left(\frac{I_{TF}}{4}\right)\left(\frac{\Psi_2^1 + \Psi_3^1 - \Psi_3^2 - \Psi_2^2}{4\pi}\right) \\ &+ \hat{z}\left(\frac{I_{TF}}{4}\right)\left(\frac{\Psi_3^1 + \Psi_4^1 - \Psi_4^2 - \Psi_3^2}{4\pi}\right) + \hat{z}\left(\frac{I_{TF}}{4}\right)\left(\frac{\Psi_4^1 + \Psi_5^1 - \Psi_5^2 - \Psi_4^2}{4\pi}\right) \qquad \text{(A24)}\end{aligned}$$

$$= \hat{z}\,\frac{I_{TF}}{2\pi}\begin{pmatrix} 0.125\left(\Psi_1^1 - \Psi_1^2\right) + 0.25\left(\Psi_2^1 - \Psi_2^2\right) + 0.25\left(\Psi_3^1 - \Psi_3^2\right) \\ + 0.25\left(\Psi_4^1 - \Psi_4^2\right) + 0.125\left(\Psi_5^1 - \Psi_5^2\right) \end{pmatrix}$$

Thus, in the sum over one poloidal interval we must premultiply the column vector of five local flux values by the row vector, [1 2 2 2 1], then divide by 16π before subtracting from the corresponding result for the other poloidal location.

Note that if all five flux values at one poloidal location were identical to each other the result would be that single value divided by 2π.

Note also that there is no benefit from repeating this summation procedure over many poloidal intervals in a TF conductor segment and summing their results, since the quantities evaluated at all intermediate poloidal locations would identically cancel each other out in taking the poloidal intervals sum. It is mathematically equivalent to directly subtract the quantities calculated on the five contours at the TF conductor segment's ends.

APPENDIX 2

Torsion Analysis Results With Nominal Stiffness Parameter Values

Using the stiffness parameter values of this memo, hear stress stress profiles were calculated for the 96 plasma equilibrium cases previously defined by J. Menard and for a single +24 kA OH precharge case. The different shear profiles are all graphed on the following pages. Peak shear stress values are collected in the following table for these cases. The maximum absolute shear was 25.234 MPa, observed for equilibrium case #1 and again in equilibrium case #16.

Table A2 and plots show peak shear stress is mostly due to OH, and reaches its maximum when the OH current is -24 kA. PF coils and plasma are smaller contributors to peak shear stress.

Table A2: TF Centerstack Max Absolute Shear Stress ; Precharge and Plasma Cases

Case# -24 kA OH	Peak Shear MPa	Case# 0 kA OH	Peak Shear MPa	Case# 13 kA OH	Peak Shear MPa	Case 24 kA OH	Peak Shear MPa
						Precharge	17.075
1	25.2342	2	7.8607	3	9.9531		
4	25.0242	5	7.7104	6	9.7952		
7	24.8916	8	7.8971	9	9.7799		
10	24.7792	11	8.1233	12	10.1388		
13	24.7974	14	8.1955	15	10.2218		
16	25.2342	17	7.8607	18	9.9531		
19	23.5284	20	7.5095	21	9.5377		
22	24.0073	23	7.7574	24	9.7794		
25	24.3660	26	7.8945	27	9.8867		
28	24.6358	29	8.1082	30	9.9733		
31	24.7383	32	8.4486	33	10.1411		
34	22.7757	35	9.6055	36	11.8424		
37	23.1024	38	9.6302	39	11.8662		
40	23.5114	41	9.5922	42	11.8414		
43	23.9825	44	9.4749	45	11.7359		
46	24.3098	47	9.1979	38	11.5040		
49	21.5879	50	8.5384	51	10.7784		
52	21.9790	53	8.6015	54	10.8492		
55	22.5061	56	8.6266	57	10.8669		
58	23.0224	59	8.5566	60	10.8048		
61	23.5439	62	8.3331	63	10.6176		
64	25.1894	65	8.9480	66	11.0566		
67	25.0718	68	8.7566	69	10.8486		
70	24.6347	71	8.1963	72	10.2964		
73	24.1861	74	7.8472	75	9.9392		
76	23.7807	77	7.5209	78	9.6075		
79	23.2512	80	7.2031	81	9.2976		
82	24.6500	83	10.1626	84	12.1672		

85	24.7093	86	9.3389	87	11.3258		
88	24.7711	89	8.7861	90	10.7808		
91	24.8086	92	8.4007	93	10.3819		
94	24.8460	95	8.0646	96	10.0348		

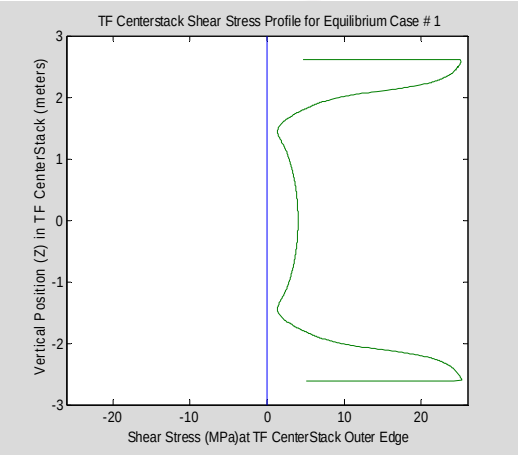
TF Centerstack Shear Stress Profile for Equilibrium Case # 1
Vertical Position (Z) in TF CenterStack (meters)
Shear Stress (MPa)at TF CenterStack Outer Edge

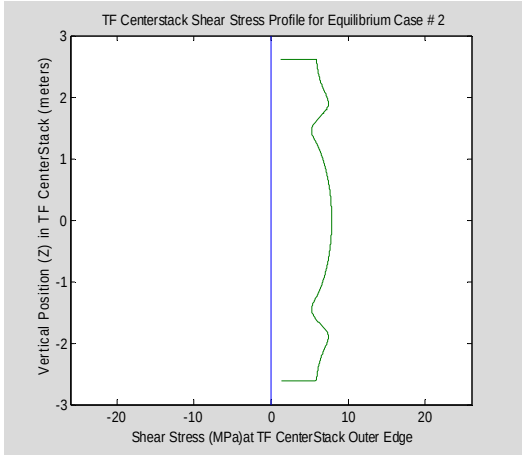
TF Centerstack Shear Stress Profile for Equilibrium Case # 2
Vertical Position (Z) in TF CenterStack (meters)
Shear Stress (MPa)at TF CenterStack Outer Edge

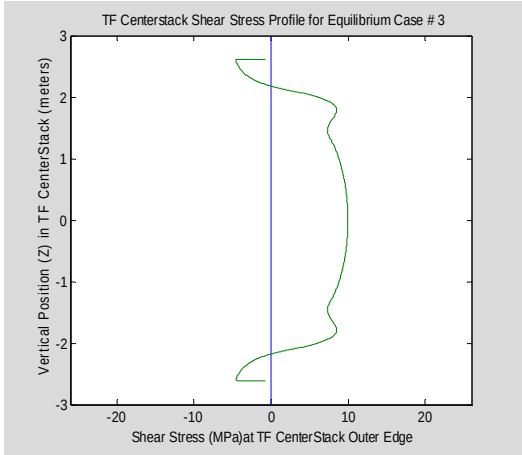
TF Centerstack Shear Stress Profile for Equilibrium Case # 3
Vertical Position (Z) in TF CenterStack (meters)
Shear Stress (MPa)at TF CenterStack Outer Edge

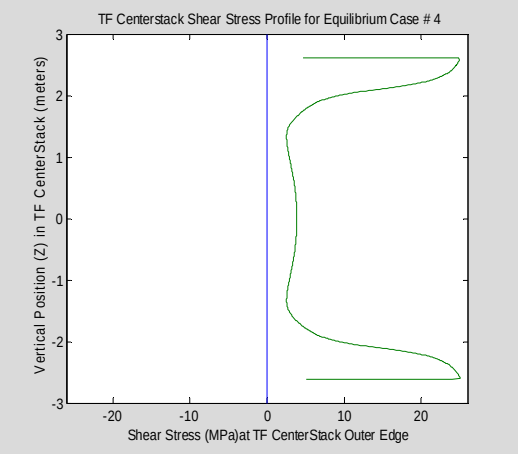
TF Centerstack Shear Stress Profile for Equilibrium Case # 4
Vertical Position (Z) in TF CenterStack (meters)
Shear Stress (MPa)at TF CenterStack Outer Edge

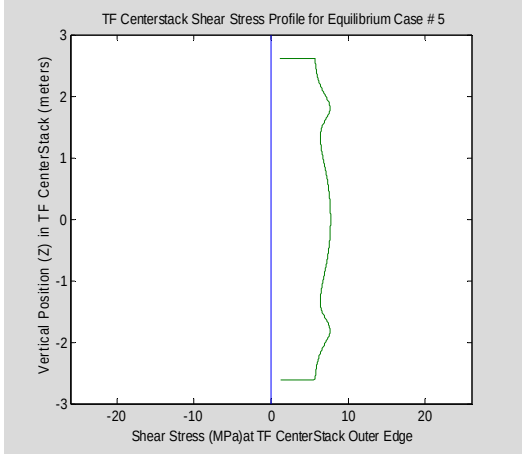
TF Centerstack Shear Stress Profile for Equilibrium Case # 5
Vertical Position (Z) in TF CenterStack (meters)
Shear Stress (MPa)at TF CenterStack Outer Edge

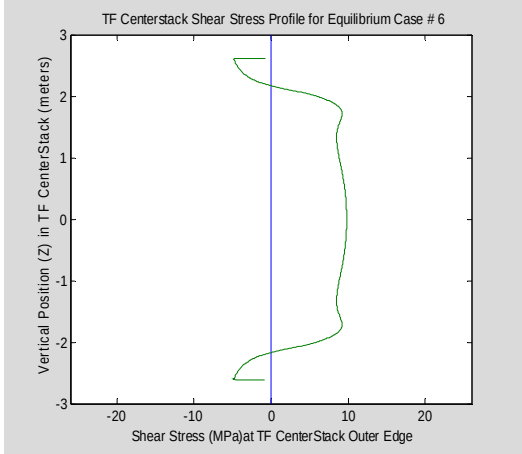
TF Centerstack Shear Stress Profile for Equilibrium Case # 6
Vertical Position (Z) in TF CenterStack (meters)
Shear Stress (MPa)at TF CenterStack Outer Edge

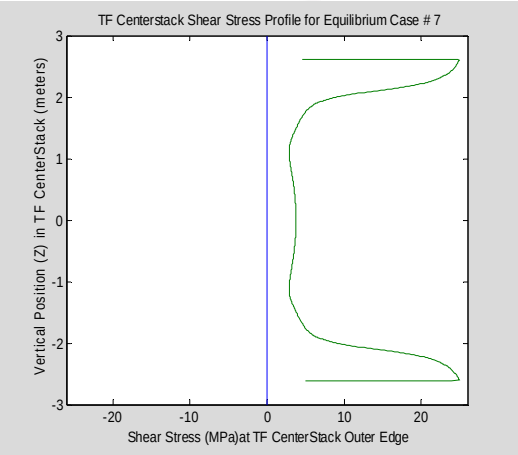
TF Centerstack Shear Stress Profile for Equilibrium Case # 7
Vertical Position (Z) in TF CenterStack (meters)
Shear Stress (MPa)at TF CenterStack Outer Edge

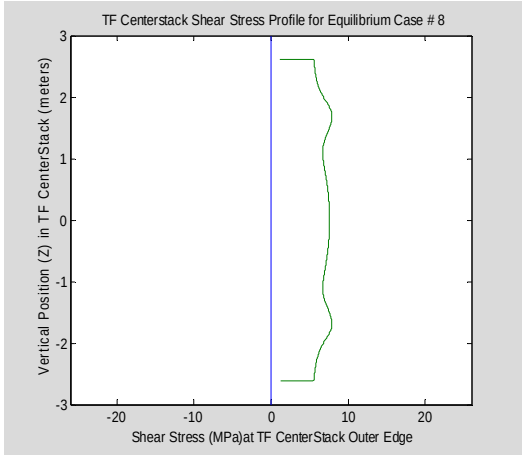
TF Centerstack Shear Stress Profile for Equilibrium Case # 8
Vertical Position (Z) in TF CenterStack (meters)
Shear Stress (MPa)at TF CenterStack Outer Edge

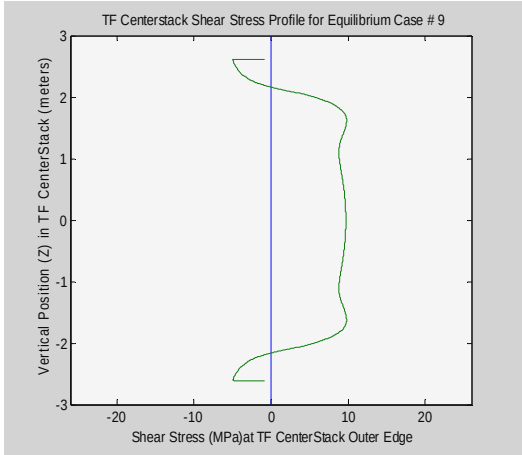
TF Centerstack Shear Stress Profile for Equilibrium Case # 9
Vertical Position (Z) in TF CenterStack (meters)
Shear Stress (MPa)at TF CenterStack Outer Edge

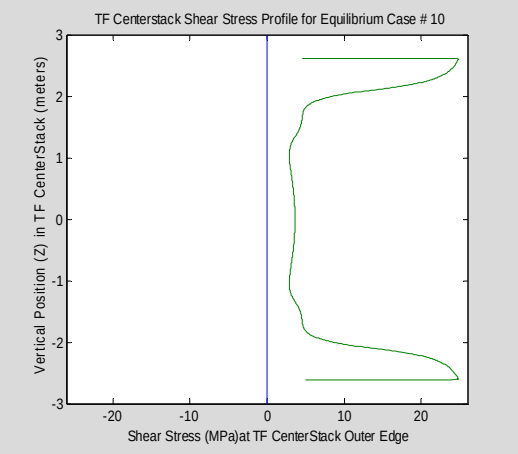
TF Centerstack Shear Stress Profile for Equilibrium Case # 10
Vertical Position (Z) in TF CenterStack (meters)
Shear Stress (MPa)at TF CenterStack Outer Edge

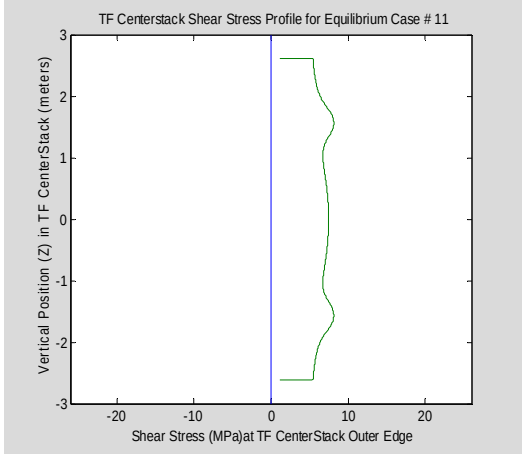
TF Centerstack Shear Stress Profile for Equilibrium Case # 11
Vertical Position (Z) in TF CenterStack (meters)
Shear Stress (MPa)at TF CenterStack Outer Edge

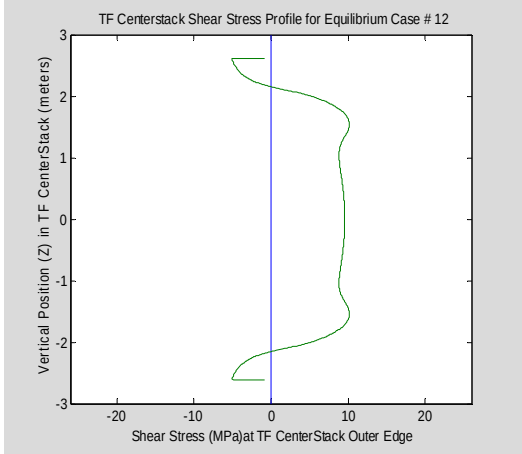
TF Centerstack Shear Stress Profile for Equilibrium Case # 12
Vertical Position (Z) in TF CenterStack (meters)
Shear Stress (MPa)at TF CenterStack Outer Edge

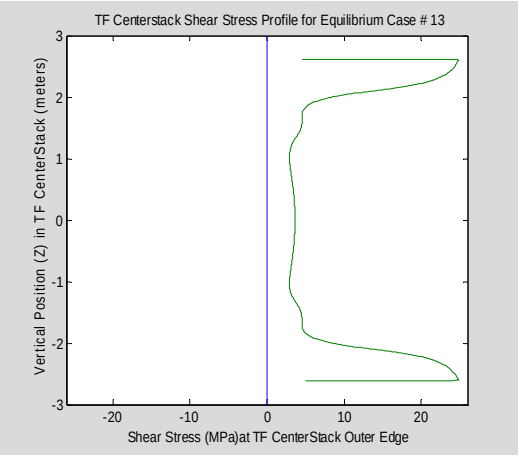
TF Centerstack Shear Stress Profile for Equilibrium Case # 13
Vertical Position (Z) in TF CenterStack (meters)
Shear Stress (MPa)at TF CenterStack Outer Edge

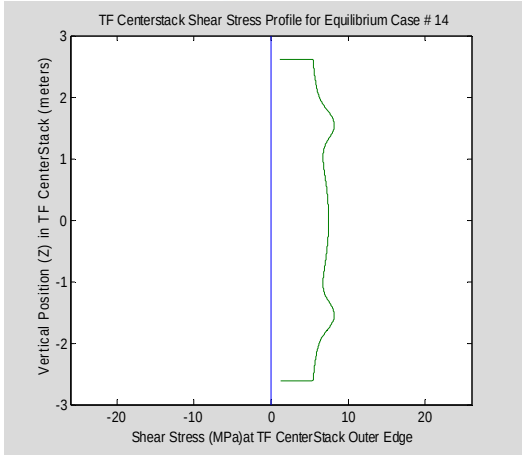
TF Centerstack Shear Stress Profile for Equilibrium Case # 14
Vertical Position (Z) in TF CenterStack (meters)
Shear Stress (MPa)at TF CenterStack Outer Edge

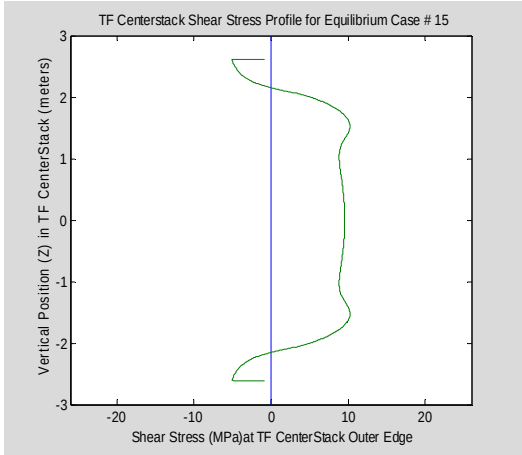
TF Centerstack Shear Stress Profile for Equilibrium Case # 15
Vertical Position (Z) in TF CenterStack (meters)
Shear Stress (MPa)at TF CenterStack Outer Edge

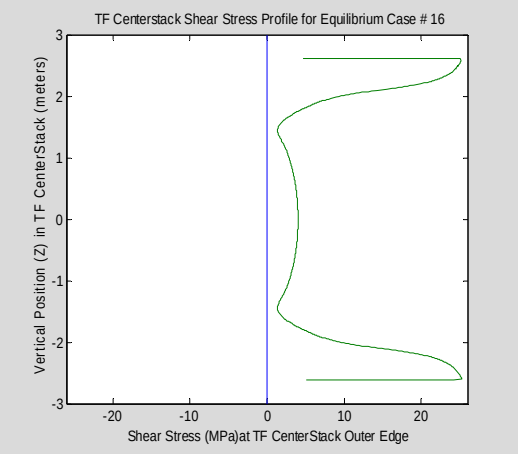
TF Centerstack Shear Stress Profile for Equilibrium Case # 16
Vertical Position (Z) in TF CenterStack (meters)
Shear Stress (MPa)at TF CenterStack Outer Edge

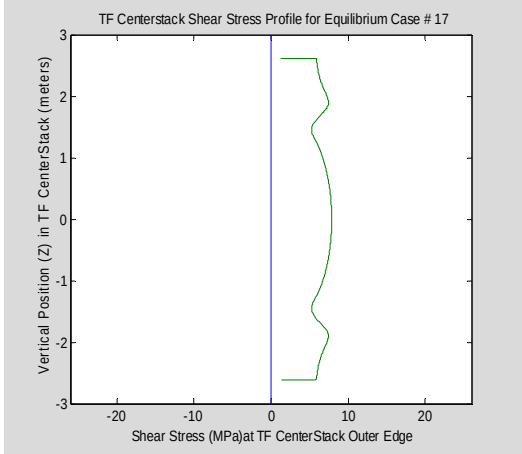
TF Centerstack Shear Stress Profile for Equilibrium Case # 17
Vertical Position (Z) in TF CenterStack (meters)
Shear Stress (MPa)at TF CenterStack Outer Edge

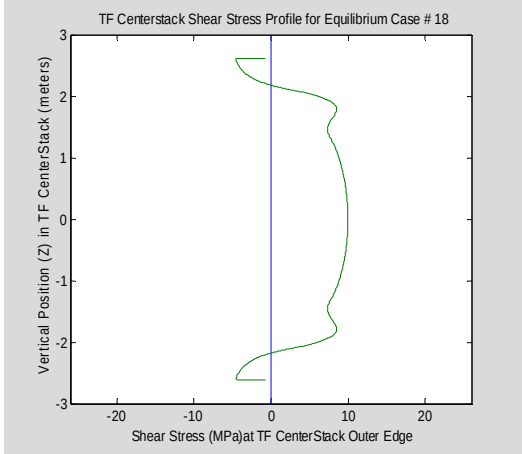
TF Centerstack Shear Stress Profile for Equilibrium Case # 18
Vertical Position (Z) in TF CenterStack (meters)
Shear Stress (MPa)at TF CenterStack Outer Edge

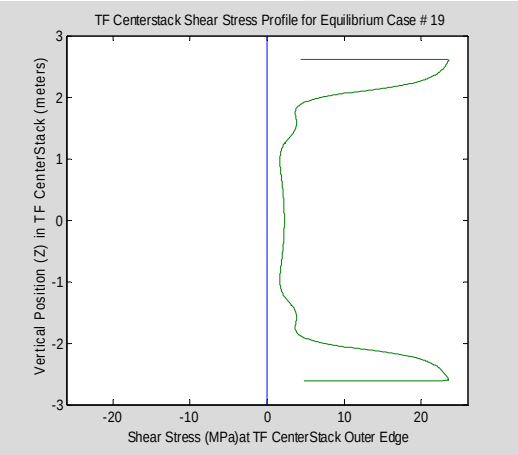
TF Centerstack Shear Stress Profile for Equilibrium Case # 19
Vertical Position (Z) in TF CenterStack (meters)
Shear Stress (MPa)at TF CenterStack Outer Edge

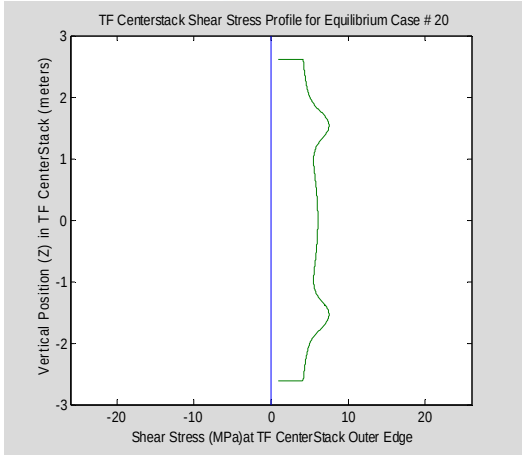
TF Centerstack Shear Stress Profile for Equilibrium Case # 20
Vertical Position (Z) in TF CenterStack (meters)
Shear Stress (MPa)at TF CenterStack Outer Edge

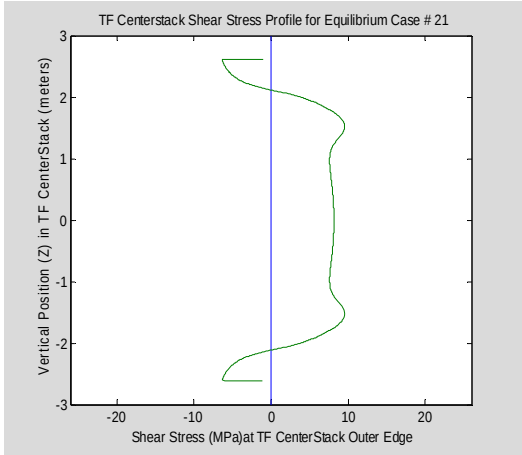
TF Centerstack Shear Stress Profile for Equilibrium Case # 21
Vertical Position (Z) in TF CenterStack (meters)
Shear Stress (MPa)at TF CenterStack Outer Edge

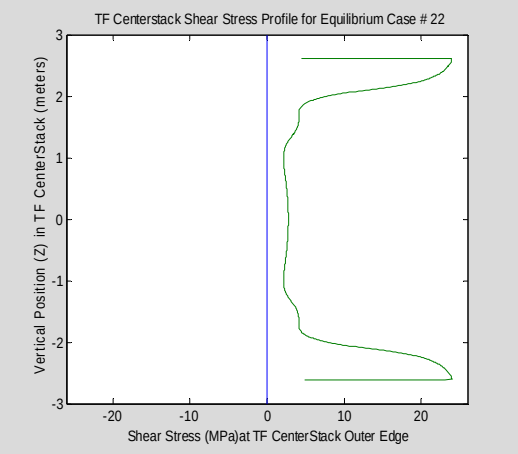
TF Centerstack Shear Stress Profile for Equilibrium Case # 22
Vertical Position (Z) in TF CenterStack (meters)
Shear Stress (MPa)at TF CenterStack Outer Edge

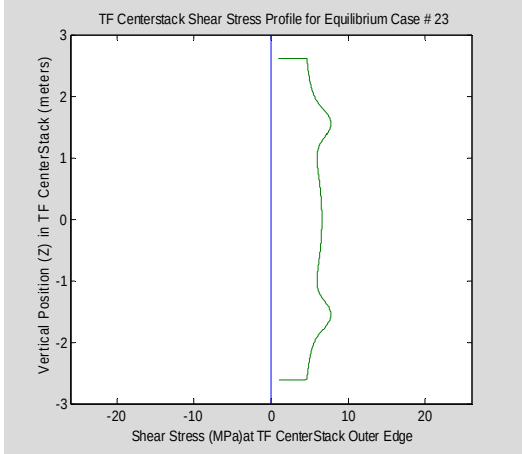
TF Centerstack Shear Stress Profile for Equilibrium Case # 23
Vertical Position (Z) in TF CenterStack (meters)
Shear Stress (MPa)at TF CenterStack Outer Edge

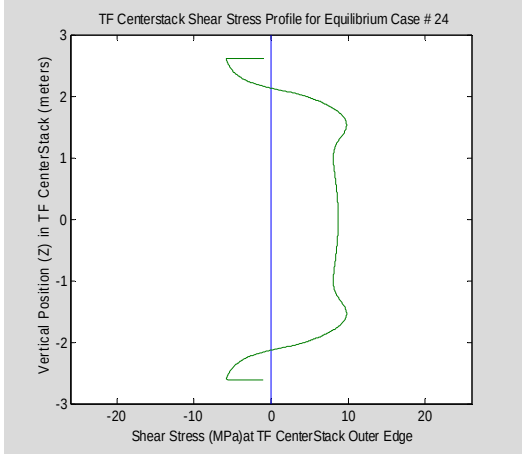
TF Centerstack Shear Stress Profile for Equilibrium Case # 24
Vertical Position (Z) in TF CenterStack (meters)
Shear Stress (MPa)at TF CenterStack Outer Edge

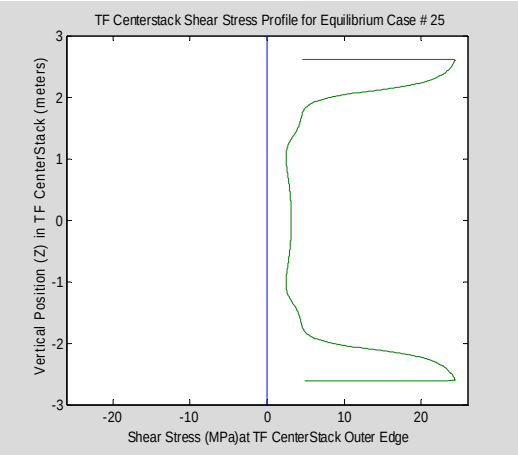
TF Centerstack Shear Stress Profile for Equilibrium Case # 25
Vertical Position (Z) in TF CenterStack (meters)
Shear Stress (MPa)at TF CenterStack Outer Edge

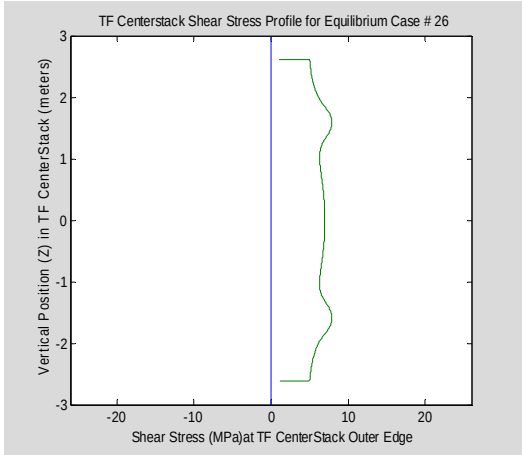
TF Centerstack Shear Stress Profile for Equilibrium Case # 26
Vertical Position (Z) in TF CenterStack (meters)
Shear Stress (MPa)at TF CenterStack Outer Edge

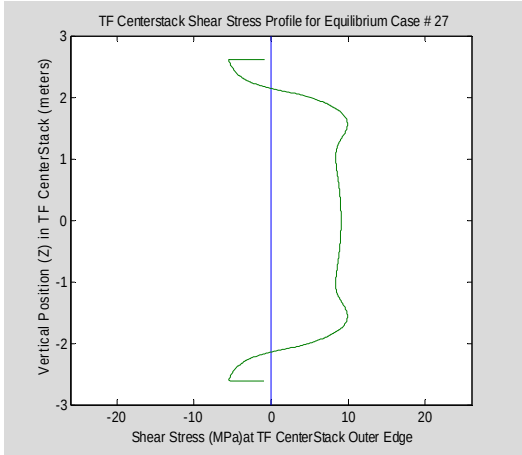
TF Centerstack Shear Stress Profile for Equilibrium Case # 27
Vertical Position (Z) in TF CenterStack (meters)
Shear Stress (MPa)at TF CenterStack Outer Edge

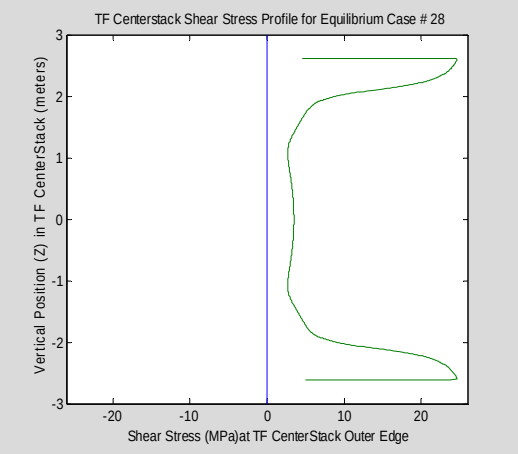
TF Centerstack Shear Stress Profile for Equilibrium Case # 28
Vertical Position (Z) in TF CenterStack (meters)
Shear Stress (MPa)at TF CenterStack Outer Edge

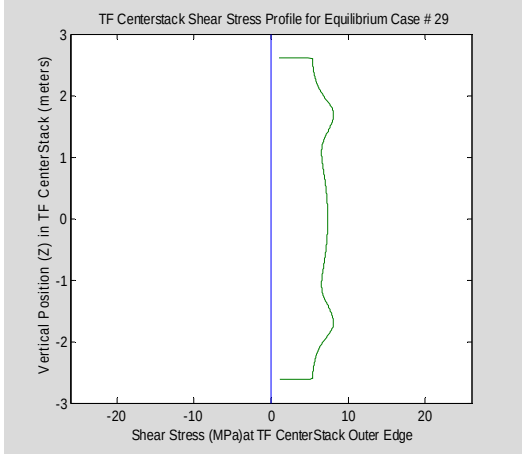
TF Centerstack Shear Stress Profile for Equilibrium Case # 29
Vertical Position (Z) in TF CenterStack (meters)
Shear Stress (MPa)at TF CenterStack Outer Edge

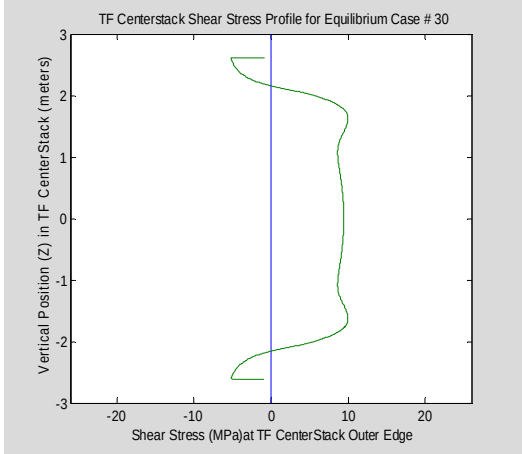
TF Centerstack Shear Stress Profile for Equilibrium Case # 30
Vertical Position (Z) in TF CenterStack (meters)
Shear Stress (MPa)at TF CenterStack Outer Edge

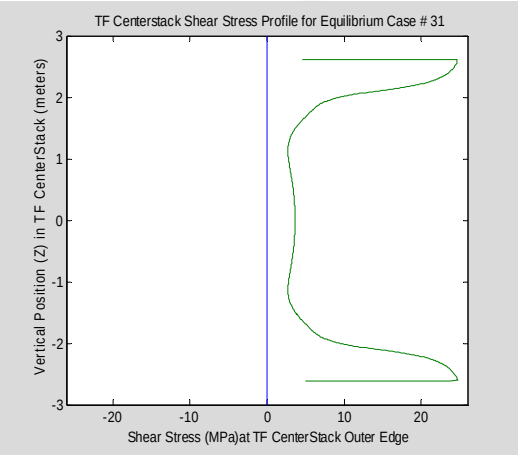
TF Centerstack Shear Stress Profile for Equilibrium Case # 31
Vertical Position (Z) in TF CenterStack (meters)
Shear Stress (MPa)at TF CenterStack Outer Edge

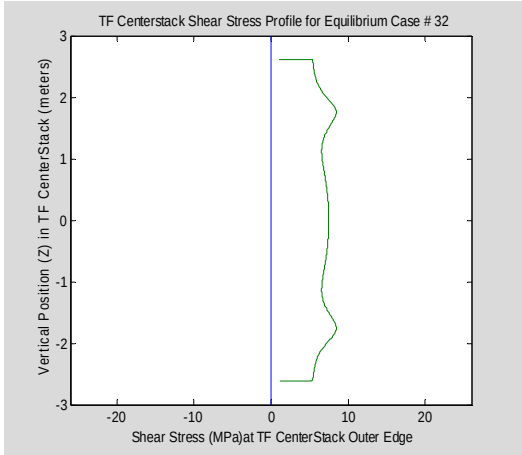
TF Centerstack Shear Stress Profile for Equilibrium Case # 32
Vertical Position (Z) in TF CenterStack (meters)
Shear Stress (MPa)at TF CenterStack Outer Edge

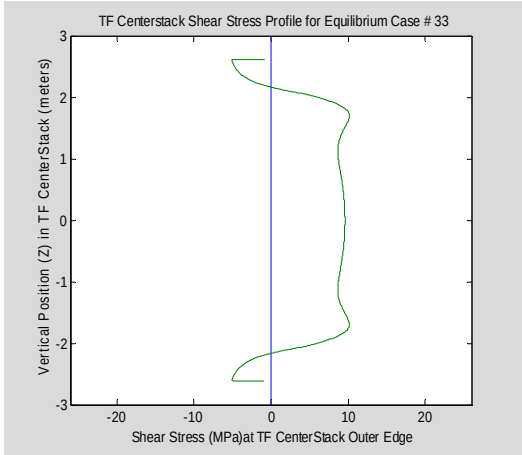
TF Centerstack Shear Stress Profile for Equilibrium Case # 33
Vertical Position (Z) in TF CenterStack (meters)
Shear Stress (MPa)at TF CenterStack Outer Edge

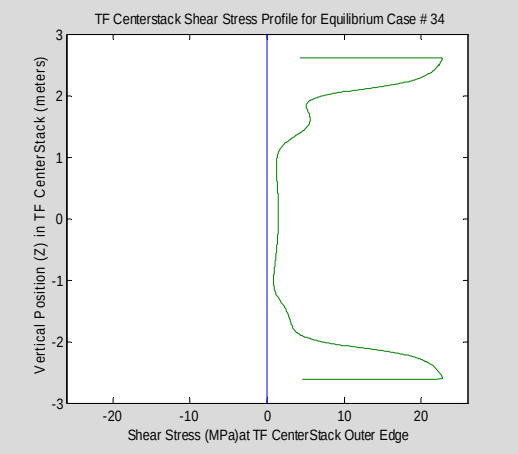
TF Centerstack Shear Stress Profile for Equilibrium Case # 34
Vertical Position (Z) in TF CenterStack (meters)
Shear Stress (MPa)at TF CenterStack Outer Edge

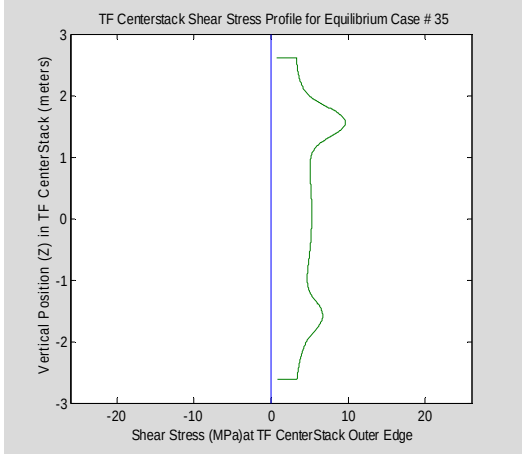
TF Centerstack Shear Stress Profile for Equilibrium Case # 35
Vertical Position (Z) in TF CenterStack (meters)
Shear Stress (MPa)at TF CenterStack Outer Edge

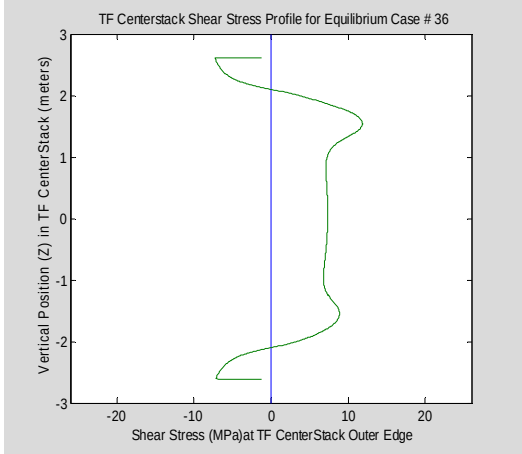
TF Centerstack Shear Stress Profile for Equilibrium Case # 36
Vertical Position (Z) in TF CenterStack (meters)
Shear Stress (MPa)at TF CenterStack Outer Edge

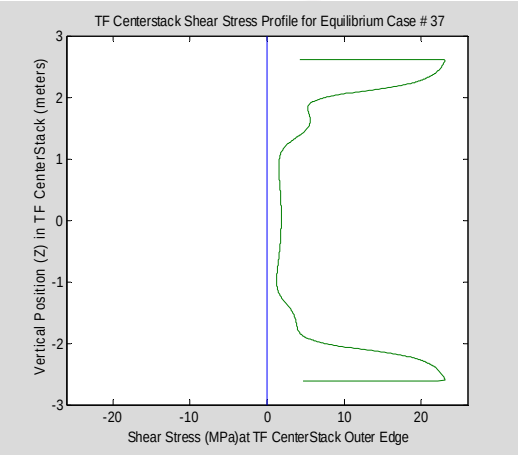
TF Centerstack Shear Stress Profile for Equilibrium Case # 37
Vertical Position (Z) in TF CenterStack (meters)
Shear Stress (MPa)at TF CenterStack Outer Edge

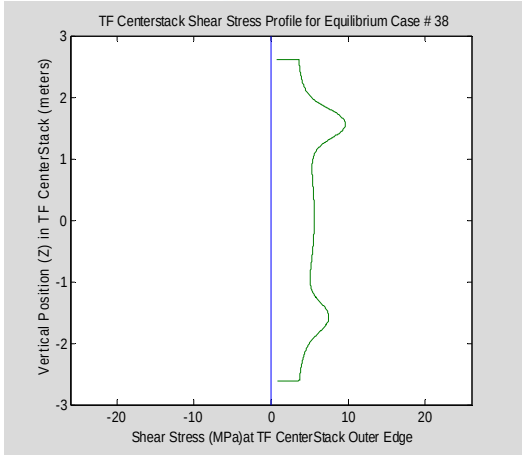
TF Centerstack Shear Stress Profile for Equilibrium Case # 38
Vertical Position (Z) in TF CenterStack (meters)
Shear Stress (MPa)at TF CenterStack Outer Edge

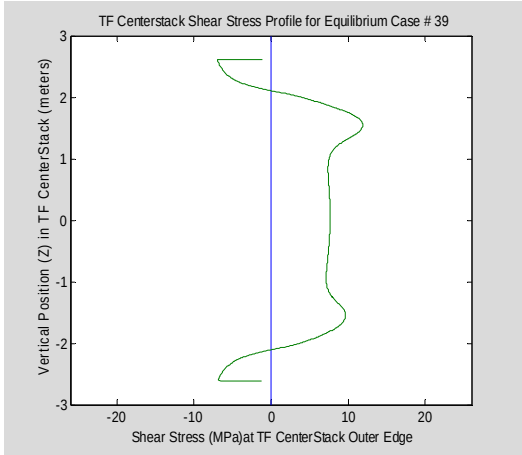
TF Centerstack Shear Stress Profile for Equilibrium Case # 39
Vertical Position (Z) in TF CenterStack (meters)
Shear Stress (MPa)at TF CenterStack Outer Edge

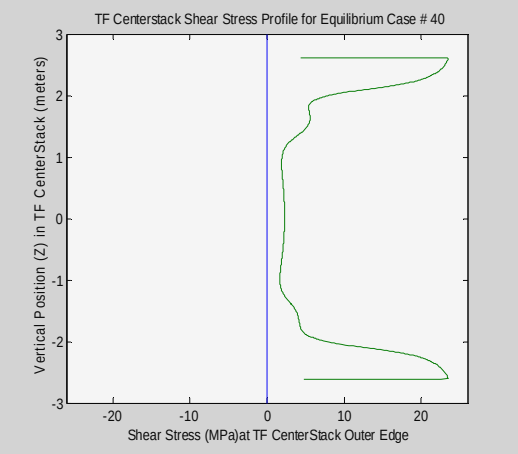
TF Centerstack Shear Stress Profile for Equilibrium Case # 40
Vertical Position (Z) in TF CenterStack (meters)
Shear Stress (MPa)at TF CenterStack Outer Edge

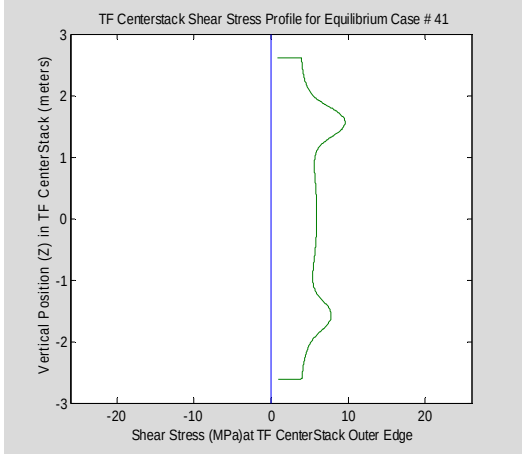
TF Centerstack Shear Stress Profile for Equilibrium Case # 41
Vertical Position (Z) in TF CenterStack (meters)
Shear Stress (MPa)at TF CenterStack Outer Edge

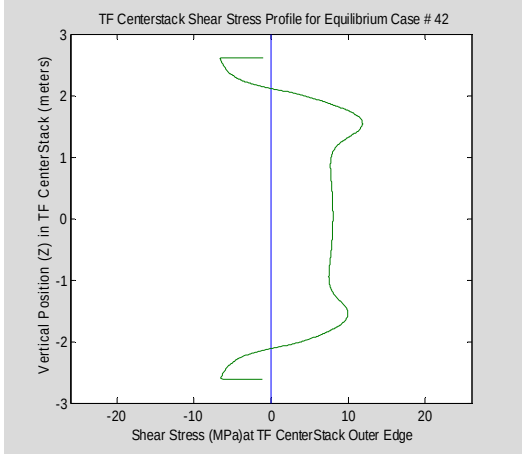
TF Centerstack Shear Stress Profile for Equilibrium Case # 42
Vertical Position (Z) in TF CenterStack (meters)
Shear Stress (MPa)at TF CenterStack Outer Edge

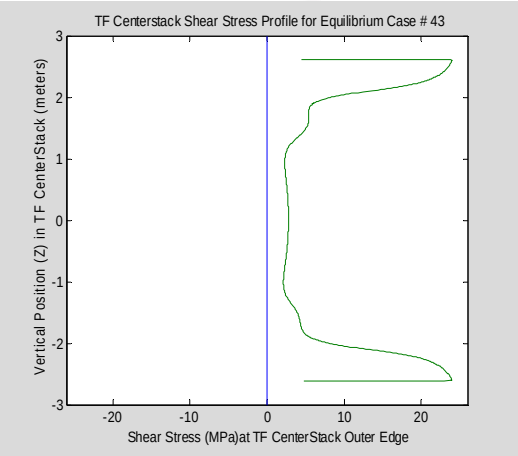
TF Centerstack Shear Stress Profile for Equilibrium Case # 43
Vertical Position (Z) in TF CenterStack (meters)
Shear Stress (MPa)at TF CenterStack Outer Edge

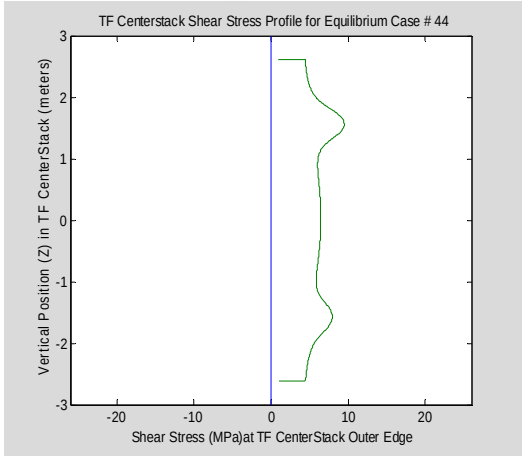
TF Centerstack Shear Stress Profile for Equilibrium Case # 44
Vertical Position (Z) in TF CenterStack (meters)
Shear Stress (MPa)at TF CenterStack Outer Edge

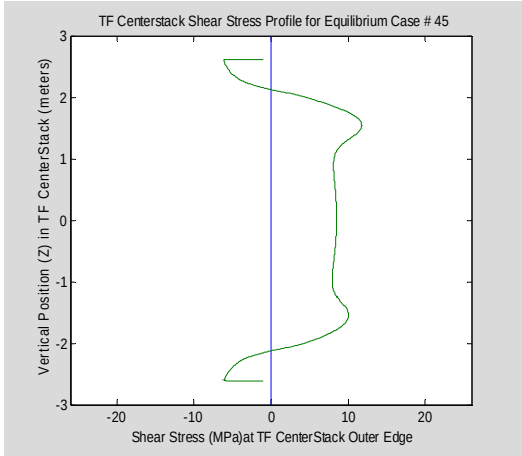
TF Centerstack Shear Stress Profile for Equilibrium Case # 45
Vertical Position (Z) in TF CenterStack (meters)
Shear Stress (MPa)at TF CenterStack Outer Edge

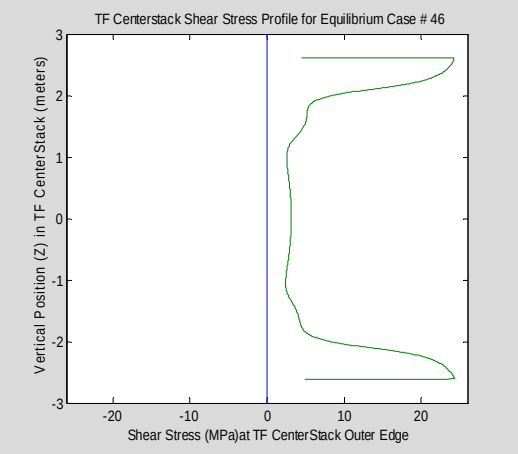
TF Centerstack Shear Stress Profile for Equilibrium Case # 46
Vertical Position (Z) in TF CenterStack (meters)
Shear Stress (MPa)at TF CenterStack Outer Edge

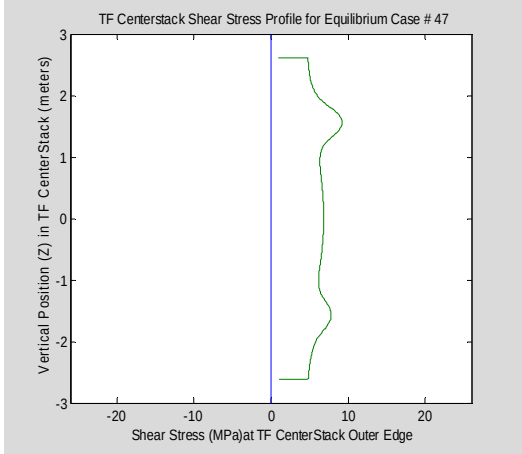
TF Centerstack Shear Stress Profile for Equilibrium Case # 47
Vertical Position (Z) in TF CenterStack (meters)
Shear Stress (MPa)at TF CenterStack Outer Edge

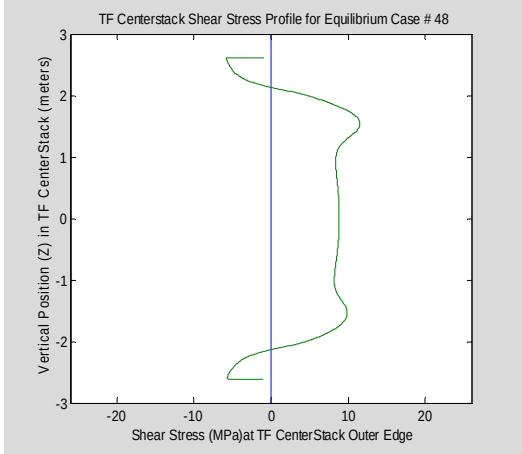
TF Centerstack Shear Stress Profile for Equilibrium Case # 48
Vertical Position (Z) in TF CenterStack (meters)
Shear Stress (MPa)at TF CenterStack Outer Edge

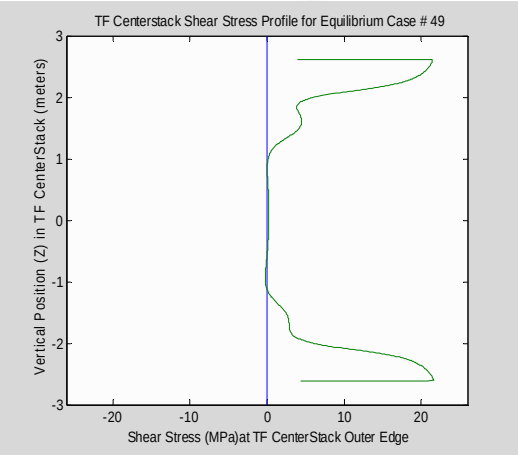
TF Centerstack Shear Stress Profile for Equilibrium Case # 49
Vertical Position (Z) in TF CenterStack (meters)
Shear Stress (MPa)at TF CenterStack Outer Edge

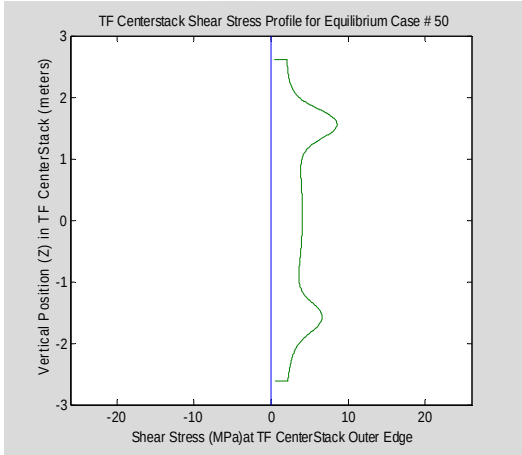
TF Centerstack Shear Stress Profile for Equilibrium Case # 50
Vertical Position (Z) in TF CenterStack (meters)
Shear Stress (MPa)at TF CenterStack Outer Edge

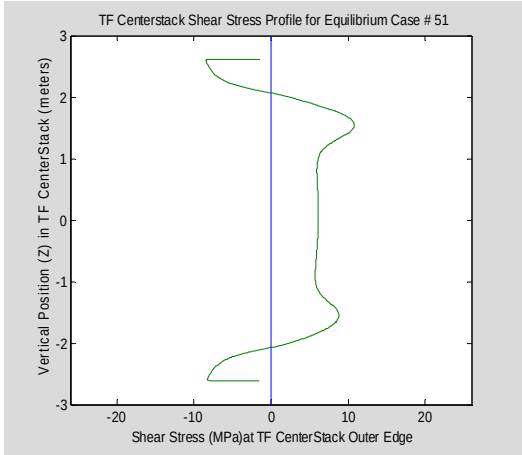
TF Centerstack Shear Stress Profile for Equilibrium Case # 51
Vertical Position (Z) in TF CenterStack (meters)
Shear Stress (MPa)at TF CenterStack Outer Edge

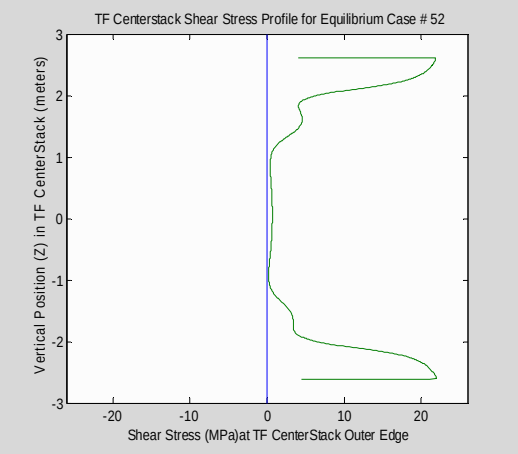
TF Centerstack Shear Stress Profile for Equilibrium Case # 52
Vertical Position (Z) in TF CenterStack (meters)
Shear Stress (MPa)at TF CenterStack Outer Edge

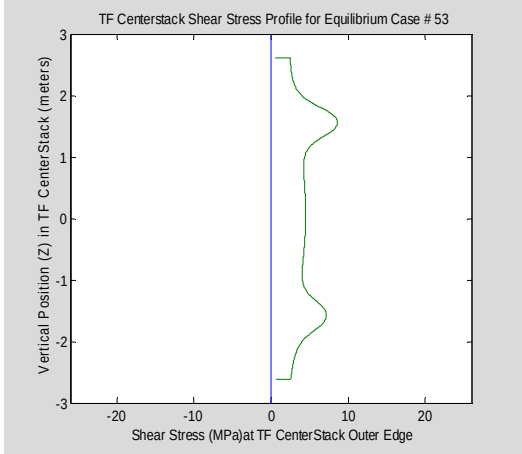
TF Centerstack Shear Stress Profile for Equilibrium Case # 53
Vertical Position (Z) in TF CenterStack (meters)
Shear Stress (MPa)at TF CenterStack Outer Edge

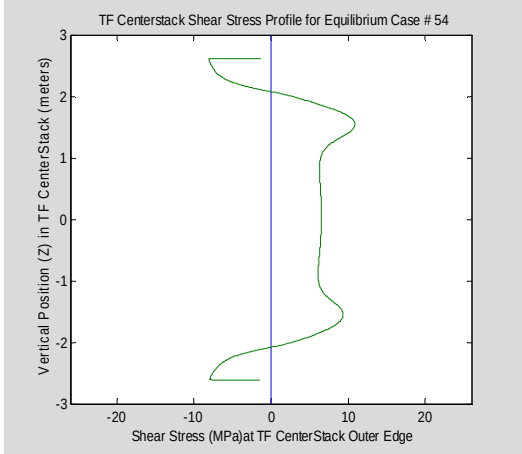
TF Centerstack Shear Stress Profile for Equilibrium Case # 54
Vertical Position (Z) in TF CenterStack (meters)
Shear Stress (MPa)at TF CenterStack Outer Edge

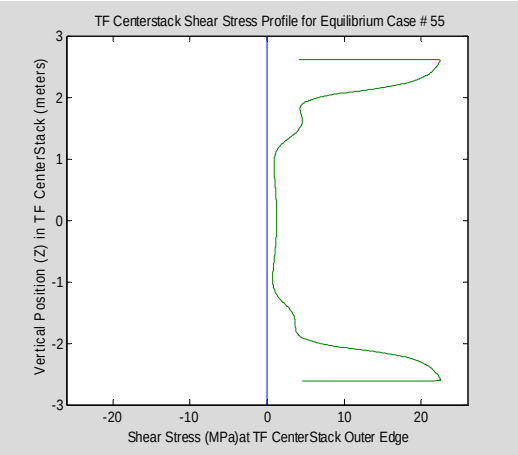
TF Centerstack Shear Stress Profile for Equilibrium Case # 55
Vertical Position (Z) in TF CenterStack (meters)
Shear Stress (MPa)at TF CenterStack Outer Edge

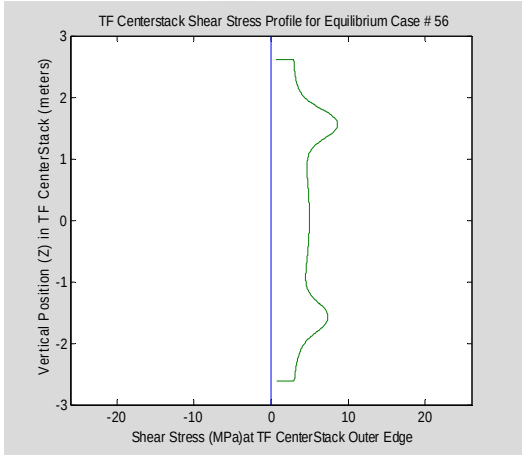
TF Centerstack Shear Stress Profile for Equilibrium Case # 56
Vertical Position (Z) in TF CenterStack (meters)
Shear Stress (MPa)at TF CenterStack Outer Edge

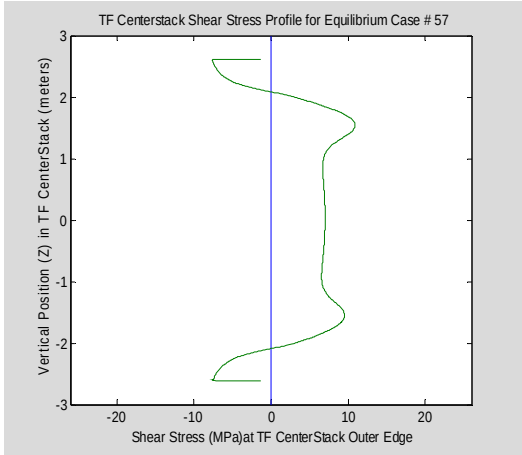
TF Centerstack Shear Stress Profile for Equilibrium Case # 57
Vertical Position (Z) in TF CenterStack (meters)
Shear Stress (MPa)at TF CenterStack Outer Edge

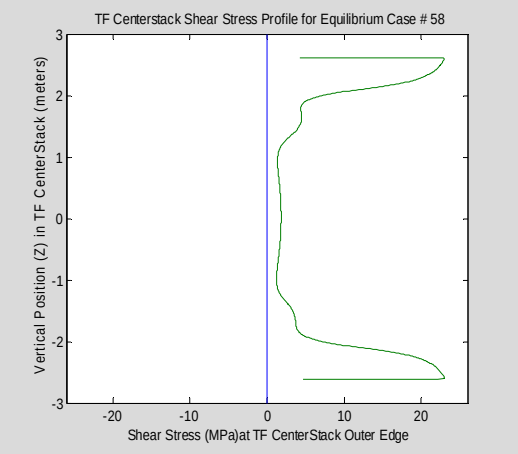
TF Centerstack Shear Stress Profile for Equilibrium Case # 58
Vertical Position (Z) in TF CenterStack (meters)
Shear Stress (MPa)at TF CenterStack Outer Edge

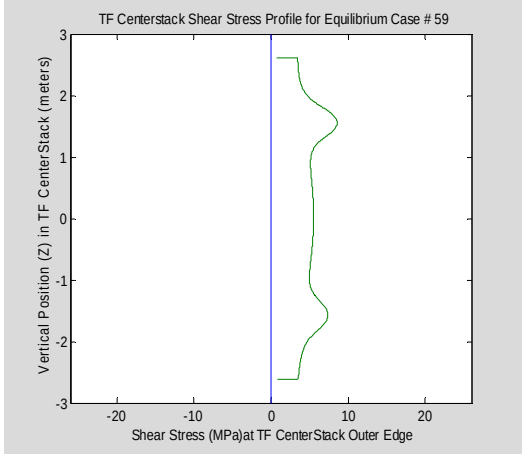
TF Centerstack Shear Stress Profile for Equilibrium Case # 59
Vertical Position (Z) in TF CenterStack (meters)
Shear Stress (MPa)at TF CenterStack Outer Edge

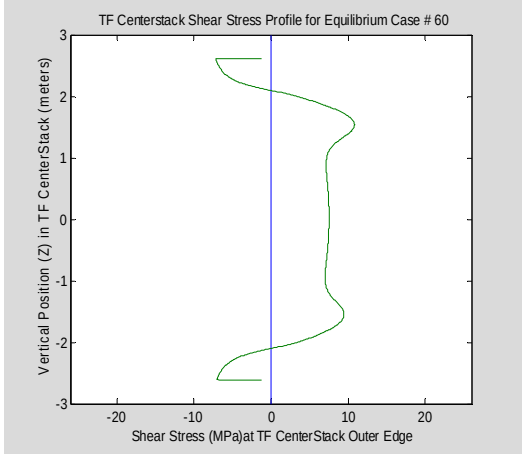
TF Centerstack Shear Stress Profile for Equilibrium Case # 60
Vertical Position (Z) in TF CenterStack (meters)
Shear Stress (MPa)at TF CenterStack Outer Edge

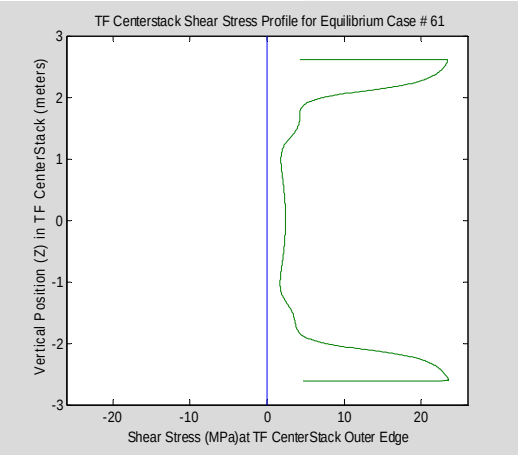
TF Centerstack Shear Stress Profile for Equilibrium Case # 61
Vertical Position (Z) in TF CenterStack (meters)
Shear Stress (MPa)at TF CenterStack Outer Edge

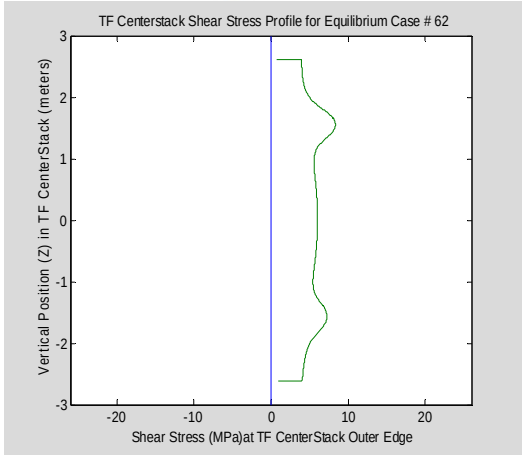
TF Centerstack Shear Stress Profile for Equilibrium Case # 62
Vertical Position (Z) in TF CenterStack (meters)
Shear Stress (MPa)at TF CenterStack Outer Edge

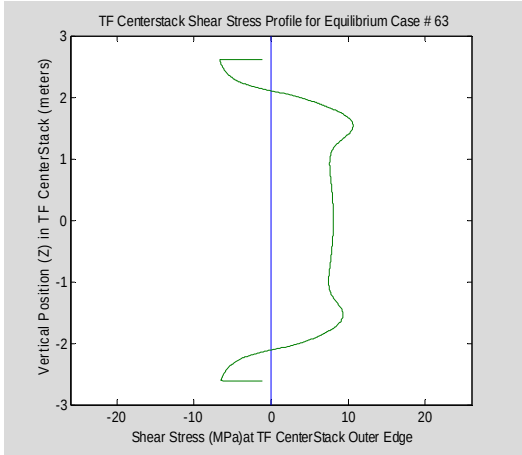
TF Centerstack Shear Stress Profile for Equilibrium Case # 63
Vertical Position (Z) in TF CenterStack (meters)
Shear Stress (MPa)at TF CenterStack Outer Edge

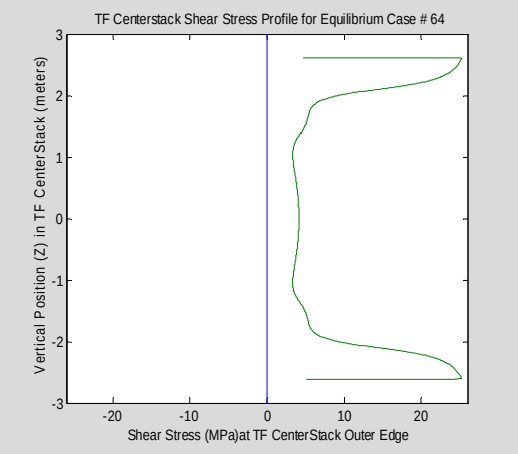
TF Centerstack Shear Stress Profile for Equilibrium Case # 64
Vertical Position (Z) in TF CenterStack (meters)
Shear Stress (MPa)at TF CenterStack Outer Edge

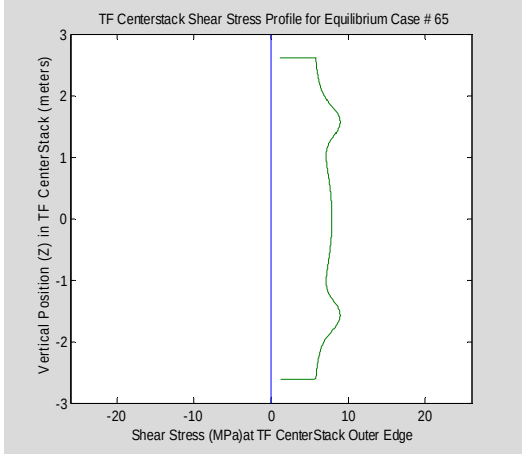
TF Centerstack Shear Stress Profile for Equilibrium Case # 65
Vertical Position (Z) in TF CenterStack (meters)
Shear Stress (MPa)at TF CenterStack Outer Edge

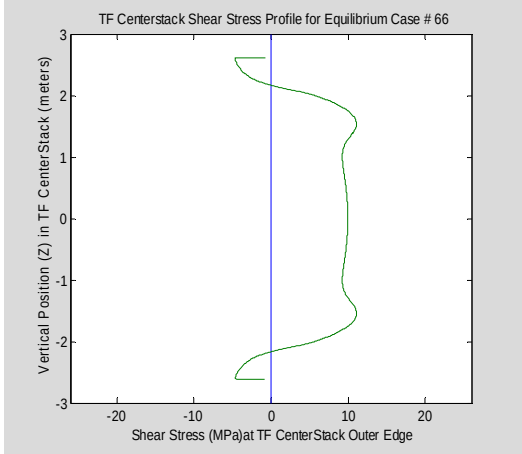
TF Centerstack Shear Stress Profile for Equilibrium Case # 66
Vertical Position (Z) in TF CenterStack (meters)
Shear Stress (MPa)at TF CenterStack Outer Edge

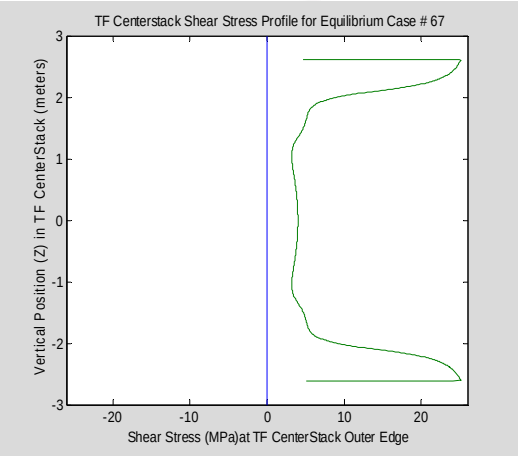
TF Centerstack Shear Stress Profile for Equilibrium Case # 67
Vertical Position (Z) in TF CenterStack (meters)
Shear Stress (MPa)at TF CenterStack Outer Edge

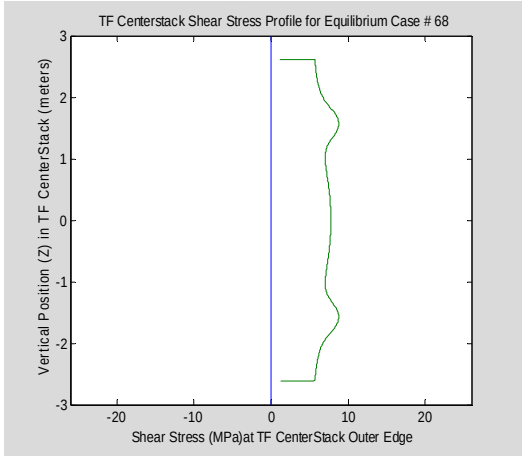
TF Centerstack Shear Stress Profile for Equilibrium Case # 68
Vertical Position (Z) in TF CenterStack (meters)
Shear Stress (MPa)at TF CenterStack Outer Edge

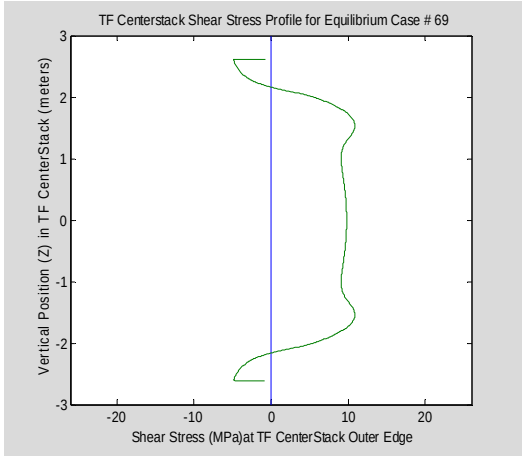
TF Centerstack Shear Stress Profile for Equilibrium Case # 69
Vertical Position (Z) in TF CenterStack (meters)
Shear Stress (MPa)at TF CenterStack Outer Edge

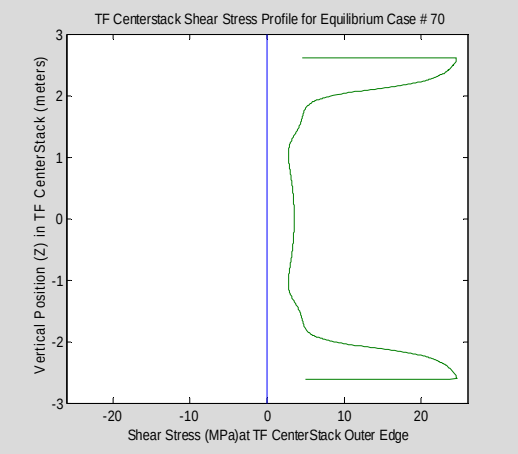
TF Centerstack Shear Stress Profile for Equilibrium Case # 70
Vertical Position (Z) in TF CenterStack (meters)
Shear Stress (MPa)at TF CenterStack Outer Edge

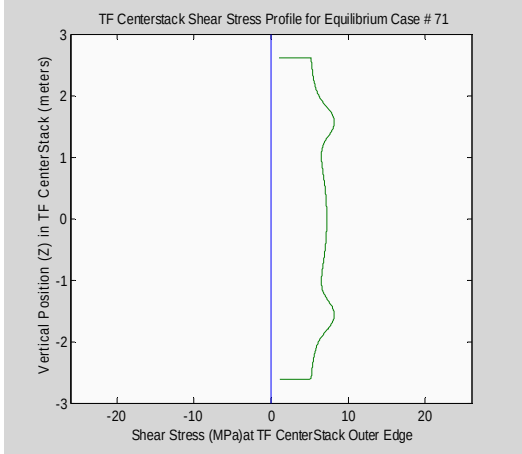
TF Centerstack Shear Stress Profile for Equilibrium Case # 71
Vertical Position (Z) in TF CenterStack (meters)
Shear Stress (MPa)at TF CenterStack Outer Edge

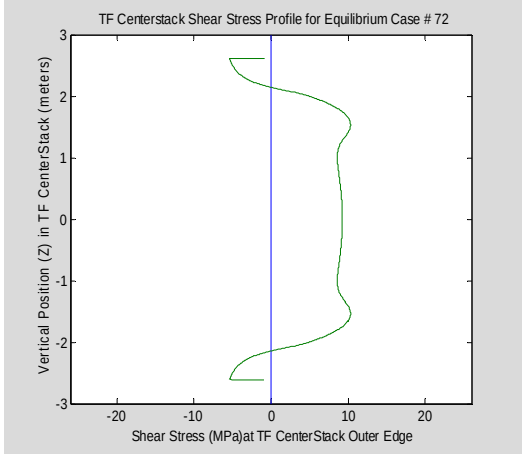
TF Centerstack Shear Stress Profile for Equilibrium Case # 72
Vertical Position (Z) in TF CenterStack (meters)
Shear Stress (MPa)at TF CenterStack Outer Edge

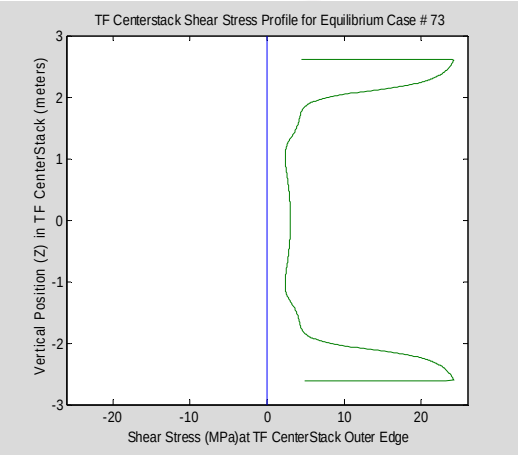
TF Centerstack Shear Stress Profile for Equilibrium Case # 73
Vertical Position (Z) in TF CenterStack (meters)
Shear Stress (MPa)at TF CenterStack Outer Edge

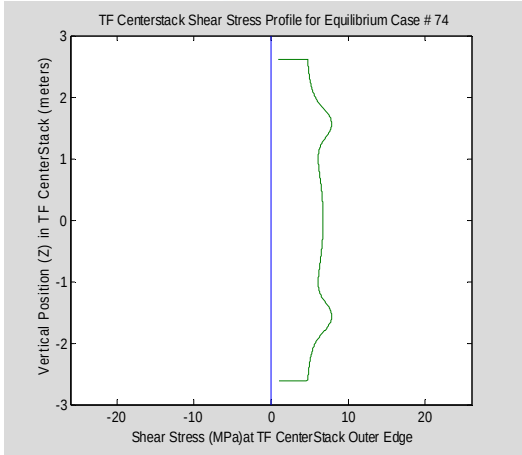
TF Centerstack Shear Stress Profile for Equilibrium Case # 74
Vertical Position (Z) in TF CenterStack (meters)
Shear Stress (MPa)at TF CenterStack Outer Edge

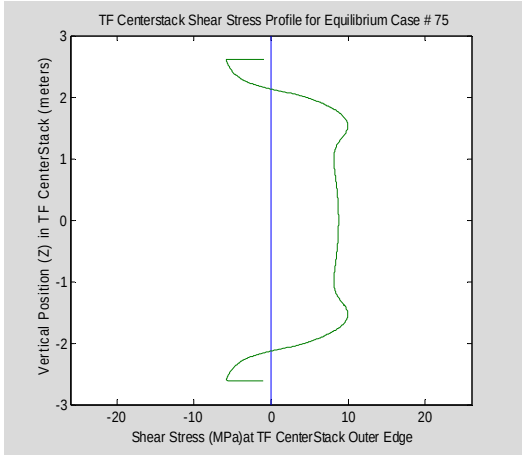
TF Centerstack Shear Stress Profile for Equilibrium Case # 75
Vertical Position (Z) in TF CenterStack (meters)
Shear Stress (MPa)at TF CenterStack Outer Edge

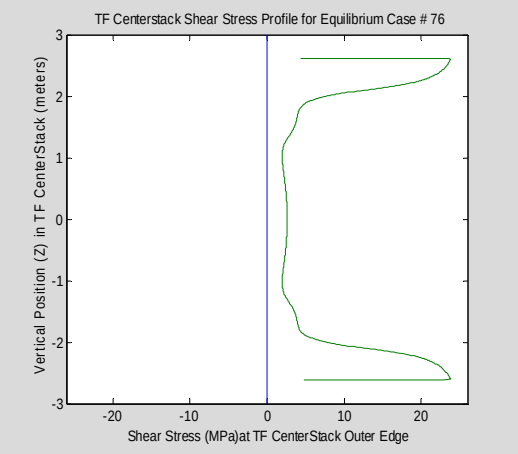
TF Centerstack Shear Stress Profile for Equilibrium Case # 76
Vertical Position (Z) in TF CenterStack (meters)
Shear Stress (MPa)at TF CenterStack Outer Edge

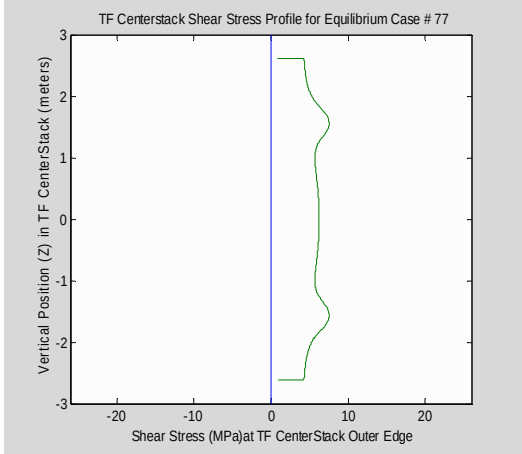
TF Centerstack Shear Stress Profile for Equilibrium Case # 77
Vertical Position (Z) in TF CenterStack (meters)
Shear Stress (MPa)at TF CenterStack Outer Edge

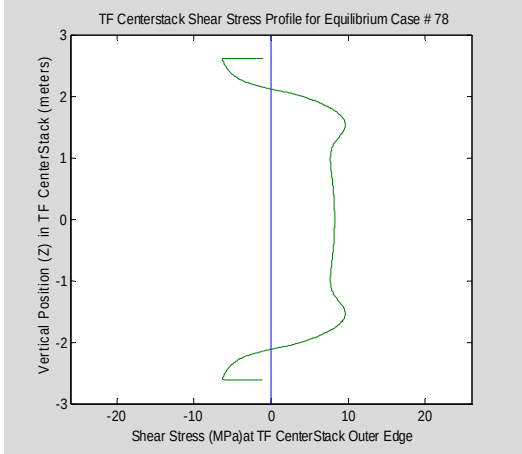
TF Centerstack Shear Stress Profile for Equilibrium Case # 78
Vertical Position (Z) in TF CenterStack (meters)
Shear Stress (MPa)at TF CenterStack Outer Edge

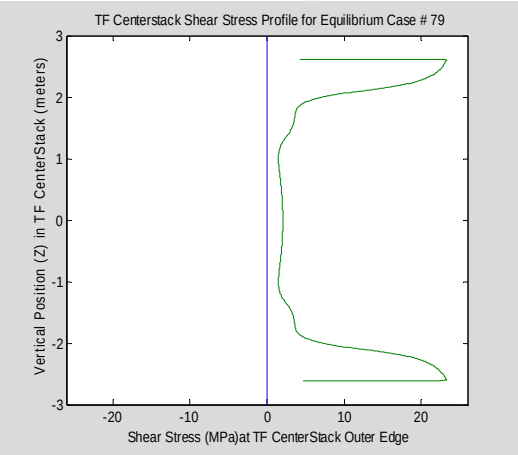
TF Centerstack Shear Stress Profile for Equilibrium Case # 79
Vertical Position (Z) in TF CenterStack (meters)
Shear Stress (MPa)at TF CenterStack Outer Edge

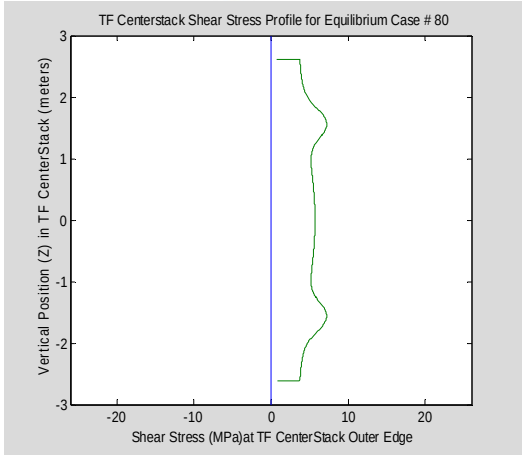
TF Centerstack Shear Stress Profile for Equilibrium Case # 80
Vertical Position (Z) in TF CenterStack (meters)
Shear Stress (MPa)at TF CenterStack Outer Edge

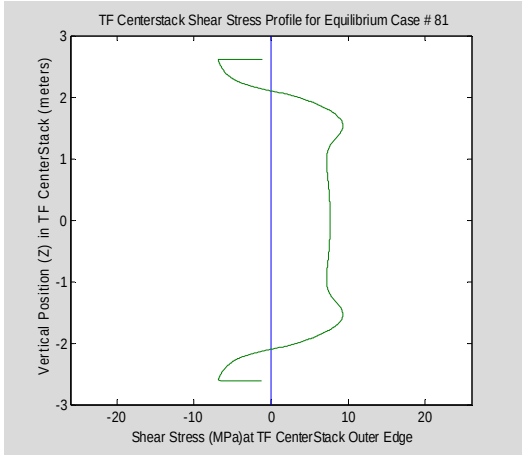
TF Centerstack Shear Stress Profile for Equilibrium Case # 81
Vertical Position (Z) in TF CenterStack (meters)
Shear Stress (MPa)at TF CenterStack Outer Edge

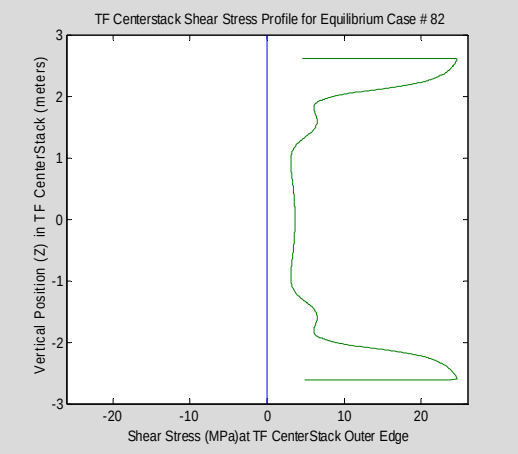
TF Centerstack Shear Stress Profile for Equilibrium Case # 82
Vertical Position (Z) in TF CenterStack (meters)
Shear Stress (MPa)at TF CenterStack Outer Edge

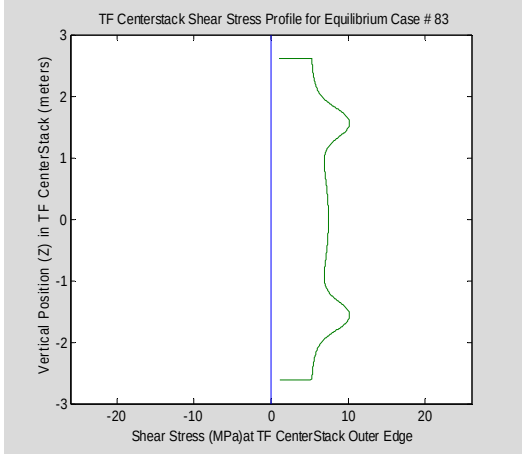
TF Centerstack Shear Stress Profile for Equilibrium Case # 83
Vertical Position (Z) in TF CenterStack (meters)
Shear Stress (MPa)at TF CenterStack Outer Edge

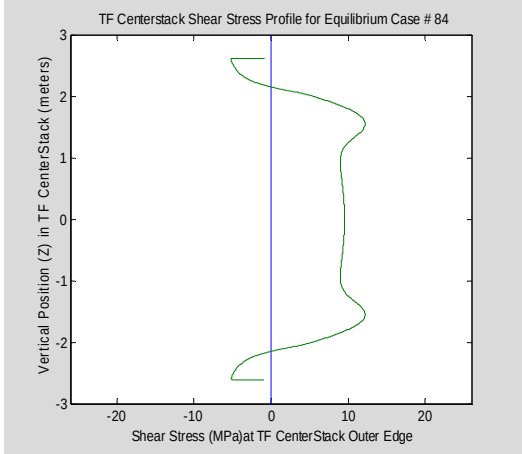
TF Centerstack Shear Stress Profile for Equilibrium Case # 84
Vertical Position (Z) in TF CenterStack (meters)
Shear Stress (MPa)at TF CenterStack Outer Edge

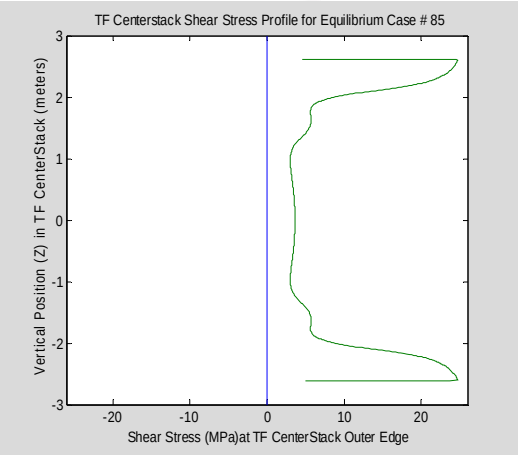
TF Centerstack Shear Stress Profile for Equilibrium Case # 85
Vertical Position (Z) in TF CenterStack (meters)
Shear Stress (MPa)at TF CenterStack Outer Edge

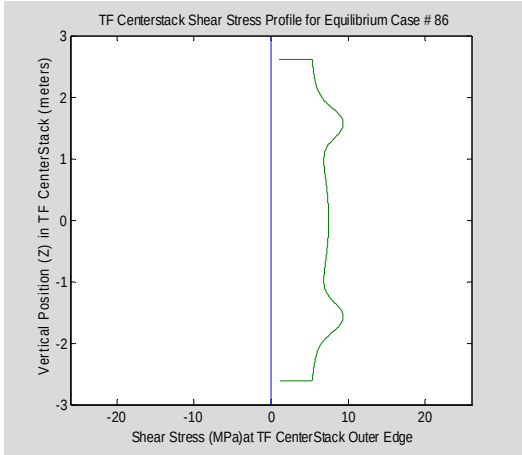
TF Centerstack Shear Stress Profile for Equilibrium Case # 86
Vertical Position (Z) in TF CenterStack (meters)
Shear Stress (MPa)at TF CenterStack Outer Edge

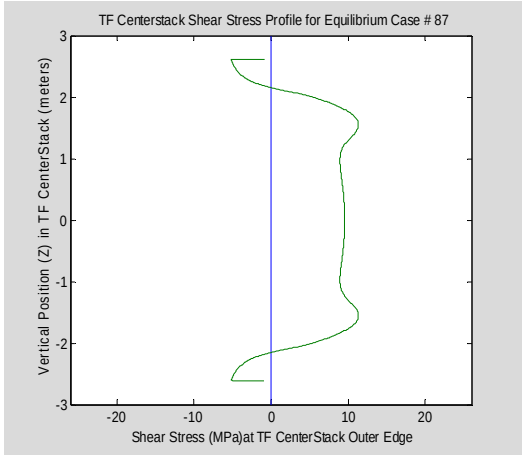
TF Centerstack Shear Stress Profile for Equilibrium Case # 87
Vertical Position (Z) in TF CenterStack (meters)
Shear Stress (MPa)at TF CenterStack Outer Edge

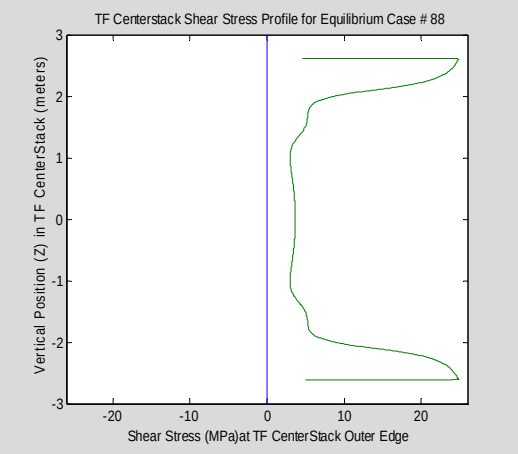
TF Centerstack Shear Stress Profile for Equilibrium Case # 88
Vertical Position (Z) in TF CenterStack (meters)
Shear Stress (MPa)at TF CenterStack Outer Edge

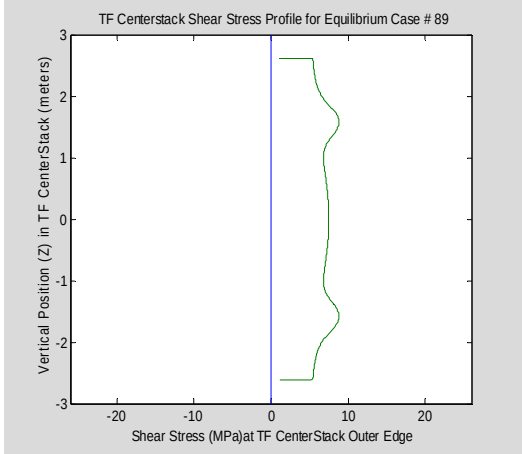
TF Centerstack Shear Stress Profile for Equilibrium Case # 89
Vertical Position (Z) in TF CenterStack (meters)
Shear Stress (MPa)at TF CenterStack Outer Edge

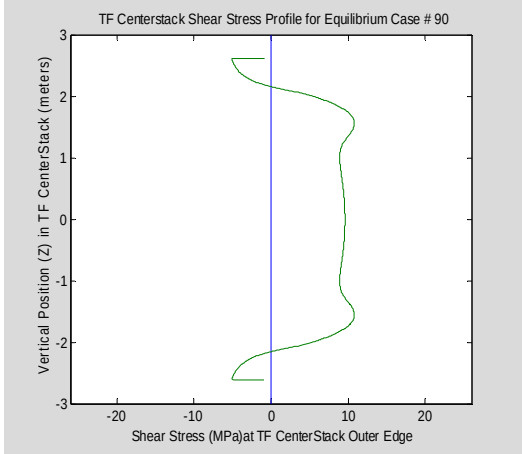
TF Centerstack Shear Stress Profile for Equilibrium Case # 90
Vertical Position (Z) in TF CenterStack (meters)
Shear Stress (MPa)at TF CenterStack Outer Edge

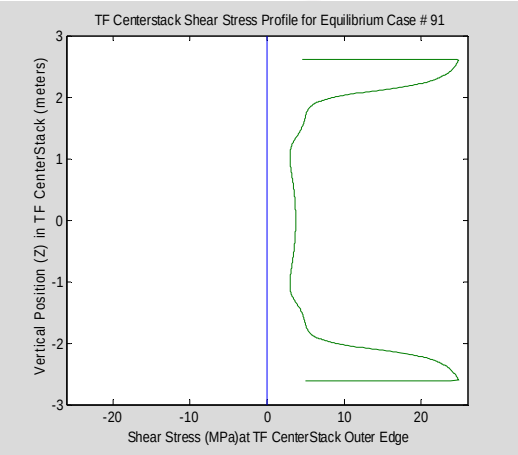
TF Centerstack Shear Stress Profile for Equilibrium Case # 91
Vertical Position (Z) in TF CenterStack (meters)
Shear Stress (MPa)at TF CenterStack Outer Edge

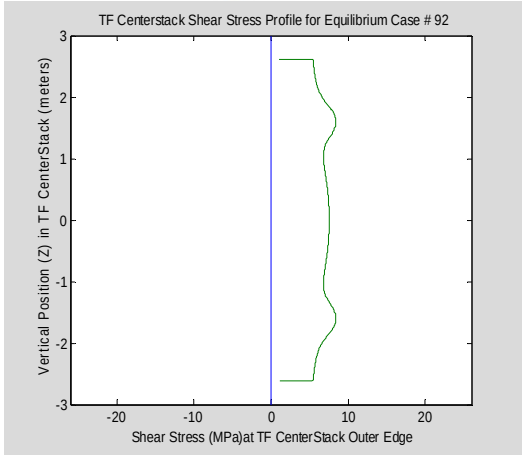
TF Centerstack Shear Stress Profile for Equilibrium Case # 92
Vertical Position (Z) in TF CenterStack (meters)
Shear Stress (MPa)at TF CenterStack Outer Edge

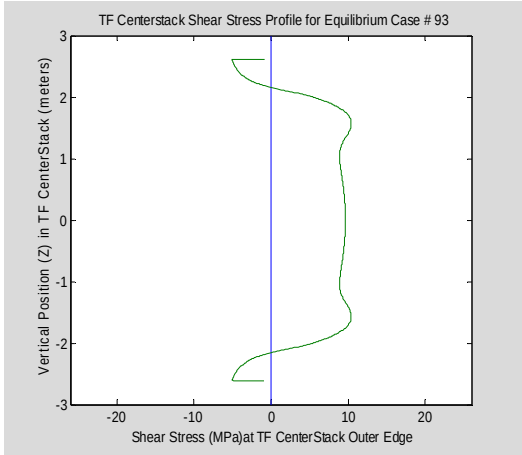
TF Centerstack Shear Stress Profile for Equilibrium Case # 93
Vertical Position (Z) in TF CenterStack (meters)
Shear Stress (MPa)at TF CenterStack Outer Edge

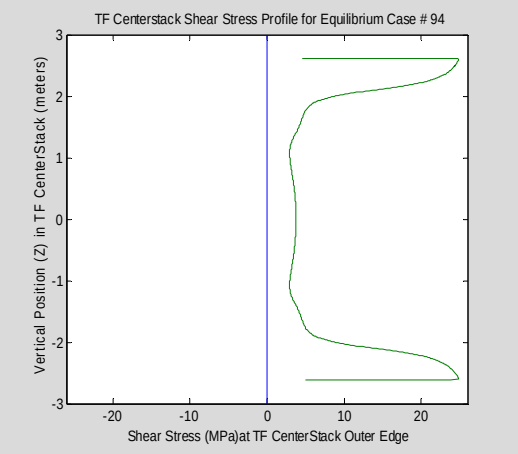
TF Centerstack Shear Stress Profile for Equilibrium Case # 94
Vertical Position (Z) in TF CenterStack (meters)
Shear Stress (MPa)at TF CenterStack Outer Edge

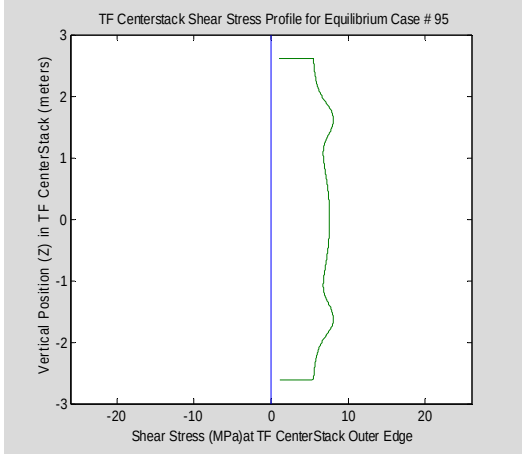
TF Centerstack Shear Stress Profile for Equilibrium Case # 95
Vertical Position (Z) in TF CenterStack (meters)
Shear Stress (MPa)at TF CenterStack Outer Edge

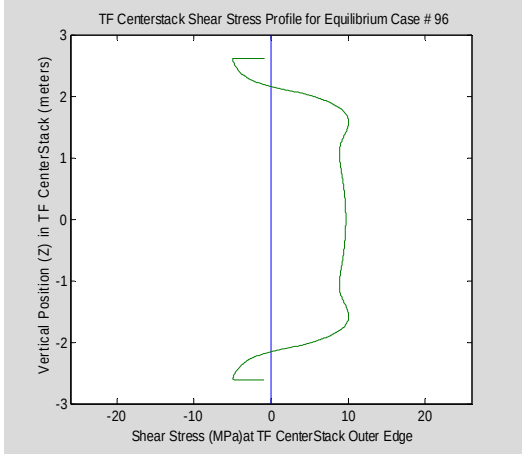
TF Centerstack Shear Stress Profile for Equilibrium Case # 96
Vertical Position (Z) in TF CenterStack (meters)
Shear Stress (MPa)at TF CenterStack Outer Edge

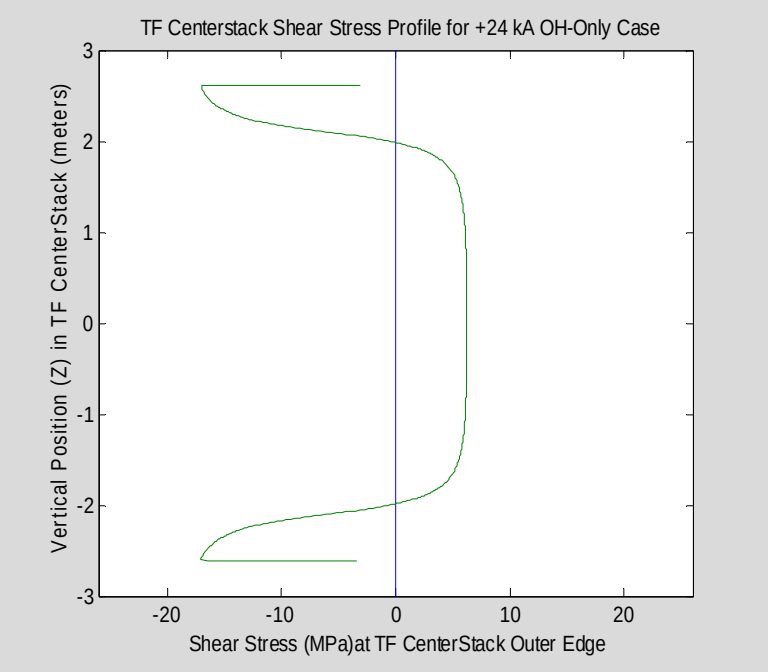
TF Centerstack Shear Stress Profile for +24 kA OH-Only Case
Vertical Position (Z) in TF CenterStack (meters)
3
2
1
0
-1
-2
-3
-20
-10
0
10
20
Shear Stress (MPa)at TF CenterStack Outer Edge

APPENDIX 3

Torsion Analysis Results With Reduced Stiffness in Upper Lid

To determine the effects on peak shear stress, the torsional stiffness of the upper lid was reduced by a factor of 20 while all other stiffness parameters were left unchanged from the values used to calculate the Appendix 2 results.

Peak shear stress values are collected in the following table for these cases. The maximum absolute shear was 19.553 MPa, observed for equilibrium case #1 and again in equilibrium case #16.

Table A3 and plots show peak shear stress is mostly due to OH, and reaches its maximum when the OH current is -24 kA. PF coils and plasma are smaller contributors to peak shear stress.

Table A3: TF Centerstack Max Absolute Shear Stress ; Precharge and Plasma Cases

Case# -24 kA OH	Peak Shear MPa	Case# 0 kA OH	Peak Shear MPa	Case# 13 kA OH	Peak Shear MPa	Case 24 kA OH	Peak Shear MPa
						Precharge	13.160
1	19.5534	2	6.5375	3	10.9944		
4	19.4016	5	6.4449	6	10.8958		
7	19.2976	8	6.6634	9	10.9114		
10	19.1926	11	6.8980	12	11.2799		
13	19.1987	14	6.9595	15	11.3530		
16	19.5534	17	6.5375	18	10.9944		
19	18.1765	20	6.5205	21	10.9161		
22	18.5628	23	6.6753	24	11.0597		
25	18.8599	26	6.7516	27	11.1091		
28	19.0966	29	6.9223	30	11.1563		
31	19.2033	32	7.2720	33	11.3294		
34	17.6028	35	8.8235	36	13.4361		
37	17.8582	38	8.7835	39	13.3987		
40	18.1871	41	8.6822	42	13.3054		
43	18.5673	44	8.4675	45	13.1140		
46	18.8337	47	8.1257	38	12.8219		
49	16.6842	50	8.0255	51	12.6412		
52	16.9927	53	8.0063	54	12.6375		
55	17.4139	56	7.9418	57	12.5644		
58	17.8337	59	7.7767	60	12.4114		
61	18.2611	62	7.4595	63	12.1297		
64	19.5428	65	7.6528	66	12.1223		
67	19.4479	68	7.4859	69	11.9422		
70	19.0970	71	7.0231	72	11.4907		
73	18.7393	74	6.7629	75	11.2275		
76	18.4170	77	6.5354	78	10.9964		
79	17.9967	80	6.3280	81	10.7971		

82	19.1319	83	9.0096	84	13.3828		
85	19.1611	86	8.1527	87	12.5073		
88	19.2045	89	7.5824	90	11.9441		
91	19.2357	92	7.1888	93	11.5370		
94	19.2686	95	6.8490	96	11.1865		

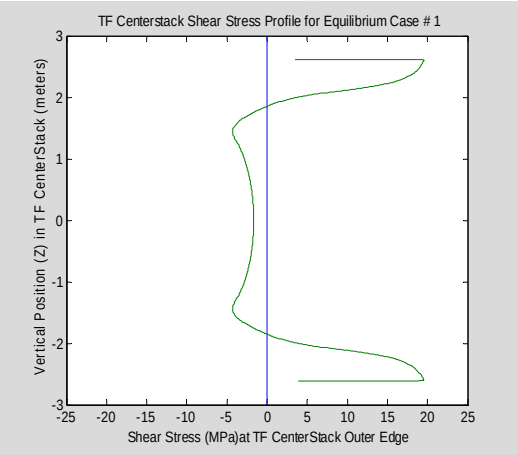
TF Centerstack Shear Stress Profile for Equilibrium Case # 1
Vertical Position (Z) in TF CenterStack (meters)
Shear Stress (MPa)at TF CenterStack Outer Edge

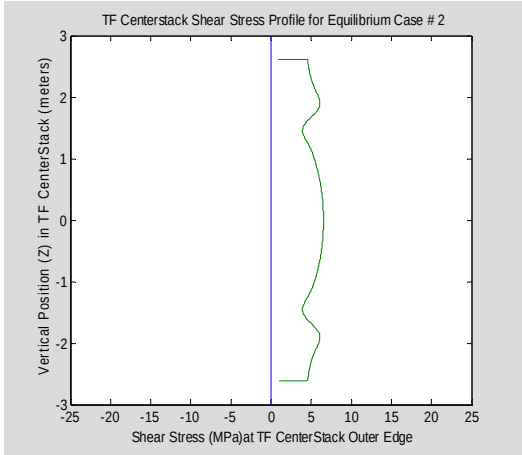
TF Centerstack Shear Stress Profile for Equilibrium Case # 2
Vertical Position (Z) in TF CenterStack (meters)
Shear Stress (MPa)at TF CenterStack Outer Edge

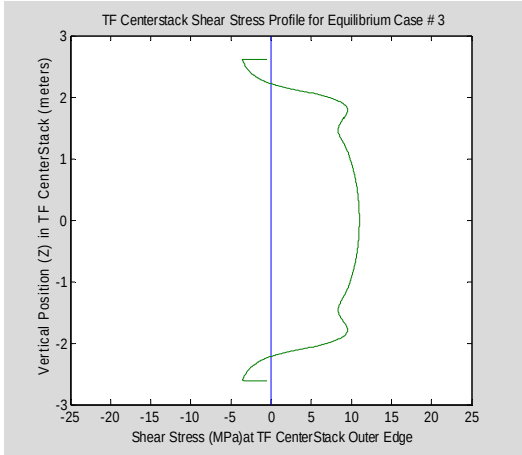
TF Centerstack Shear Stress Profile for Equilibrium Case # 3
Vertical Position (Z) in TF CenterStack (meters)
Shear Stress (MPa)at TF CenterStack Outer Edge

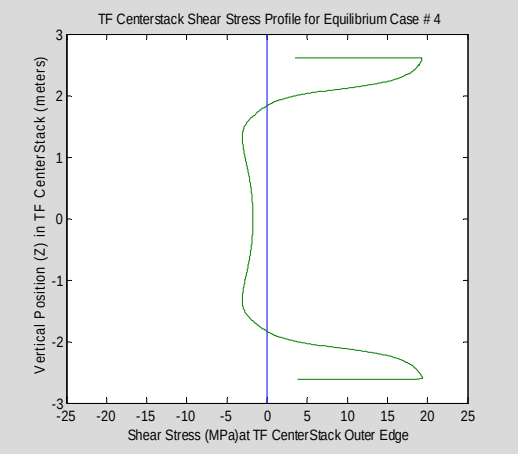
TF Centerstack Shear Stress Profile for Equilibrium Case # 4
Vertical Position (Z) in TF CenterStack (meters)
Shear Stress (MPa)at TF CenterStack Outer Edge

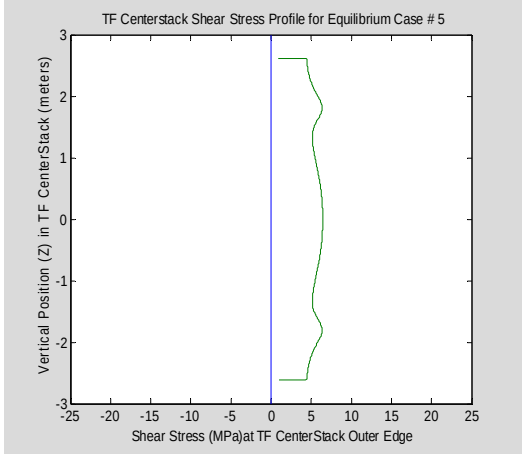
TF Centerstack Shear Stress Profile for Equilibrium Case # 5
Vertical Position (Z) in TF CenterStack (meters)
Shear Stress (MPa)at TF CenterStack Outer Edge

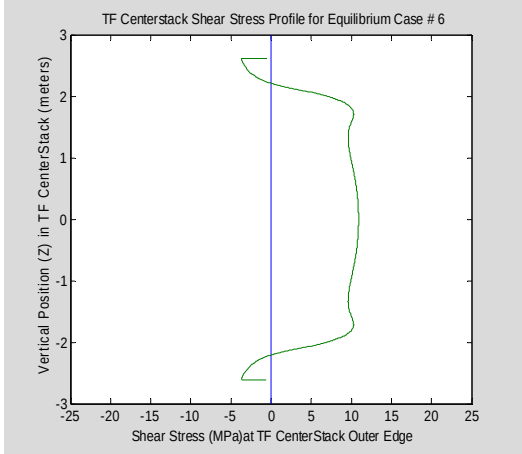
TF Centerstack Shear Stress Profile for Equilibrium Case # 6
Vertical Position (Z) in TF CenterStack (meters)
Shear Stress (MPa)at TF CenterStack Outer Edge

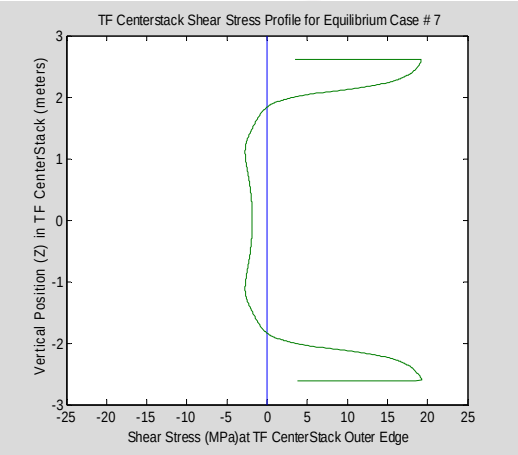
TF Centerstack Shear Stress Profile for Equilibrium Case # 7
Vertical Position (Z) in TF CenterStack (meters)
Shear Stress (MPa)at TF CenterStack Outer Edge

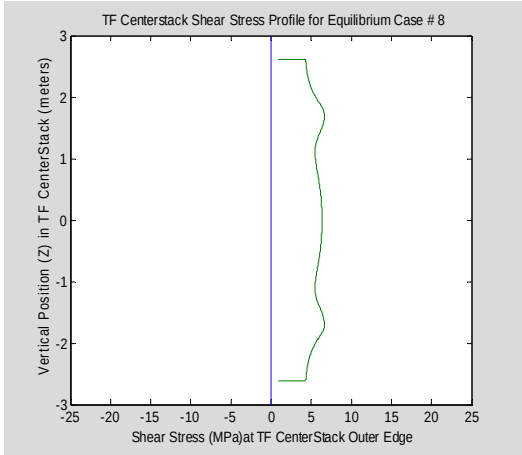
TF Centerstack Shear Stress Profile for Equilibrium Case # 8
Vertical Position (Z) in TF CenterStack (meters)
Shear Stress (MPa)at TF CenterStack Outer Edge

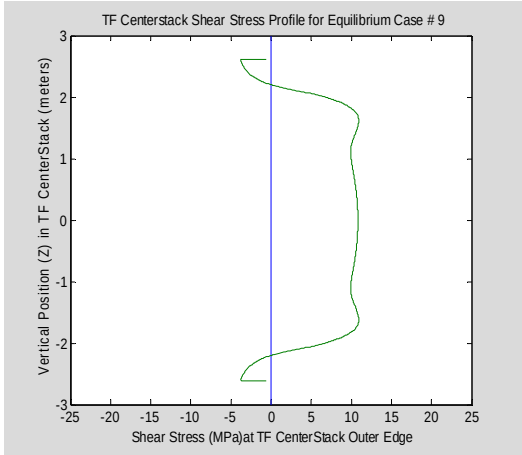
TF Centerstack Shear Stress Profile for Equilibrium Case # 9
Vertical Position (Z) in TF CenterStack (meters)
Shear Stress (MPa)at TF CenterStack Outer Edge

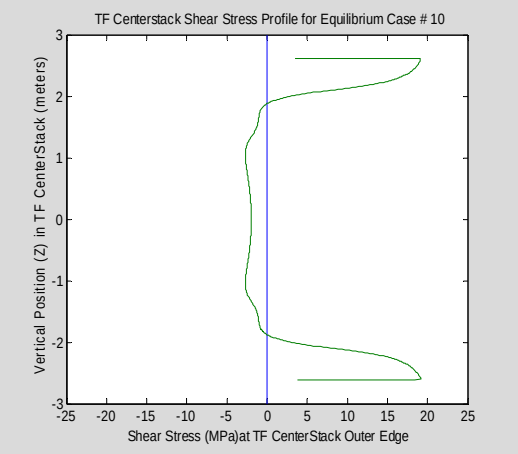
TF Centerstack Shear Stress Profile for Equilibrium Case # 10
Vertical Position (Z) in TF CenterStack (meters)
Shear Stress (MPa)at TF CenterStack Outer Edge

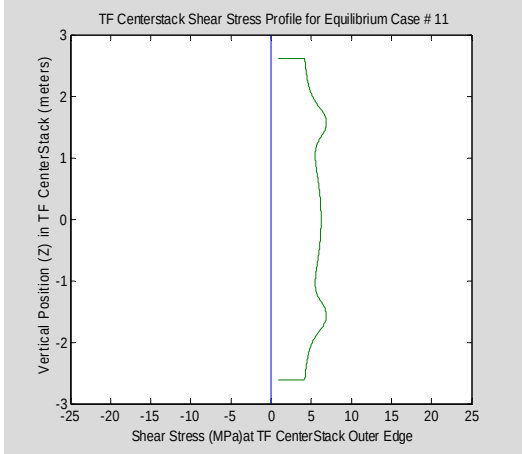
TF Centerstack Shear Stress Profile for Equilibrium Case # 11
Vertical Position (Z) in TF CenterStack (meters)
Shear Stress (MPa)at TF CenterStack Outer Edge

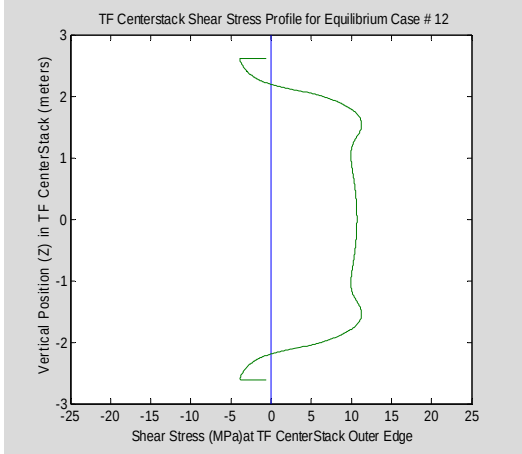
TF Centerstack Shear Stress Profile for Equilibrium Case # 12
Vertical Position (Z) in TF CenterStack (meters)
Shear Stress (MPa)at TF CenterStack Outer Edge

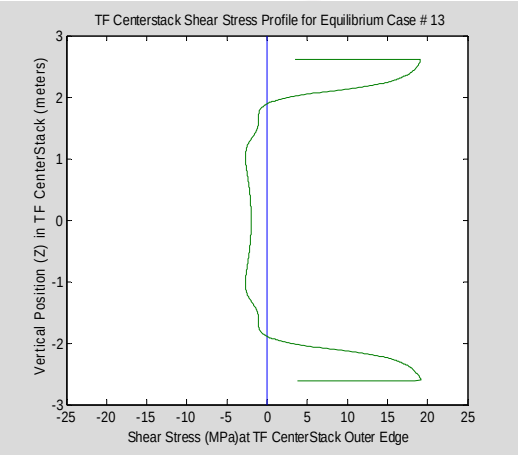
TF Centerstack Shear Stress Profile for Equilibrium Case # 13
Vertical Position (Z) in TF CenterStack (meters)
Shear Stress (MPa)at TF CenterStack Outer Edge

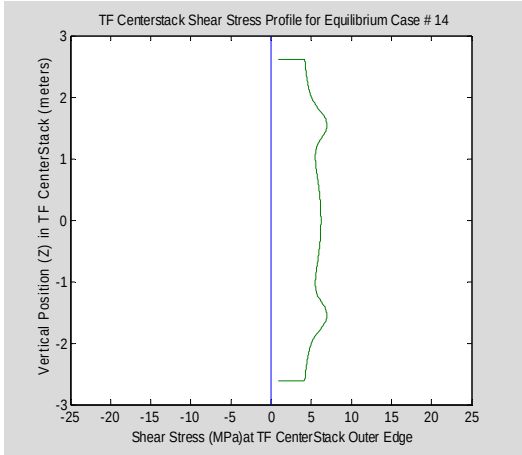
TF Centerstack Shear Stress Profile for Equilibrium Case # 14
Vertical Position (Z) in TF CenterStack (meters)
Shear Stress (MPa)at TF CenterStack Outer Edge

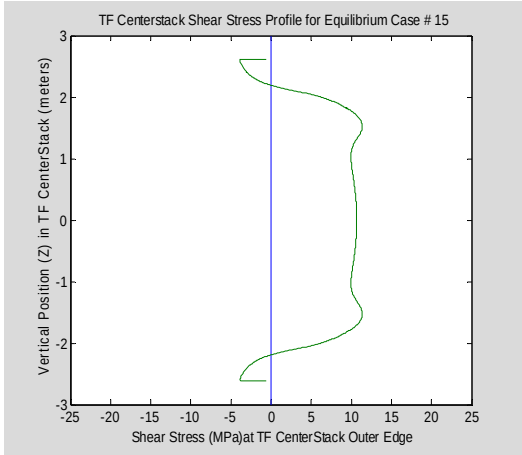
TF Centerstack Shear Stress Profile for Equilibrium Case # 15
Vertical Position (Z) in TF CenterStack (meters)
Shear Stress (MPa)at TF CenterStack Outer Edge

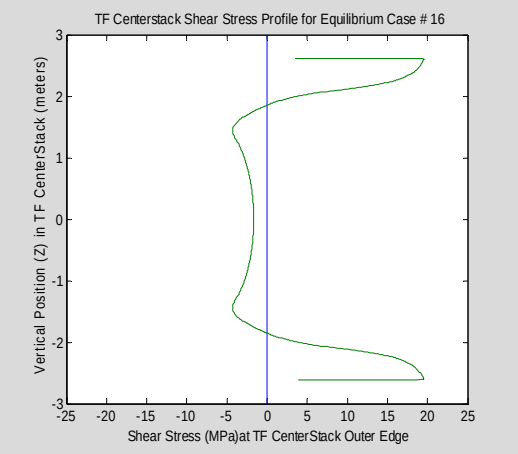
TF Centerstack Shear Stress Profile for Equilibrium Case # 16
Vertical Position (Z) in TF CenterStack (meters)
Shear Stress (MPa)at TF CenterStack Outer Edge

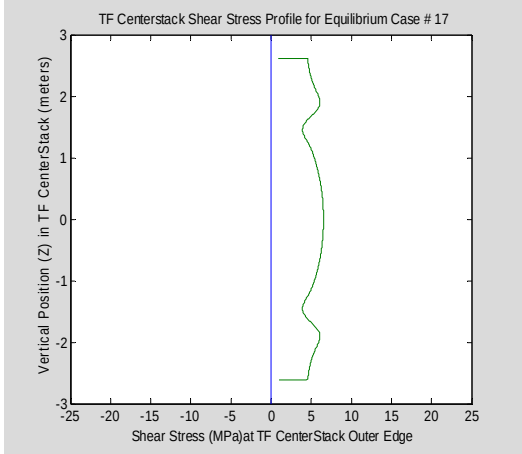
TF Centerstack Shear Stress Profile for Equilibrium Case # 17
Vertical Position (Z) in TF CenterStack (meters)
Shear Stress (MPa)at TF CenterStack Outer Edge

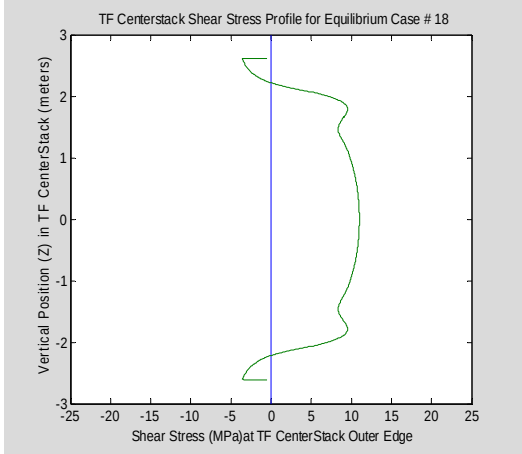
TF Centerstack Shear Stress Profile for Equilibrium Case # 18
Vertical Position (Z) in TF CenterStack (meters)
Shear Stress (MPa)at TF CenterStack Outer Edge

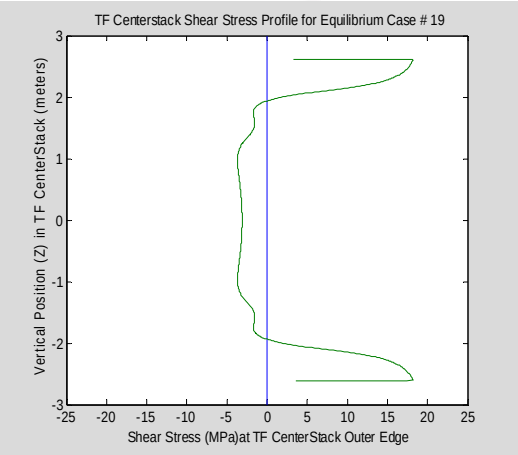
TF Centerstack Shear Stress Profile for Equilibrium Case # 19
Vertical Position (Z) in TF CenterStack (meters)
Shear Stress (MPa)at TF CenterStack Outer Edge

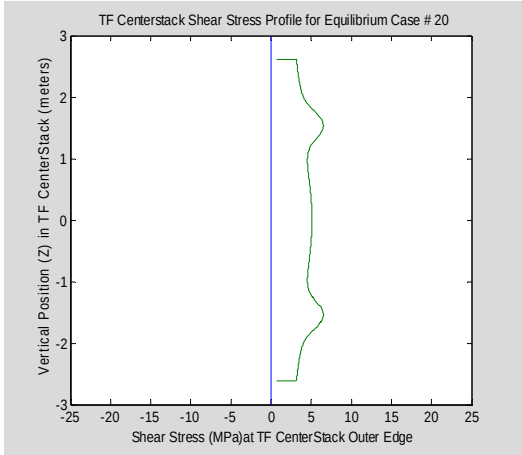
TF Centerstack Shear Stress Profile for Equilibrium Case # 20
Vertical Position (Z) in TF CenterStack (meters)
Shear Stress (MPa)at TF CenterStack Outer Edge

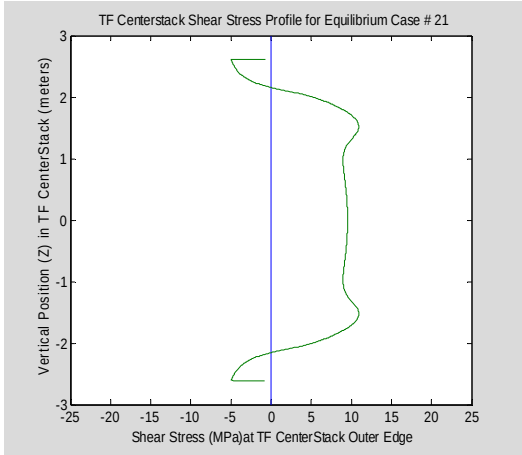
TF Centerstack Shear Stress Profile for Equilibrium Case # 21
Vertical Position (Z) in TF CenterStack (meters)
Shear Stress (MPa)at TF CenterStack Outer Edge

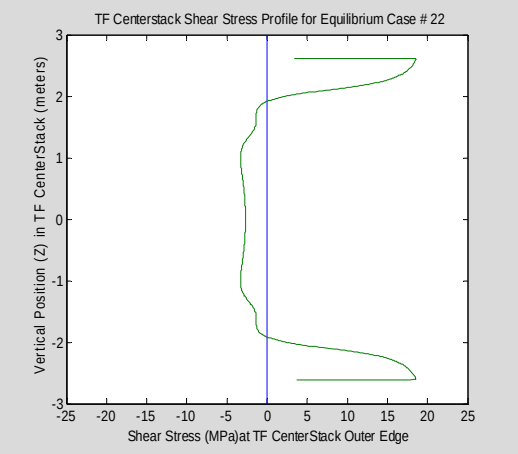
TF Centerstack Shear Stress Profile for Equilibrium Case # 22
Vertical Position (Z) in TF CenterStack (meters)
Shear Stress (MPa)at TF CenterStack Outer Edge

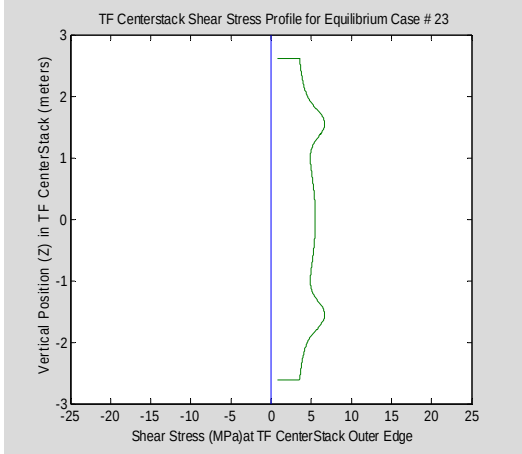
TF Centerstack Shear Stress Profile for Equilibrium Case # 23
Vertical Position (Z) in TF CenterStack (meters)
Shear Stress (MPa)at TF CenterStack Outer Edge

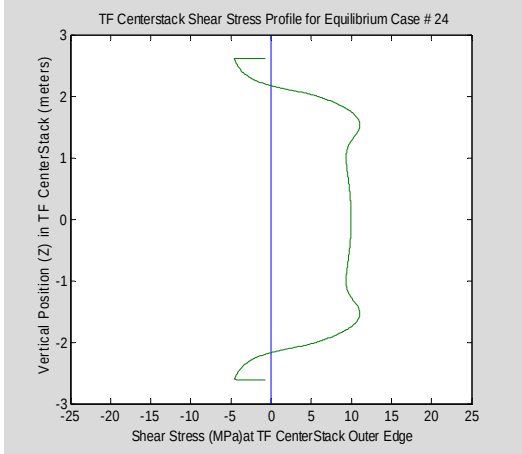
TF Centerstack Shear Stress Profile for Equilibrium Case # 24
Vertical Position (Z) in TF CenterStack (meters)
Shear Stress (MPa)at TF CenterStack Outer Edge

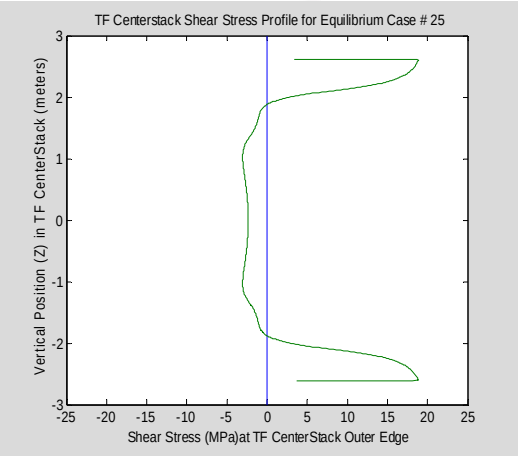
TF Centerstack Shear Stress Profile for Equilibrium Case # 25
Vertical Position (Z) in TF CenterStack (meters)
Shear Stress (MPa)at TF CenterStack Outer Edge

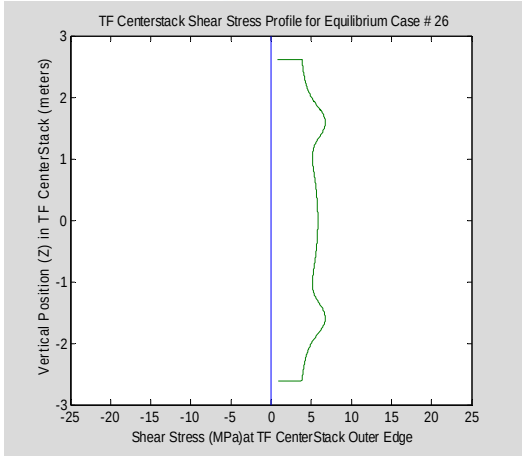
TF Centerstack Shear Stress Profile for Equilibrium Case # 26
Vertical Position (Z) in TF CenterStack (meters)
Shear Stress (MPa)at TF CenterStack Outer Edge

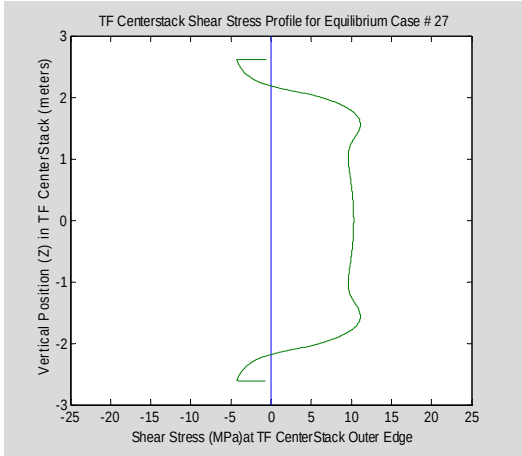
TF Centerstack Shear Stress Profile for Equilibrium Case # 27
Vertical Position (Z) in TF CenterStack (meters)
Shear Stress (MPa)at TF CenterStack Outer Edge

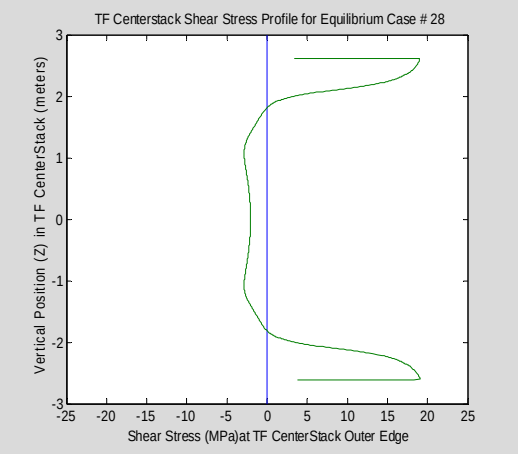
TF Centerstack Shear Stress Profile for Equilibrium Case # 28
Vertical Position (Z) in TF CenterStack (meters)
Shear Stress (MPa)at TF CenterStack Outer Edge

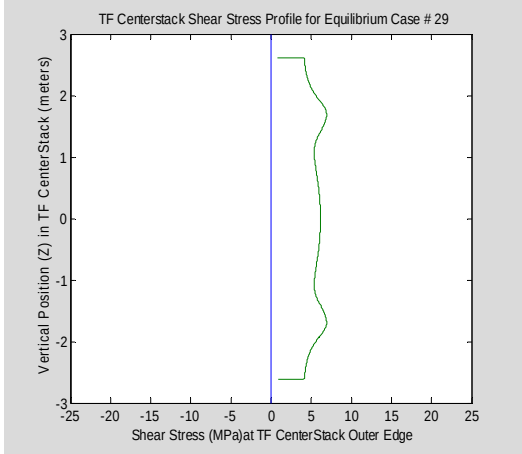
TF Centerstack Shear Stress Profile for Equilibrium Case # 29
Vertical Position (Z) in TF CenterStack (meters)
Shear Stress (MPa)at TF CenterStack Outer Edge

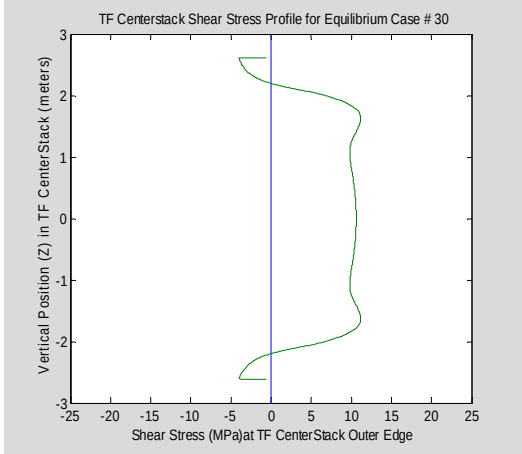
TF Centerstack Shear Stress Profile for Equilibrium Case # 30
Vertical Position (Z) in TF CenterStack (meters)
Shear Stress (MPa)at TF CenterStack Outer Edge

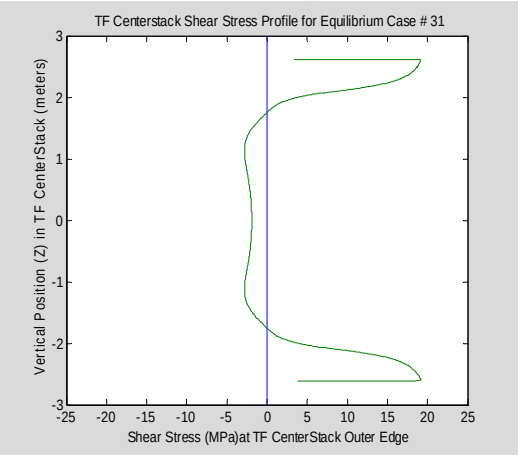
TF Centerstack Shear Stress Profile for Equilibrium Case # 31
Vertical Position (Z) in TF CenterStack (meters)
Shear Stress (MPa)at TF CenterStack Outer Edge

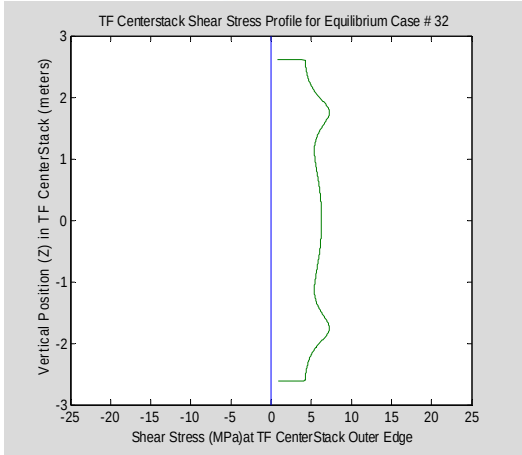
TF Centerstack Shear Stress Profile for Equilibrium Case # 32
Vertical Position (Z) in TF CenterStack (meters)
Shear Stress (MPa)at TF CenterStack Outer Edge

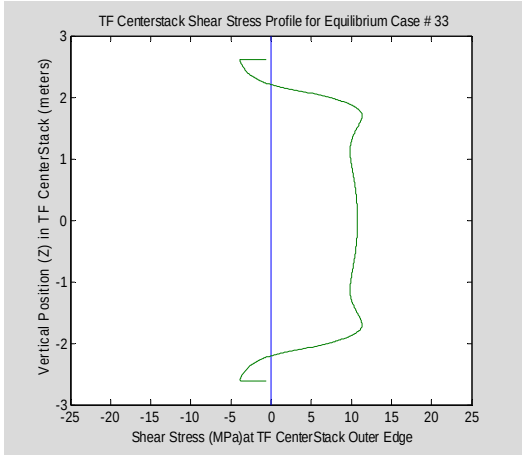
TF Centerstack Shear Stress Profile for Equilibrium Case # 33
Vertical Position (Z) in TF CenterStack (meters)
Shear Stress (MPa)at TF CenterStack Outer Edge

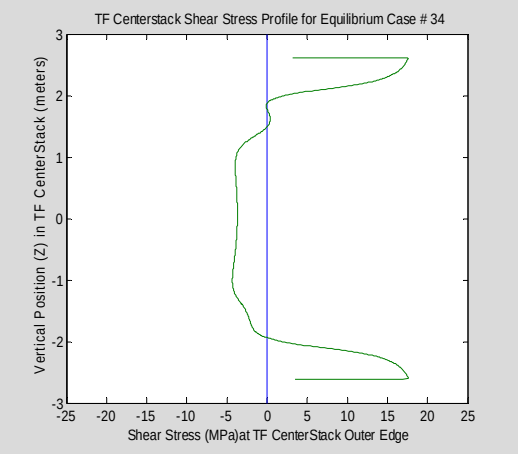
TF Centerstack Shear Stress Profile for Equilibrium Case # 34
Vertical Position (Z) in TF CenterStack (meters)
Shear Stress (MPa)at TF CenterStack Outer Edge

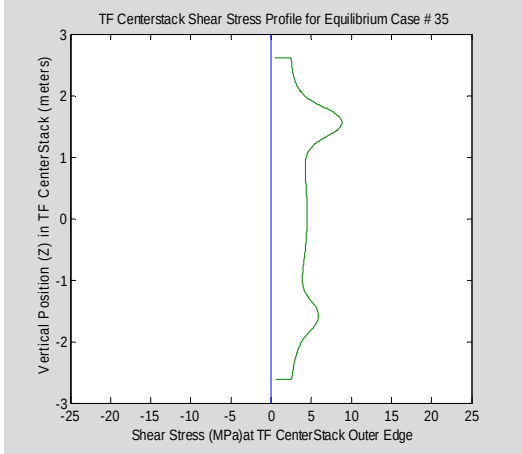
TF Centerstack Shear Stress Profile for Equilibrium Case # 35
Vertical Position (Z) in TF CenterStack (meters)
Shear Stress (MPa)at TF CenterStack Outer Edge

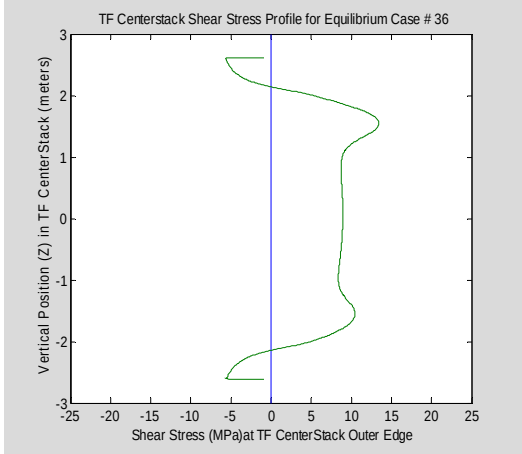
TF Centerstack Shear Stress Profile for Equilibrium Case # 36
Vertical Position (Z) in TF CenterStack (meters)
Shear Stress (MPa)at TF CenterStack Outer Edge

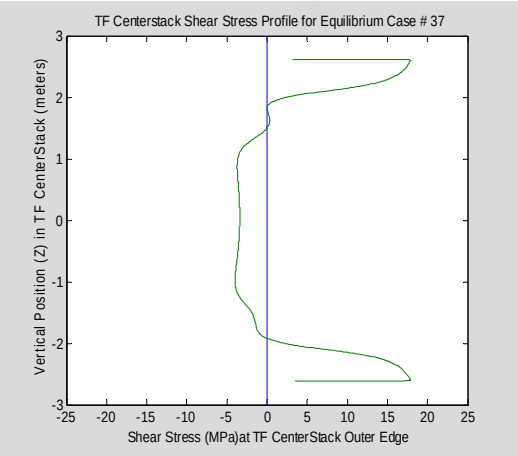
TF Centerstack Shear Stress Profile for Equilibrium Case # 37
Vertical Position (Z) in TF CenterStack (meters)
Shear Stress (MPa)at TF CenterStack Outer Edge

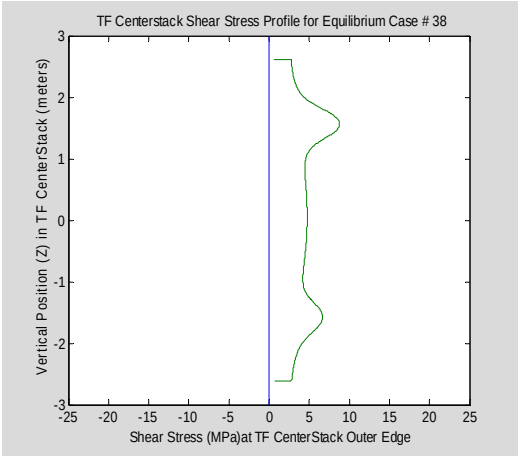
TF Centerstack Shear Stress Profile for Equilibrium Case # 38
Vertical Position (Z) in TF CenterStack (meters)
Shear Stress (MPa)at TF CenterStack Outer Edge

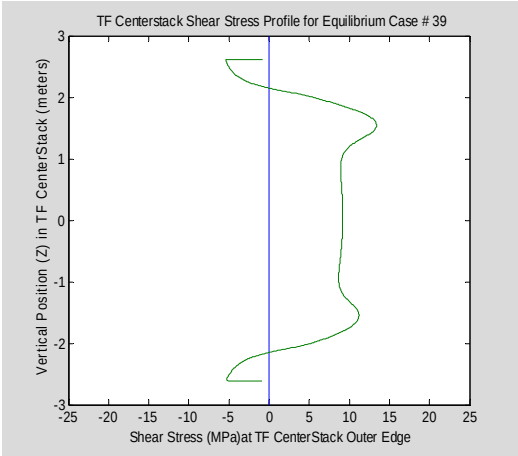
TF Centerstack Shear Stress Profile for Equilibrium Case # 39
Vertical Position (Z) in TF CenterStack (meters)
Shear Stress (MPa)at TF CenterStack Outer Edge

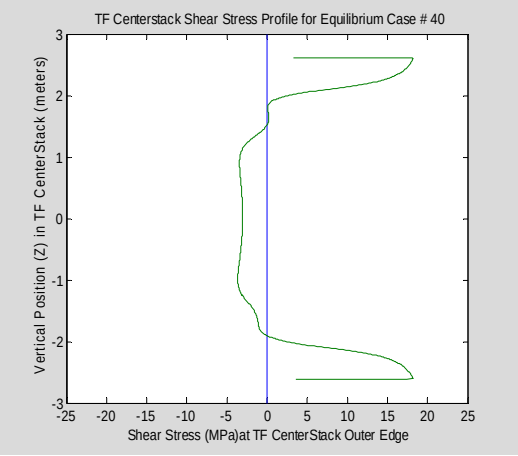
TF Centerstack Shear Stress Profile for Equilibrium Case # 40
Vertical Position (Z) in TF CenterStack (meters)
Shear Stress (MPa)at TF CenterStack Outer Edge

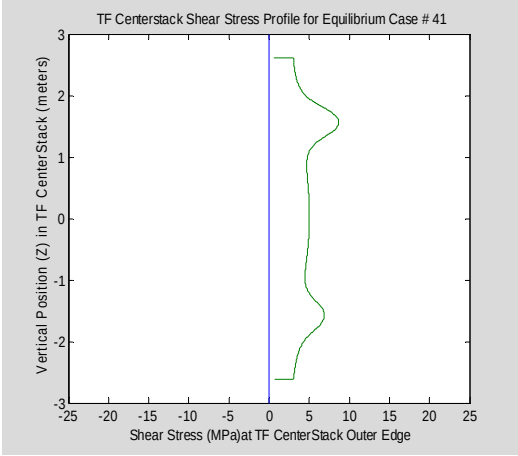
TF Centerstack Shear Stress Profile for Equilibrium Case # 41
Vertical Position (Z) in TF CenterStack (meters)
Shear Stress (MPa)at TF CenterStack Outer Edge

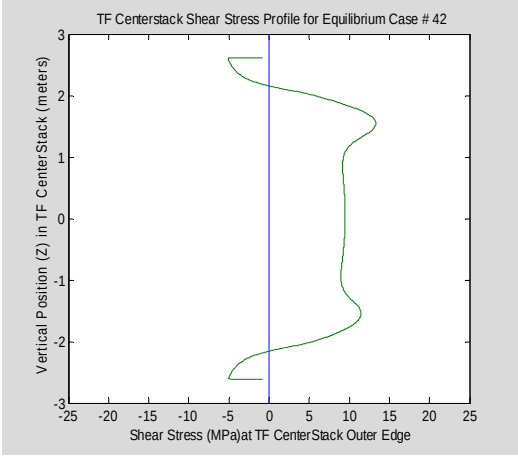
TF Centerstack Shear Stress Profile for Equilibrium Case # 42
Vertical Position (Z) in TF CenterStack (meters)
Shear Stress (MPa)at TF CenterStack Outer Edge

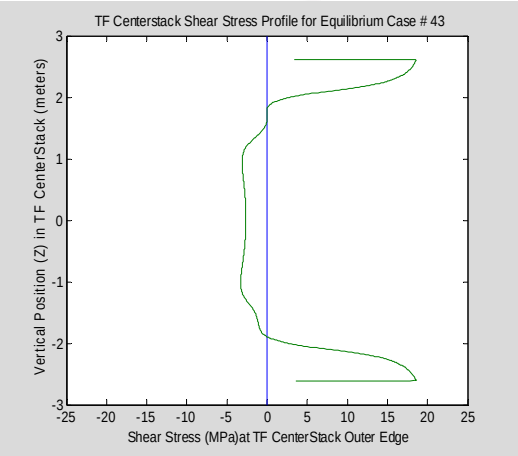
TF Centerstack Shear Stress Profile for Equilibrium Case # 43
Vertical Position (Z) in TF CenterStack (meters)
Shear Stress (MPa)at TF CenterStack Outer Edge

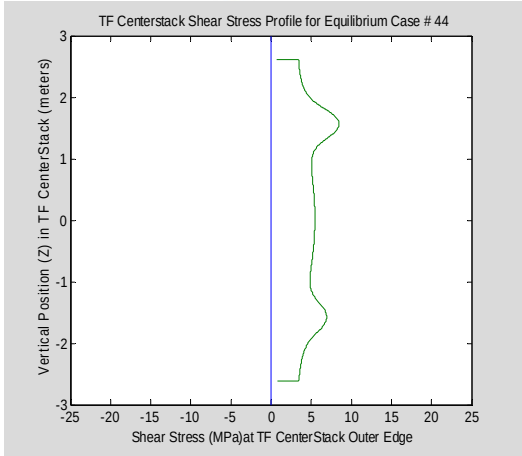
TF Centerstack Shear Stress Profile for Equilibrium Case # 44
Vertical Position (Z) in TF CenterStack (meters)
Shear Stress (MPa)at TF CenterStack Outer Edge

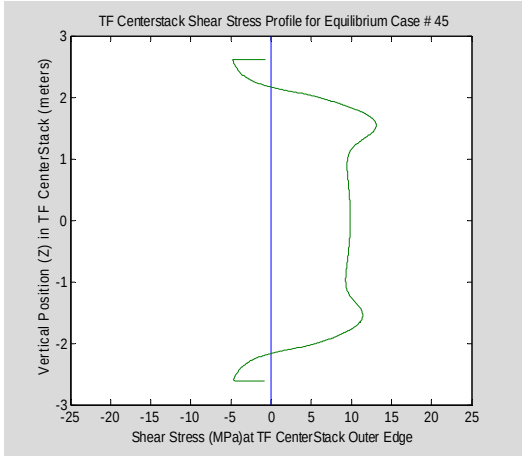
TF Centerstack Shear Stress Profile for Equilibrium Case # 45
Vertical Position (Z) in TF CenterStack (meters)
Shear Stress (MPa)at TF CenterStack Outer Edge

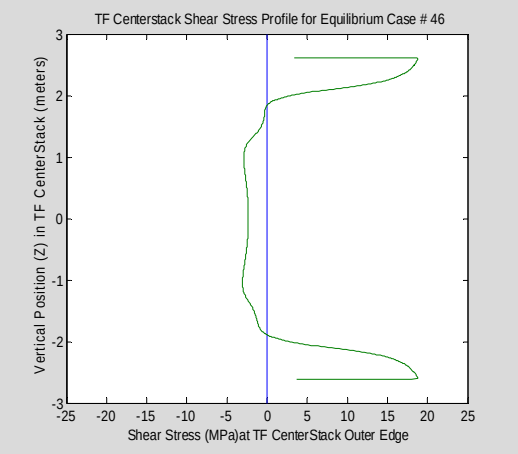
TF Centerstack Shear Stress Profile for Equilibrium Case # 46
Vertical Position (Z) in TF CenterStack (meters)
Shear Stress (MPa)at TF CenterStack Outer Edge

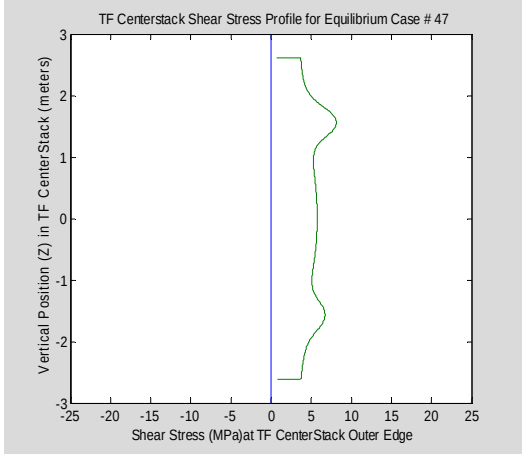
TF Centerstack Shear Stress Profile for Equilibrium Case # 47
Vertical Position (Z) in TF CenterStack (meters)
Shear Stress (MPa)at TF CenterStack Outer Edge

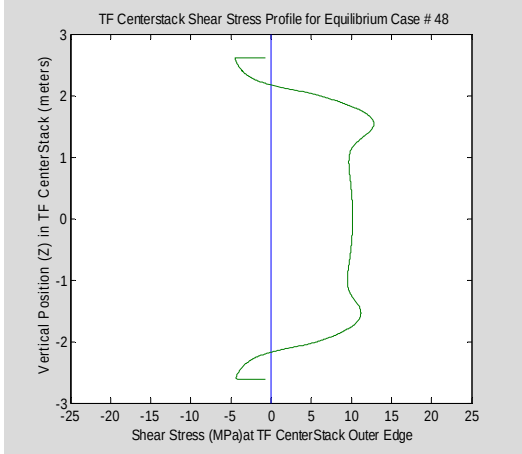
TF Centerstack Shear Stress Profile for Equilibrium Case # 48
Vertical Position (Z) in TF CenterStack (meters)
Shear Stress (MPa)at TF CenterStack Outer Edge

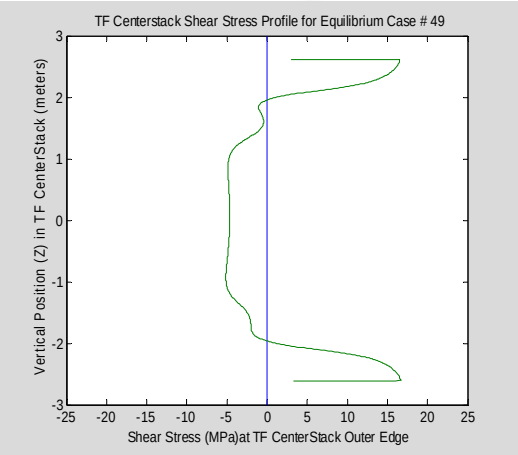
TF Centerstack Shear Stress Profile for Equilibrium Case # 49
Vertical Position (Z) in TF CenterStack (meters)
Shear Stress (MPa)at TF CenterStack Outer Edge

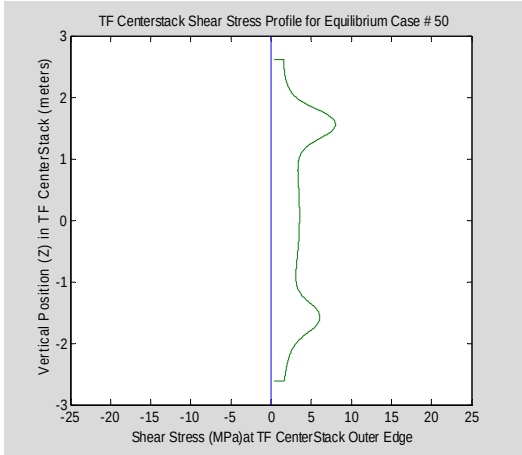
TF Centerstack Shear Stress Profile for Equilibrium Case # 50
Vertical Position (Z) in TF CenterStack (meters)
Shear Stress (MPa)at TF CenterStack Outer Edge

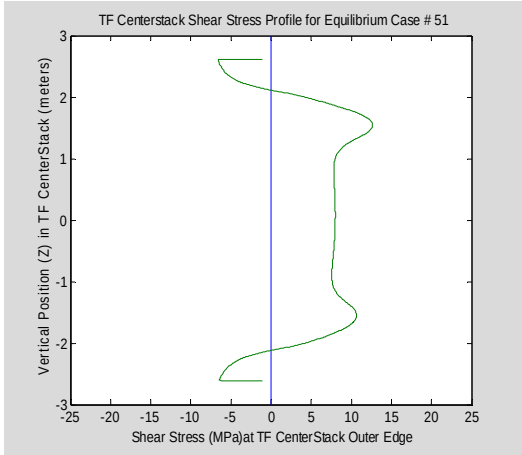
TF Centerstack Shear Stress Profile for Equilibrium Case # 51
Vertical Position (Z) in TF CenterStack (meters)
Shear Stress (MPa)at TF CenterStack Outer Edge

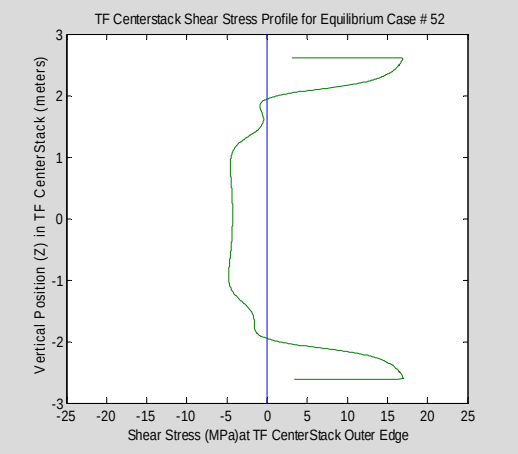
TF Centerstack Shear Stress Profile for Equilibrium Case # 52
Vertical Position (Z) in TF CenterStack (meters)
Shear Stress (MPa)at TF CenterStack Outer Edge

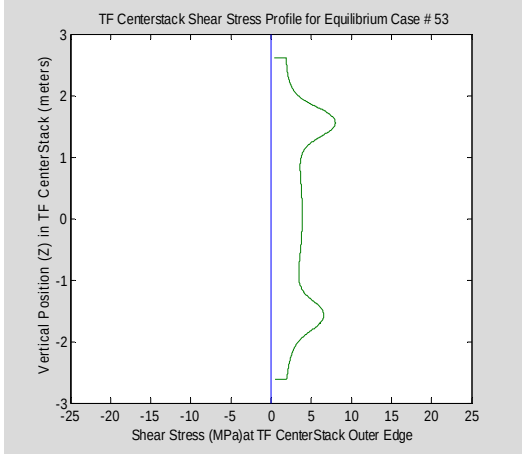
TF Centerstack Shear Stress Profile for Equilibrium Case # 53
Vertical Position (Z) in TF CenterStack (meters)
Shear Stress (MPa)at TF CenterStack Outer Edge

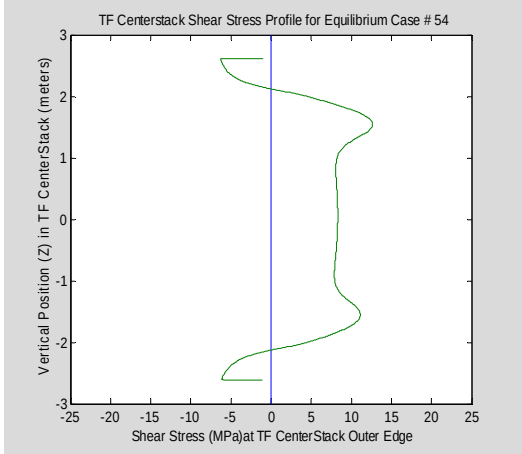
TF Centerstack Shear Stress Profile for Equilibrium Case # 54
Vertical Position (Z) in TF CenterStack (meters)
Shear Stress (MPa)at TF CenterStack Outer Edge

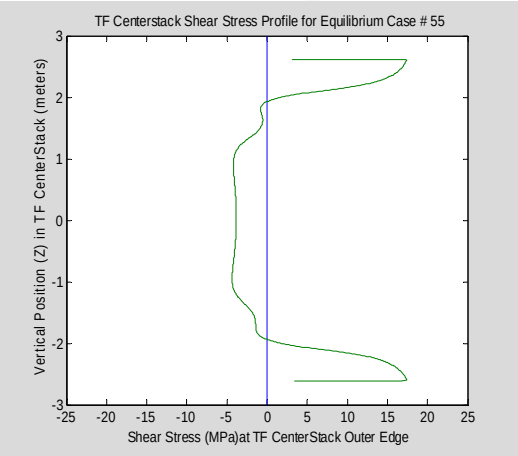
TF Centerstack Shear Stress Profile for Equilibrium Case # 55
Vertical Position (Z) in TF CenterStack (meters)
Shear Stress (MPa)at TF CenterStack Outer Edge

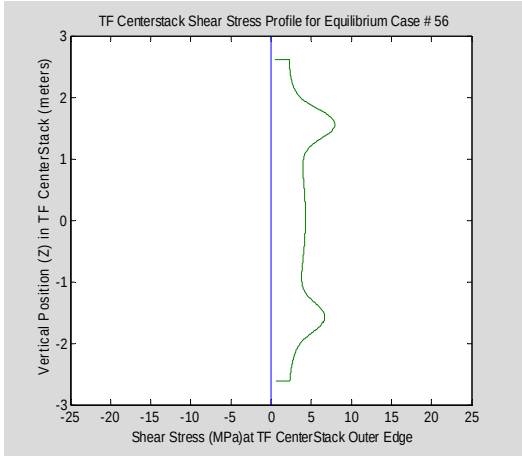
TF Centerstack Shear Stress Profile for Equilibrium Case # 56
Vertical Position (Z) in TF CenterStack (meters)
Shear Stress (MPa)at TF CenterStack Outer Edge

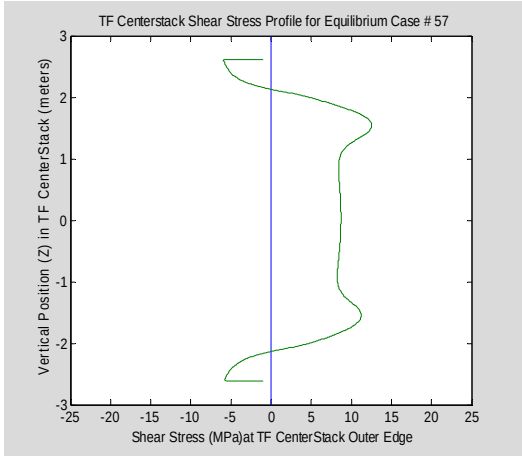
TF Centerstack Shear Stress Profile for Equilibrium Case # 57
Vertical Position (Z) in TF CenterStack (meters)
Shear Stress (MPa)at TF CenterStack Outer Edge

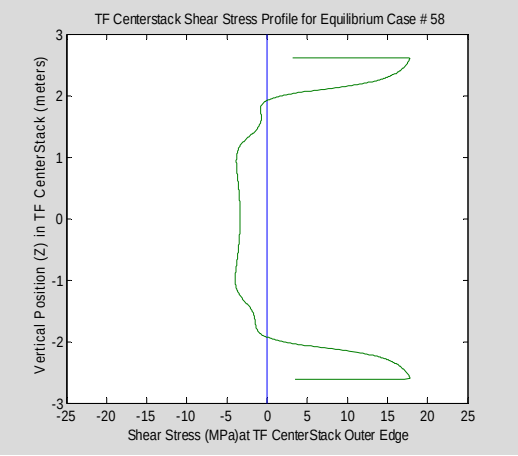
TF Centerstack Shear Stress Profile for Equilibrium Case # 58
Vertical Position (Z) in TF CenterStack (meters)
Shear Stress (MPa)at TF CenterStack Outer Edge

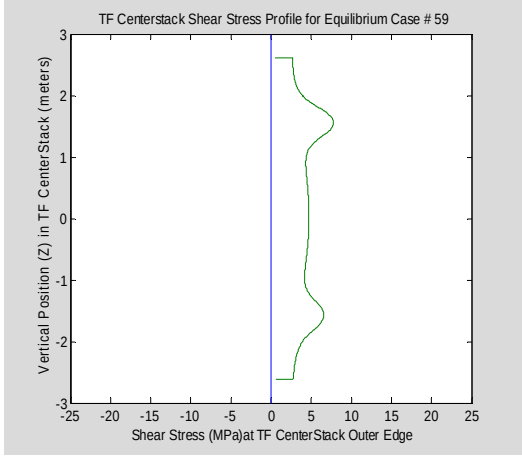
TF Centerstack Shear Stress Profile for Equilibrium Case # 59
Vertical Position (Z) in TF CenterStack (meters)
Shear Stress (MPa)at TF CenterStack Outer Edge

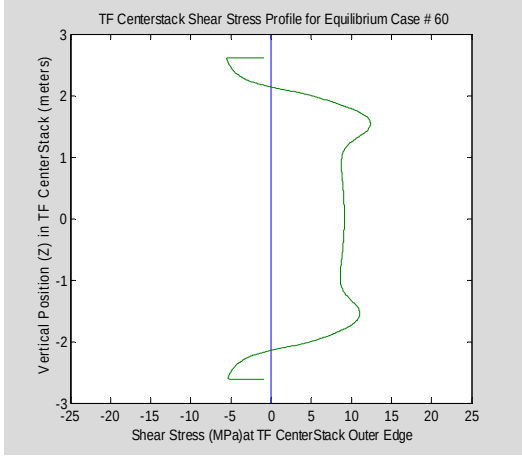
TF Centerstack Shear Stress Profile for Equilibrium Case # 60
Vertical Position (Z) in TF CenterStack (meters)
Shear Stress (MPa)at TF CenterStack Outer Edge

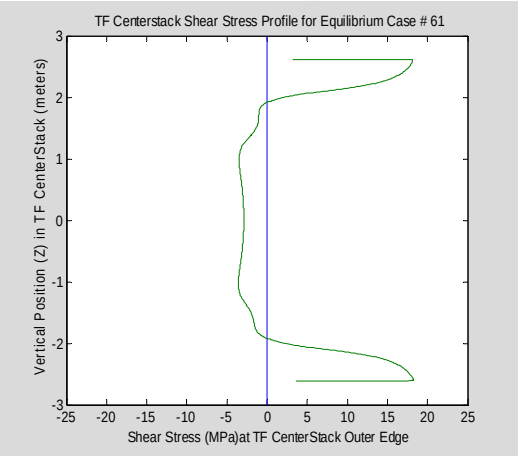
TF Centerstack Shear Stress Profile for Equilibrium Case # 61
Vertical Position (Z) in TF CenterStack (meters)
Shear Stress (MPa)at TF CenterStack Outer Edge

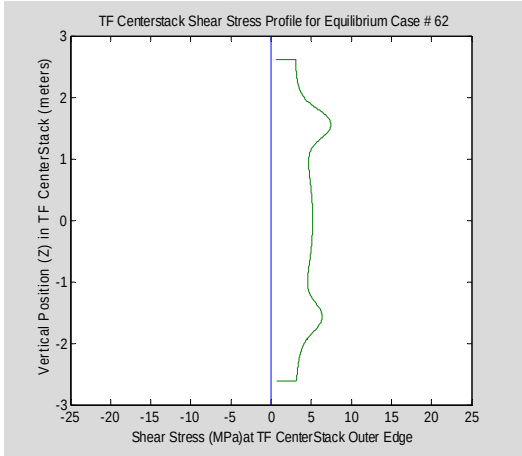
TF Centerstack Shear Stress Profile for Equilibrium Case # 62
Vertical Position (Z) in TF CenterStack (meters)
Shear Stress (MPa)at TF CenterStack Outer Edge

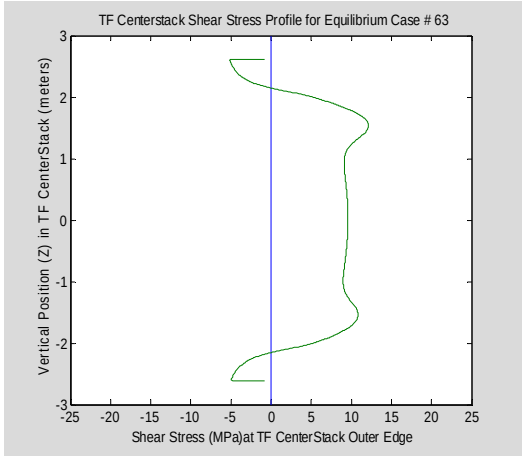
TF Centerstack Shear Stress Profile for Equilibrium Case # 63
Vertical Position (Z) in TF CenterStack (meters)
Shear Stress (MPa)at TF CenterStack Outer Edge

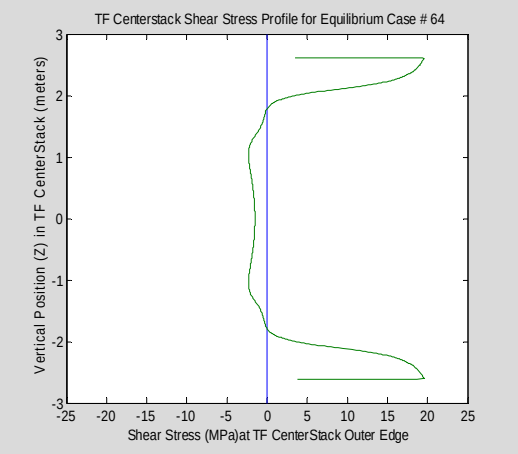
TF Centerstack Shear Stress Profile for Equilibrium Case # 64
Vertical Position (Z) in TF CenterStack (meters)
Shear Stress (MPa)at TF CenterStack Outer Edge

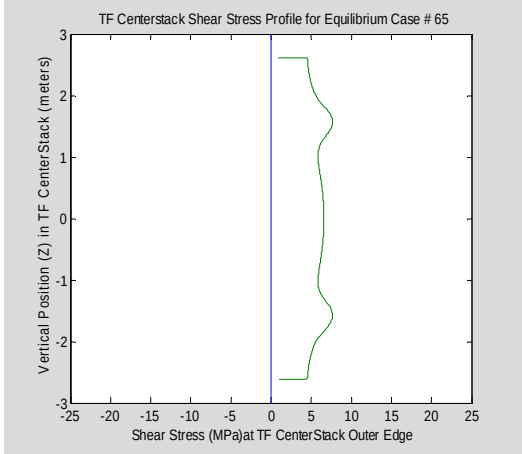
TF Centerstack Shear Stress Profile for Equilibrium Case # 65
Vertical Position (Z) in TF CenterStack (meters)
Shear Stress (MPa)at TF CenterStack Outer Edge

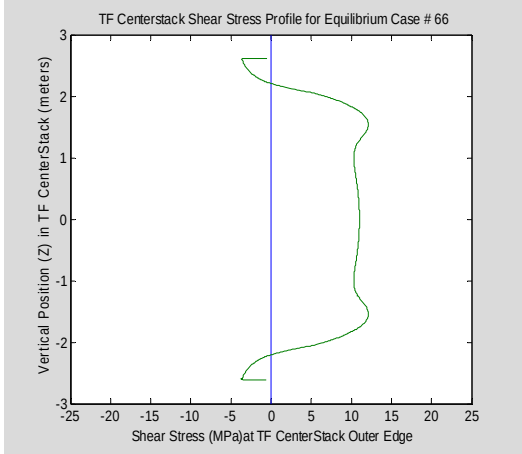
TF Centerstack Shear Stress Profile for Equilibrium Case # 66
Vertical Position (Z) in TF CenterStack (meters)
Shear Stress (MPa)at TF CenterStack Outer Edge

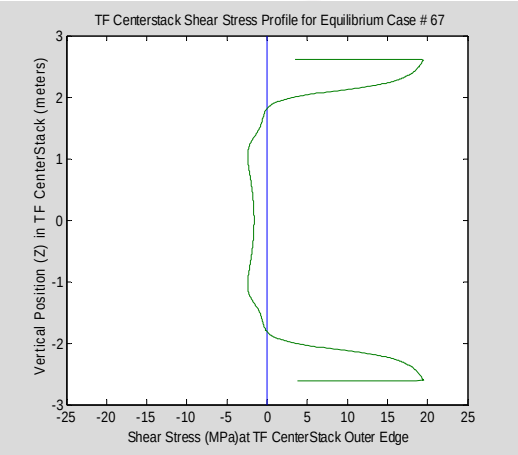
TF Centerstack Shear Stress Profile for Equilibrium Case # 67
Vertical Position (Z) in TF CenterStack (meters)
Shear Stress (MPa)at TF CenterStack Outer Edge

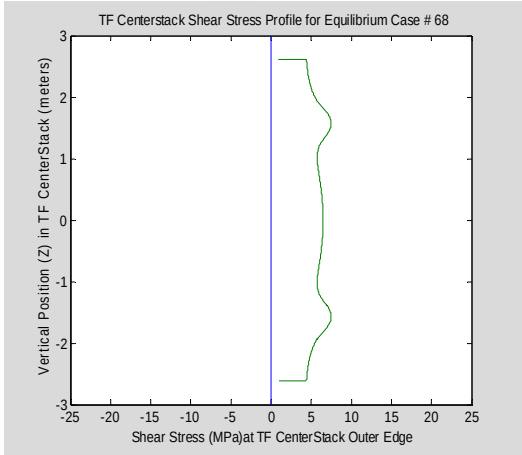
TF Centerstack Shear Stress Profile for Equilibrium Case # 68
Vertical Position (Z) in TF CenterStack (meters)
Shear Stress (MPa)at TF CenterStack Outer Edge

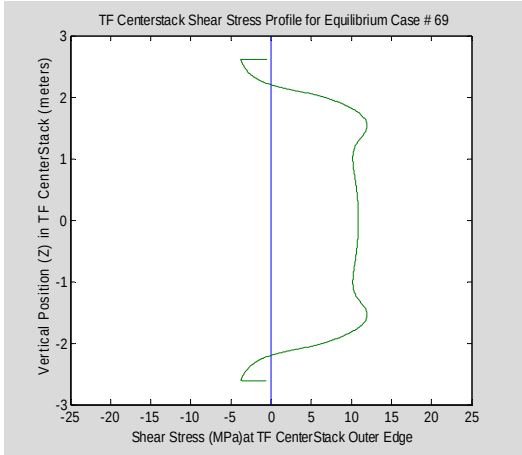
TF Centerstack Shear Stress Profile for Equilibrium Case # 69
Vertical Position (Z) in TF CenterStack (meters)
Shear Stress (MPa)at TF CenterStack Outer Edge

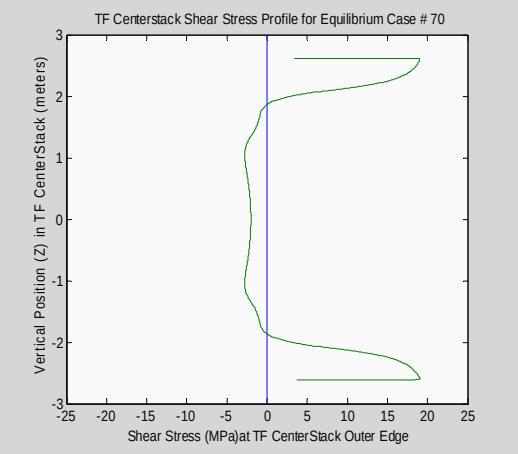
TF Centerstack Shear Stress Profile for Equilibrium Case # 70
Vertical Position (Z) in TF CenterStack (meters)
Shear Stress (MPa)at TF CenterStack Outer Edge

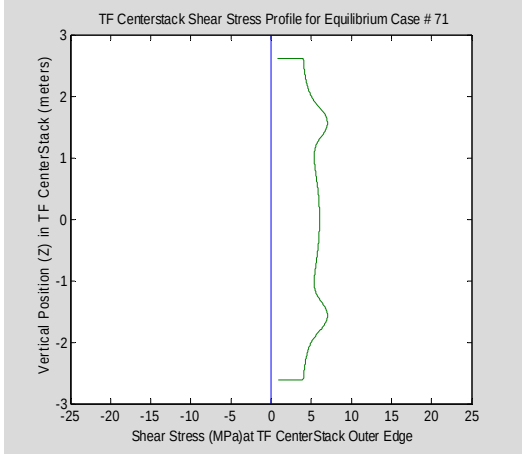
TF Centerstack Shear Stress Profile for Equilibrium Case # 71
Vertical Position (Z) in TF CenterStack (meters)
Shear Stress (MPa)at TF CenterStack Outer Edge

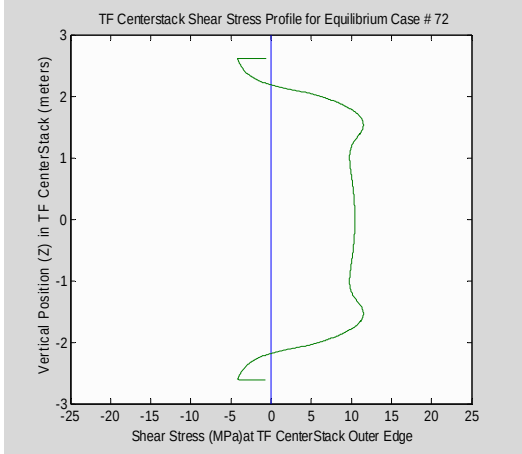
TF Centerstack Shear Stress Profile for Equilibrium Case # 72
Vertical Position (Z) in TF CenterStack (meters)
Shear Stress (MPa)at TF CenterStack Outer Edge

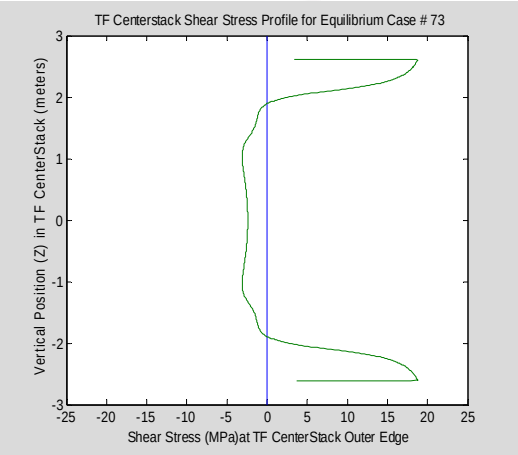
TF Centerstack Shear Stress Profile for Equilibrium Case # 73
Vertical Position (Z) in TF CenterStack (meters)
Shear Stress (MPa)at TF CenterStack Outer Edge

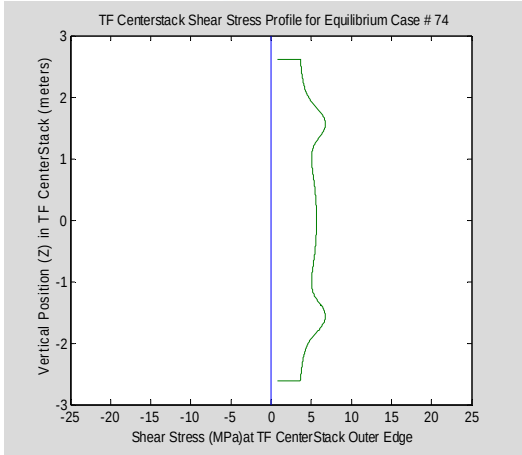
TF Centerstack Shear Stress Profile for Equilibrium Case # 74
Vertical Position (Z) in TF CenterStack (meters)
Shear Stress (MPa)at TF CenterStack Outer Edge

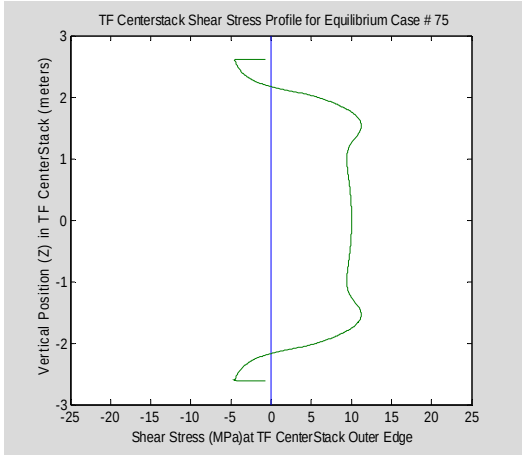
TF Centerstack Shear Stress Profile for Equilibrium Case # 75
Vertical Position (Z) in TF CenterStack (meters)
Shear Stress (MPa)at TF CenterStack Outer Edge

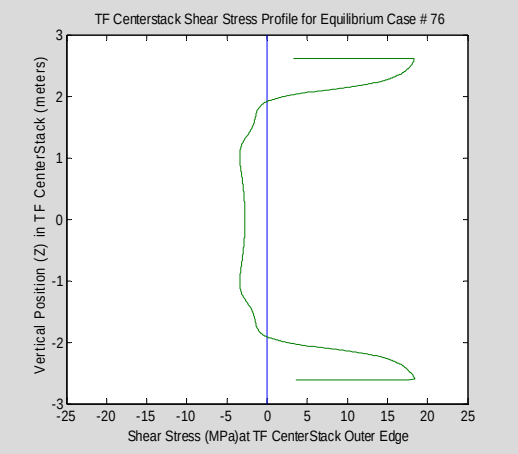
TF Centerstack Shear Stress Profile for Equilibrium Case # 76
Vertical Position (Z) in TF CenterStack (meters)
Shear Stress (MPa)at TF CenterStack Outer Edge

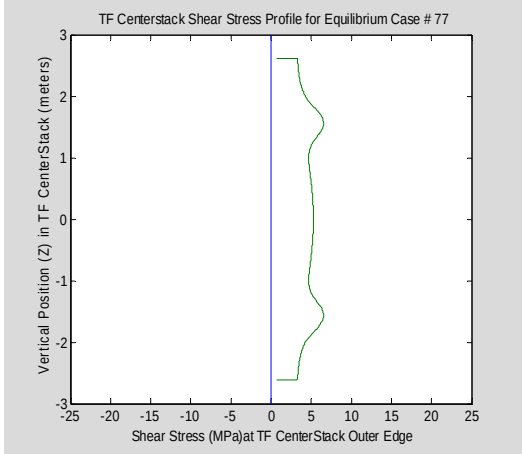
TF Centerstack Shear Stress Profile for Equilibrium Case # 77
Vertical Position (Z) in TF CenterStack (meters)
Shear Stress (MPa)at TF CenterStack Outer Edge

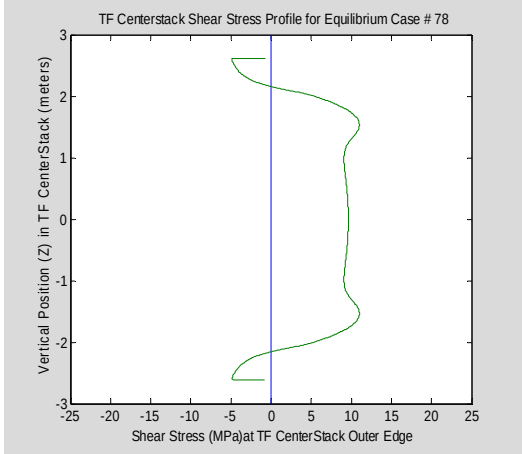
TF Centerstack Shear Stress Profile for Equilibrium Case # 78
Vertical Position (Z) in TF CenterStack (meters)
Shear Stress (MPa)at TF CenterStack Outer Edge

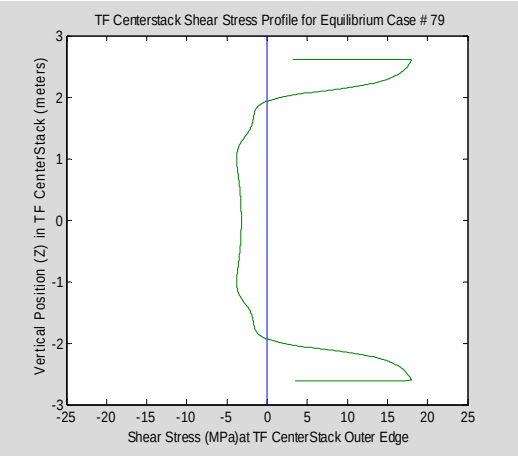
TF Centerstack Shear Stress Profile for Equilibrium Case # 79
Vertical Position (Z) in TF CenterStack (meters)
Shear Stress (MPa)at TF CenterStack Outer Edge

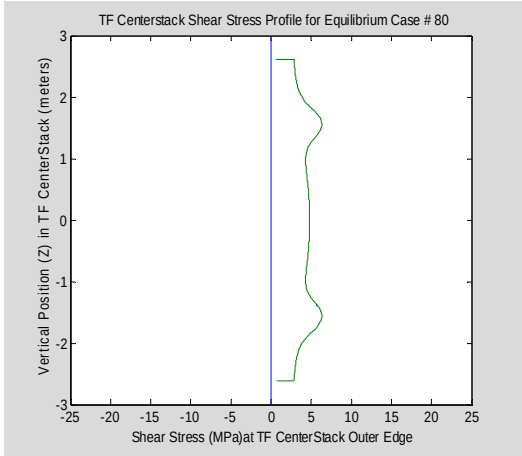
TF Centerstack Shear Stress Profile for Equilibrium Case # 80
Vertical Position (Z) in TF CenterStack (meters)
Shear Stress (MPa)at TF CenterStack Outer Edge

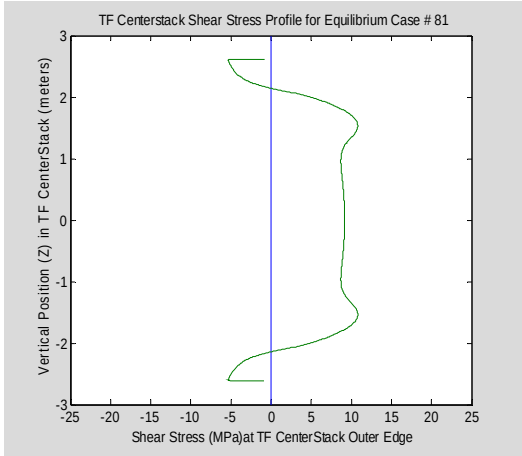
TF Centerstack Shear Stress Profile for Equilibrium Case # 81
Vertical Position (Z) in TF CenterStack (meters)
Shear Stress (MPa)at TF CenterStack Outer Edge

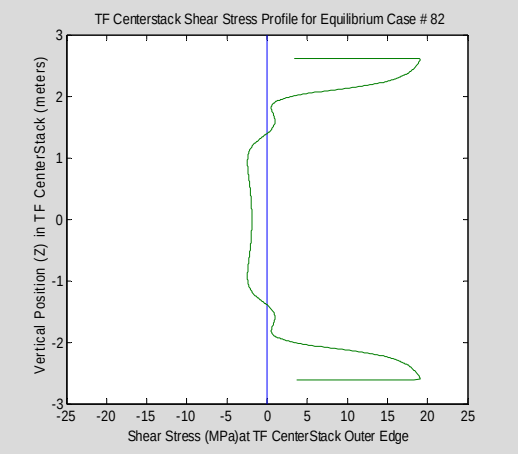
TF Centerstack Shear Stress Profile for Equilibrium Case # 82
Vertical Position (Z) in TF CenterStack (meters)
Shear Stress (MPa)at TF CenterStack Outer Edge

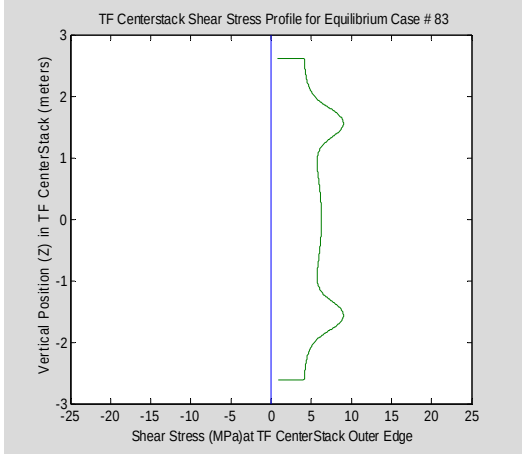
TF Centerstack Shear Stress Profile for Equilibrium Case # 83
Vertical Position (Z) in TF CenterStack (meters)
Shear Stress (MPa)at TF CenterStack Outer Edge

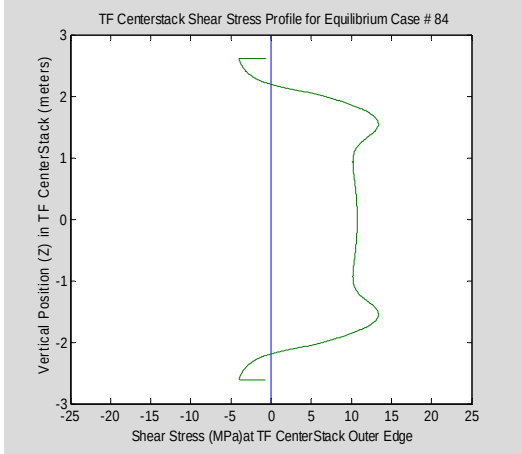
TF Centerstack Shear Stress Profile for Equilibrium Case # 84
Vertical Position (Z) in TF CenterStack (meters)
Shear Stress (MPa)at TF CenterStack Outer Edge

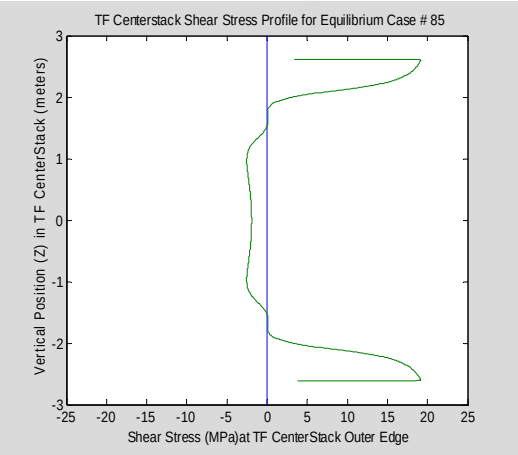
TF Centerstack Shear Stress Profile for Equilibrium Case # 85
Vertical Position (Z) in TF CenterStack (meters)
Shear Stress (MPa)at TF CenterStack Outer Edge

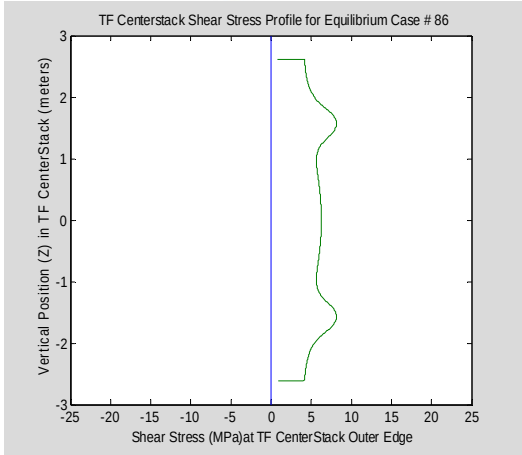
TF Centerstack Shear Stress Profile for Equilibrium Case # 86
Vertical Position (Z) in TF CenterStack (meters)
Shear Stress (MPa)at TF CenterStack Outer Edge

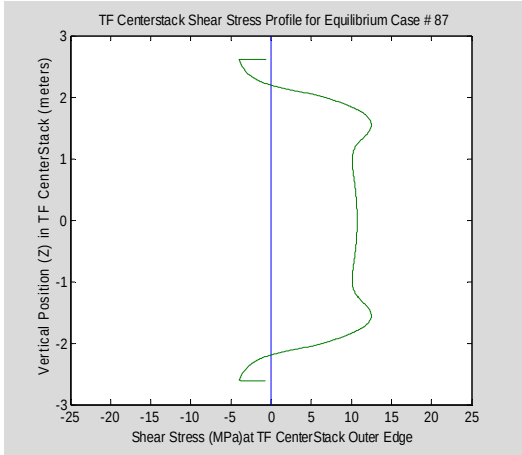
TF Centerstack Shear Stress Profile for Equilibrium Case # 87
Vertical Position (Z) in TF CenterStack (meters)
Shear Stress (MPa)at TF CenterStack Outer Edge

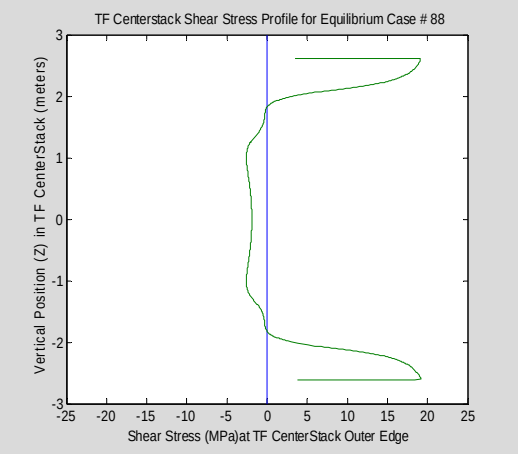
TF Centerstack Shear Stress Profile for Equilibrium Case # 88
Vertical Position (Z) in TF CenterStack (meters)
Shear Stress (MPa)at TF CenterStack Outer Edge

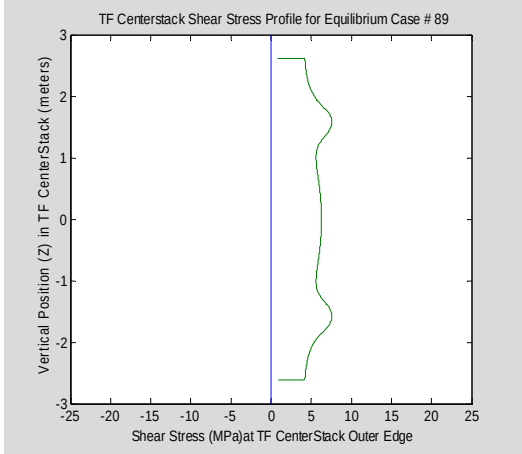
TF Centerstack Shear Stress Profile for Equilibrium Case # 89
Vertical Position (Z) in TF CenterStack (meters)
Shear Stress (MPa)at TF CenterStack Outer Edge

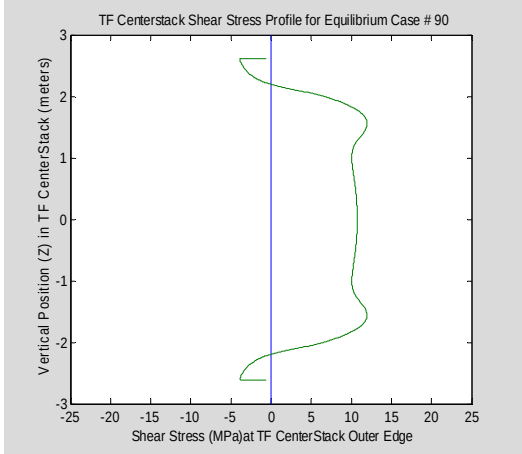
TF Centerstack Shear Stress Profile for Equilibrium Case # 90
Vertical Position (Z) in TF CenterStack (meters)
Shear Stress (MPa)at TF CenterStack Outer Edge

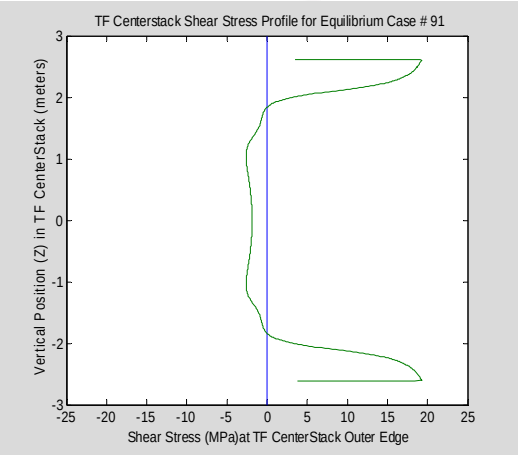
TF Centerstack Shear Stress Profile for Equilibrium Case # 91
Vertical Position (Z) in TF CenterStack (meters)
Shear Stress (MPa)at TF CenterStack Outer Edge

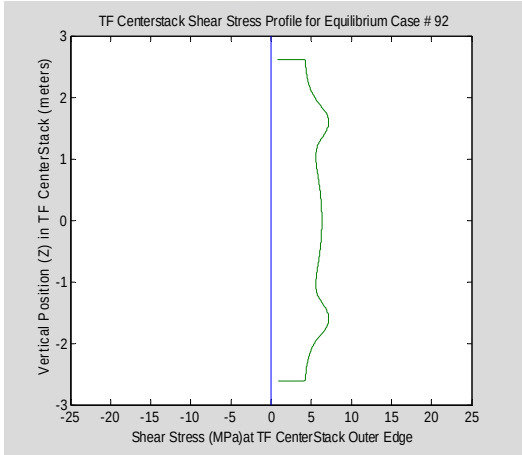
TF Centerstack Shear Stress Profile for Equilibrium Case # 92
Vertical Position (Z) in TF CenterStack (meters)
Shear Stress (MPa)at TF CenterStack Outer Edge

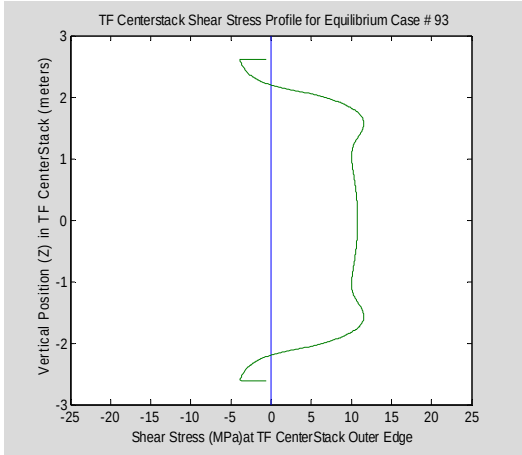
TF Centerstack Shear Stress Profile for Equilibrium Case # 93
Vertical Position (Z) in TF CenterStack (meters)
Shear Stress (MPa)at TF CenterStack Outer Edge

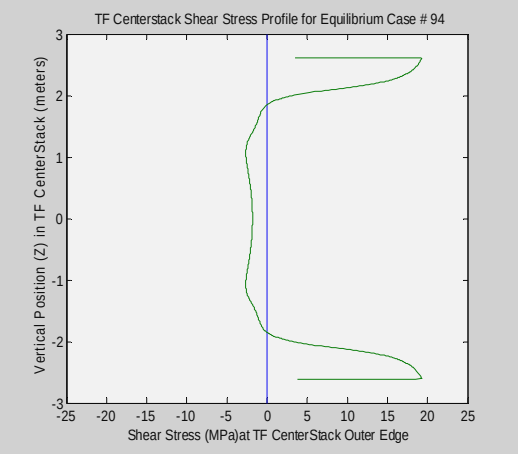
TF Centerstack Shear Stress Profile for Equilibrium Case # 94
Vertical Position (Z) in TF CenterStack (meters)
Shear Stress (MPa)at TF CenterStack Outer Edge

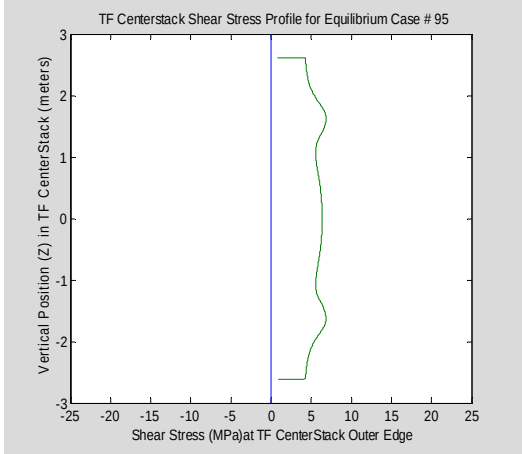
TF Centerstack Shear Stress Profile for Equilibrium Case # 95
Vertical Position (Z) in TF CenterStack (meters)
Shear Stress (MPa)at TF CenterStack Outer Edge

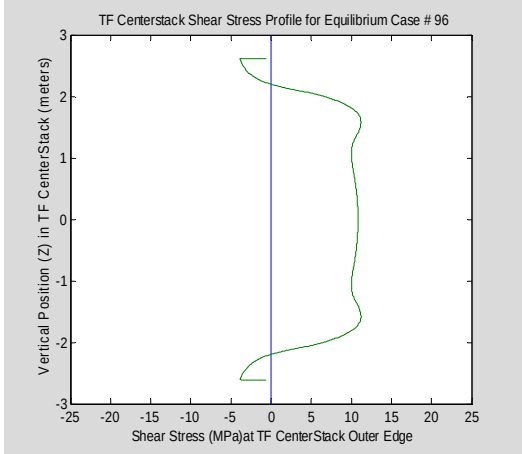
TF Centerstack Shear Stress Profile for Equilibrium Case # 96
Vertical Position (Z) in TF CenterStack (meters)
Shear Stress (MPa)at TF CenterStack Outer Edge

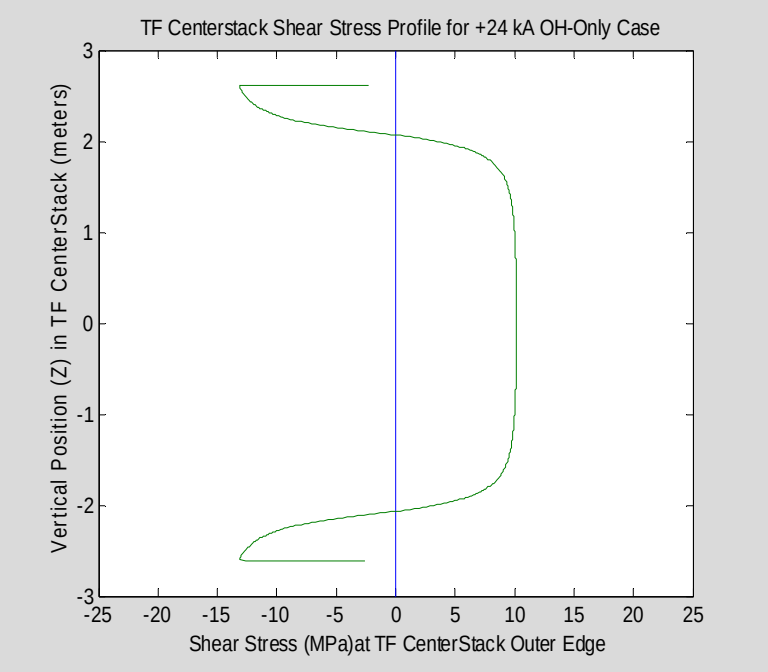
TF Centerstack Shear Stress Profile for +24 kA OH-Only Case
Vertical Position (Z) in TF CenterStack (meters)
Shear Stress (MPa)at TF CenterStack Outer Edge
3
2
1
0
-1
-2
-3
-25
-20
-15
-10
-5
0
5
10
15
20
25